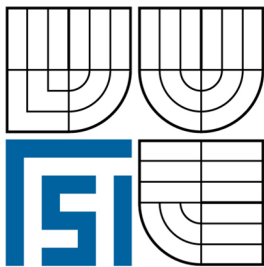# VYSOKÉ UČENÍ TECHNICKÉ V BRNĚ
BRNO UNIVERSITY OF TECHNOLOGY

FAKULTA STROJNÍHO INŽENÝRSTVÍ
ÚSTAV MECHANIKY TĚLES, MECHATRONIKY A BIOMECHANIKY

FACULTY OF MECHANICAL ENGINEERING
INSTITUTE OF MECHANICS OF SOLIDS, MECHATRONICS AND BIOMECHNICS

SOLUTION OF GENERAL STRESS CONCENTRATORS IN ANISOTROPIC MEDIA BY COMBINATION OF FEM AND THE COMPLEX POTENTIAL THEORY

ŘEŠENÍ OBECNÝCH KONCENTRÁTORŮ NAPĚTÍ V ANISOTROPNÍCH PROSTŘEDÍCH POMOCÍ KOMBINACE MKP A TEORIE KOMPLEXNÍCH POTENCIÁLŮ

DISERTAČNÍ PRÁCE
DOCTORAL THESIS

AUTOR PRÁCE Ing. OLDŘICH ŠEVEČEK
AUTHOR

VEDOUCÍ PRÁCE prof. RNDr. MICHAL KOTOUL, DrSc
SUPERVISOR

BRNO 2009

Abstract:

The presented Ph.D. thesis has originated in the framework of the postgraduate study under tuition of my supervisor Prof. RNDr. Michal Kotoul, DrSc. The thesis focuses to the solution of the problems of general stress concentrators in anisotropic media. Particularly, it is a problem of cracks terminating on the interface of two dissimilar materials or problems of general multi-material wedge. The work is possible to sectionalize into three parts. The first part is dedicated to the search study in the area of interest, the second part to the methods chosen for the achievement of the thesis aims. These aims are as follows: the description of the stress field in the vicinity of the general stress concentrator, the inclusion of the effect of crack bridging into the resulting stress field, and definition of the fracture criteria for the crack impinging at the interface in dissimilar anisotropic media. The last, third, part contains several demonstrative examples – applications of methods on specific bi-material models. For the description of the stress field the so-called Lechnitskii-Stroh formalism and continuously distributed dislocation technique, exploiting the complex potential theory. The first step is the singularity analysis of the general stress concentrator, next the calculation of the generalized stress intensity factor and of the T-stress. The obtained asymptotic expansion for stresses and displacements is subsequently used for the fracture criterion definition, where the theory of Finite Fracture Mechanics and matched asymptotic expansions is used for its derivation. All the needed calculations are performed in the mathematical softwares MAPLE 10.0 and MATLAB 7.1 and in the finite element system ANSYS 10.0. The two-state Ψ-integral is widely applied in this work – especially for the calculation of the generalized stress intensity factor or T-stress, calculation of the bridging effect and for the application of the fracture criteria.

Keywords:

Abstrakt:

Předkládaná disertační práce vznikla v rámci doktorského studia pod vedením mého školitele Prof. RNDr. Michala Kotoula, DrSc. Práce se věnuje problematice obecných koncentrátorů napětí v anisotropních prostředích. Zejména se jedná o problém trhlin končících na rozhraní dvou různých materiálů, či problém obecného více-materiálového klínu. Práce je členěna do několika částí, kde první je věnována rešerši v oblasti řešené problematiky, druhá část je potom věnována jednotlivým metodám zvolených pro splnění cílů práce, tj. popis pole napětí v okolí obecného koncentrátoru, zahrnutí vlivu přemostění trhliny do výsledného pole napětí a definici lomových kritérií pro obecný koncentrátor v anisotropním prostředí. Poslední část je věnována ukázkovým příkladům, tedy aplikaci metod na konkrétní bi-materiálové modely. U popisu pole napětí je využit tzv. Lechnického-Strohův formalismus a technika spojitě rozložených dislokací využívající teorii komplexních potenciálů. Prvním krokem je analýza singularity obecného koncentrátoru, dále výpočet zobecněného součinitele intensity napětí a T-napětí. Získaný asymptotický rozvoj pro napětí a posuvy se následně uplatní při formulaci lomových kritérií, přičemž je použita teorie tzv. „konečné lomové mechaniky" a teorie sdružených asymptotických rozvojů. Veškeré potřebné výpočty jsou prováděny v matematických softwarech MAPLE 10.0 a MATLAB 7.1 a konečnoprvkovém systému ANSYS 10.0. V práci je široce uplatněn tzv. dvoustavový Ψ-integrál, založený na Bettiho recipročním teorému. Využit je pro výpočet zobecněného součinitele intensity napětí, T-napětí, výpočtu přemostění i při aplikaci lomových kritérií.

Klíčová slova:

Anisotropní bimateriál, dvoustavový integrál, zobecněný faktor intensity napětí, T-napětí, MKP, přemostěná trhlina, lomová kritéria.

Bibliographic citation of this work:

ŠEVEČEK, O. *Solution of general stress concentrators in anisotropic media by combination of FEM and the complex potential theory.* Brno: Brno University of Technology, Faculty of Mechanical Engineering, 2009. 123 p. Supervisor of the doctoral thesis prof. RNDr. Michal Kotoul, DrSc.

Bibliografická citace této práce:

ŠEVEČEK, O. *Solution of general stress concentrators in anisotropic media by combination of FEM and the complex potential theory.* Brno: Vysoké učení technické v Brně, Fakulta strojního inženýrství, 2009. 123 s. Vedoucí disertační práce prof. RNDr. Michal Kotoul, DrSc.

Čestné prohlášení

Prohlašuji, že jsem tuto disertační práci zpracoval samostatně na základě konzultací s mým školitelem prof. RNDr. Michalem Kotoulem, DrSc. a s použitím uvedené literatury.

V Brně dne 29. 6. 2009

....

Ing. Oldřich Ševeček

Acknowledgements:

I would like to personally express big thanks to my supervisor Prof. RNDr. Michal Kotoul, DrSc. for his inspiring tuitions through the whole doctoral study and the related research and for his, at all points, very kind access to me as a Ph.D. student. Thanks belong also to my collegue, Ing. Tomáš Profant, Ph.D, who was very conducive to me during the solution of the complex mathematical problems.

At the end, I would like to also express thanks to my girlfriend and family for their persistent support during the whole doctoral study and writing of this thesis.

Contents

1   Introduction

The increasing use of fibre-reinforced composites (or other modern materials) in high performance structures has brought a renewed interest in the analysis of cracks in anisotropic and moreover heterogeneous media. Without the tools for the assessment of fracture-mechanics behaviour of these materials it is impossible to apply them into any critical machine parts, where the unexpected failure can have a catastrophic consequence. Therefore, there is a necessity to correctly assess the singular points in constructions (potential stress concentrators) and be able to predict their future behaviour during the operation. Lot of recent works have been focused on the description of the general stress concentrators in isotropic media. As a consequence, this field is explored quite well. However, in case of the anisotropic materials, there are certain complications which generally disallow applying the same approaches as for isotropic materials. Therefore, it is necessary to find other possible ways how to involve general anisotropy into the solution and assessment of the general stress concentrators.

Most matrices of the advanced composite materials are brittle. They prone to cracking under very low applied stresses and the failure frequently occurs in the form of multiple matrix cracking. The orientations of these cracks may vary depending on the relative position of the reinforcement in relation to the load. The stress field in the neighbourhood of crack is governed by the overall anisotropic material response. The existence of material interfaces in composites, especially in laminates, brings other problems in the analysis of cracks – the problem of cracks terminating at the interface of two anisotropic (most often orthotropic) solids and the problem of interfacial cracks [22]. These problems are also encountered in the technology of protective coatings. For the assessment of crack behaviour in the aforementioned situations it is essential to investigate and describe the stress field near the crack tip. Although the FE analysis is capable of capturing the singular stress behaviour near a corner or a crack tip in homogeneous regions with a refined mesh of conventional elements, this traditional FE approach fails to accurately capture the appropriate singular behaviour near a corner or a crack tip at the junction of dissimilar materials. A very promising approach to an accurate calculation of the near crack tip fields consists in the application of so-called two-state (or mutual) conservation integrals - [34], [40], [80], [107]. The two-state conservation integrals, e.g. in conjunction with a displacement-based FEM provide an efficient tool for calculating the stress intensities and elastic T-stresses without need of the very fine mesh in the singular point vicinity. This is a major advantage over the singular finite elements [93], and other various special techniques such as the boundary collocation or the singular hybrid FEM.

The problem complexity can be further increased by presence of the bridging phase which can significantly influence the resulting stress field in the vicinity of the crack tip. These situations can be often found for example in laminated structures composed of layers which are reinforced by long fibres. In spite of the crack existence in some layer, there may be present intact bridging fibres which positively influence the fracture behaviour of the structure (due to the crack closure effect). Therefore, this fact should be also involved in the stress field analysis which stands as a basis for the subsequent fracture-mechanics behaviour assessment. The main objective of this assessment and of the whole described problems is to understand the mechanism of competition between the crack deflection along the interface and penetration into the adjoining material and be able to design such a construction which will exhibit the desired behaviour. The solved problems are very topical and will provide a basis of the subsequent research following this thesis.

2 Analysis of the investigated problems

2.1 Basic terms

General stress concentrator:

Generally the singular stress field in the vicinity of a singular point exhibits the asymptotic behaviour $\sigma_{ij} \approx r^{\delta-1}$, where r is the distance from the singular point, δ is called a characteristic eigenvalue of the singularity and $1-\delta$ is called as a stress singularity exponent. In the case of sharp crack in homogenous media, this singularity exponent is equal to 0.5. If the singularity exponent differs from this value, the stress concentrator is called a general stress concentrator. In that case the characteristic eigenvalue (or singularity exponent) can generally acquire a value from the interval (0,1). It can be also generally complex, whereas the real part is from interval (0,1).

For instance, the following configurations give rise to the general stress concentrators:

- o Cracks or notches with tip on the interface of two dissimilar materials (can be positioned at arbitrary angle to the interface)

- o Interfacial cracks

- o V-notch

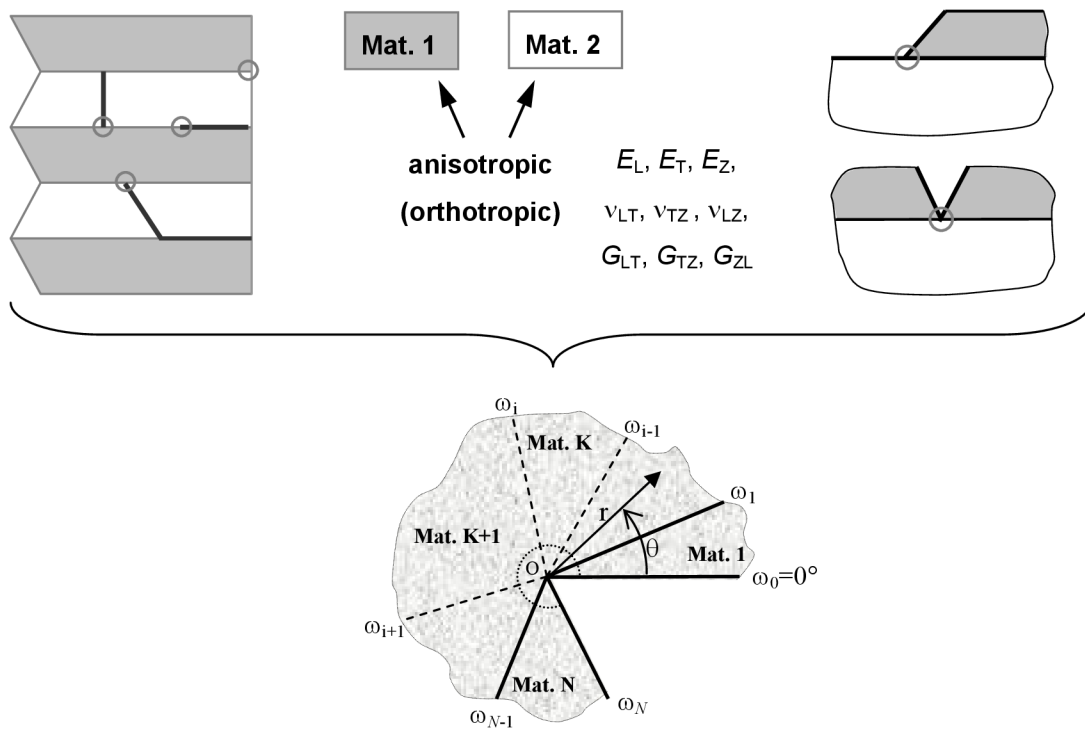- o Generally a junction of several materials (covers all previous cases)

Fig. 1 Different types of the general stress concentrators – crack terminating at the interface of two dissimilar materials, interfacial crack, notch and V-notch and a general multimaterial wedge.

Complex potential theory:

The Lechnitskii formalism is the oldest and the most frequently used formalism in engineering practise employed for the description of plane deformation of anisotropic media – see [52], [53], [54] and [55]. This formalism is in fact a generalization of the Muschelishvilli theory [67] of complex potentials in plane isotropic elasticity which assumes that stresses are dependent only on coordinates x_1 a x_2. Therefore, in relations outgoing from the Lechnitskii theory the components of the reduced compliance matrix occur. The opposite situation is in the case of the Stroh formalism which comes out of the works [20] and [85]. The Stroh formalism assumes that displacements U_i ($i=1, 2, 3$) are dependent on coordinates x_1 and x_2 (axes of coordinate system with origin at the crack tip). Due to this assumption, instead of the compliance matrix components in the corresponding relations, the components of the stiffness matrix are present. The advantage of the Stroh formalism is its mathematical elegance and its power in the solution of 2D anisotropic elastic problems.

In case of the general plane anisotropic elasticity it is necessary to consider all components of the stress and strain tensor. Each anisotropic material can be characterized by three complex numbers μ_i ($i=1, 2, 3$) and their complex conjugate opposites. The numbers μ_i are eigenvalues of the matrix 3×3 whose elements depends on material elastic properties. A significant simplification can be made if the stiffness (or compliance) matrix has a symmetry planes, as e.g. in the case of orthotropic materials. In such a case the number of characteristic material eigenvalues is reduced to two and the nonzero components of stress (strain) tensor are reduced only to σ_{ij} or ε_{ij}, where $i, j = 1, 2$.

The singular stress and displacement field in the vicinity of the crack tip is useful to express as a functions of polar coordinates r and θ:

$$U_i = H\, r^\delta g_i(\theta)\,, \quad \sigma_{ij} = H\, r^{\delta-1} f_{ij}(\theta)\,, \tag{1}$$

where δ is a characteristic eigenvalue of the given singularity which is obtained as a solution of the singular eigenvalue problem. The Generalized Stress Intensity Factor H depends on the external load and on the whole body geometry.

Generalized Stress Intensity Factor (GSIF):

Within the framework of the linear-elastic fracture mechanics, the stress field in the vicinity of the general stress concentrator is possible to write (for the general case of loading) in the following form:

$$\sigma_{ij\,(tip)} = H_1 \cdot r^{\delta_1-1} \cdot f_{ij1}(\phi,\alpha,\beta,\delta_1,\theta) + H_2 \cdot r^{\delta_2-1} \cdot f_{ij2}(\phi,\alpha,\beta,\delta_2,\theta) + \ldots T^{(1)}\delta_{i1}\delta_{j1} + T^{(2)}\delta_{i2}\delta_{j2} + O(r^\delta). \tag{2}$$

Expansion (2) is called a Williams asymptotic stress expansion [2]. The first two terms are singular (generally there can be also more of them or only one). The amplitude of the singular term is then called a Generalized Stress Intensity Factor and is denoted as H_1 or H_2. Here, H_1 corresponds to the GSIF of a stronger singularity and H_2 to the GSIF of a weaker singularity (note that H_1 can be matched with the stress intensity factor K_I for a crack in homogenous body, where characteristic eigenvalues δ_1 and δ_2 are equal to 1/2). Variables r and θ denote the polar coordinates, T is the T-stress and $O(r^\delta)$ are the higher order terms which are negligible in comparison with the previous ones for $r\to0$.

T-stress:

The T-stress is a non-singular term in the Williams asymptotic expansion (2) denoted as T. It represents stress component σ_{xx} acting parallely with the crack faces. This term is not dependent on the distance from the crack tip (on the polar coordinate r). The T-stress is a second fracture-mechanics parameter which mostly characterizes the influence of the body geometry and it can be also used for the description of the constraint effect at the crack tip. T-stress can be tensile (positive) or compressive (negative). Its value is changing with the applied stress, specimen geometry and is also dependent on the boundary conditions. Since it can have a significant influence on the fracture-mechanics behaviour of the stress concentrator, there is necessary to have some available methods for its determination. Some of them are mentioned in the chapter 4.1.4 with the corresponding references to the literature.

2.2   Definition of the studied problem

The main subject of the thesis is the analysis of the behaviour of the general stress concentrators in the anisotropic media. The goal is to work up a suitable technique for the description of the stress field in the vicinity of the general stress concentrator with involvement of a possible crack bridging effect. Subsequently, to set up a criterion which will have made possible to predict failure behaviour originated at the given loading conditions. All materials are considered to be orthotropic (or generally anisotropic). In case of the full orthotropy the nine independent material characteristics are required to its description and in case of the transverse isotropic material only five independent elastic constants are needed (due to the material symmetry). All studied problems are restricted to the validity of the linear elastic fracture mechanics (LEFM). Solution of these problems is of a high importance for the fracture-mechanics analysis of e.g. laminated composite structures composed of anisotropic laminae, analysis of the protective surface layers or some general multimaterial wedges.

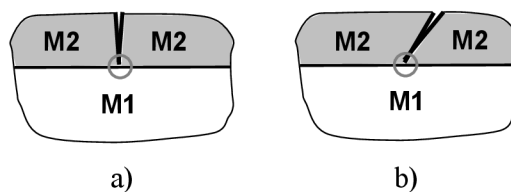a)   b)

Fig. 2 Geometric configurations of general stress concentrators in anisotropic media solved within the thesis: a) crack perpendicular to the bi-material interface; b) crack situated at arbitrary angle to the bi-material interface.

3   Problem formulation

In order to describe fracture-mechanics behaviour of the studied general stress concentrators (Fig. 2), first the stress field has to be investigated and subsequently the suitable fracture criterion defined. Namely the following steps are required to perform:

☞ In the first step it is necessary to obtain the characteristic eigenvalue(s) of the given singularity which are in case of the general stress concentrator different from 1/2. The studied geometric configurations are depicted in Fig. 2. In literature one can find several approaches which can be used for the singularity analysis. In case of isotropic materials, it is possible to employ analytical solution as was proposed by Williams and used e.g. in [68]. However, the approach is not very suitable for the case of junction of more than two materials, especially in case of generally anisotropic materials. It is due to resulting very long analytical expressions which are significantly difficult to manipulate. For this reason, it is better to employ e.g. some semi-analytical methods based on the complex potential theory and Stroh formalism which simplify the problem.

☞ In the second step, the stress distribution in the vicinity of the general stress concentrator has to be determined. This step is in fact connected with the step no. one. That is, after the appropriate eigenvalues of the given singularity are found, the eigenvectors describing the distribution of the stress field can be calculated (by the same method).

☞ In the third step, the amplitude of the singular term in Williams asymptotic expansion (2) (Generalized Stress Intensity Factor - GSIF) has to be determined for a selected configuration. It is an important fracture-mechanics parameter, which involves the information about the loading conditions. To refine the local stress field description, considering the T-stress may improve a characterization of the fracture behaviour. In many cases, it can have a significant influence on this behaviour. The GSIF or the T-stress can be calculated e.g. using a combination of the FEM and two-state integral method based on Betti's theorem. For the same purpose the Continuously Distributed Dislocation technique can be used as well.

☞ The fourth step (optional) depends on the solved material configuration. It involves a case, when the crack is bridged by long fibres and the goal is to quantify the bridging effect and its influence on the applied GSIF (from the third step). These crack bridging situation can be very often found e.g. in some laminated structures composed of plies with long fibres, where the possible crack in some ply is bridged by these fibres. If the bridging effect exists, it should be taken into account, because it can have a significant influence on the crack stability.

☞ In the last step, the appropriate fracture criterion for the general stress concentrators is to be set up and defined. Within the thesis, the criteria based upon the energetic approach, are to be applied. The main goal is to propose a procedure which allows to predict a fracture stemming from the concentrator. Particularly, the possibility of crack deflection along the interface (single or double) or further penetration of the main crack across the interface into the next material will be considered. The competition between these processes will be assessed.

4   Summary of references relating to the solved problems

With regards to the solved problems (as stated in the previous sections), this chapter will be divided into three main parts which will include the recherché study in the field of the thesis topic. The main objective is to give information concerning the current state of research and to find suitable techniques for the solution of the defined problems. In the fourth, summarizing part of this chapter all findings with respect to own work objectives are classified.

4.1   Description of the stress field in the vicinity of the general stress concentrator

4.1.1   Singularity analysis

In the first stage of the analysis of the stress field induced by the general stress concentrator, the eigenvalues and eigenvectors pertaining to the given singularity have to be found. These eigenvalues determine the stress singularity exponent – the order of the stress singularity in the Williams-like asymptotic expansion (2). The eigenvectors determine the shape and distribution of the stress field (see function $f_{ij}(\theta)$ in (1)). Note that when the eigenvalue changes from real to complex at some combinations of elastic constants and crack/wedge geometry, multiple eigenvalues corresponding to the same independent eigenfunction may occur. For the singularity analysis, two main categories of numerical methods are available – explicit and implicit methods - [71]:

a) Explicit methods

An explicit form of the transcendent equation for the eigenvalues of the singular problem – roots of this equation are the eigenvalues of the singular problem operator is derived. Analytical solution was proposed e.g. by Williams or Westergaard and used in works [33], [68] or [76] for a solution of the problem of crack terminating at the interface in isotropic solids. However, from practical point of view, this solution is limited to isotropic materials (or very special cases of anisotropy) and at present, only to the problems of maximum tri-material wedge. As was already mentioned, it is because it leads to very long analytical expressions which are significantly difficult to manipulate. For the bi-material case, the authors of [16], using similar techniques, obtained explicit eigenequations with each expression corresponding to a different boundary condition. In [108] an explicit closed form expression for the eigenequation for a tri-material wedge includes the uni- and bi-material cases. The eigenequation was again derived as the determinant of a 2x2 matrix. Its roots were sought in a given region of the complex plane. As is noted in the above papers, the uniform expression for a tri-material wedge is 15 pages long and is almost impossible to work out by hand, while for a four-material wedge, the size of the expression is too big to handle even with symbolic manipulation programs. Therefore some other approaches based on the semi-analytical solution have to be used.

- L.E.S. method

The method is named after Lechnitskii [55], Eshelby [20] and Stroh [85] who introduced the complex potentials for anisotropic bodies. The complex potentials formally satisfy the equilibrium, the compatibility equations and the elastic/strain laws but the specific form of the solution is gained by matching boundary conditions. The stresses σ_{ij}, displacements U_i and a resulting force T_i along the half-line leading from the origin of coordinate system is possible to write in the following form:

$$\sigma_{ij} = H \cdot r^{\delta-1} \cdot f_{ij}\left(\theta,...\right), \quad U_i = H \cdot r^{\delta} \cdot g_i\left(\theta,...\right), \quad -T_i = H \cdot r^{\delta} \cdot F_i\left(\theta,...\right), \tag{3}$$

where $f_{ij}(\theta,...)$, $g_i(\theta,...)$ and $F_i(\theta,...)$ are the functions of the polar coordinate θ, material elastic properties (given by material stiffness matrix), further of the characteristic material eigenvalues μ_i (see chapter 2.1), and mainly of the searched singularity exponent (characteristic eigenvalue of the singularity δ). The means of obtaining the complex numbers μ_i have been proposed by Lechnitskii [55], Eshelby et al. [20] and summarized by Suo in [86].

Providing a perfect bonding between two adjacent materials and application of appropriate boundary conditions (equivalent displacements U_i and resulting force T_i along the interface of the adjoining materials and traction free crack surfaces) we get a system of 4N homogenous linear equations [17] (N is the number of material wedges). This system is shortly possible to write in the following form:

$$\mathbf{K}(\delta)\mathbf{v} = 0, \tag{4}$$

where for non trivial solution all equations have to be linear dependent, so the determinant of system matrix $\mathbf{K}$ have to be zero ($\det(\mathbf{K})=0$). From this condition we get a non-linear equation whose roots are the searched characteristic singularity eigenvalues δ. The real part of the least root from interval (0,1) define a singularity exponent (δ_1-1) – see (2).

- *Transfer matrix method:*

The procedure originally developed by Ting [95], [96], [97] is an efficient tool for the singular characterization of non-degenerate anisotropic multimaterial corners. The ith material wedge occupies the polar sector $\omega_{i-1} < \theta < \omega_i$, $i = 1, . . . ,N$ (see Fig. 1). Perfect bonding is considered between material wedges. Fixed or free boundary conditions are considered at the external faces. The solution can be written in the condensed form using the complex variable $z_\alpha = x_1 + p_\alpha x_2 = r(\cos\theta + p_\alpha \sin\theta) = r\zeta_\alpha(\theta)$:

$$\mathbf{w}\left(r,\theta\right) = r^{\delta}\mathbf{X}\mathbf{Z}^{\delta}\left(\theta\right)\mathbf{q}, \tag{5}$$

where $\mathbf{w}^T(r,\theta) = [\mathbf{u}(r,\theta),\mathbf{\Phi}(r,\theta)]^T$, $\mathbf{u}$ stands for the displacement vector and $\mathbf{\Phi}$ is the stress function vector. p_α are three distinct complex numbers with positive imaginary parts, which are obtained as the roots of the characteristic equation

$$\det\left[c_{i1k1} + p\left(c_{i1k2} + c_{i2k1}\right) + p^2 c_{i2k2}\right] = 0. \tag{6}$$

c_{ijkl} is the tensor of elastic constants, i.e. $\sigma_{ij} = c_{ijkl}u_{k,l}$, the matrices $\mathbf{X}$ and $\mathbf{Z}$ are defined as

$$\mathbf{X} = \begin{bmatrix} \mathbf{A} & \overline{\mathbf{A}} \\ \mathbf{L} & \overline{\mathbf{L}} \end{bmatrix}, \quad \mathbf{Z}^{\delta} = \begin{bmatrix} \left\langle \zeta_*^{\delta} \right\rangle & 0 \\ 0 & \left\langle \overline{\zeta}_*^{\delta} \right\rangle \end{bmatrix}, \tag{7}$$

where $\mathbf{A}$ and $\mathbf{L}$ are matrices given by $L_{i\alpha} = A_{k\alpha}\left(c_{i2k1} + p_\alpha c_{i2k2}\right)$, $A_{k\alpha}$ denotes the eigenvector corresponding to the eigenvalue p_α above, the overbar denotes the complex conjugate. $\left\langle \zeta_*^{\delta} \right\rangle = \mathrm{diag}\left[\zeta_1^{\delta}, \zeta_2^{\delta}, \zeta_3^{\delta}\right]$. $\delta \in (0,1)$ is the characteristic eigenvalue of the singularity, $\mathbf{q}^T = \left[\mathbf{v}, \tilde{\mathbf{v}}\right]^T$ is the corresponding eigenvector which can be determined up to a multiplicative constant. If δ is a real number, then $\tilde{\mathbf{v}} = \overline{\mathbf{v}}$. Ting's procedure makes use of a transfer matrix, which transfers the displacements and stress function vector components from one edge of the material wedge to the other. Using the continuity conditions introduced by the hypothesis of perfect bonding between the wedges, $\mathbf{w}_i(r, \omega_i) = \mathbf{w}_{i+1}(r, \omega_i)(i = 1, . . . ,N-1)$, and the transfer matrix for each wedge, it is easy to arrive at an

expression for the whole multimaterial corner, as it relates the variables between its external faces (ω_0 and ω_N):

$$
\begin{bmatrix} \mathbf{u}_N(r,\omega_N) \\ \mathbf{\Phi}_N(r,\omega_N) \end{bmatrix} = \begin{bmatrix} \mathbf{K}_N^{(1)} & \mathbf{K}_N^{(2)} \\ \mathbf{K}_N^{(3)} & \mathbf{K}_N^{(4)} \end{bmatrix} \begin{bmatrix} \mathbf{u}_1(r,\omega_0) \\ \mathbf{\Phi}_1(r,\omega_0) \end{bmatrix},
\tag{8}
$$

where $\mathbf{K}_N$ is obtained by the product of the sequence of the successive transfer matrices $\mathbf{E}_i$ of all the wedges in the corner:

$$
\mathbf{K}_N = \mathbf{E}_N \cdot \mathbf{E}_{N-1} \cdot \ldots \mathbf{E}_2 \cdot \mathbf{E}_1, \quad \mathbf{E}_i = \mathbf{X}\mathbf{Z}^\delta(\omega_i)\left[\mathbf{Z}^\delta(\omega_{i-1})\right]^{-1}\mathbf{X}^{-1}.
\tag{9}
$$

This is worthy of note that Ting's procedure directly yields a linear system whose size is 3×3 or 6×6, irrespective of the number of materials N, contrary to traditional analytical procedures leading to a linear system of ($6N \times 6N$).

- Continuously distributed dislocation technique

This technique can be used for modelling of arbitrary cracks (opened or closed ones) [26] and it is based on the so-called Bueckner's principle. The basic idea is to use the superposition of the stress field present in the uncracked body, together with the unknown distribution of edge dislocations, chosen so that the crack faces become traction free. In other words, the crack is modelled by means of the continuous distribution of edge dislocations along the crack with a certain dislocation density which is unknown in the beginning of the solution and has to be determined. The goal is to set up an integral equation where the appropriate fundamental solution for the isolated dislocation is integrated along the crack line (the dislocations are distributed with certain dislocation density). By solving resulting Fredholm's integral equation the dislocation density is found. When this function of dislocations distribution is known, arbitrary quantity (stress or displacement) in the vicinity of the crack tip can be calculated. Also GSIF or the T-stress can be determined.
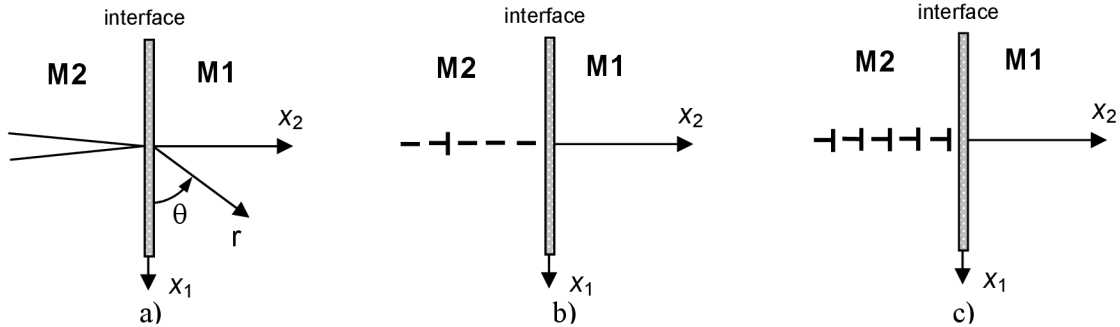
Fig. 3. Modelling of the crack by means of the CDD technique: a) crack perpendicular to the bi-material interface; b) Isolated dislocation in the semi-infinite plane; c) Array of dislocations distributed along the crack plane with certain dislocation density.

On the basis of work of Suo [86] it is possible to write the stress field component (e.g. σ_{1i}) induced by one isolated dislocation with Burger's vector b_i placed in the point (x_{1o}, x_{2o}) in infinite anisotropic bi-material in the following form:

$$
\sigma_{1i}(x_{1o}, x_{2o}) = -\frac{1}{4\pi}\sum_\alpha L_{i\alpha}^{II} p_\alpha^{II}\left[\sum_\beta\left(G_{\alpha\beta}\bar{M}_{\beta k}^{II}\frac{d_k}{z_\alpha - \bar{\varsigma}_\beta}\right) + M_{\alpha k}^{II}\frac{d_k}{z_\alpha - \varsigma_\alpha}\right] + C.C., \quad z \in 2
\tag{10}
$$

$$
\sigma_{1i}(x_{1o}, x_{2o}) = -\frac{1}{4\pi}\sum_\alpha L_{i\alpha}^I p_\alpha^I\sum_\beta\left(C_{\alpha\beta}M_{\beta k}^{II}\frac{d_k}{z_\alpha - \varsigma_\beta}\right) + C.C., \quad z \in 1
\tag{11}
$$

where the indices *I* a *II* refers to the material 1 and 2 respectively and *C.C.* is an expression complex conjugate to the previous one. The matrices *L* and *M* contain information about the bimaterial elastic properties and p_α are the characteristic material eigenvalues–see [86].

Introduce the local density of the Burger's vector f_k in some position *(x₁=0, x₂)* and define

$$d_k = f_k\left(x_{2o}\right)dx_{2o}, \tag{12}$$

where d_k is the elementary Burger's vector between x_{2o} and $x_{2o}+ dx_{2o}$. By integration of (10) along the whole crack one obtain the integral equation for stresses induced by the dislocation density f_k in position *(0, x₂)*:

$$\sigma_{1i}\left(x_2\right) = -\frac{1}{4\pi}\left\{\sum_\alpha L_{i\alpha}^{II}\left[\sum_\beta \left(G_{\alpha\beta}\overline{M}_{\beta k}^{II}\frac{p_\alpha^{II}}{\overline{p}_\beta^{II}}\int_{-\infty}^{0}\frac{f_k\left(x_{2o}\right)\mathrm{d}\,x_{2o}}{\frac{p_\alpha^{II}}{\overline{p}_\beta^{II}}x_2 - x_{2o}}\right) + M_{\alpha k}^{II}\int_{-\infty}^{0}\frac{f_k\left(x_{2o}\right)\mathrm{d}\,x_{2o}}{x_2 - x_{2o}}\right] + C.C.\right\}. \tag{13}$$

The asymptotic stress field in the vicinity of the crack tip is possible to model using (13) with dislocation density f_k:

$$f_k\left(x_{2o}\right) = H\cdot v_k\left(-x_{2o}\right)^{-\delta}, \quad x_{2o} < 0, \tag{14}$$

where δ is the characteristic eigenvalue of the singularity which is searched, v_k are components of the corresponding eigenvector and *H* is the generalized stress intensity factor. By substitution (14) into (13), integration and application of the boundary condition of traction free crack surfaces one obtains:

$$\mathrm{Re}\left\{\left[\sum_\alpha\sum_\beta L_{i\alpha}^{II}G_{\alpha\beta}\overline{M}_{\beta k}^{II}\left(-\frac{\overline{p}_\beta^{II}}{p_\alpha^{II}}\right)^{-\delta}\csc\left(\pi\delta\right) - \delta_{ik}\cot\left(\pi\delta\right)\right]\right\}v_k = 0 \quad\Rightarrow\quad \mathbf{D}(\delta)\cdot v_k = 0 \tag{15}$$

The eigenvalues δ are obtained from the characteristic eigenequation:

$$\det\left[\mathbf{D}\left(\delta\right)\right] = 0. \tag{16}$$

The potentials for the interaction of an edge dislocation with the interface of two anisotropic materials can be obtained by invoking the standard analytical continuation arguments along the interface, as described by Suo in [86] and [87]. This work describes how the presence of other singularities, as for example the bimaterial interfaces, influences the solution for the edge dislocation which is placed in the infinite homogenous plane.

- Babuska's method:

The eigenpairs δ, **q** (as defined in the Transfer matrix method paragraph) can also be evaluated using the method developed by Papadakis and Babuska in [71]. Their method can be used with multi-material wedges, with anisotropic materials and general boundary conditions under the assumption of plane strain. Along the interfaces at $\theta = \omega_i$, the following continuity conditions are assumed $\left[\mathbf{U}\right]_i = 0$, $\left[\mathbf{t}\right]_i = 0$ where **U** is the displacement vector, **t** is the traction vector and the brackets denote a jump along $\theta = \omega_i$. The problem of finding the characteristic exponent δ can be viewed as the following eigenvalue problem: Find the characteristic exponent δ such that there exists $\mathbf{F} \neq 0$ such that

$$\frac{\partial\mathbf{F}\left(\theta\right)}{\partial\theta} = \mathcal{H}\left(\delta;\theta\right)\mathbf{F}\left(\theta\right) \text{ in } \omega_i \leq \theta \leq \omega_{i+1}, \tag{17}$$

$$\mathbf{O}_1\left(\delta\right)\left[\mathbf{F}\left(\omega_i\right)\right] = 0 \text{ for } \theta=\omega_i, \quad \mathbf{O}_2\left(\delta\right)\left[\mathbf{F}\left(\omega_{i+1}\right)\right] = 0 \text{ for } \theta=\omega_{i+1},$$

$\mathcal{H}$ is a 4×4 matrix whose elements depend in a complicated manner upon elastic constants and the angle θ, $\mathbf{O}_1$, $\mathbf{O}_2$ are 2×4 matrices and $\mathbf{F}(\theta)$ is 4×1 vector $\mathbf{F}(\theta)=\left[u_r,u_\theta,u_r',u_\theta'\right]^T$, where u_r and u_θ stand for radial and tangential displacement component respectively. The general idea in solving the above problem is as follows: First construct two initial value problems using the matrix $\mathcal{H}(\delta,\ \theta)$ and start with two independent initial vectors that satisfy the left boundary conditions

$$\mathbf{F}'(\theta)=\mathcal{H}(\delta;\theta)\mathbf{F}(\theta),\ \mathbf{F}(0)=\zeta_0 \quad\text{and}\quad \mathbf{F}'(\theta)=\mathcal{H}(\delta;\theta)\mathbf{F}(\theta),\mathbf{F}(0)=\psi_0, \qquad (18)$$

where ζ_0, ψ_0 are two linearly independent vectors which satisfy the boundary conditions $\mathbf{O}_1(\delta)\zeta_0=0$, $\mathbf{O}_2(\delta)\psi_0=0$; ζ_0 ψ_0 can be determined a priori. Then the fact that a linear combination of the solution of the two initial value problems $k_1\zeta(\theta)+k_2\psi(\theta)$ will be a solution of Eq. 7 only if it satisfies the right-hand side boundary conditions, leads to the formation of the determinant of a matrix which depends on δ. Specifically, in each material, two initial value problems are solved and the interface conditions are used to calculate two independent vectors which will be used as the initial vectors for the initial value problem in the next material. Finally, $k_1\zeta(\theta)+k_2\psi(\theta)$ solves Eq. (17) if k_1, k_2 are chosen to satisfy

$$\mathbf{O}_2(\delta)\left(k_1\zeta(\omega_N)+k_2\psi(\omega_N)\right)=0 \quad\text{or equivalently}\quad \mathbf{D}(\delta)\begin{bmatrix}k_1\\k_2\end{bmatrix}=0. \qquad (19)$$

For non zero k_1 a k_2 satisfying (19) the determinant det[$\mathbf{D}(\delta)$] must vanish. A special iterative procedure named Shoot was developed to solve the problem in equations (17) - (19). This method has been also used in work [46] for calculation of eigenvalues of the multimaterial wedge.
A special iterative procedure named Shoot was developed to solve the problem (17)-(19) in the MATLAB 7.1 and presented in [46] and [74].
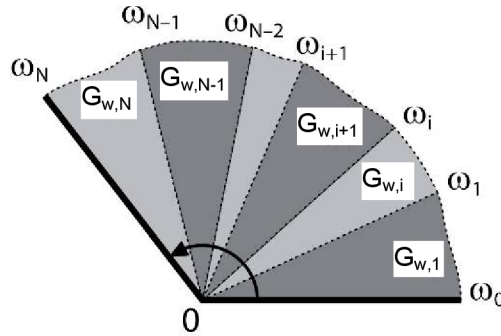
Fig. 4 Scheme of multimaterial wedge.

b) Implicit methods

These methods do not lead to the closed form of the equation for the eigenvalues, they are slower, however they can be used also for the anisotropic materials and multi-material wedges as well. For example a method based on the variational formulation of the solved problem is available [49]. The main idea is to replace the classical formulation by the variational one by the construction of functional as sesquilinear form [71]. The classical approximation for the finding of functional minimum using FEM leads to the homogenous system of algebraic equations for eigenvalues and eigenvectors. In other words, the problem of infinite dimension is converted into discrete one. These methods will not be a subject of the thesis so the more detailed information will not be given here.

4.1.2 Description of the singular stress field

Crack in anisotropic homogenous body

The problem of a crack in general anisotropic material under LEFM conditions is presented in work [81]. Three methods are presented for the calculation of the stress intensity factors for various anisotropic materials. All of the methods employ the displacement field obtained by means of the finite element method. The first one is known as displacement extrapolation and requires the values of the crack face displacements. The other two are conservative integrals based upon the J-integral. One employs symmetric and asymmetric fields to separate the mode I and II stress intensity factors. The second is the M-integral which also allows the calculation of K_I and K_II separately. All of these methods were originally presented for isotropic materials. Displacement extrapolation and the M-integral are extended for orthotropic and monoclinic materials, whereas the J_I- and J_II-integrals are only extended for orthotropic material in which the crack and material directions coincide. Results are obtained by these methods for several problems appearing in the literature. Good to excellent agreement is found in comparison to published values. New results are obtained for several problems. In Part II, the M-integral is extended for more general anisotropies. In these cases, three-dimensional problems must be solved, requiring a three-dimensional M-integral. Similar problem were studied also in work [38].

Crack terminating at the interface of two different anisotropic materials

Number of works has been devoted to the problem of singularity analysis of cracks terminating at the interface in anisotropic media – e.g. [56], [97]. Ting in [97] studies the order of stress singularities at the tip of a crack which is normal to and ends at an interface between two anisotropic elastic layers in a composite material. Work [56] extends this study on problem of inclined crack at the bi-material interface. Equations for determining the stress singularity exponent are derived. The works are based on the complex potential theory which is analyzed in more details in [95].

Multimaterial wedge in anisotropic media

In the paper [10] the singular stress states induced at the tip of linear elastic multimaterial corners are characterized in terms of the order of stress singularities and angular variation of stresses and displacements. Linear elastic materials of an arbitrary nature are considered, namely anisotropic, orthotropic, transversely isotropic, isotropic, etc. Thus, in terms of Stroh formalism of anisotropic elasticity, the scope of that work includes mathematically non-degenerate and degenerate materials. Multimaterial corners composed of materials of different nature (Fig. 1) are typically present at any metal-composite, or composite-composite adhesive joint. Several works are available in the literature dealing with a singularity analysis of multimaterial corners but involving (in the vast majority) only materials of the same nature (e.g., either isotropic or orthotropic). Although many different corner configurations have been studied in literature, with almost any kind of boundary conditions, there is an obvious lack of a general procedure for the singularity characterization of multimaterial corners without any limitation in the nature of the materials. With the procedure developed in [10], and implemented in a computer code, multimaterial corners, with no limitation in the nature of the materials and any homogeneous orthogonal boundary conditions, could be analyzed. This work is based on an original idea of Ting [95] in which an efficient procedure for a singularity analysis of anisotropic non-degenerate multimaterial corners is introduced by means of the use of a transfer matrices (as mentioned in chapter 4.1.1) – see also [44].

4.1.3 Overview of references focusing on the GSIFs and T-stress calculation

The next stage of the stress field analysis consist in the GSIF calculation (parameter H in (2)). There are several approaches for the calculation of the singular term amplitude in the Williams asymptotic expansion. One of the simplest is based on the comparison of numerical calculations of the stress (or displacement) field in front of the crack tip (e.g. by FEM) with the appropriate analytical expressions for stresses or displacements. GSIF is then extracted for $r \to 0$ – see e.g. works [68], [99]. This approach is called a "direct method" and it can be used for cases where only one singularity is present. The accuracy of this method is strongly dependent on the element size at the crack tip. The higher accuracy is desired, the smaller elements have to be placed in the vicinity of the crack tip. This condition can therefore lead to high computation times and to dis-economy of this approach. Note, that stress intensity factor in case of general stress concentrators cannot be calculated using any function integrated in commercial FE software (these functions are designed only for cracks in homogenous media - [3]). A specific FE post-processing approach is also proposed in work [6].

Another, much more effective method, which can be used, for the GSIF calculation (eventually also the T-stress calculation) is based on the method of two state (interactive) integrals in combination with FEM – e.g. [1], [17], [32], [39]. This method enables to determine the local stress field parameters in the vicinity of the crack tip using the deformation and stress field in the remote points, where the numerical results obtained e.g. using FE analysis are more accurate. The two-state integrals, which are path independent, are based on the J-integral [22], [32] or M-integral [23]. The physical meaning of the M-integral is interpreted as an energy release rate with respect to the unit expansion of 2D-cavity.

The application of the two-state integrals requires knowledge of the so-called auxiliary solution in the form of eigenfunctions of the appropriate singular problem [39]. The value of the two-state integral is possible to express in the closed form from the local stress-strain field and from an auxiliary solution.

The auxiliary solution has been found for the semi-infinite or finite crack, generally terminating at the interface of two anisotropic materials. In the connection with a description of V-notches or other general stress concentrators it is necessary to point out that J-integral is not path independent, so it cannot be applied for the calculation of GSIF in these cases. On contrary the two-state M-integral is path independent for the case of V-notch configurations [23].

GSIF can also be determined using the so-called Ψ-integral [17]. This method which turned out to be very efficient is an implication of the Betti's reciprocity theorem. Major advantage of this integral consists in its path independency also for cases of multimaterial wedges in anisotropic media [84] – that is result of its definition. The reciprocal theorem of elastostatics states that in the absence of body forces and residual stresses the reciprocal theorem states that the following integral is path independent

$$\Psi(\mathbf{U}, \mathbf{V}) = \int_{\Gamma} \left[\sigma_{ij}(\mathbf{U}) n_i V_j - \sigma_{ij}(\mathbf{V}) n_i U_j \right] \mathrm{d}s, \qquad (20)$$

where Γ is any contour surrounding the crack tip and $\mathbf{U}$, $\mathbf{V}$ are two admissible displacement fields. The asymptotic expansion of the displacements $\mathbf{U}(x)$ is possible to write in the following form

$$\mathbf{U}(x) = \mathbf{U}(0) + H_1 r^{\delta_1} \mathbf{u}_1(\theta) + H_2 r^{\delta_2} \mathbf{u}_2(\theta) + T r^{\delta_3} \mathbf{u}_3(\theta) + \ldots = \sum_{i=0}^{\infty} k_i r^{\delta_i} \mathbf{u}_i(\theta), \quad \delta_3 = 1, \qquad (21)$$

where H_1 ,H_2 are the generalized stress intensity factors $\mathbf{u}_i(\theta)$, $i = 1,2$ are the angular distribution of the displacements corresponding to the singular terms in the stress asymptotic expansion and $\mathbf{u}_3(\theta)$ is the angular distribution of displacements for the T-stress. In the following we will consider $\mathbf{U}(0) = 0$. T-stress is a non-singular stress component $\sigma_{22}(0,x_2)$ (observe, that the crack lies along the x_2 axis) acting at the crack tip, $T = \sigma_{22}(0, x_2)\big|_{x_2 \to 0^-}$. Due to the elastic mismatch, there exists also the non-singular stress component σ_{11} ahead of the crack tip, i.e. in the material M1, contrary to homogeneous materials, where T-stress is the only non-singular in-plane stress component. If the following displacement fields are considered $\mathbf{U} = \mathcal{U}_i(x) = r^{\delta_i} \mathbf{u}_i(\theta)$, $\mathbf{V} = \mathcal{U}_j(x) = r^{\delta_j} \mathbf{u}_j(\theta)$, (where δ_i, δ_j are obtained by solving the eigenvalue problem, see the Section 4.1.1, it can be proved [49], [101], that the contour integral Ψ is equal to zero for -$\delta_i \neq \delta_j$ and non-zero if -$\delta_i = \delta_j$. Since the basis function corresponding to coefficients $k_1 = H_1$, $k_2 = H_2$, $k_3 = T$ in the asymptotic expansion for $\mathbf{U}$ are $r^{\delta_1} \mathbf{u}_1(\theta), r^{\delta_2} \mathbf{u}_2(\theta), r^{\delta_3} \mathbf{u}_3(\theta)$, it holds

$$\Psi\left(\mathbf{U}, r^{-\delta_1} \mathbf{u}_{-1}\right) = \sum_{i=1}^{\infty} k_i \Psi\left(r^{\delta_i} \mathbf{u}_i, r^{-\delta_1} \mathbf{u}_{-1}\right) = k_1 \Psi\left(r^{\delta_1} \mathbf{u}_1, r^{-\delta_1} \mathbf{u}_{-1}\right)$$

$$\Psi\left(\mathbf{U}, r^{-\delta_2} \mathbf{u}_{-2}\right) = \sum_{i=1}^{\infty} k_i \Psi\left(r^{\delta_i} \mathbf{u}_i, r^{-\delta_2} \mathbf{u}_{-2}\right) = k_2 \Psi\left(r^{\delta_2} \mathbf{u}_2, r^{-\delta_2} \mathbf{u}_{-2}\right), \qquad (22)$$

$$\Psi\left(\mathbf{U}, r^{-\delta_3} \mathbf{u}_{-3}\right) = \sum_{i=1}^{\infty} k_i \Psi\left(r^{\delta_i} \mathbf{u}_i, r^{-\delta_3} \mathbf{u}_{-3}\right) = k_3 \Psi\left(r^{\delta_3} \mathbf{u}_3, r^{-\delta_3} \mathbf{u}_{-3}\right)$$

where $\Psi\left(r^{\delta_1} \mathbf{u}_1, r^{-\delta_1} \mathbf{u}_{-1}\right)$ is computed analytically along the path Γ_1 surrounding the crack tip with diameter approaching zero, while $\Psi\left(\mathbf{U}, r^{-\delta_1} \mathbf{u}_{-1}\right)$ is computed along Γ_2 which is any remote integration path with finite diameter (see Fig. 5). Thus, the GSIFs $H_1 = k_1$, $H_2 = k_2$ can be computed as follows:

$$H_1 = \frac{\Psi\left(\mathbf{U}, r^{-\delta_1} \mathbf{u}_{-1}\right)}{\Psi\left(r^{\delta_1} \mathbf{u}_1, r^{-\delta_1} \mathbf{u}_{-1}\right)}, \quad H_2 = \frac{\Psi\left(\mathbf{U}, r^{-\delta_2} \mathbf{u}_{-2}\right)}{\Psi\left(r^{\delta_2} \mathbf{u}_2, r^{-\delta_2} \mathbf{u}_{-2}\right)}. \qquad (23)$$

Observe, that the dual displacement fields (so called extraction solutions) $r^{-\delta_i} \mathbf{u}_{-i}(\theta)$ are singular at the crack tip, hence they have unbounded energy near the crack tip and thus correspond to some concentrated sources at the crack tip. They are mathematical tools which allow extracting asymptotic coefficient terms from the complete exact solution $\mathbf{U}$. Since the exact solution $\mathbf{U}$ is not known, a finite element solution $\mathbf{U}^h$ can be used as an approximation for $\mathbf{U}$ so to obtain an approximation for GSIFs see e.g. [74], [75]. Thus, one gets e.g. for H_1

$$H_1 \doteq \frac{\Psi\left(\mathbf{U}^h, r^{-\delta_1} \mathbf{u}_{-1}\right)}{\Psi\left(r^{\delta_1} \mathbf{u}_1, r^{-\delta_1} \mathbf{u}_{-1}\right)} = \frac{\int_{\Gamma_2}\left[\sigma\left(\mathbf{U}^h\right) \cdot \mathbf{n} \cdot r^{-\delta_1} \mathbf{u}_{-1} - \sigma\left(r^{-\delta_1} \mathbf{u}_{-1}\right) \cdot \mathbf{n} \cdot \mathbf{U}^h\right] \mathrm{d}s}{\int_{\Gamma_\varepsilon}\left[\sigma\left(r^{\delta_1} \mathbf{u}_1\right) \cdot \mathbf{n} \cdot r^{-\delta_1} \mathbf{u}_{-1} - \sigma\left(r^{-\delta_1} \mathbf{u}_{-1}\right) \cdot \mathbf{n} \cdot r^{\delta_1} \mathbf{u}_1\right] \mathrm{d}s} \qquad (24)$$

and similarly for H_2.

Due to the path independence, the Ψ-integral standing in the denominator of Eq. (23) is evaluated along an infinitesimal path that shrinks to the crack tip.
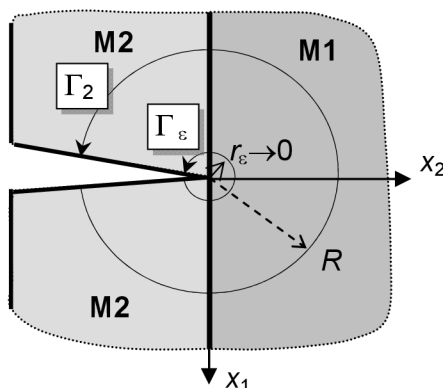
Fig. 5 Integration paths surrounding the singular point.

4.1.4 Description of the non-singular stress field

The non-singular term in the Williams asymptotic stress expansion – the T-stress - is often neglected. However, when aiming to describe the stress field in the vicinity of the crack tip more exactly, it should be also paid the same attention to the T-stress as to GSIF. The singular terms in the Williams asymptotic expansion corresponds to the characteristic eigenvalues $\delta \in (0,1)$. The T-stress term is related to the characteristic eigenvalue $\delta = 1$, so it is no more singular.

It is well known that the T-stress co-determinates plastic zone size at the crack front (for metals), microcracking region (or phase transformation region) – for brittle materials and structural ceramics. T-stress also has a significant influence on the crack initiation angles in brittle fracture [64]. In general, numerical determination of T-stresses requires careful handling, because of their location in the vicinity of singular points. A closed form solution of the T-stress in plane elasticity crack problems in homogenous materials is possible to find for example in [36]. However, for the case of general stress concentrators, this solution can be very complicated or even impossible. There exist lot of other methods for the T-stress determination in case of stress concentrators in homogenous media [79], but most of them fail if they are applied on general stress concentrators. In these cases there are several other possibilities and approaches how the T-stress can be obtained:

Calculation of the T-stress using FEM

Estimation of the T-stress using the FE analysis is possible with a quite good accuracy for cracks in the homogenous materials. However in case of the general stress concentrators this analysis becomes controversial due to the presence of media discontinuity at the interface. This approach can be used only as a first approximation, but cannot be taken as an accurate solution. The T-stress is estimated by this method as a stress in direction of the crack face at distance $r \rightarrow 0$ from the crack tip. The estimation is strongly dependent on the mesh refinement in the vicinity of the crack tip.

Calculation of the T-stress using contour integrals

Calculation of the T-stress in the anisotropic linear elastic homogenous solid is presented in papers [106] and [88]. The T-stress is calculated using the path independent line integral and Betti's reciprocal work theorem, together with selected auxiliary fields. To determine the T-stress, special auxiliary fields for a crack under moment acting about axis x_3 at the crack tip are used. Through the use of Stroh formalism in the anisotropic elasticity, analytical expression for the T-stress is derived in a compact form that has surprisingly

simple structure in terms of one of the Barnett-Lothe tensors, L – see e.g.. [105]. The solution forms for degenerated materials, monoclinic, orthotropic, and isotropic materials are also presented. However, all the presented theory is applicable only to the case of crack in the homogenous body. In case of the general stress concentrators the application of J-integral is not possible, because it become path dependent. Therefore is necessary to use other path-independent integral such as for example the Ψ-integral as it was proposed in the previous chapter for the calculation of GSIF. Of course, in that case, first the suitable auxiliary field has to be constructed. The work [41] discusses a calculation of the T-stress in functionally graded materials using the M-integral, where arbitrarily oriented cracks are considered. Authors [82] developed techniques for calculation of the T-stress based on the interactive integrals in combination with the Boundary Element method to the solution of the crack problem.

Similar arguments which lead to Eq. (23), apply also for T-stress calculation, i.e. $T = k_3$ can be computed as follows

$$T = \frac{\Psi\left(\mathbf{U}, r^{-1}\mathbf{u}_{-3}\right)}{\Psi\left(r\mathbf{u}_3, r^{-1}\mathbf{u}_{-3}\right)}, \tag{25}$$

see also Eq. (22). Similarly like with GSIF a finite element solution $\mathbf{U}^h$ can be used as an approximation for $\mathbf{U}$ so to obtain an approximation for T

$$T \doteq \frac{\Psi\left(\mathbf{U}^h, r^{-1}\mathbf{u}_{-3}\right)}{\Psi\left(r^{-1}\mathbf{u}_3, r^{-1}\mathbf{u}_{-3}\right)} = \frac{\int_{\Gamma_2}\left[\boldsymbol{\sigma}\left(\mathbf{U}^h\right)\cdot\mathbf{n}\cdot r^{-1}\mathbf{u}_{-3} - \boldsymbol{\sigma}\left(r^{-1}\mathbf{u}_{-3}\right)\cdot\mathbf{n}\cdot\mathbf{U}^h\right]\mathrm{d}s}{\int_{\Gamma_\varepsilon}\left[\boldsymbol{\sigma}\left(r^{-1}\mathbf{u}_3\right)\cdot\mathbf{n}\cdot r^{-1}\mathbf{u}_{-3} - \boldsymbol{\sigma}\left(r^{-1}\mathbf{u}_{-3}\right)\cdot\mathbf{n}\cdot r^{-1}\mathbf{u}_3\right]\mathrm{d}s}. \tag{26}$$

In equations (25), (26) $\mathbf{u}_{-3}(\theta)$ denotes the extraction solution for the T-stress. Physically, this solution corresponds to the concentrated moment about x_3 acting at the crack tip.

Calculation of the T-stress using CDD technique

As suggested by Broberg [11], the T-stress can also be determined using dislocation arrays. Determination of the T-stresses via dislocation arrays leads to a Fredholm equation that can be solved very accurately and provides more accurate values of the T-stress comparing to common finite element methods. However, the application of this method requires determining the solution for a dislocation in a complicated domain. Such an approach is not economical, but there are strategies, which may be employed to overcome this problem. These strategies start with a dislocation in a crack free infinite domain aiming to determine stresses along the curve $\partial\Omega$ which stands for the boundary of finite body. Introducing tractions along $\partial\Omega$ such that they negate stresses found previously and solving for stresses along the dislocation plane e.g. by FEM, one can finally derive the regular part of the dislocation solution for a specified finite domain [42].

Modelling of a finite crack perpendicular to the bi-material interface, and terminating in front of the interface at distance l, is presented in [35] and [104]. The continuously distributed dislocation technique is used here. The materials are considered as isotropic. The complete solutions of the problem, including the T-stress and the stress intensity factors are obtained. The latter mentioned paper also discusses a comparison of the stress intensity factors between the finite and infinite problem.

4.2   Crack bridging problem

Fibre reinforced ceramic materials have promising potential e.g. for high-temperature applications. Under the tensile loading of the composite in the fibre direction, the brittle matrix can undergo extensive cracking normal to the fibres, but the associated matrix cracking stress may be substantially greater than the critical fracture stress of the unreinforced ceramic. Furthermore, with the intact fibres, the composite material can continue to sustain additional load up to the fibre bundle fracture stress. In papers [13] and [14], the critical conditions for the onset of widespread matrix cracking are studied analytically on the basis of fracture mechanics theory. Two distinct situations concerning the fibre-matrix interface are considered: (i) unbonded fibres initially held in the matrix by thermal or other strain mismatches, but susceptible to frictional slip, and (ii) fibres that initially are weakly bonded to the matrix, but may be debonded by the stresses near the tip of an advancing matrix crack. The results generalize those of the Aveston-Cooper-Kelly theory [4] for case (i). Theoretical results are compared with experimental data for a SiC fibre, Lithium-Alumina-Silicate glass matrix composite.

4.2.1   Generalized bridging stress intensity factor

To quantitatively express the influence of the bridging fibres on the resulting stress field the value of the generalized bridging stress intensity factor H_{br} caused by the bridging stress have to be calculated. As a result, the local generalized stress intensity factor $H_{tip}=H_{appl}-H_{br}$ acting in the very crack tip is lower than the remote applied stress intensity H_{appl}. One of the possible ways how to calculate the influence of the bridging effect can be found e.g. in [43] or [66]. The contribution [43] deals with a theoretical and experimental analysis of the bridged crack in the chevron-notched three point bending specimen made of the glass matrix composite reinforced by long SiC fibres. The fracture toughness (K_{IC}) values are determined using the chevron notch technique and compared with the theoretical predictions based on micromechanical analysis exploiting weight functions. The weight functions are further used together with appropriate bridging models to theoretical prediction of R-curve. The generalized bridging stress intensity factor is then calculated using the following formula:

$$H_{br} = \int_{-h}^{0} W\left(x_2,h\right) \sigma_{br}\left(x_2\right) \mathrm{d}\, x_2 \; , \tag{27}$$

where $W(x_2,h)$ is the mentioned weight function which can be obtained numerically using the FE analysis as was proposed for example in [78]. The weight function depends on the component geometry, but it is independent of the applied loading. The stress intensity factor at the tip of a crack in a chevron-notched specimen is there calculated for the direct line loading of the crack surfaces by a constant traction. The traction is applied in different positions between the apex of the chevron notch and the crack tip so that the whole weight function is obtained. This technique can be modified for the solution of the plane crack problems by use of pair of concentrated forces instead of the line loading.

The bridging stress σ_{br} can be calculated using the recurrent formulas and suitable bridging models as is presented in paper [43]. In work [21] is possible to find a procedure which allows determining of the bridging stress from the measured R-curve. After the weight function and bridging stress is calculated, the generalized bridging stress intensity factor H_{br} can be determined and the local GSIF H_{tip} as well. The applied stress intensity factor H_{appl} can be calculated on the unbridged configuration e.g. using some of the two state integral methods as mentioned in chapter 4.1.3.

The bridging crack problems can also be solved efficiently using the continuously distributed dislocation technique. This technique leads to a Fredholm integral equation that can be solved very accurately using e.g. polynomial-base Galerkin method. For the bi-material half-space, see Fig. 3, the solution can be worked out due to recent findings of Choi and Earmme [37], who studied singularities in anisotropic trimaterials. An integral equation is obtained by choosing the dislocation distribution to meet the traction conditions along the line of the crack and within crack bridging zone:

$$\frac{\left(\operatorname{Im}\left(\mathbf{A}^{II}\mathbf{M}^{II}\right)\right)_{ik}^{-1}}{2\pi} \int_{-h}^{0} \frac{f_k\left(x_{2o}\right)\mathrm{d}\,x_{2o}}{x_2 - x_{2o}} + \int_{-h}^{0} N_{1ik}\left(x_2, x_{2o}\right)f_k\left(x_{2o}\right)\mathrm{d}\,x_{2o} = \sigma_{1i}^{appl}\left(x_2\right) + \delta_{1i}\sigma_{br}\left(v\left(x_2\right)\right). \quad (28)$$

Here, N_{1ik} are regular kernels in the closed interval $[-h,0]$ (along the crack), $\sigma_{1i}^{appl}\left(x_2\right)$ denotes the negated stresses in $x_1=0$ produced by the given boundary loads, acting on a specimen with boundary $\partial\Omega$, but without cracks and dislocations. σ_{br} is the bridging stress as a function of the upper crack face displacement. $f_k(x_{2o})$ is the unknown dislocation density which has to be non-singular at an open end. The integral equation may be solved using the Gauss-Jacobi quadrature. Once the dislocation density $f_k(x_{2o})$ is found, the displacement of the upper crack face $v(x_2)$ is also known and from $\sigma_{br}\left[v\left(x_2\right)\right]$, the bridging stress as a function of position follows. After the bridging stress and dislocation density is known, arbitrary stress component in front of the crack tip can be calculated. Afterwards the resulting local generalized stress intensity factor is obtained as the following limit:

$$H_{tip} = \lim_{r \to 0} r^{1-\delta}\sigma_{11}\left(r, \theta = \pi / 2\right). \quad (29)$$

4.2.2 Bridging models

To calculate a bridging stress or bridging crack face closure effect the bridging model has to be defined. The bridging models generally describe a relation between the crack face displacements and the bridging stress. In literature is possible to find several different models, describing different behaviours in dependency on the crack opening displacements - Budiansky et al. [12], [14] or Thouless et al. [94]. Some possible types of constraints between fibre and matrix are depicted in Fig. 6:
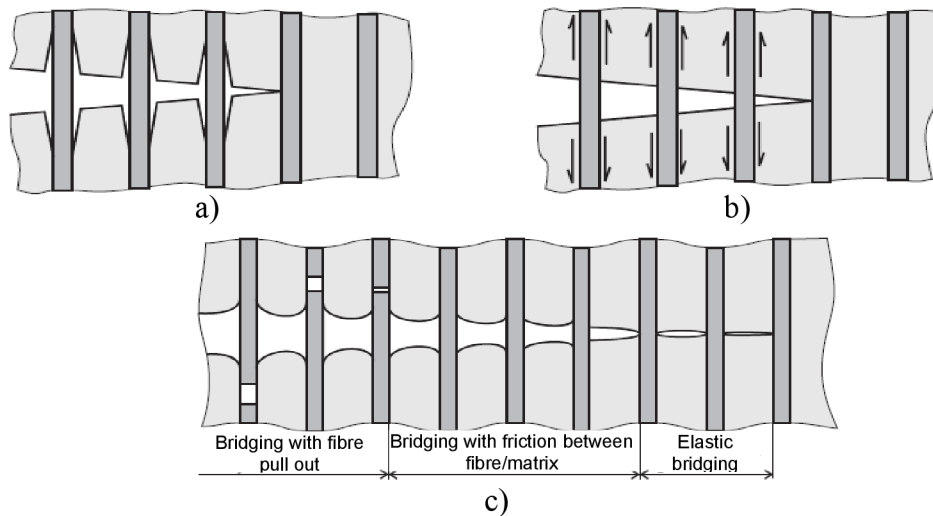

Fig. 6 Interface fibre/matrix: a) decohesion of fibre in matrix; b) frictional constraint between fibre and matrix; c) characteristic bridging areas and corresponding types of constraints between fibre and matrix.

4.3 Problems of fracture criteria

It is now well established that the increase of the toughness of ceramics laminates or ceramic-matrix composites can be achieved by introducing weak interfaces between layers or between the fibre and the matrix [60]. Deflection along the interface then results in a crack blunting and this effect increases the required energy for the next crack propagation. Understanding the mechanism of the crack deflection along the interface is thus essential to determine for example the suitable interlayer and the optimum interface toughness which are necessary to favour this phenomenon [47]. Various attempts have been made to attain this objective.

The discontinuity in the elastic properties at the interface strongly influences the behaviour of the energy release rate of the crack in the vicinity of the interface. In the case of a strong singularity (crack lies in a stiffer material and a characteristic eigenvalue $\delta < 1/2$), the energy release rates $G_p(a_p=0)$, $G_d(a_d=0)$ for a crack terminating at the interface are infinite and interface penetration or deflection is thus possible at any finite load level. In contrast, the presence of a weak singularity (crack lies in a softer material, $\delta > 1/2$) implies that the energy release rates $G_p(a_p=0)$, $G_d(a_d=0)$ for a crack terminating at the interface are zero and interface penetration or deflection is not predicted for any applied load. This is a drawback of the classical differential theory which can be used with success for cracks in homogenous media however not in the case of cracks propagating near the interface. The mentioned problem of zero or infinite energy release rates may be overcome with the help of the so-called *finite fracture mechanics* [61], where the crack increment of a finite length is used instead of the infinitesimal one. The evolution of the energy release rates in three different cases are depicted in the following figure:
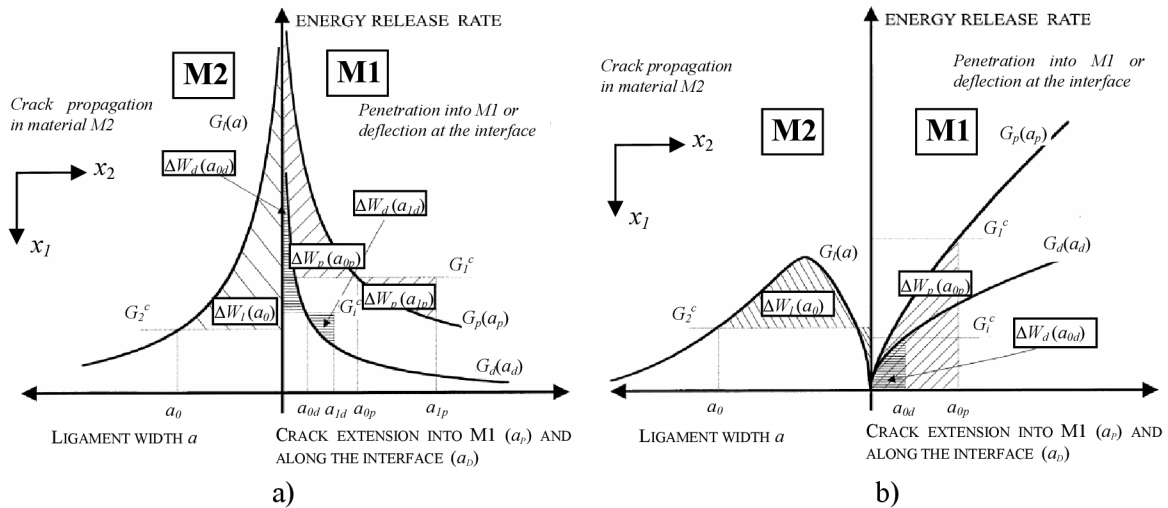
Fig. 7 Evolution of the energy release rates $G_l(a)$, $G_p(a_p)$, $G_d(a_d)$, depending on the crack increments (a, a_p, a_d) – taken over from [61]: a) case of a strong singularity ($\delta < 1/2$; $E_{1x} < E_{2x}$); b) case of a weak singularity ($\delta > 1/2$; $E_{1x} > E_{2x}$).

The first case (left side of both graphs) describes energy release rate $G_l(a)$ of the crack which is approaching interface from the left with some ligament width a (Fig. 8.a). On the right hand side the curves express energy release rates $G_p(a_p)$ and $G_d(a_d)$ when the crack extends into the material M1- or is deflected along the interface. The problem of infinite or zero release rates is obvious.

With the help of the asymptotic analysis, He and Hutchinson [28] derived a deflection criterion which compares the ratio of the interfacial toughness G_c^i over the toughness of the penetrated material G_c^1. The results can be used to determine the range of interface toughness relative to bulk material toughness which ensures that cracks will be deflected into interface. The paper [27] moreover discusses an influence of residual stresses, caused by the thermal expansion misfit, on the energy release rates for interface cracking and crack penetration. The approach used by He and Hutchinson was extended by taking anisotropy into account in [62] and was confirmed by Tullock et al. [98]. Martin el al. [61] improved the criterion which does not require any assumption concerning the crack extension ratio. The capability of an interface to deflect a crack is usually analyzed in terms of the competition between deflection and penetration for a stationary crack terminating at the interface at a normal angle – e.g. [30], [51] and [61]. Problems of cracks terminating at arbitrary angle to the interface are solved in work [28]. The solution procedure used in that work is similar to, or extension of, the integral equation methods used in the earlier papers – e.g. [15] where only crack perpendicular to the bi-material interface have been considered. In all cases, the materials on either side of the interface are taken to be elastic and isotropic.

Other approach, where the tendency of crack to deflect or penetrate at an interface between two dissimilar elastic materials in finite-sized sample is investigated by means of the boundary element method (BEM), can be found in papers [57] and [98]. The ratio of the energy release rate of a deflecting crack to the maximum energy release rate of a penetrating crack is computed as a function of Dundurs' elastic parameters for several double-edged notch specimen geometries and loading conditions. For moderate differences in relative stiffnesses of the two materials and when the crack is advancing toward a stiffer material, there have been found no difference between the singly and doubly deflected crack and the numerical calculations are in excellent agreement with recent analytical predictions as e.g. in [27]. However when the crack is advancing into a material of much lower modulus, the numerical calculations for a doubly deflected crack are smaller than the analytical predictions.

4.3.1 Matched asymptotic analysis

Matched asymptotic analysis is powerful tool for deriving the change in potential energy induced by a finite crack increment growth [48], [51] or [101]. It is performed within the framework of 2D linear elasticity. As shown in Fig. 8, different crack paths are considered (single or double deflection along the interface and the penetration into the material M1). In order to keep a validity of the asymptotic analysis, the condition of a_d, $a_p \rightarrow 0$ must hold. It means that a ratio of $a/L_c \ll 1$, where L_c is a characteristic size of the main crack. It is worthy of note that the asymptotic assumptions of the small crack extensions imply that the constant loading conditions have no influence on the energy balance.

The following figure shows four different crack paths in the vicinity of the interface which have been considered in the previously mentioned works. The crack either approaches the interface by an increment a (Fig. 8 a) or penetrate into the material M1 with increment a_p (Fig. 8 b) or is deflected along the interface by increment a_d (singly or doubly – Fig. 8 c, d) - [62], [61].
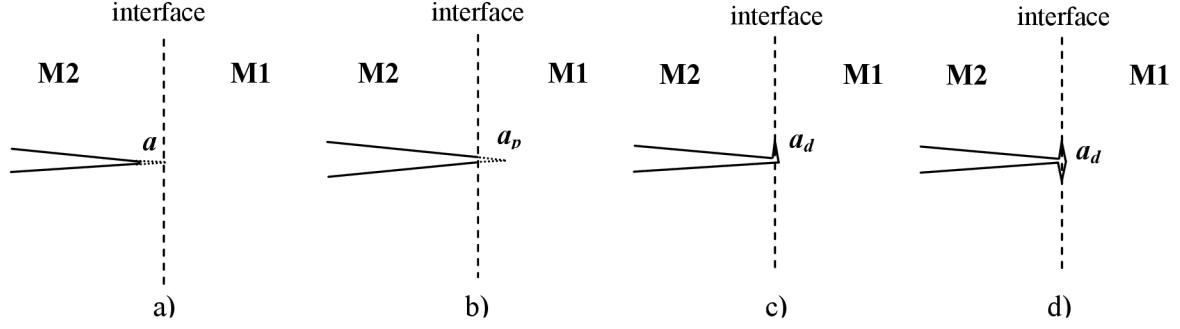
Fig. 8 Different crack paths: a) propagation towards the interface (ligament a); b) crack penetrating into the material M1; c) singly deflected crack; d) doubly deflected crack.

The competition between the deflection of the main crack along the interface and the penetration into the substrate can be assessed so that the crack will follow the path which maximizes the additional energy ΔW released by the fracture. If crack deflection occurs preferentially to penetration at the interface, the following condition must be satisfied:

$$\Delta W_d = \delta W_d - G_c^i a_d > \Delta W_p = \delta W_p - G_c^1 a_p, \tag{30}$$

where G_c^i is the interface toughness, G_c^1 is the fracture toughness of the material M1 [22] and δW is a change of the potential energy between the original and new crack position. The Ψ integral also plays a useful role in the calculation of the change of the potential energy δW between the unperturbed state $\mathbf{U}^0$ (without the crack extension) and perturbed state $\mathbf{U}^\varepsilon$ (with the small finite crack extension). The change of the potential energy δW between the unperturbed state $\mathbf{U}^0$ (without the crack extension) and perturbed state $\mathbf{U}^\varepsilon$ (with the small finite crack extension) is given by the relation:

$$\delta W = W^0 - W^\varepsilon = \frac{1}{2} \int_\Gamma \left(\sigma_{ij}\left(\mathbf{U}^0\right) n_i U_j^\varepsilon - \sigma_{ij}\left(\mathbf{U}^\varepsilon\right) n_i U_j^0 \right) ds = \frac{1}{2} \Psi\left(\mathbf{U}^0, \mathbf{U}^\varepsilon\right). \tag{31}$$

Remark 1: Derivation of the relation (31) can be done as follows. The change of the potential energy δW between the unperturbed state $\mathbf{U}^0$ (without the crack extension) and the perturbed state $\mathbf{U}^\varepsilon$ (with the small finite crack extension) is given by the relation:

$$\delta W = W^0 - W^\varepsilon = \left(\int_\Omega \frac{1}{2} \sigma_{ij}\left(\mathbf{U}^0\right) \varepsilon_{ij}\left(\mathbf{U}^0\right) dS - \int_{\partial\Omega_\sigma} p_j U_j^0 \, ds \right) - \left(\int_{\Omega^\varepsilon} \frac{1}{2} \sigma_{ij}\left(\mathbf{U}^\varepsilon\right) \varepsilon_{ij}\left(\mathbf{U}^\varepsilon\right) dS - \frac{1}{2} \int_{\partial\Omega_\sigma^\varepsilon} p_j U_j^\varepsilon \, ds \right) =$$

$$\frac{1}{2} \int_{\partial\Omega} \sigma_{ij}\left(\mathbf{U}^0\right) U_j^0 n_i \, ds - \int_{\partial\Omega_\sigma} p_j U_j^0 \, ds - \frac{1}{2} \int_{\partial\Omega^\varepsilon} \sigma_{ij}\left(\mathbf{U}^\varepsilon\right) U_j^\varepsilon n_i \, ds + \int_{\partial\Omega_\sigma^\varepsilon} p_j U_j^\varepsilon \, ds = \tag{32}$$

$$-\frac{1}{2} \int_{\partial\Omega_\sigma} p_j U_j^0 \, ds + \frac{1}{2} \int_{\partial\Omega_u} \sigma_{ij}\left(\mathbf{U}^0\right) g_j n_i \, ds + \frac{1}{2} \int_{\partial\Omega_\sigma^\varepsilon} p_j U_j^\varepsilon \, ds - \frac{1}{2} \int_{\partial\Omega_u^\varepsilon} \sigma_{ij}\left(\mathbf{U}^\varepsilon\right) g_j n_i \, ds,$$

where the boundary conditions

$$\sigma_{ij} n_i = p_j \quad \text{on } \partial\Omega_\sigma^\varepsilon = \partial\Omega_\sigma \quad \text{and } U_j = g_j \quad \text{on } \partial\Omega_u^\varepsilon = \partial\Omega_u \tag{33}$$

were applied.

Now consider the domain D obtained from the original domain Ω by excluding the singularity by using a contour Γ, see Fig. 9. The boundary ∂D consists of $\partial\Omega$ and the contour Γ. Consider following integrals

$$\int_D \sigma_{ij}\left(\mathbf{U}^\varepsilon\right)\varepsilon_{ij}\left(\mathbf{U}^0\right)\mathrm{d}S = \int_{\partial\Omega} \sigma_{ij}\left(\mathbf{U}^\varepsilon\right)n_j U_i^0\,\mathrm{d}s + \int_\Gamma \sigma_{ij}\left(\mathbf{U}^\varepsilon\right)n_j U_i^0\,\mathrm{d}s =$$
$$= \int_{\partial\Omega_\sigma} p_j U_j^0\,\mathrm{d}s + \int_{\partial\Omega_u} \sigma_{ij}\left(\mathbf{U}^\varepsilon\right)g_j n_i\,\mathrm{d}s + \int_\Gamma \sigma_{ij}\left(\mathbf{U}^\varepsilon\right)n_j U_i^0\,\mathrm{d}s \tag{34}$$

$$\int_D \sigma_{ij}\left(\mathbf{U}^0\right)\varepsilon_{ij}\left(\mathbf{U}^\varepsilon\right)\mathrm{d}S = \int_{\partial\Omega} \sigma_{ij}\left(\mathbf{U}^0\right)n_j U_i^\varepsilon\,\mathrm{d}s + \int_\Gamma \sigma_{ij}\left(\mathbf{U}^0\right)n_j U_i^\varepsilon\,\mathrm{d}s =$$
$$\int_{\partial\Omega_\sigma} p_j U_j^\varepsilon\,\mathrm{d}s + \int_{\partial\Omega_u} \sigma_{ij}\left(\mathbf{U}^0\right)g_j n_i\,\mathrm{d}s + \int_\Gamma \sigma_{ij}\left(\mathbf{U}^0\right)n_j U_i^\varepsilon\,\mathrm{d}s, \tag{35}$$

where again the boundary conditions (33) were applied. Applying the reciprocal theorem to the left sides of Eqs. (34), (35) one gets:

$$\int_\Gamma \sigma_{ij}\left(\mathbf{U}^\varepsilon\right)n_j U_i^0\,\mathrm{d}s - \int_\Gamma \sigma_{ij}\left(\mathbf{U}^0\right)n_j U_i^\varepsilon\,\mathrm{d}s =$$
$$= \int_{\partial\Omega_\sigma} p_j U_j^\varepsilon\,\mathrm{d}s + \int_{\partial\Omega_u} \sigma_{ij}\left(\mathbf{U}^0\right)g_j n_i\,\mathrm{d}s - \int_{\partial\Omega_\sigma} p_j U_j^0\,\mathrm{d}s - \int_{\partial\Omega_u} \sigma_{ij}\left(\mathbf{U}^\varepsilon\right)g_j n_i\,\mathrm{d}s. \tag{36}$$

The right-hand side of Eq. (36) is equal to the right-hand side of (32). Thus the change of the potential energy δW can be put into the form

$$\delta W = \frac{1}{2}\int_\Gamma \left(\sigma_{ij}\left(\mathbf{U}^0\right)n_i U_j^\varepsilon - \sigma_{ij}\left(\mathbf{U}^\varepsilon\right)n_i U_j^0\right)ds = \frac{1}{2}\Psi\left(\mathbf{U}^0,\mathbf{U}^\varepsilon\right), \tag{37}$$

where the flow direction of the contour Γ (and consequently the direction of the normal on this contour) was reversed.
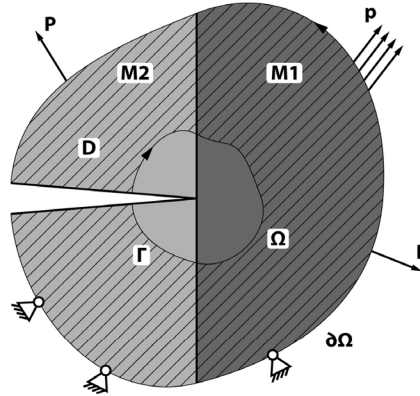
Fig. 9 Scheme of domain Ω and its boundary $\partial\Omega$, subdomain D and the contour Γ which excludes the crack tip.

A very efficient tool for the calculation of the change of the potential energy in the case of generalized stress concentrators such as crack cracks impinging a bi-material interface and/or multimaterial wedges is the matched asymptotic expansion method [49], [101], which does not require carrying out repeatedly a full field analysis. Let the domain Ω with crack impinging the interface is perturbed by a small deflected (double) crack extension of length a_d or small penetrating crack extension of length a_p. The small perturbation parameter ε is introduced by definition as $\varepsilon = a/L \ll 1$, $a = a_p, a_d$, where L is the characteristic length of Ω. Denote the perturbed domain as Ω^ε. The displacement $\mathbf{U}^\varepsilon$ of

the perturbed elasticity problem due to the crack extension can be expressed as the unperturbed solution $\mathbf{U}^0(x)$, ($x = (x_1, x_2)$), defined in Ω (Ω is the limit of Ω^ε as $\varepsilon \to 0$), plus a small correction

$$\mathbf{U}^\tau (x) = \mathbf{U}^0 (x) + k_1 (\varepsilon) \mathbf{U}^1 (x) + \dots \quad \text{with} \quad \lim_{\tau \to 0} k_1 (\varepsilon) = 0, \tag{38}$$

which may be rearranged into the form

$$\mathbf{U}^\varepsilon (x) = k_0 (\varepsilon) \mathcal{U}_0 (x) + k_1 (\varepsilon) \mathcal{U}_1 (x) + \dots = \sum_{i=0}^{\infty} k_i (\varepsilon) \mathcal{U}_i (x), \tag{39}$$

where $\lim_{\varepsilon \to 0} k_{i+1} (\varepsilon) / k_i (\varepsilon) = 0$, $\forall i = 1, 2, \dots$ and $\{\mathcal{U}_1, \mathcal{U}_2, \dots\}$ form a set of linearly independent basis functions, $\mathcal{U}_i (x) = r^{\delta_i} \mathbf{u}_i (\theta)$, where the eigenvalues δ_i are positive or negative, see also the Section 4.1.1. Observe that the basis functions $\{\mathcal{U}_i\}$ satisfy the elasticity problem on the same domain $\Omega \approx \Omega^\varepsilon$ but with zero body force and with homogeneous boundary conditions. Such an expansion is called 'outer' and is valid in the whole domain Ω (or Ω^ε) except near the former main crack tip where the geometry is perturbed. A second scale to the problem can be introduced, represented by the scaled-up coordinates $y = x/\varepsilon$, or $(y_1, y_2) = (x_1/\varepsilon, x_2/\varepsilon)$. In order to have a description of the near fields, the domain Ω^ε is stretched ($\times 1/\varepsilon$) and as $\varepsilon \to 0$ it leads to the unbounded 'inner' domain Ω^{in} spanned by the stretched variables y_1 and y_2. The inner domain becomes unbounded for $\varepsilon \to 0$. The solution can be expanded in this domain as:

$$\mathbf{V}^\varepsilon (y) = F_0 (\varepsilon) \mathcal{V}_0 (y) + F_1 (\varepsilon) \mathcal{V}_1 (y) + \dots = \sum_{i=0}^{\infty} F_i (\varepsilon) \mathcal{V}_i (y), \tag{40}$$

where $\lim_{\varepsilon \to 0} F_{i+1} (\varepsilon) / F_i (\varepsilon) = 0$, $\forall i = 1, 2, \dots$ and $\{\mathcal{V}_0, \mathcal{V}_1, \mathcal{V}_2, \dots\}$ form a set of linearly independent basis functions. This expansion is called 'inner'. Conditions at infinity are missing to define well-posed problem for the unknown functions $\mathcal{V}_i (y)$. They derive from the matching conditions based on the existence of an intermediate area where both expansions (39) and (40) hold. In other words, the behaviour of the outer terms in Eq. (39) or Eq (40) when approaching the singular point must match with the behaviour of the inner terms in Eq. (40) at infinity. This common area is near the crack tip in the outer domain and far from it in the inner domain. The expansion of the elastic solution in positive powers of the distance r to the crack tip is a generalization of the Williams series. The successive terms have a finite energy in the vicinity of the tip. The behaviour at infinity is described by similar series but with negative powers in order to have a bounded energy at infinity.

To get a physical insight, consider the domain Ω^ε perturbed due to a small crack extension a while freezing the far-field boundary conditions. Since a is very small, the asymptotic solution far from the crack tip will still be the same as in Eq. (21). To meet the traction-free condition on the crack extension a, however, the displacement field for the disturbed domain will be given as a superposition of the elastic state of Eq. (21) and another elastic state whose displacement field is given by the eigenfunction expansion of a Laurent series type obtained by taking $\mathcal{U}_i (x) = r^{\delta_i} \mathbf{u}_i (\theta)$, with $\delta_i < 0$. This assumes an essential similarity to the case of a crack under small-scale yielding: in the situation of small-scale yielding an eigenfunction expansion of negative powers occurs in addition to the inverse square singularity, which represents the leading term in the outer solution (see [29]). Note that the appearance of any eigenvalue $\delta_i < 0$ in the expansion for the perturbed domain would yield a finite displacement at the boundary and therefore would violate the boundary condition on the far-field, where the displacement field is frozen according to Eq. (21).

4.3.2 Measuring of the interfacial toughness

In order to decide whether the crack will deflect along the interface or cross the interface, the very important mechanical property – interfacial toughness has to be known - see (30). In accordance to the literature, there exist many methods to measure this characteristic for different types of material configurations with interfaces. It starts with measurement of the interfacial toughness for thin films on substrates [100] where the films of thickness 30-30000 nm are considered. Methods of superlayer test, indentation test (Fig. 10 c)), scratch test and sandwich specimen test are used for its determination. Similar problem is also investigated in [65] and [69]. In the work [110], the method of three point bending test is used for the measurement of the interfacial toughness of Si_3N_4/BN composite (Fig. 10 a)). This method can be modified to four point bending test (Fig. 10 b)) in order to measure the mixed mode interfacial fracture toughness [103]. A comparison of other types of test specimen for measuring of the interfacial toughness is given in [70]. Proposed specimens are well-suited for investigating interfacial toughness over a wide range of mode mixity on which is this characteristic strongly dependent.
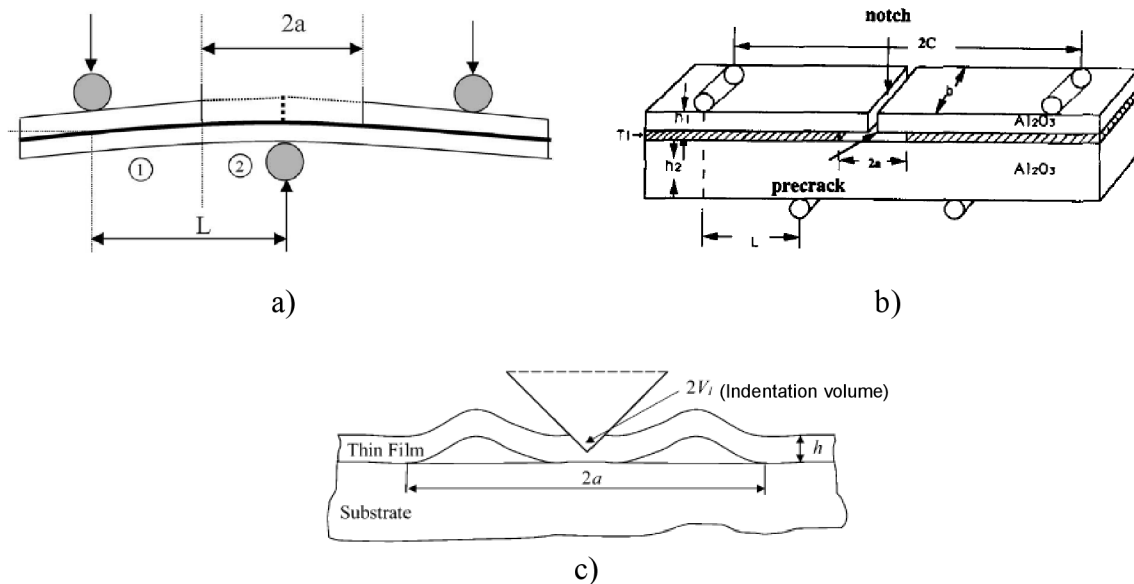
a)   b)

c)

Fig. 10 Some of the measuring methods for the interfacial toughness a) three point bending test, b) four-point bend test, c) indentation test.

5 Application of methods for the stress field description in the vicinity of the general stress concentrator

5.1 Analysis of the singular and auxiliary (extraction) fields

5.1.1 CDD technique

The semi-infinite crack is modelled as an array of continuously distributed edge dislocations along the negative x_2-axis, see Fig. 11. The potential functions for an isolated dislocation located at the point (x_{1o}, x_{2o}) in an infinite homogeneous anisotropic medium is

$$\Phi_{\alpha o}(z) = q_\alpha \ln(z - \varsigma_\alpha), \tag{41}$$

where

$$\varsigma_\alpha = x_{1o} + p_\alpha x_{2o}, \quad \alpha=1,..3 \tag{42}$$

and

$$q_\alpha = \frac{1}{4\pi} M_{\alpha k} d_k, \tag{43}$$

where the vector d_k is related to the Burgers vector b_i through the equation

$$b_i = B_{ik} d_k, \quad \text{with } B_{ik} = \frac{i}{2} \sum_\alpha \left(A_{i\alpha} M_{\alpha k} - \overline{A}_{i\alpha} \overline{M}_{\alpha k} \right) = -\text{Im} \left(\sum_\alpha A_{i\alpha} M_{\alpha k} \right), \tag{44}$$

where the matrix $M_{\alpha k}$ is defined as the inverse of $L_{i\alpha}$, $M_{\alpha k} L_{k\beta} = \delta_{\alpha\beta}$. The quantities p_α, $A_{i\alpha}$, $L_{i\alpha}$ are given by Lekhniskii [55]. For the plane deformation, the elastic field can be represented in terms of the complex potential functions $\Phi_1(z_1)$, $\Phi_2(z_2)$, $\Phi_3(z_3)$, each of which is holomorphic in its arguments $z_\alpha = x_1 + p_\alpha x_2$. Here, p_α are three distinct complex numbers with positive imaginary parts, which are obtained as the roots of the characteristic equation

$$\det \left[c_{i1k1} + p \left(c_{i1k2} + c_{i2k1} \right) + p^2 c_{i2k2} \right] = 0, \tag{45}$$

where

c_{ijkl} is the tensor of elastic constants, i.e. $\sigma_{ij} = c_{ijkl} u_{k,l}$, which satisfies the symmetry conditions

$$c_{ijkl} = c_{ijlk} = c_{jikl} = c_{klij}. \tag{46}$$

With these holomorphic functions, the representation for the displacements U_i and stresses σ_{ij} is

$$U_i = 2\text{Re} \left[\sum_{\alpha=1}^3 A_{i\alpha} \Phi_\alpha(z_\alpha) \right], \quad \sigma_{2i} = 2\text{Re} \left[\sum_{\alpha=1}^3 L_{i\alpha} \Phi'_\alpha(z_\alpha) \right], \quad \sigma_{1i} = -2\text{Re} \left[\sum_{\alpha=1}^3 L_{i\alpha} p_\alpha \Phi'_\alpha(z_\alpha) \right]. \tag{47}$$

Here, ()' designates the derivative with respect to the associated arguments, and **A** and **L** are matrices given by

$$L_{i\alpha} = A_{k\alpha} \left(c_{i2k1} + p_\alpha c_{i2k2} \right), \tag{48}$$

where $A_{k\alpha}$ denotes the eigenvector corresponding to the eigenvalue p_α above.
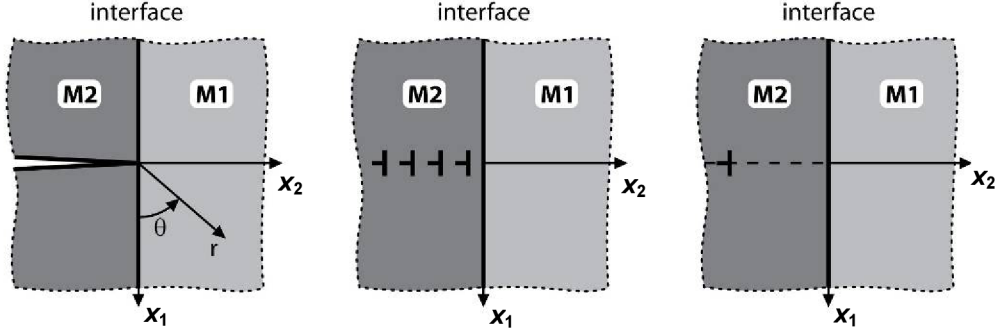
Fig. 11 Semi-infinite crack terminating perpendicular to the interface between two anisotropic materials.

The potentials for the interaction of an edge dislocation with the interface of two anisotropic materials can be obtained in terms of Eq. (41)

$$\mathbf{\Phi}_o(z) = \left[q_1 \ln(z - \varsigma_1), q_2 \ln(z - \varsigma_2), q_3 \ln(z - \varsigma_3) \right]^T, \tag{49}$$

by invoking the standard analytical continuation arguments along the interface, as described by Suo [86]. The solution for the two media can be written as

$$\mathbf{\Phi}(z) = \mathbf{\Phi}^I(z), \quad z \in 1, \quad \mathbf{\Phi}(z) = \mathbf{\Phi}^{II}(z) + \mathbf{\Phi}_o(z), \quad z \in 2, \tag{50}$$

$$\mathbf{\Phi}^I(z) = \mathbf{C}\mathbf{\Phi}_o(z), \quad \mathbf{C} = i\mathbf{M}^I \mathbf{H}^{-1} \left(\mathbf{A}^{II} \mathbf{M}^{II} - \bar{\mathbf{A}}^{II} \bar{\mathbf{M}}^{II} \right) \mathbf{L}^{II}, \quad z \in 1, \quad \mathbf{H} = i \left(\mathbf{A}^I \mathbf{M}^I - \bar{\mathbf{A}}^{II} \bar{\mathbf{M}}^{II} \right),$$

$$\mathbf{\Phi}^{II}(z) = \mathbf{G}\bar{\mathbf{\Phi}}_o(z), \quad \mathbf{G} = -i\mathbf{M}^{II} \bar{\mathbf{H}}^{-1} \left(\bar{\mathbf{A}}^{II} \bar{\mathbf{M}}^{II} - \bar{\mathbf{A}}^I \bar{\mathbf{M}}^I \right) \bar{\mathbf{L}}^{II}, \quad z \in 2. \tag{51}$$

The solution for the stress field produced by an isolated dislocation located at point (x_{1o}, x_{2o}) with the Burgers vector b_i in an infinite anisotropic bi-material follows from (47), (50) and (51) as

$$\sigma_{1i}(x_1, x_2) = -\frac{1}{4\pi} \sum_\alpha L_{i\alpha}^{II} p_\alpha^{II} \left[\sum_\beta \left(G_{\alpha\beta} \bar{M}_{\beta k}^{II} \frac{d_k}{z_\alpha - \bar{\varsigma}_\beta} \right) + M_{\alpha k}^{II} \frac{d_k}{z_\alpha - \varsigma_\alpha} \right] + C.C., \quad z \in 2, \tag{52}$$

$$\sigma_{2i}(x_1, x_2) = \frac{1}{4\pi} \sum_\alpha L_{i\alpha}^{II} \left[\sum_\beta \left(G_{\alpha\beta} \bar{M}_{\beta k}^{II} \frac{d_k}{z_\alpha - \bar{\varsigma}_\beta} \right) + M_{\alpha k}^{II} \frac{d_k}{z_\alpha - \varsigma_\alpha} \right] + C.C., \quad z \in 2, \tag{53}$$

$$\sigma_{1i}(x_1, x_2) = -\frac{1}{4\pi} \sum_\alpha L_{i\alpha}^I p_\alpha^I \sum_\beta \left(C_{\alpha\beta} M_{\beta k}^{II} \frac{d_k}{z_\alpha - \varsigma_\beta} \right) + C.C., \quad z \in 1, \tag{54}$$

$$\sigma_{2i}(x_1, x_2) = \frac{1}{4\pi} \sum_\alpha L_{i\alpha}^I \sum_\beta \left(C_{\alpha\beta} M_{\beta k}^{II} \frac{d_k}{z_\alpha - \varsigma_\beta} \right) + C.C., \quad z \in 1, \tag{55}$$

where C.C. denotes the complex conjugate of the preceding expression, superscript I and II refers to the material 1 and 2 respectively, and the convention of summing over repeated Latin indices is used. Introduce a function f_k at a point on the crack ($x_1=0$, x_2) which relates to the elemental Burgers vector δb_i between x_{2o} and $x_{2o} + \delta x_{2o}$ as

$$\delta b_i = B_{ik} \delta d_k = B_{ik} f_k(x_{2o}) \delta x_{2o}, \tag{56}$$

and integrate (52) along the whole crack. The tractions produced at a point $(0, x_2)$ by the density function f_k can be expressed as

$$\sigma_{1i}(x_2) = -\frac{1}{4\pi}\left\{\sum_\alpha L^{II}_{i\alpha}\left[\sum_\beta\left(G_{\alpha\beta}\bar{M}^{II}_{\beta k}\frac{p^{II}_\alpha}{\overline{p}^{II}_\beta}\int_{-\infty}^0\frac{f_k(x_{2o})\,\mathrm{d}\,x_{2o}}{\frac{p^{II}_\alpha}{\overline{p}^{II}_\beta}x_2-x_{2o}}\right)+M^{II}_{\alpha k}\int_{-\infty}^0\frac{f_k(x_{2o})\,\mathrm{d}\,x_{2o}}{x_2-x_{2o}}\right]\right\}+$$

$$+\sum_\alpha\overline{L}^{II}_{i\alpha}\left[\sum_\beta\left(\overline{G}_{\alpha\beta}M^{II}_{\beta k}\frac{\overline{p}^{II}_\alpha}{p^{II}_\beta}\int_{-\infty}^0\frac{f_k(x_{2o})\,\mathrm{d}\,x_{2o}}{\frac{\overline{p}^{II}_\alpha}{p^{II}_\beta}x_2-x_{2o}}\right)+\overline{M}^{II}_{\alpha k}\int_{-\infty}^0\frac{f_k(x_{2o})\,\mathrm{d}\,x_{2o}}{x_2-x_{2o}}\right]\right\}. \tag{57}$$

The asymptotic stress field near the crack tip is modelled as a continuous distribution of dislocations with density function

$$f_k(x_{2o}) = Hv_k(-x_{2o})^{\delta-1}, \quad x_{2o} < 0, \tag{58}$$

where δ is the stress singularity exponent, which is yet unknown, v_k are the components of corresponding eigenvector, and H is the generalized stress intensity factor (GSIF). Substitute Eq. (58) in (57), integrate and apply the traction-free condition on the plane of the crack to obtain

$$\mathrm{Re}\left\{\left[\sum_\alpha\sum_\beta L^{II}_{i\alpha}G_{\alpha\beta}\bar{M}^{II}_{\beta k}\left(-\frac{\overline{p}^{II}_\beta}{p^{II}_\alpha}\right)^{-\delta}\csc(\pi\delta)-\delta_{ik}\cot(\pi\delta)\right]\right\}v_k = 0. \tag{59}$$

Eq. (59) can be briefly written as

$$\mathbf{D}(\delta)\mathbf{v} = 0, \quad\text{where}\quad D_{ik}(\delta) = \mathrm{Re}\left\{\left[\sum_\alpha\sum_\beta L^{II}_{i\alpha}G_{\alpha\beta}\bar{M}^{II}_{\beta k}\left(-\frac{\overline{p}^{II}_\beta}{p^{II}_\alpha}\right)^{-\delta}\csc(\pi\delta)-\delta_{ik}\cot(\pi\delta)\right]\right\}. \tag{60}$$

The parameter δ is calculated from the characteristic equation

$$\mathrm{Det}\left[\mathbf{D}(\delta)\right] = 0 \tag{61}$$

and the eigenvector $\mathbf{v}$ is determined from Eq. (60) up to a multiplicative constant.
Taking

$$z_\alpha = r\left(\cos\theta + p^{II}_\alpha\sin\theta\right) = r\tau^{II}_\alpha(\theta)\ \text{ for }z_\alpha\in 2,\ z_\alpha = r\left(\cos\theta + p^{I}_\alpha\sin\theta\right) = r\tau^{I}_\alpha(\theta)\ \text{ for }z_\alpha\in 1 \tag{62}$$

the stresses induced by the distribution of dislocation in Eq. (58) can be expressed as

$$\sigma_{1i}(r,\theta) = -\frac{H}{2r^{1-\delta}}\mathrm{Re}\left\{\sum_\alpha L^{II}_{i\alpha}p^{II}_\alpha\sum_\beta\left[G_{\alpha\beta}\bar{M}^{II}_{\beta k}\left(\overline{p}^{II}_\beta\right)^{-\delta}+\delta_{ik}\left(p^{II}_\alpha\right)^{-\delta}\right]\frac{(-1)^{1-\delta}}{\tau^{II}_\alpha(\theta)^{1-\delta}}\left(\cot(\pi\delta)-i\right)v_k\right\},$$

$$\theta\in\left(-\frac{\pi}{2},0\right)\cup\left(\pi,\frac{3}{2}\pi\right), \tag{63}$$

$$\sigma_{2i}\left(r,\theta\right)=\frac{H}{2r^{1-\delta}}\text{Re}\left\{\sum_{\alpha}L_{i\alpha}^{II}\sum_{\beta}\left[G_{\alpha\beta}\overline{M}_{\beta k}^{II}\left(\overline{p}_{\beta}^{II}\right)^{-\delta}+\delta_{ik}\left(p_{\alpha}^{II}\right)^{-\delta}\right]\frac{\left(-1\right)^{1-\delta}}{\tau_{\alpha}^{II}\left(\theta\right)^{1-\delta}}\left(\cot\left(\pi\delta\right)-i\right)v_{k}\right\},$$

$$\theta\in\left(-\frac{\pi}{2},0\right)\cup\left(\pi,\frac{3}{2}\pi\right),$$ (64)

$$\sigma_{1i}\left(r,\theta\right)=-\frac{H}{2r^{1-\delta}}\text{Re}\left\{\sum_{\alpha}L_{i\alpha}^{I}p_{\alpha}^{I}\sum_{\beta}C_{\alpha\beta}M_{\beta k}^{II}\left(p_{\beta}^{II}\right)^{-\delta}\frac{\left(-1\right)^{1-\delta}}{\tau_{\alpha}^{I}\left(\theta\right)^{1-\delta}}\left(\cot\left(\pi\delta\right)-i\right)v_{k}\right\},\quad\theta\in\left(0,\pi\right),$$ (65)

$$\sigma_{2i}\left(r,\theta\right)=\frac{H}{2r^{1-\delta}}\text{Re}\left\{\sum_{\alpha}L_{i\alpha}^{I}\sum_{\beta}C_{\alpha\beta}M_{\beta k}^{II}\left(p_{\beta}^{II}\right)^{-\delta}\frac{\left(-1\right)^{1-\delta}}{\tau_{\alpha}^{I}\left(\theta\right)^{1-\delta}}\left(\cot\left(\pi\delta\right)-i\right)v_{k}\right\},\quad\theta\in\left(0,\pi\right).$$ (66)

Apparently, the previous results can be written in the form of (47), where the function Φ'_{α} is given by

$$\Phi'_{\alpha}=\frac{H}{4r^{1-\delta}}\sum_{\beta}\left[G_{\alpha\beta}\overline{M}_{\beta k}^{II}\left(\overline{p}_{\beta}^{II}\right)^{-\delta}+\delta_{ik}\left(p_{\alpha}^{II}\right)^{-\delta}\right]\frac{\left(-1\right)^{1-\delta}}{\tau_{\alpha}^{II}\left(\theta\right)^{1-\delta}}\left(\cot\left(\pi\delta\right)-i\right)v_{k},\quad\text{for }z\in 2,$$ (67)

hence

$$\Phi_{\alpha}=\frac{Hr^{\delta}}{4\delta}\sum_{\beta}\left[G_{\alpha\beta}\overline{M}_{\beta k}^{II}\left(\overline{p}_{\beta}^{II}\right)^{-\delta}+\delta_{ik}\left(p_{\alpha}^{II}\right)^{-\delta}\right]\frac{\left(-1\right)^{1-\delta}}{\tau_{\alpha}^{II}\left(\theta\right)^{1-\delta}}\left(\cot\left(\pi\delta\right)-i\right)v_{k},\quad\text{for }z\in 2$$ (68)

and

$$\Phi'_{\alpha}=\frac{H}{4r^{1-\delta}}\sum_{\beta}C_{\alpha\beta}M_{\beta k}^{II}\left(p_{\beta}^{II}\right)^{-\delta}\frac{\left(-1\right)^{1-\delta}}{\tau_{\alpha}^{I}\left(\theta\right)^{1-\delta}}\left(\cot\left(\pi\delta\right)-i\right)v_{k},\quad\text{for }z\in 1,$$ (69)

hence

$$\Phi_{\alpha}=\frac{Hr^{\delta}}{4\delta}\sum_{\beta}C_{\alpha\beta}M_{\beta k}^{II}\left(p_{\beta}^{II}\right)^{-\delta}\frac{\left(-1\right)^{1-\delta}}{\tau_{\alpha}^{I}\left(\theta\right)^{1-\delta}}\left(\cot\left(\pi\delta\right)-i\right)v_{k},\quad\text{for }z\in 1.$$ (70)

Using Eqs. (47), (68) and (70), the displacement field can be expressed as

$$U_{i}=\frac{Hr^{\delta}}{2\delta}\text{Re}\left\{\sum_{\alpha}A_{i\alpha}\sum_{\beta}\left[G_{\alpha\beta}\overline{M}_{\beta k}^{II}\left(\overline{p}_{\beta}^{II}\right)^{-\delta}+\delta_{ik}\left(p_{\alpha}^{II}\right)^{-\delta}\right]\frac{\left(-1\right)^{1-\delta}}{\tau_{\alpha}^{II}\left(\theta\right)^{1-\delta}}\left(\cot\left(\pi\delta\right)-i\right)v_{k}\right\},\quad\text{for }z\in 2$$ (71)

and

$$U_{i}=\frac{Hr^{\delta}}{2\delta}\text{Re}\left\{\sum_{\alpha}A_{i\alpha}\sum_{\beta}C_{\alpha\beta}M_{\beta k}^{II}\left(p_{\beta}^{II}\right)^{-\delta}\frac{\left(-1\right)^{1-\delta}}{\tau_{\alpha}^{I}\left(\theta\right)^{1-\delta}}\left(\cot\left(\pi\delta\right)-i\right)v_{k}\right\},\quad\text{for }z\in 1.$$ (72)

CDD technique can be also used for the determination of the dual (auxiliary) fields which are needed for the application of Ψ-integral.

Assume the the following distribution of dislocations $f_{k}^{*}\left(x_{2}\right)$

$$f_k^* \left(x_2\right) = \frac{w_k}{\left(-x_2\right)^{\delta+1}}, \quad -\infty < x_2 < 0, \tag{73}$$

where w_k is the eigenvector of matrix $\mathbf{D}$ in Eq. (60) corresponding to the eigenvalue $\delta^* = -\delta$.

The dual displacement field can be expressed as

$$U_{-1i}\left(r,\theta\right) = \frac{r^{-\delta}}{-2\delta} \operatorname{Re}\left\{\sum_\alpha A_{i\alpha} \sum_\beta \left[G_{\alpha\beta}\bar{M}_{\beta k}^{II}\left(\bar{p}_\beta^{II}\right)^{-\delta} + \delta_{ik}\left(p_\alpha^{II}\right)^{-\delta}\right]\frac{(-1)^{1-\delta}}{\tau_\alpha^{II}\left(\theta\right)^\delta}\left(\cot\left(\pi\delta\right)-i\right)w_k\right\},$$
$$\theta \in \left(-\frac{\pi}{2},0\right) \cup \left(\pi,\frac{3}{2}\pi\right), \tag{74}$$

$$U_{-1i}\left(r,\theta\right) = \frac{r^{-\delta}}{-2\delta} \operatorname{Re}\left\{\sum_\alpha A_{i\alpha} \sum_\beta C_{\alpha\beta}M_{\beta k}^{II}\left(p_\beta^{II}\right)^{-\delta}\frac{(-1)^{1-\delta}}{\tau_\alpha^{I}\left(\theta\right)^\delta}\left(\cot\left(\pi\delta\right)-i\right)w_k\right\}, \quad \theta \in \left(0,\pi\right). \tag{75}$$

and correspondingly the dual stress field $\sigma_{ij}\left[U_{-1i}\left(r,\theta\right)\right]$.

Using the results (63)-(72) and (74)-(75) together with corresponding results for the dual stress field one can compute the Ψ-integral $\Psi\left(r^{\delta_1}\mathbf{u}_1, r^{-\delta_1}\mathbf{u}_{-1}\right)$ along the path Γ_1 surrounding the crack tip with diameter approaching zero as follows

$$\Psi\left(r^{\delta_1}\mathbf{u}_1, r^{-\delta_1}\mathbf{u}_{-1}\right) = c_1 - c_2, \tag{76}$$

where

$$c_1 = \frac{1}{-4\delta}\left\{\int_{-\frac{\pi}{2}}^{0} \operatorname{Re}\left\{\sum_\alpha L_{i\alpha}^{II}\left(\sin\theta - p_\alpha^{II}\cos\theta\right)\sum_\beta \left[G_{\alpha\beta}\bar{M}_{\beta k}^{II}\left(\bar{p}_\beta^{II}\right)^{-\delta} + \delta_{ik}\left(p_\alpha^{II}\right)^{-\delta}\right]\frac{(-1)^{1-\delta}}{\tau_\alpha^{II}\left(\theta\right)^{1-\delta}}\left(\cot\left(\pi\delta\right)-i\right)v_k\right\} \times \right.$$

$$\times \operatorname{Re}\left\{\sum_\alpha A_{i\alpha} \sum_\beta \left[G_{\alpha\beta}\bar{M}_{\beta k}^{II}\left(\bar{p}_\beta^{II}\right)^{-\delta} + \delta_{ik}\left(p_\alpha^{II}\right)^{-\delta}\right]\frac{(-1)^{1-\delta}}{\tau_\alpha^{II}\left(\theta\right)^\delta}\left(\cot\left(\pi\delta\right)-i\right)w_k\right\}d\theta +$$

$$+\int_{0}^{\pi} \operatorname{Re}\left\{\sum_\alpha L_{i\alpha}^{I}\left(\sin\theta - p_\alpha^{I}\cos\theta\right)\sum_\beta C_{\alpha\beta}M_{\beta k}^{II}\left(p_\beta^{II}\right)^{-\delta}\frac{(-1)^{1-\delta}}{\tau_\alpha^{I}\left(\theta\right)^{1-\delta}}\left(\cot\left(\pi\delta\right)-i\right)v_k\right\} \times$$

$$\times \operatorname{Re}\left\{\sum_\alpha A_{i\alpha} \sum_\beta C_{\alpha\beta}M_{\beta k}^{II}\left(p_\beta^{II}\right)^{-\delta}\frac{(-1)^{1-\delta}}{\tau_\alpha^{I}\left(\theta\right)^\delta}\left(\cot\left(\pi\delta\right)-i\right)w_k\right\}d\theta + \tag{77}$$

$$+\int_{\pi}^{\frac{3\pi}{2}} \operatorname{Re}\left\{\sum_\alpha L_{i\alpha}^{II}\left(\sin\theta - p_\alpha^{II}\cos\theta\right)\sum_\beta \left[G_{\alpha\beta}\bar{M}_{\beta k}^{II}\frac{1}{p_\alpha^{II}}\left(\frac{\bar{p}_\beta^{II}}{p_\alpha^{II}}\right)^{-\delta} + \frac{\delta_{ik}}{p_\alpha^{II}}\right]\frac{(-1)^{1-\delta}}{\tau_\alpha^{II}\left(\theta\right)^{1-\delta}}v_k\right\} \times$$

$$\times \operatorname{Re}\left\{\sum_\alpha A_{i\alpha} \sum_\beta \left[G_{\alpha\beta}\bar{M}_{\beta k}^{II}\left(\bar{p}_\beta^{II}\right)^{-\delta} + \delta_{ik}\left(p_\alpha^{II}\right)^{-\delta}\right]\frac{(-1)^{1-\delta}}{\tau_\alpha^{II}\left(\theta\right)^\delta}\left(\cot\left(\pi\delta\right)-i\right)w_k\right\}d\theta\right\},$$

$$
c_2 = \frac{1}{-4\delta} \left\{ \int_{-\frac{\pi}{2}}^{0} \mathrm{Re} \left\{ \sum_{\alpha} L_{i\alpha}^{II} \left(\sin\theta - p_{\alpha}^{II} \cos\theta \right) \sum_{\beta} \left[G_{\alpha\beta} \bar{M}_{\beta k}^{II} \left(\bar{p}_{\beta}^{II} \right)^{-\delta} + \delta_{ik} \left(p_{\alpha}^{II} \right)^{-\delta} \right] \frac{(-1)^{1-\delta}}{\tau_{\alpha}^{II}(\theta)^{1-\delta^*}} \left(\cot(\pi\delta) - i \right) w_k \right\} \times \right.
$$

$$
\times \mathrm{Re} \left\{ \sum_{\alpha} A_{i\alpha} \sum_{\beta} \left[G_{\alpha\beta} \bar{M}_{\beta k}^{II} \left(\bar{p}_{\beta}^{II} \right)^{-\delta} + \delta_{ik} \left(p_{\alpha}^{II} \right)^{-\delta} \right] \frac{(-1)^{1-\delta}}{\tau_{\alpha}^{II}(\theta)^{1-\delta}} \left(\cot(\pi\delta) - i \right) v_k \right\} \mathrm{d}\theta \ +
$$

$$
+ \int_{0}^{\pi} \mathrm{Re} \left\{ \sum_{\alpha} L_{i\alpha}^{I} \left(\sin\theta - p_{\alpha}^{I} \cos\theta \right) \sum_{\beta} C_{\alpha\beta} M_{\beta k}^{II} \left(p_{\beta}^{II} \right)^{-\delta} \frac{(-1)^{1-\delta}}{\tau_{\alpha}^{I}(\theta)^{1-\delta^*}} \left(\cot(\pi\delta) - i \right) w_k \right\} \times
$$

$$
\times \mathrm{Re} \left\{ \sum_{\alpha} A_{i\alpha} \sum_{\beta} C_{\alpha\beta} M_{\beta k}^{II} \left(p_{\beta}^{II} \right)^{-\delta} \frac{(-1)^{1-\delta}}{\tau_{\alpha}^{I}(\theta)^{1-\delta}} \left(\cot(\pi\delta) - i \right) v_k \right\} \mathrm{d}\theta +
$$

$$
+ \int_{\pi}^{\frac{3\pi}{2}} \left\{ \int_{-\frac{\pi}{2}}^{0} \mathrm{Re} \left\{ \sum_{\alpha} L_{i\alpha}^{II} \left(\sin\theta - p_{\alpha}^{II} \cos\theta \right) \sum_{\beta} \left[G_{\alpha\beta} \bar{M}_{\beta k}^{II} \left(\bar{p}_{\beta}^{II} \right)^{-\delta} + \delta_{ik} \left(p_{\alpha}^{II} \right)^{-\delta} \right] \frac{(-1)^{1-\delta}}{\tau_{\alpha}^{II}(\theta)^{1-\delta^*}} \left(\cot(\pi\delta) - i \right) w_k \right\} \times \right.
$$

$$
\left. \times \mathrm{Re} \left\{ \sum_{\alpha} A_{i\alpha} \sum_{\beta} \left[G_{\alpha\beta} \bar{M}_{\beta k}^{II} \left(\bar{p}_{\beta}^{II} \right)^{-\delta} + \delta_{ik} \left(p_{\alpha}^{II} \right)^{-\delta} \right] \frac{(-1)^{1-\delta}}{\tau_{\alpha}^{II}(\theta)^{1-\delta}} \left(\cot(\pi\delta) - i \right) v_k \right\} \mathrm{d}\theta \right\}.
$$

(78)

5.1.2 L.E.S. method

Choose the coordination system so that the material containing crack is in the area $x_2 < 0$. Both of these materials are homogenous and linear elastic and the Hooke´s law is valid for the deformations:

$$\varepsilon_i = \sum_{j=1,2,6} s_{ij} \sigma_j, \quad (i=1,2,6). \tag{79}$$

Here the rule of short tensor index notation was applied

$$1 \leftrightarrow 11, \quad 2 \leftrightarrow 22, \quad 6 \leftrightarrow 12 \leftrightarrow 21. \tag{80}$$

Where s_{ij} is a compliance matrix and the Eq. (79) holds for the case of the plane stress. In the case of plane strain it is necessary to perform a conversion of the compliance matrix components according to the relation

$$s'_{ij} = s_{ij} - \frac{s_{i3} s_{j3}}{s_{33}}, \quad (i, j = 1, 2, 6). \tag{81}$$

The compliance matrix s_{ij} of an orthotropic material has in terms of usual engineering constants the following form

$$s_{ij} = \begin{bmatrix} \dfrac{1}{E_1} & -\dfrac{v_{21}}{E_2} & -\dfrac{v_{31}}{E_3} & 0 & 0 & 0 \\[2mm] -\dfrac{v_{12}}{E_1} & \dfrac{1}{E_2} & -\dfrac{v_{32}}{E_3} & 0 & 0 & 0 \\[2mm] -\dfrac{v_{13}}{E_1} & -\dfrac{v_{23}}{E_2} & \dfrac{1}{E_3} & 0 & 0 & 0 \\[2mm] 0 & 0 & 0 & \dfrac{1}{G_{23}} & 0 & 0 \\[2mm] 0 & 0 & 0 & 0 & \dfrac{1}{G_{31}} & 0 \\[2mm] 0 & 0 & 0 & 0 & 0 & \dfrac{1}{G_{12}} \end{bmatrix}. \tag{82}$$

The subscripts 1,2,3 denotes the appropriate material direction, where the direction 1 is called the Longitudinal (L), 2 – Transversal (T) and 3 as Z. Note, that a general orthotropic material is characterized by 9 independent elastic constants and the matrix s_{ij} is symmetric ($s_{ij} = s_{ji}$) - in other words, the appropriate non-diagonal components has to be in terms of usual engineering constants equal.

Orthotropic materials are characterized by the complex numbers μ_i, $\text{Im}(\mu_i) > 0$, where $i=1,2$ and $\text{Im}(.)$ denotes the complex number imaginary part. Numbers μ_i are depending on material characteristics and can be obtained as the roots of the 4th order equation

$$\lambda \mu^4 + 2\rho \lambda^{1/2} \mu^2 + 1 = 0, \tag{83}$$

where

$$\lambda = \frac{s_{11}}{s_{22}}, \quad \rho = \frac{2s_{12} + s_{66}}{2\sqrt{s_{11} s_{22}}}. \tag{84}$$
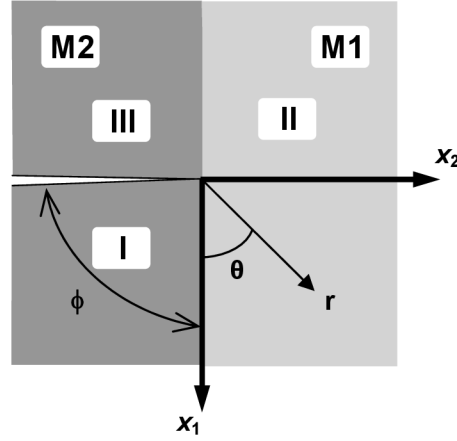
Fig. 12 Semi-infinite crack, perpendicular to the interface of two orthotropic materials.

Eq. (83) is a special case of the characteristic equation of the 6th order presented by Lechnitskii [52]. The roots μ_i of the characteristic equation (83) are as follows

$$\mu_1 = i\lambda^{-1/4}(n+m), \quad \mu_2 = i\lambda^{-1/4}(n-m) \quad \text{for} \quad 1 < \rho < \infty,$$

$$\mu_1 = \lambda^{-1/4}(in+m), \quad \mu_2 = \lambda^{-1/4}(in-m) \quad \text{for} \quad -1 < \rho < 1, \tag{85}$$

$$\mu_1 = \mu_2 = i\lambda^{-1/4} \quad \text{for} \quad \rho = 1,$$

where

$$n = \sqrt{\frac{1+\rho}{2}}, \quad m = \sqrt{\left|\frac{1-\rho}{2}\right|}. \tag{86}$$

The case $\rho=1$ corresponds to material with cubic symmetry and $\lambda=\rho=1$ corresponds to isotropic material. These are the so-called degenerate cases of anisotropy, where the L.E.S. formalism cannot be applied directly. One of the ways to overcome the problems with material symmetry was introduced by Suo [86]. This is an analogy to the Muschelishvilli´s complex potential method.

For the two aligned orthotropic media, it is possible to define two generalized Dundurs' parameters α and β [25], which are the only bi-material constants that enter the solution for the problem involving dissimilar materials with prescribed tractions at the boundary. Thus, the solution for the problem under consideration should depend upon λ and ρ for each material and the two bi-material parameters α and β (indices M1, M2 denotes pertinence of the matrix components s_{ij} to the given material –see Fig. 12):

$$\alpha = \frac{\left[\sqrt{(s_{11}s_{22})_{M2}}/\sqrt{(s_{11}s_{22})_{M1}} - 1\right]}{\left[\sqrt{(s_{11}s_{22})_{M2}}/\sqrt{(s_{11}s_{22})_{M1}} + 1\right]}, \quad \beta = \frac{\left[\sqrt{s_{11}s_{22}} + s_{12}\right]_{M2} - \left[\sqrt{s_{11}s_{22}} + s_{12}\right]_{M1}}{\sqrt{H_{11}H_{22}}}, \tag{87}$$

where

$$H_{11} = \left[2n\lambda^{1/4}\sqrt{s_{11}s_{22}}\right]_{M1} + \left[2n\lambda^{1/4}\sqrt{s_{11}s_{22}}\right]_{M2},$$

$$H_{22} = \left[2n\lambda^{-1/4}\sqrt{s_{11}s_{22}}\right]_{M1} + \left[2n\lambda^{-1/4}\sqrt{s_{11}s_{22}}\right]_{M2}. \tag{88}$$

Both parameters α and β can take the value from interval (-1, 1). For the case of anisotropic material, i.e. for $\rho \neq 1$, is possible to write the relations for displacements U_i,

stresses σ_{ij}, and the resulting force T_i along the half-line leading from the CS origin:

$$U_i = 2\operatorname{Re}\left\{\sum_{j=1}^{2} A_{ij} f_j(z_j)\right\}, \quad T_i = -2\operatorname{Re}\left\{\sum_{j=1}^{2} L_{ij} f_j(z_j)\right\}$$

$$\sigma_{2i} = 2\operatorname{Re}\left\{\sum_{j=1}^{2} L_{ij} f_j'(z_j)\right\}, \quad \sigma_{1i} = -2\operatorname{Re}\left\{\sum_{j=1}^{2} L_{ij} \mu_j f_j'(z_j)\right\}$$

(89)

where $z_j = x_1 + ix_2$, $(.)'$ denotes differentiation with respect to z_j and the matrices A_{ij}, L_{ij} are defined by

$$\mathbf{A} = \begin{bmatrix} s_{11}\mu_1^2 + s_{12} & s_{11}\mu_2^2 + s_{12} \\ s_{12}\mu_1 + s_{22}/\mu_1 & s_{12}\mu_2 + s_{22}/\mu_2 \end{bmatrix} \quad \mathbf{L} = \begin{bmatrix} -\mu_1 & -\mu_2 \\ 1 & 1 \end{bmatrix}.$$

(90)

In case of the isotropic material, i.e. for $\lambda=\rho=1$, the relations for displacements U_i, stresses σ_{ij}, and the resulting force T_i along the half-line leading from the can be written in the following form

$$U_i = 2\operatorname{Re}\left\{\sum_{j=1}^{2} A_{ij}^* g_j(z)\right\}, \quad T_i = 2\operatorname{Re}\left\{\sum_{j=1}^{2} B_{ij}^* g_j(z)\right\}$$

$$\sigma_{2i} = 2\operatorname{Re}\left\{\sum_{j=1}^{2} B_{ij}^* g_j'(z)\right\}, \quad \sigma_{1i} = 2\operatorname{Re}\left\{\sum_{j=1}^{2} L_{ij}^* g_j'(z)\right\},$$

(91)

where $z = x_1 + ix_2$, $(.)'$ denotes differentiation with respect to z and the matrices A_{ij}, L_{ij} are defined by

$$\mathbf{A}^* = \frac{1}{4Gi}\begin{bmatrix} \kappa i & -i \\ \kappa & 1 \end{bmatrix}, \quad \mathbf{B}^* = \frac{1}{2}\begin{bmatrix} i & -i \\ 1 & 1 \end{bmatrix}, \quad \mathbf{L}^* = \frac{1}{2}\begin{bmatrix} 3 & -1 \\ i & -i \end{bmatrix}.$$

(92)

where $\kappa = 3 - 4\nu$ for plane strain and $\kappa = (3-\nu)/(1+\nu)$ for plane stress, ν and G are Poisson's ratio and shear modulus. The vector function $g_j(z)$ depends on Muschelishvilli´s potentials $\varphi(z)$, $\psi(z)$ and is possible to write as follows

$$\mathbf{g}(z) = \left[\varphi(z), \psi(z) + (\bar{z} - z)\varphi'(z)\right]^T = \mathbf{f}^*(z) + (\bar{z} - z)\mathbf{Q}^*\mathbf{f}^{*'}(z),$$

$$\mathbf{g}'(z) = \left[\varphi'(z), \psi'(z) + (\bar{z} - z)\varphi''(z)\right]^T = \mathbf{f}^{*'}(z) + (\bar{z} - z)\mathbf{Q}^*\mathbf{f}^{*''}(z),$$

(93)

where $(\overline{.})$ is a complex conjugate expression

$$\mathbf{f}^*(z) = \left[\varphi(z), \psi(z)\right]^T, \quad \mathbf{Q}^* = \begin{bmatrix} 0 & 0 \\ 1 & 0 \end{bmatrix}.$$

(94)

The stresses in the crack tip region are proportional to $r^{\delta-1}$ and displacements to r^δ. r denotes the distance from the crack tip and the exponent δ is, for a crack perpendicular to the interface of two different materials, a real number. The exponent δ depends on the local boundary conditions (i.e. on the character of the crack faces loading and the character of the interface between the materials) and the material characteristics of both materials. The unknown potentials $f_j(z_j)$, $\varphi(z)$ and $\psi(z)$ are sought in the following form

$$f_j^J(z_j^J) = \phi_j^J z_j^{J\delta}, \quad \varphi^J(z) = \phi_1^{*J} z^\delta, \quad \psi^J(z) = \phi_2^{*J} z^\delta, \quad (j = 1, 2, \ J = I, II, III), \tag{95}$$

where ϕ_j^J and ϕ_j^{*J} are vectors of complex coefficients. The superscripts denotes the appropriate bi-material region (see Fig. 12), the subscript denotes either the pertinence to characteristic number μ_j of the orthotropic material or pertinence to the potential of the isotropic material. The coordinates z_j and z are considered as polar (see Fig. 12)

$$z_j^J = r\left(\cos\theta + \mu_j^J \sin\theta\right), \quad z = r\left(\cos\theta + i\sin\theta\right). \tag{96}$$

In the crack tip region, the following boundary conditions have to be satisfied

$$T_i = 0 \quad \text{for} \quad \theta = -\frac{\pi}{2}, \frac{3\pi}{2},$$
$$U_i^I = U_i^{II}, \ T_i^I = T_i^{II} \quad \text{for} \quad \theta = 0, \tag{97}$$
$$U_i^{II} = U_i^{III}, \ T_i^{II} = T_i^{III} \quad \text{for} \quad \theta = \pi, \ i = 1, 2,$$

The goal is to find the unknown singularity exponent δ and the corresponding unknown eigenvectors ϕ_j^J or ϕ_j^{*J} so that the boundary conditions (97) are satisfied.

Substituting the assumed form of the potential solution $f_j(z_j)$, $\varphi(z)$ and $\psi(z)$ from (95) into (89) or (91) one obtain for the case of the anisotropic media the following relations

$$\mathbf{U}^J = \mathbf{A}^J \mathbf{Z}^{J\delta} \mathbf{\Phi}^J + \overline{\mathbf{A}}^J \overline{\mathbf{Z}}^{J\delta} \overline{\mathbf{\Phi}}^J,$$
$$-\mathbf{T}^J = \mathbf{L}^J \mathbf{Z}^{J\delta} \mathbf{\Phi}^J + \overline{\mathbf{L}}^J \overline{\mathbf{Z}}^{J\delta} \overline{\mathbf{\Phi}}^J, \tag{98}$$

where

$$Z^{J\delta} = \mathrm{diag}\left[z_1^{J\delta}, z_2^{J\delta} \right] = \mathrm{diag}\left[(x_1 + \mu_1^J x_2)^\delta, (x_1 + \mu_2^J x_2)^\delta \right]$$
$$= r^\delta \mathrm{diag}\left[(\cos\theta + \mu_1^J \sin\theta)^\delta, (\cos\theta + \mu_2^J \sin\theta)^\delta \right]. \tag{99}$$

For the case of the isotropic media one obtains

$$\mathbf{U}^J = \mathbf{A}^{*J} \mathbf{Z}^{*\delta} \mathbf{\Phi}^{*J} + \overline{\mathbf{A}}^{*J} \overline{\mathbf{Z}}^{*\delta} \overline{\mathbf{\Phi}}^{*J},$$
$$-\mathbf{T}^J = \mathbf{B}^{*J} \mathbf{Z}^{*\delta} \mathbf{\Phi}^{*J} + \overline{\mathbf{B}}^{*J} \overline{\mathbf{Z}}^{*\delta} \overline{\mathbf{\Phi}}^{*J}, \tag{100}$$

where

$$Z^{*\delta} = \begin{bmatrix} z^\delta & 0 \\ (\overline{z} - z)\delta z^{\delta-1} & z^\delta \end{bmatrix} = \begin{bmatrix} (x_1 + ix_2)^\delta & 0 \\ -2ix_2\delta(x_1 + ix_2)^{\delta-1} & (x_1 + ix_2)^\delta \end{bmatrix}$$
$$= \begin{bmatrix} r^\delta(\cos\theta + i\sin\theta)^\delta & 0 \\ -2r^\delta i\delta(\cos\theta + i\sin\theta)^{\delta-1}\sin\theta & r^\delta(\cos\theta + i\sin\theta)^\delta \end{bmatrix}. \tag{101}$$

For the bi-material composed of two anisotropic media, the boundary conditions (97) and relations for the displacements and resulting force (98) lead to the following homogenous algebraic equation system

$$\begin{bmatrix} \mathbf{B}_0^I & -\overline{\mathbf{B}}_0^I & -\mathbf{B}_0^{II} & \overline{\mathbf{B}}_0^{II} & \mathbf{0} & \mathbf{0} \\ \mathbf{X}_0^I & \overline{\mathbf{X}}_0^I & -\mathbf{X}_0^{II} & -\overline{\mathbf{X}}_0^{II} & \mathbf{0} & \mathbf{0} \\ \mathbf{0} & \mathbf{0} & \mathbf{B}_I^{II} & -\overline{\mathbf{B}}_1^{II} & -\mathbf{B}_1^{III} & \overline{\mathbf{B}}_1^{III} \\ \mathbf{0} & \mathbf{0} & \mathbf{X}_1^{II} & \overline{\mathbf{X}}_1^{II} & -\mathbf{X}_1^{III} & -\overline{\mathbf{X}}_1^{III} \\ \mathbf{X}_2^I & \overline{\mathbf{X}}_2^I & \mathbf{0} & \mathbf{0} & \mathbf{0} & \mathbf{0} \\ \mathbf{0} & \mathbf{0} & \mathbf{0} & \mathbf{0} & \mathbf{X}_3^{III} & \overline{\mathbf{X}}_3^{III} \end{bmatrix} \begin{bmatrix} \mathbf{L}^I \Phi^I \\ \overline{\mathbf{L}}^I \overline{\Phi}^I \\ \mathbf{L}^{II} \Phi^{II} \\ \overline{\mathbf{L}}^{II} \overline{\Phi}^{II} \\ \mathbf{L}^{III} \Phi^{III} \\ \overline{\mathbf{L}}^{III} \overline{\Phi}^{III} \end{bmatrix} = \mathbf{0}, \qquad (102)$$

where in the system matrix on the left-hand side of (102), the $\mathbf{0}=\mathbf{0}_{ij}$ denotes the zero matrix 2×2, on the right-hand side the $\mathbf{0}=\mathbf{0}_i$ is a vector 12×1, I_{ij} denotes the unit matrix 2×2 and

$$\mathbf{B}_j^{*J} = \mathrm{i}\mathbf{A}^{*J}\mathbf{Z}_j^{*\delta}\mathbf{B}^{*J-1}, \quad \mathbf{X}_j^{*J} = \mathbf{B}^{*J}\mathbf{Z}_j^{*\delta}\mathbf{B}^{*J-1}, \quad (j=0,1,2,3, \quad J=I,II,III)$$

$$\mathbf{Z}_0^J = \mathrm{diag}[1,1], \quad \mathbf{Z}_1^J = \mathrm{diag}\left[e^{\mathrm{i}\pi\delta}, e^{\mathrm{i}\pi\delta}\right], \qquad (103)$$

$$\mathbf{Z}_2^J = \mathrm{diag}\left[\left|\mu_1^J\right|^\delta e^{-\mathrm{i}\phi\delta}, \left|\mu_2^J\right|^\delta e^{-\mathrm{i}\phi\delta}\right], \quad \mathbf{Z}_3^J = \mathrm{diag}\left[\left|\mu_1^J\right|^\delta e^{i(2\pi-\phi)\delta}, \left|\mu_2^J\right|^\delta e^{i(2\pi-\phi)\delta}\right].$$

where ϕ is the angle forming by the interface and the crack, see Fig. 12. The system of twelve algebraic equations (102) is possible to reduce to the system of two equations

$$\mathbf{K}(\delta)\mathbf{v}^I = \mathbf{0}, \qquad (104)$$

where $\mathbf{0}=\mathbf{0}_i$ is a vector 2×1 and for the vector v_i^I holds

$$\mathbf{v}^I = \frac{1}{H}\mathbf{L}^I\Phi^I. \qquad (105)$$

where H is a generalized stress intensity factor (GSIF) – see e.g. (1). The parameter δ indicates the dependency of the matrix $\mathbf{K}$ (of type 2×2) on this parameter, whereas $\mathbf{K}$ can be written as follows

$$\mathbf{K} = \overline{\mathbf{X}}_1^{II}(\mathbf{I}-\mathbf{Y}_2^I) + (\mathbf{X}_1^{III} - \overline{\mathbf{X}}_1^{III}\mathbf{Y}_3^{III})(\mathbf{B}_1^{III} + \overline{\mathbf{B}}_1^{III}\mathbf{Y}_3^{III})^{-1}\mathbf{B}_1^{II}(\mathbf{I}-\mathbf{Y}_2^I)$$
$$+ \left(\mathbf{X}_1^{II} - \overline{\mathbf{X}}_1^{II} - (\mathbf{X}_1^{III} - \overline{\mathbf{X}}_1^{III}\mathbf{Y}_3^{III})(\mathbf{B}_1^{III} + \overline{\mathbf{B}}_1^{III}\mathbf{Y}_3^{III})^{-1}(\mathbf{B}_1^{II} + \overline{\mathbf{B}}_1^{II})\right) \qquad (106)$$
$$\times (\mathbf{B}_0^{II} + \overline{\mathbf{B}}_0^{II})^{-1}\left(\mathbf{B}_0^I + \mathbf{B}_0^I\mathbf{Y}_2^I + \mathbf{B}_0^{II}(\mathbf{I}-\mathbf{Y}_2^I)\right),$$

where

$$\mathbf{Y}_j^J = (\overline{\mathbf{X}}_j^J)^{-1}\mathbf{X}_j^J. \qquad (107)$$

Note, that in all matrices of Eq. (106) there are expressions containing the unknown parameter δ in the exponent. Hence, to effectively handle the components of the matrix $\mathbf{K}$ it is useful to express some of the inverse matrices on the right-hand side of Eq. (106) by means of the adjoint matrix. Specifically, it holds

$$(\mathbf{B}_1^{III} + \overline{\mathbf{B}}_1^{III}\mathbf{Y}_3^{III})^{-1} = \left(\det(\mathbf{B}_1^{III} + \overline{\mathbf{B}}_1^{III}\mathbf{Y}_3^{III})\right)^{-1}(\mathbf{B}_1^{III} + \overline{\mathbf{B}}_1^{III}\mathbf{Y}_3^{III})^{adj}, \qquad (108)$$

where the superscript *adj* denotes the adjoint matrix. By substitution of Eq. (108) into (106) one gets

$$\det(\mathbf{B}_1^{III} + \overline{\mathbf{B}}_1^{III}\mathbf{Y}_3^{III})\mathbf{K} = \det(\mathbf{B}_1^{III} + \overline{\mathbf{B}}_1^{III}\mathbf{Y}_3^{III})\overline{\mathbf{X}}_1^{II}(\mathbf{I} - \mathbf{Y}_2^{I})$$

$$+(\mathbf{X}_1^{III} - \overline{\mathbf{X}}_1^{III}\mathbf{Y}_3^{III})(\mathbf{B}_1^{III} + \overline{\mathbf{B}}_1^{III}\mathbf{Y}_3^{III})^{adj}\overline{\mathbf{B}}_1^{II}(\mathbf{I} - \mathbf{Y}_2^{I})$$

$$+\left(\det(\mathbf{B}_1^{III} + \overline{\mathbf{B}}_1^{III}\mathbf{Y}_3^{III})(\mathbf{X}_1^{II} - \overline{\mathbf{X}}_1^{II})\right. \tag{109}$$

$$\left.-(\mathbf{X}_1^{III} - \overline{\mathbf{X}}_1^{III}\mathbf{Y}_3^{III})(\mathbf{B}_1^{III} + \overline{\mathbf{B}}_1^{III}\mathbf{Y}_3^{III})^{adj}(\mathbf{B}_1^{II} + \overline{\mathbf{B}}_1^{II})\right)$$

$$\times(\mathbf{B}_0^{II} + \overline{\mathbf{B}}_0^{II})^{-1}\left(\mathbf{B}_0^{I} + \mathbf{B}_0^{I}\mathbf{Y}_2^{I} + \mathbf{B}_0^{II}(\mathbf{I} - \mathbf{Y}_2^{I})\right).$$

The vector $\mathbf{v}^I$ in the system of algebraic equations (104) is generally a complex vector – see [73]. This fact complicates subsequent numerical calculations. Using the relations

$$\text{Re}\left\{\mathbf{v}^I\right\} = \frac{1}{2}(\mathbf{v}^I + \overline{\mathbf{v}}^I) = \frac{1}{2}(\mathbf{I} - \mathbf{Y}_2^I)\mathbf{v}^I ,$$

$$\text{Im}\left\{\mathbf{v}^I\right\} = \frac{1}{2i}(\mathbf{v}^I - \overline{\mathbf{v}}^I) = -\frac{1}{2}i(\mathbf{I} + \mathbf{Y}_2^I)\mathbf{v}^I \tag{110}$$

$$= -i(\mathbf{I} + \mathbf{Y}_2^I)(\mathbf{I} - \mathbf{Y}_2^I)^{-1}\text{Re}\left\{\mathbf{v}^I\right\}$$

the system of equations (104) can be converted to the form

$$2\mathbf{KI}(\mathbf{I} - \mathbf{Y}_2^I)^{-1}\text{Re}\left\{\mathbf{v}^I\right\} = \mathbf{0} . \tag{111}$$

The similar procedure can be applied to the combinations of anisotropic/isotropic bi-materials. Namely, using the boundary conditions (97) and relations (98), (100) one obtains a system of algebraic equations for the case of bi-material composed of isotropic material (region II) and anisotropic material (region I, III – see Fig. 12)

$$
\begin{bmatrix}
\mathbf{B}_0^{*I} & -\overline{\mathbf{B}}_0^{*I} & -\mathbf{B}_0^{II} & \overline{\mathbf{B}}_0^{II} & 0 & 0 \\
\mathbf{X}_0^{*I} & \overline{\mathbf{X}}_0^{*I} & -\mathbf{X}_0^{II} & -\overline{\mathbf{X}}_0^{II} & 0 & 0 \\
0 & 0 & \mathbf{B}_I^{II} & -\overline{\mathbf{B}}_1^{II} & -\mathbf{B}_1^{*III} & \overline{\mathbf{B}}_1^{*III} \\
0 & 0 & \mathbf{X}_1^{II} & \overline{\mathbf{X}}_1^{II} & -\mathbf{X}_1^{*III} & -\overline{\mathbf{X}}_1^{*III} \\
\mathbf{X}_2^{*I} & \overline{\mathbf{X}}_2^{*I} & 0 & 0 & 0 & 0 \\
0 & 0 & 0 & 0 & \mathbf{X}_3^{*III} & \overline{\mathbf{X}}_3^{*III}
\end{bmatrix}
\begin{bmatrix}
\mathbf{B}^{*I}\mathbf{\Phi}^I \\
\overline{\mathbf{B}}^{*I}\overline{\mathbf{\Phi}}^I \\
\mathbf{L}^{II}\mathbf{\Phi}^{II} \\
\overline{\mathbf{L}}^{II}\overline{\mathbf{\Phi}}^{II} \\
\mathbf{B}^{*III}\mathbf{\Phi}^{III} \\
\overline{\mathbf{B}}^{*III}\overline{\mathbf{\Phi}}^{III}
\end{bmatrix} = \mathbf{0}, \tag{112}
$$

where

$$\mathbf{B}_j^{*J} = i\mathbf{A}^{*J}\mathbf{Z}_j^{*\delta}\mathbf{B}^{*J-1}, \quad \mathbf{X}_j^{*J} = \mathbf{B}^{*J}\mathbf{Z}_j^{*\delta}\mathbf{B}^{*J-1}, \quad (j = 0, 1, 2, 3, \quad J = I, II, III)$$

$$\mathbf{Z}_0^* = \text{diag}[1, 1], \quad \mathbf{Z}_1^* = \text{diag}\left[e^{i\pi\delta}, e^{i\pi\delta}\right], \tag{113}$$

$$\mathbf{Z}_2^* = \begin{bmatrix} e^{-i\phi\delta} & 0 \\ 2i\delta e^{-i\phi(\delta-1)} & e^{-i\phi\delta} \end{bmatrix}, \quad \mathbf{Z}_3^J = \begin{bmatrix} e^{i(2\pi-\phi)\delta} & 0 \\ 2i\delta e^{i(2\pi-\phi)(\delta-1)} & e^{i(2\pi-\phi)\delta} \end{bmatrix}.$$

Similarly as the system (102) also the system (112) can be converted to the form (104) or (111), whereas the changes consist only in the replacement of appropriate matrices B_j^J, or $\mathbf{X}_j^J$ by the matrices B_j^{*J} or X_j^{*J}. The following relation must hold in order the solution of the equation system (104) would exist

$$\det(\mathbf{K}(\delta)) = 0. \tag{114}$$

The relation (114) leads to nonlinear equation with parameter δ, which has at least one

real root within the interval (0, 1) – another real or complex roots may be present.

Remark 2: It can easily be proved that if δ is a root of the characteristic equation $Det[\mathbf{K}(\delta)] = 0$ then $-\delta$ also verifies this equation. A general proof of this property for general stress concentrator can be found e.g. in [71]. The corresponding displacement field - so called dual displacement field or extraction solution, is singular at the crack tip, hence it has unbounded energy near the crack tip and thus corresponds to some concentrated source at the crack tip. It is a mathematical tool which allows extracting asymptotic coefficient terms from the complete exact solution using the concept of so-called Ψ-integral based upon the reciprocal theorem.

Remark 3: The zero eigenvalue of matrix $\mathbf{K}$ and the corresponding exponent $\pm\delta_1$ eventually $\pm\delta_2$ can be of multiplicity 2. In that case when searching the eigenvectors corresponding to the given eigenvalue of the matrix, two cases can arise. In the first case the two linearly independent vectors $\mathbf{v}^{Ja}$ and $\mathbf{v}^{Ib}$ are found and any linear combination of these vectors provides the vector $\mathbf{v}^J$. In the second case, the only one eigenvector $\mathbf{v}^I$ can be found, while besides to the solution (95) the following solution given in [71] has to be considered.

$$f_j^I(z_j^J) = r^\delta \left[\ln(r^{1-\delta} z_j^{J\delta} \phi_j^J) + \frac{d}{d\delta}\left(r^{-\delta} z_j^{J\delta} \phi_j^J\right)\bigg|_{\delta=\pm\delta_{I,II}} \right],$$

$$\varphi^I(z) = r^\delta \left[\ln(r^{1-\delta} z^\delta \phi_1^{*J}) + \frac{d}{d\delta}\left(r^{-\delta} z^\delta \phi_1^J\right)\bigg|_{\delta=\pm\delta_{I,II}} \right], \tag{115}$$

$$\psi^I(z) = r^\delta \left[\ln(r^{1-\delta} z^\delta \phi_2^{*J}) + \frac{d}{d\delta}\left(r^{-\delta} z^\delta \phi_2^J\right)\bigg|_{\delta=\pm\delta_{I,II}} \right].$$

5.2   Numerical calculation of GSIF using Ψ-integral

This section is devoted to the demonstration of Ψ-integral technique for a crack impinging perpendicularly at the orthotropic material interface.

Numerical calculations were performed using the FEM system ANSYS. The specimen is made of two layers M1 and M2 of composite such as Graphite/Epoxy T300/5208 system. Elastic constants are taken from the work [38] and are the following: E_L=137GPa, E_T= E_Z=10.8GPa G_{ZT} = 3.36 GPa, G_{ZL} = G_{TL} = 5.65 GPa, ν_{TZ} = 0.49, ν_{ZL} = ν_{TL} = 0.238. Material properties of some other fibre reinforced composites and particular laminae can be found in more details also in the paper [83]. The appropriate material directions of the considered material configurations are obvious from the Fig. 13. The width of substrate was ranging from 40 mm to 100 mm, and the specimen length was 100 mm. As indicated in Fig. 13, three different mutual orientations of layers M1 and M2 were considered with the axis of material symmetry either parallel or perpendicular to the material interface. For each of considered configurations the eigenvalue problem (60) was solved. Both the pair of quantities, δ, $\mathbf{u}_1$, pertaining to the real solution, and the pair of quantities, $\delta^* = -\delta$, $\mathbf{u}_{-1}$, pertaining to the auxiliary solution (see 4.1.3), were found. Calculated characteristic eigenvalues of the singularity δ and δ^* are listed in the Table 1.

Configuration	Characteristic eigenvalue δ (CDD/ L.E.S. method)	Characteristic eigenvalue of the auxiliary solution $\delta^* = -\delta$ (CDD/ L.E.S. method)	GSIF (CDD/L.E.S.)
A	0.328318	-0.328318	6.48
	0.328770	-0.328770	6.62
B	0. 671682	-0. 671682	2.71
	0.671825	-0.671825	2.82
C	0.661490	-0.661490	1.02
	0.661486	-0.661486	1.13

Table 1. Results of the singularity analysis and GSIF calculation for different material configurations - see Fig. 13.
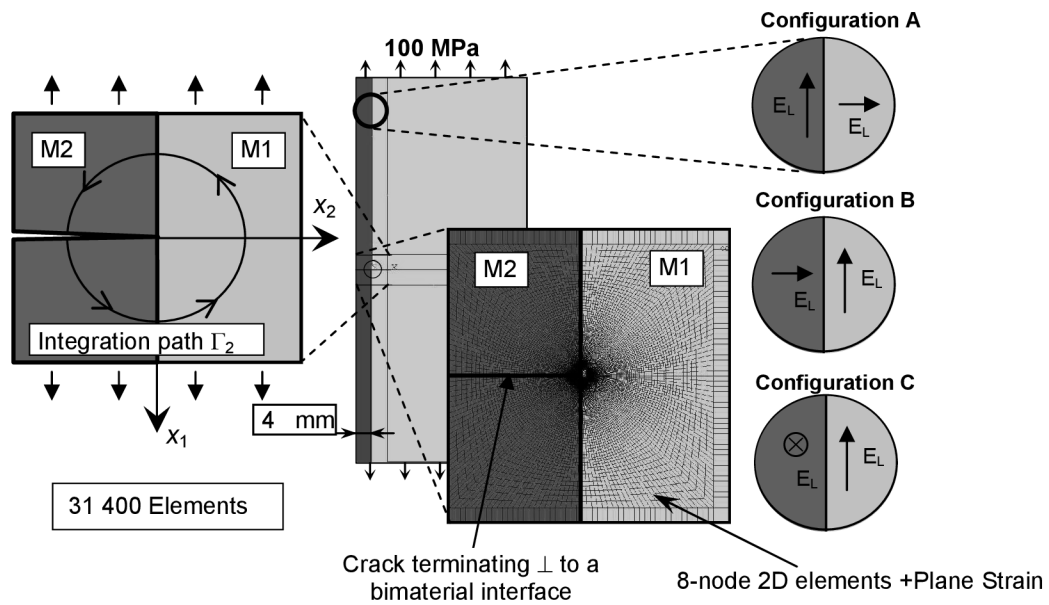
Fig. 13 2D finite element mesh used to model the cracked specimen.

Having eigenvalues and eigenvectors calculated, the near tip singular field and the auxiliary solution can be found from Equations (63)-(66), (71)-(72), and (74)-(75). In addition, expressions (77) and (78) can be set up which allows evaluating the GSIF from Eqs. (23) and (76). Both the stress field and the displacement field data obtained by means of FE computations were stored in files which were further used as an input for the calculation of the Ψ-integral using MATLAB 7.1. Calculated values of GSIF for different configurations are given in the Table 1.

It is a matter of interest to compare the stress field and the displacement field, calculated by FEM at some distance from the crack tip, with the analytical singular fields (63)-(66), (71)-(72) making use of the calculated values of GSIF. Specifically, a circular path with the radius $R=1$mm centred at the crack tip was chosen. The results are summarized in the Fig. 14-Fig. 17 and were also presented by author in [90].

Fig. 14 The courses of stress components, a) – c), and displacement components, d)- e), along the circular path with the radius $R = 1$ mm for the configuration A.

Fig. 15 Example of the courses of the auxiliary stress fields for the singular term, a) – c), and the auxiliary displacement components, d)- e), along the circular path with the radius $R = 1$ mm for the configuration A.

Fig. 16 The courses of stress components, a) – c), and displacement components, d)- e), along the circular path with the radius $R = 1$ mm for the configuration B.
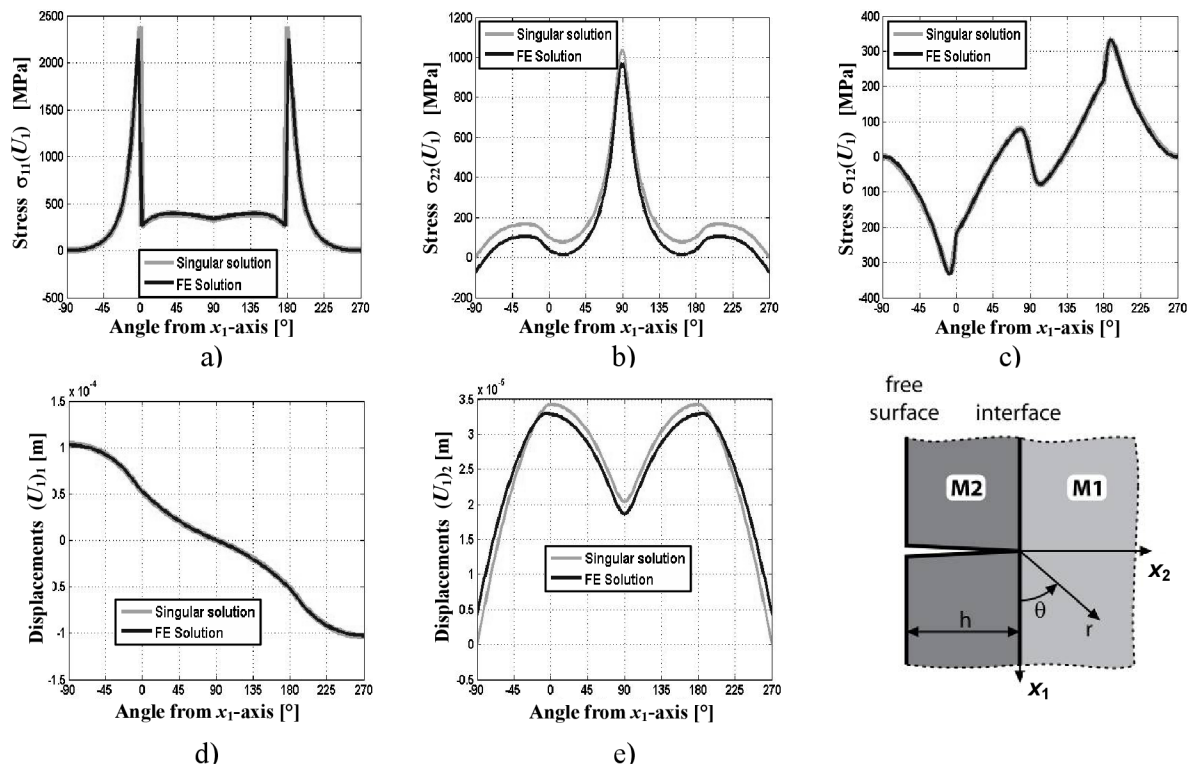

Fig. 17 The courses of stress components, a) – c), and displacement components, d)- e), along the circular path with the radius $R = 1$ mm for the configuration C.
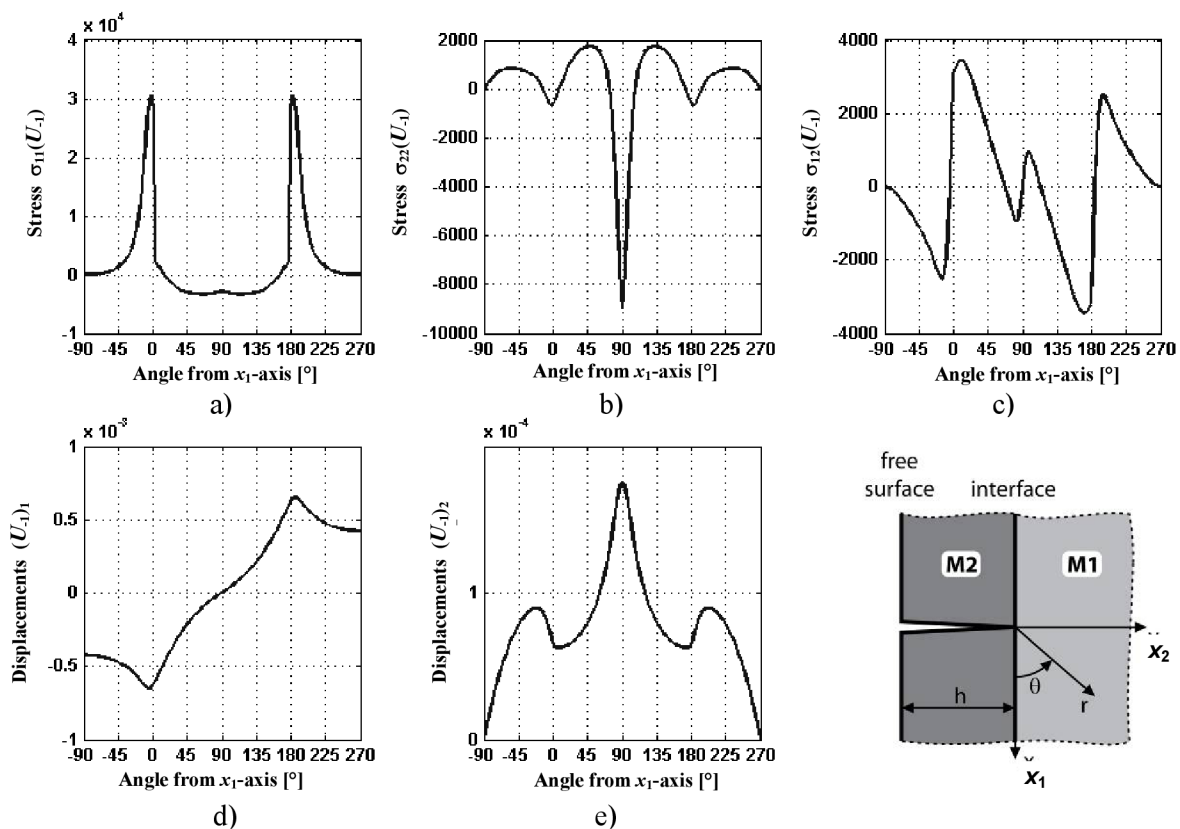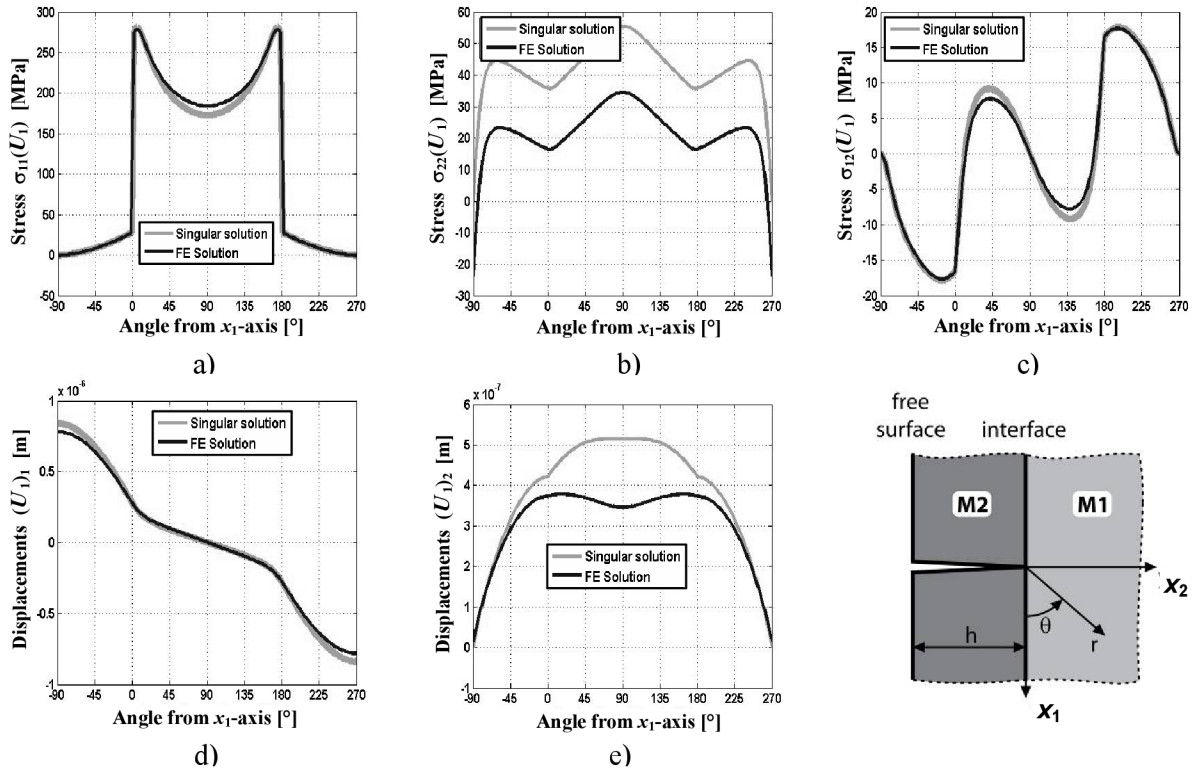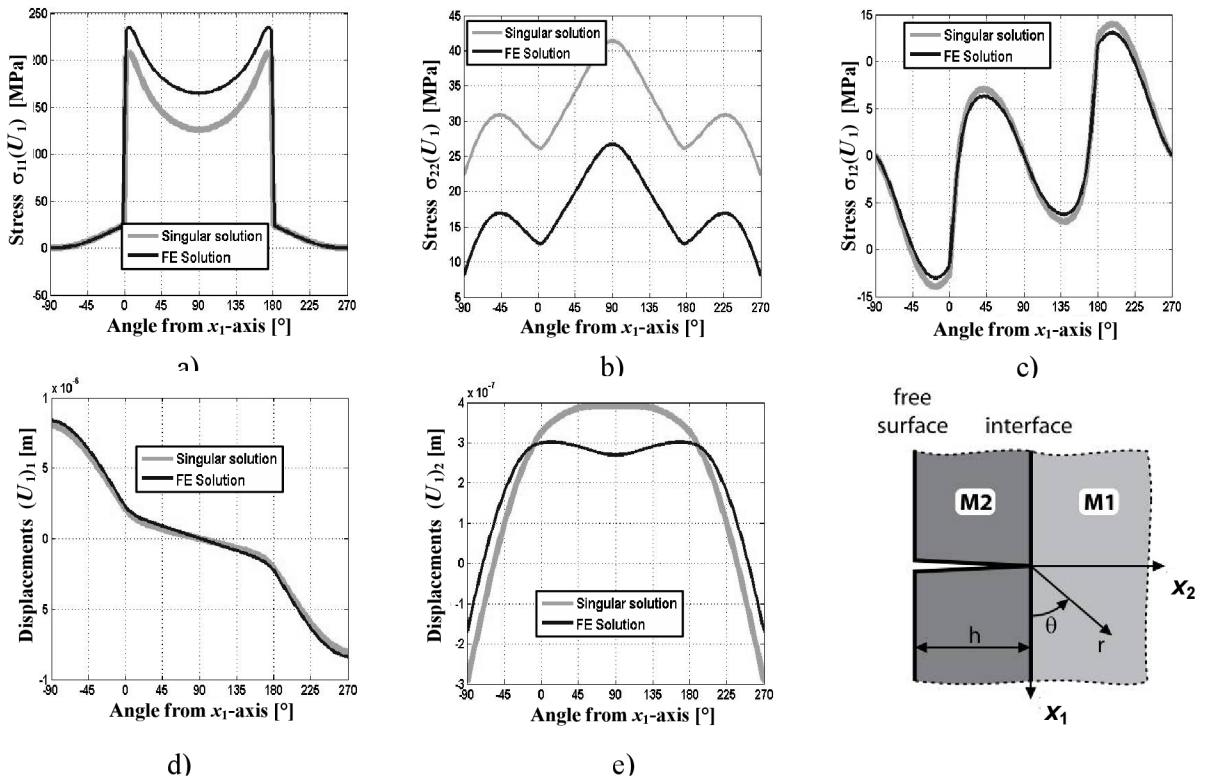
5.3 T-stress determination

5.3.1 T-stress calculation using the CDD technique

In general, numerical determination of T-stresses requires careful handling, because of their location in the vicinity of singular points. As suggested by Broberg [11], the T-stress can also be determined using dislocation arrays. The determination of T-stresses via dislocation arrays leads to a Fredholm equation that can be solved very accurately and provides more accurate values of T-stress comparing to common finite elements methods. However, the application of this method requires determining the solution for a dislocation in a complicated domain. Such an approach is not economical, but there are strategies, which may be employed to overcome this problem. These strategies start with a dislocation in a crack free infinite domain aiming to determine stresses along the curve $\partial\Omega$ which stands for the boundary of finite body. Introducing tractions along $\partial\Omega$ such that they negate stresses found previously and solving for stresses along the dislocation plane e.g. by FEM, one can finally derive the regular part of the dislocation solution for a specified finite domain. Thus, in the case of given finite bi-material plate, one obtains for stresses acting along $x_1 = 0$, $x_2 \in 2$

$$\sigma_{1i}\left(x_1=0,x_2\right)=-\frac{1}{4\pi}\sum_{\alpha}L_{i\alpha}^{II}p_{\alpha}^{II}\left[\sum_{\beta}\left(G_{\alpha\beta}\bar{M}_{\beta k}^{II}\frac{d_k}{p_{\alpha}y-\bar{p}_{\beta}x_{2o}}\right)+M_{\alpha k}^{II}\frac{d_k}{p_{\alpha}\left(x_2-x_{2o}\right)}\right]+C.C.+h_{1ik}\left(x_2,x_{2o}\right)d_k, \ x_2\in 2, (116)$$

where $h_{1ik}(x_2, x_{2o})$ denotes the regular part of the dislocation solution. Form a dislocation array by introducing the density function $f_k(x_{2o})$ and integrate over the crack length l_c

$$\sigma_{1i}\left(x_2\right)=-\frac{1}{4\pi}\left\{\sum_{\alpha}L_{i\alpha}^{II}\left[\sum_{\beta}\left(G_{\alpha\beta}\bar{M}_{\beta k}^{II}\frac{p_{\alpha}^{II}}{\bar{p}_{\beta}^{II}}\int_{l_c}\frac{f_k\left(x_{2o}\right)\mathrm{d}x_{2o}}{\frac{p_{\alpha}^{II}}{\bar{p}_{\beta}^{II}}x_2-x_{2o}}\right)+M_{\alpha k}^{II}\int_{l_c}\frac{f_k\left(x_{2o}\right)\mathrm{d}x_{2o}}{x_2-x_{2o}}\right]\right\}+$$

$$+\sum_{\alpha}\bar{L}_{i\alpha}^{II}\left[\sum_{\beta}\left(\bar{G}_{\alpha\beta}M_{\beta k}^{II}\frac{\bar{p}_{\alpha}^{II}}{p_{\beta}^{II}}\int_{l_c}\frac{f_k\left(x_{2o}\right)\mathrm{d}x_{2o}}{\frac{\bar{p}_{\alpha}^{II}}{p_{\beta}^{II}}x_2-x_{2o}}\right)+\bar{M}_{\alpha k}^{II}\int_{l_c}\frac{f_k\left(x_{2o}\right)\mathrm{d}x_{2o}}{x_2-x_{2o}}\right]\right\}+\int_{l_c}h_{1ik}\left(x_2,x_{2o}\right)f_k\left(x_{2o}\right)\mathrm{d}x_{2o}. \tag{117}$$

For a crack with traction free faces, the left side of (117) should equal to $-\sigma_{1i}^{appl}\left(x_2\right)$, the negated stresses in $x_1=0$ produced by the given boundary loads, acting on a plate with boundary $\partial\Omega$, but without cracks and dislocations. This gives integral equations for $f_k(x_{2o})$

$$\frac{1}{4\pi}\left\{\sum_{\alpha}L_{i\alpha}^{II}\left[\sum_{\beta}\left(G_{\alpha\beta}\bar{M}_{\beta k}^{II}\frac{p_{\alpha}^{II}}{\bar{p}_{\beta}^{II}}\int_{l_c}\frac{f_k\left(x_{2o}\right)\mathrm{d}x_{2o}}{\frac{p_{\alpha}^{II}}{\bar{p}_{\beta}^{II}}x_2-x_{2o}}\right)+M_{\alpha k}^{II}\int_{l_c}\frac{f_k\left(x_{2o}\right)\mathrm{d}x_{2o}}{x_2-x_{2o}}\right]\right\}+$$

$$+\sum_{\alpha}\bar{L}_{i\alpha}^{II}\left[\sum_{\beta}\left(\bar{G}_{\alpha\beta}M_{\beta k}^{II}\frac{\bar{p}_{\alpha}^{II}}{p_{\beta}^{II}}\int_{l_c}\frac{f_k\left(x_{2o}\right)\mathrm{d}x_{2o}}{\frac{\bar{p}_{\alpha}^{II}}{p_{\beta}^{II}}x_2-x_{2o}}\right)+\bar{M}_{\alpha k}^{II}\int_{l_c}\frac{f_k\left(x_{2o}\right)\mathrm{d}x_{2o}}{x_2-x_{2o}}\right]\right\}-\int_{l_c}h_{1ik}\left(x_2,x_{2o}\right)f_k\left(x_{2o}\right)\mathrm{d}x_{2o}=\sigma_{1i}^{appl}\left(x_2\right). \tag{118}$$

In general, numerical methods have to be used to determine $-\sigma_{1i}^{appl}(x_2)$. The crack may be closed at both ends (an internal crack) or only at one end (edge crack). In the second case, $f_k(x_{2o})$ has to be non-singular at an open end, and, e.g. for the case in Fig. 18 with the

left end at the point $y=-h$, $f_k(x_{2o})$ is sought in the form

$$f_k(x_{2o}) = \frac{g_k(x_{2o})}{x_{2o}^{1-\delta}},$$ (119)

where g_k is a bounded function. After $f_k(x_{2o})$ is found, all interesting quantities can be calculated, for instance the GSIF and/or T-stress. The T-stress component acting in the direction perpendicular to crack front is found after calculating σ_{22} (notice that the coordinate axis y lies in the crack direction), the expression for which is found in analogy with Eq. (117) after addition of $\sigma_{22}^{appl}(x_2)$. This stress is the tangential stress in $x_2 = 0$ produced by the given boundary loads, acting on a bi-material plate with the boundary $\partial\Omega$, but without crack and dislocations. Thus

$$\sigma_{22}(x_2) = \frac{1}{4\pi}\left\{\sum_\alpha L_{2\alpha}^{II}\left[\sum_\beta\left(G_{\alpha\beta}\bar{M}_{\beta k}^{II}\frac{1}{\bar{p}_\beta^{II}}\int_{l_c}\frac{f_k(x_{2o})\,dx_{2o}}{\frac{p_\alpha^{II}}{\bar{p}_\beta^{II}}x_2 - x_{2o}}\right) + \frac{M_{\alpha k}^{II}}{p_\alpha^{II}}\int_{l_c}\frac{f_k(x_{2o})\,dx_{2o}}{x_2 - x_{2o}}\right]\right\} +$$

$$+ \sum_\alpha \bar{L}_{2\alpha}^{II}\left[\sum_\beta\left(\bar{G}_{\alpha\beta}M_{\beta k}^{II}\frac{1}{p_\beta^{II}}\int_{l_c}\frac{f_k(x_{2o})\,dx_{2o}}{\frac{\bar{p}_\alpha^{II}}{p_\beta^{II}}x_2 - x_{2o}}\right) + \frac{\bar{M}_{\alpha k}^{II}}{\bar{p}_\alpha^{II}}\int_{l_c}\frac{f_k(x_{2o})\,dx_{2o}}{x_2 - x_{2o}}\right]\right\} +$$ (120)

$$+ \int_{l_c} h_{22k}(x_2, x_{2o})f_k(x_{2o})\,dx_{2o} + \sigma_{22}^{appl}(x_2),$$

where $h_{22k}(x_2, x_{2o})$ is found in the same way as $h_{1ik}(x_2, x_{2o})$. The singular integral in (120) can be eliminated using (118):

$$\sigma_{22}(x_2) = \frac{1}{4\pi}\left\{\sum_\alpha L_{2\alpha}^{II}\left[\sum_\beta\left(G_{\alpha\beta}\bar{M}_{\beta k}^{II}\frac{1}{\bar{p}_\beta^{II}}\int_{l_c}\frac{f_k(x_{2o})\,dx_{2o}}{\frac{p_\alpha^{II}}{\bar{p}_\beta^{II}}x_2 - x_{2o}}\right) + \right.\right.$$

(121)

$$\frac{M_{\alpha k}^{II}}{p_\alpha^{II}}\left(\sigma_{11}^{appl}(x_2) + \int_{l_c}h_{11k}(x_2, x_{2o})f_k(x_{2o})\,dx_{2o} - \frac{1}{4\pi}\left(\sum_\alpha L_{1\alpha}^{II}\left[\sum_\beta\left(G_{\alpha\beta}\bar{M}_{\beta 1}^{II}\frac{p_\alpha^{II}}{\bar{p}_\beta^{II}}\int_{l_c}\frac{f_1(x_{2o})\,dx_{2o}}{\frac{p_\alpha^{II}}{\bar{p}_\beta^{II}}x_2 - x_{2o}}\right)\right] + C.C.\right)\right)\right] + C.C.\right\}$$

$$+ \int_{l_c} h_{22k}(x_2, x_{2o})f_k(x_{2o})\,dx_{2o} + \sigma_{22}^{appl}(x_2).$$

The T-stress is found as $\sigma_{22}(x_2)\big|_{x_2 \to 0^-}$.

Remark 4: To determine the T-stress using the Ψ-integral, the auxiliary elastic field with stress singularity $\hat{\sigma}_{ij} \propto r^{-2}$ as r $\to$ 0 must be used and can be obtained from the solution for a concentrated moment acting at the crack tip.

In this work, an emphasis is put on the analysis of a crack in a thin layer terminating perpendicular to a layer/substrate interface. For a sufficiently large specimen, the semi-analytical solution for $h_{22k}(x_2, x_{2o})$ and $h_{1ik}(x_2, x_{2o})$ can be worked out due to recent findings by Choi and Earmme [37], who studied singularities in anisotropic trimaterials. Namely, authors in [37] used the so-called alternating technique that generalizes the formulas in Eqs. (50) and (51), and for the case in Fig. 18, it gives the following relations for potentials

$$\Phi_{\alpha}(z) = \begin{cases} \sum\limits_{n=1}^{\infty} \left[\Phi_{\alpha}^{n}(z) + \sum\limits_{\beta} \left(\mathbf{M}^{II}\overline{\mathbf{L}}^{II} \right)_{\alpha\beta} \Phi_{\beta}^{n} \left(z - p_{\alpha}^{II}h + p_{\beta}^{II}h \right) \right], & z \in 2, \\ C_{\alpha\beta}\overline{\Phi}_{\beta o}(z) + \sum\limits_{\beta}\sum\limits_{\gamma} \left(\mathbf{CM}^{II} \right)_{\alpha\beta} \overline{L}_{\beta\gamma}^{II} \sum\limits_{n=1}^{\infty} \Phi_{\beta}^{n} \left(z - p_{\beta}^{II}h + p_{\gamma}^{II}h \right), & z \in 1, \end{cases} \tag{122}$$

in which the recurrence formula for $\Phi_{\alpha}^{n}(z)$ is

$$\Phi_{\alpha}^{n+1}(z) = \begin{cases} \Phi_{\alpha o}(z) + \sum\limits_{\beta} G_{\alpha\beta}\overline{\Phi}_{\beta o}(z), & \text{if } n = 0, \\ \sum\limits_{\beta} G_{\alpha\beta} \left(\overline{\mathbf{M}}^{II}\mathbf{L}^{II} \right)_{\beta\gamma} \Phi_{\gamma}^{n} \left(z - \overline{p}_{\beta}^{II}h + \overline{p}_{\gamma}^{II}h \right), & \text{if } n = 1,2,3.. \end{cases} \tag{123}$$

Detailed parametric FEM computations were carried out to find bounds within which the semi-analytical solution (122) can be used for the specimen considered.
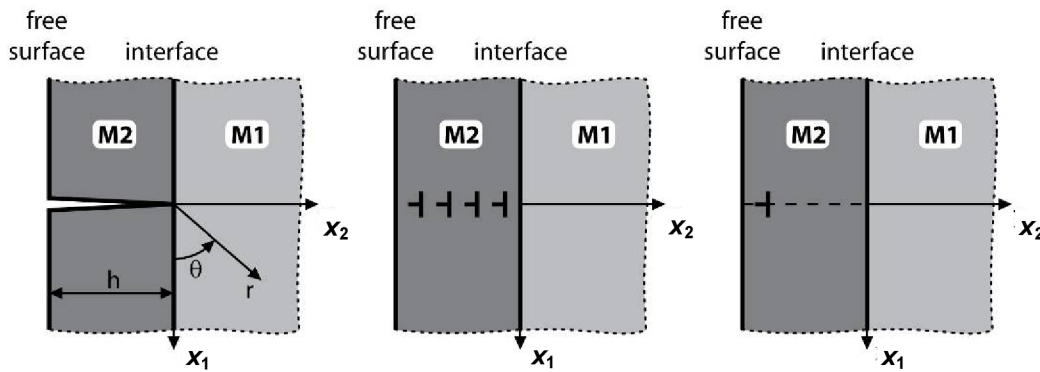
Fig. 18 Scheme of the bi-material half-plane.

5.4 Numerical calculations of GSIF and T-stress using CDD

Note that for all material configurations, the stress component σ_{22} calculated using FEM along the circular path is shifted against the singular term by a negative constant value. This shift can be attributed to the influence of T-stress. Remember that the FE solution contains all terms of the Williams-like asymptotic expansion for crack terminating at the interface. Apparently, at the distance $R=1$mm, the T-stress prevails over the higher order terms in the asymptotic expansion.

It is worth mentioning that the displacement component U_2 obtained from FEM exhibits a qualitatively different behaviour in comparison to the behaviour of the singular solution pertaining to the configurations B and C. Analogous to the stress field, this difference is due to the higher order terms in the asymptotic expansion which are included in the FE solution. Since the higher order terms in the asymptotic expansion of $U_2 \sim T.x_2$ +..., the difference depends on location. A confirmation of this statement provides Fig. 19 which shows the courses of the displacement component U_2 obtained by both the FEM and the singular solution along the circular path of the radius $R = 0.01$ mm and the path of the radius $R = 0.001$ mm, respectively. Clearly, with decreasing distance from the crack tip, the FE solution approaches the singular solution.

a)   b)
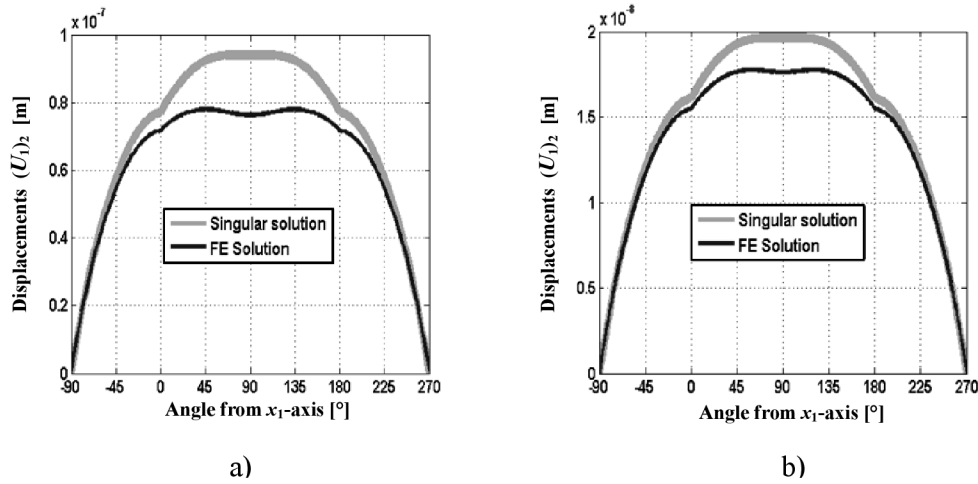
Fig. 19 The courses of the displacement component uy obtained by both the FEM and the singular solution a) along the circular path of the radius $R = 0.01$ mm; b) along the circular path of the radius $R = 0.001$ mm.

As to the comparison of the results pertaining to the configuration A with the results pertaining to the configurations B and C respectively, it should first be noted that the resolution of the graphs for the configurations B and C is of 2 orders higher than that used for the configuration A. Second, the exponent of the singularity in the case of the configuration A (strong singularity) is twice the size of that pertaining to the configurations B and C (weak singularity), see Table 1. Thus, the singular term dominated region for the configuration A is larger compared with the singular term dominated region for the configurations B and C respectively, which explains a minor influence of the higher order terms in the asymptotic expansion at the distance $R = 1$ mm.

Fig. 20 shows the component σ_{22}, calculated using FEM, plotted against the distance from the crack tip for $\theta = -\pi/2$ in case of the configuration A. As stated above, the T-stress is found as $\sigma_{22}(y)|_{x_2 \to 0^-}$. It is rather difficult to estimate this limit from Fig. 20 since the curve exhibits a turning point very close to the crack tip and sharply increases behind this point. Thus, a rough estimate of the T-stress is about of -50 MPa.
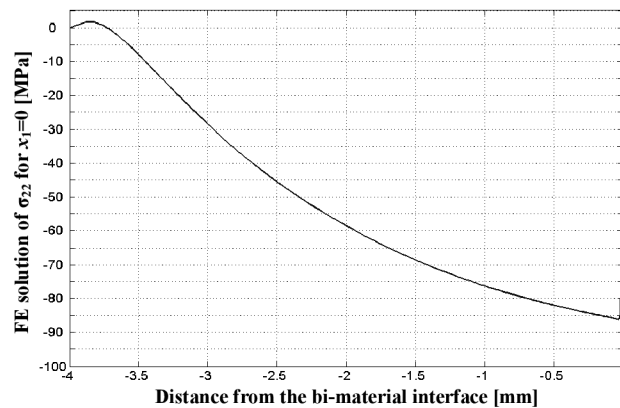
Fig. 20 Plot of FE solution for $\sigma_{22}(x_2)$ along the crack.

In the next step, detailed parametric FE computations were carried out to verify whether the semi-analytical solution (122) can be used for the given specimen. To this end, a dislocation with the Burgers vector $b = (0.01,0)$ mm was introduced into the FE mesh and the stress components σ_{11} and σ_{12} were calculated along the dislocation plane. The

dislocation was modelled as a constant displacement along the dislocation plane ensuring opposite sign of the displacement at the opposite faces of dislocation plane. The difference of the opposite displacements defines the Burgers vector. The value of the Burgers vector was carefully chosen with respect to the element size near the crack tip, which is of the order of μm.
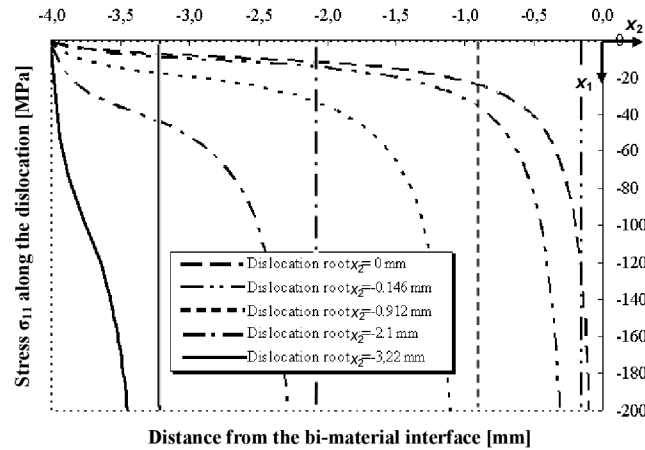
Fig. 21 Plots of the stress component σ_{11} versus the distance from the bi-material interface for several positions of the dislocation root along which the stress σ_{11} is plotted.

Fig. 22 compares results obtained for two substrate widths, i.e. 40 mm and 100 mm. Apparently there is only a slight difference in values of the stress σ_{11}. Subsequent increase of the substrate width did not provide any marked change of σ_{11}. The FE calculations of σ_{11} obtained for the width of substrate of 100 mm were compared with the calculations of σ_{11} based upon the semi-analytical solution (122) when the infinite series was truncated at n=4. This comparison is displayed in Fig. 23 revealing a very good agreement between FE calculations and the calculations based upon truncated series in Eq. (122). Thus, for the given specimen, the truncated semi-analytical solution of Choi and Earmme [37] can be used as a fundamental solution for crack modelling using DDT – see also [89].
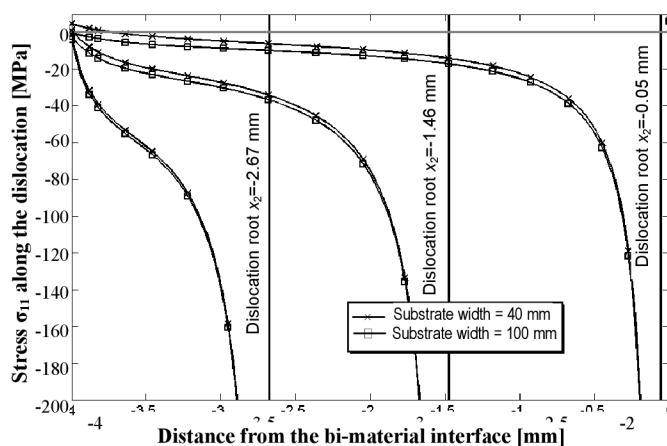
Fig. 22 Plots of the stress component σ_{11} versus the distance from the bi-material interface for several positions of the dislocation root and two substrate widths.

The integral equation (118), in which the regular kernel $h_{11k}(x_2, x_{2o})$ was obtained from the truncated semi-analytical solution of Choi and Earmme [37], was solved numerically for the unknown dislocation density in the case of the orthotropic bi-materials specified above. The procedure involves the reduction of the integral equations and constraints to a system of algebraic equations using the collocation technique. It is useful to separate the singular part from the regular part of the integral equation. Since the material interface and the crack plane correspond to the material symmetry planes, and the specimen is subjected to simple tensile loading conditions, the Burgers vector component b_2 is equal to zero. In such a case, there is more expedient to work directly with the dislocation density $\delta b_1 / \delta x_2$ rather then with the density function f_k introduced in Eq. (56). The density function f_k follows from Eq. (56) as

$$f_k\left(x_{2o}\right) = B_{ki}^{-1} \frac{\delta b_i}{\delta x_{2o}} = B_{k1}^{-1} \frac{\delta b_1}{\delta x_{2o}} = B_{k1}^{-1} b_1' \tag{124}$$

and Eq. (118) simplifies to the form

$$\sigma_{11}^{appl}\left(x_2\right) - \frac{1}{4\pi} \left\{ 2\operatorname{Re}\left(B_{11}^{-1}\right) \int_{-h}^{0} \frac{b_1'\left(x_{2o}\right)}{x_{2o} - x_2} dx_{2o} + \int_{-h}^{0} b_1'\left(x_{2o}\right) K_{x_1 x_1}\left(x_2, x_{2o}\right) dx_{2o} \right\} = 0. \tag{125}$$

The regular kernel $K_{x_1 x_1}(x_2, x_{2o})$ describes the interaction of a dislocation with the bi-material interface and with the free surface. $K_{x_1 x_1}(x_2, x_{2o})$ possesses a complicated structure and depends on elastic constants of both materials and on the layer width. Due to its algebraic complexity, it is not given here. The substitutions

$$s = 2\frac{x_{2o}}{h} + 1, \quad t = 2\frac{x_{2o}}{h} + 1, \tag{126}$$

allow to reduce the integral equation (125) to the form

$$\sigma_{11}^{appl}\left(t\right) - \frac{1}{4\pi} \left\{ 2\operatorname{Re}\left(B_{11}^{-1}\right) \int_{-1}^{1} \frac{b_1'\left(s\right)}{s - t} ds + \frac{h}{2} \int_{-1}^{1} b_1'\left(s\right) K_{x_1 x_1}\left(t, s\right) ds \right\} = 0. \tag{127}$$

Fig. 23 Comparison of FE calculations of σ_{11} with the calculations of σ_{11} based upon the semi-analytical solution (122) with the infinite series truncated at n = 4.

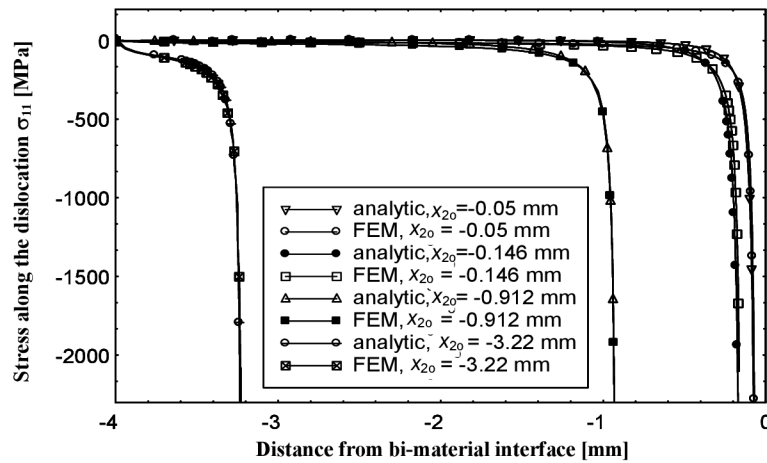The dislocation density is sought in the form $b_1'(s) = (1-s)^{\delta-1}(1+s)^{1-\delta} g(s)$, where $g(s)$ is a bounded function. As mentioned elsewhere [26], this choice means that $b_1'(-1)$ must vanish, i.e. that crack faces at the mouth are forced to be parallel and the solution is over-constrained. Nevertheless, this incorrect end-point behaviour at the crack mouth had a negligible effect on the calculated stress intensity factor. The integral equation may be solved using the Gauss-Jacobi quadrature. The function $g(s)$ is sought in the form of linear combination of Jacobi polynomials $P_n^{(1-\delta,\delta-1)}(s)$

$$g(s) = \sum_{n=0}^{\infty} c_n P_n^{(1-\delta,\delta-1)}(s) \cong \sum_{n=0}^{N_B} c_n P_n^{(1-\delta,\delta-1)}(s). \tag{128}$$

The kernel $K_{x_1x_1}(t,s)$ in Eq. (127) is known only in discrete points $s = s_i$ and its dependence on the variable s is approximated by the following truncated series of Jacobi polynomials:

$$K_{x_1x_1}(t_i,s) \cong \sum_{n=0}^{N_f} d_n(t_i) P_n^{(1-\delta,\delta-1)}(s). \tag{129}$$

The preceding approximation is performed for collocation points $t = t_i$, $i = 0,1\ldots.$ N_B - 1 at which the boundary conditions along crack faces, $\sigma_{11} = \sigma_{12} = 0$, are controlled. A convenient set is given by

$$t_i = \cos\left(\frac{\pi}{2}\frac{2i+1}{N_B}\right). \tag{130}$$

Using Eqs. (128) and (129) in the integral equation (127) and employing the integral relations given in [19] one obtains the system of algebraic equations through which the unknown coefficients c_n can be evaluated:

$$\sigma_{11}^{appl}(t_i) - \frac{1}{2}\text{Re}\left(B_{11}^{-1}\right)\sum_{n=0}^{N_B} c_n\left[\cot(\pi\delta)(1-t_i)^{1-\delta}(1+t_i)^{\delta-1} P_n^{(1-\delta,\delta-1)}(t_i) - \right.$$
$$\left. -\frac{\Gamma(\delta)\Gamma(n+\delta)}{\Gamma(n+1)}\text{F}\left(n+1,-n;\delta;\frac{1-t_i}{2}\right)\right] + \frac{h}{2}\sum_{n=0}^{N} c_n d_n(t_i)\Theta_n^{(1-\delta,\delta-1)} = 0, \tag{131}$$

where

$$\Theta_n^{(1-\delta,\delta-1)} = \frac{2}{2n+1}\frac{\Gamma(n-\delta+2)\Gamma(n+\delta)}{n!\Gamma(n+1)}, \tag{132}$$

$$N = \begin{cases} N_B \text{ for } N_B \le N_f \\ N_f \text{ for } N_B > N_f \end{cases}. \tag{133}$$

$\text{F}(n_1,n_2,n_3,x_1)$ stands for the hypergeometric function, $\Gamma(n)$ is the Gamma function and $i= 0,1..N_B -1$.

The strength of the singularity in stress may be quantified in the usual way by defining the GSIF H. Using the function-theoretic methods described in [26], [19] one obtains:

$$H = \lim_{r \to 0} \sqrt{2\pi} r^{\delta-1} \sigma_{11}(r, \theta = \pi/2) =$$

$$= \mathrm{Re} \left\{ \frac{i e^{i\pi(\delta-1)} \sqrt{2\pi}}{1 - e^{2\pi i(\delta-1)}} g(1) \left[L_{11}^I p_1^I \left(\frac{C_{11} M_{11}^{II}}{p_1^{II}} \left(\frac{p_1^{II}}{p_1^I} h \right)^{\delta-1} + \frac{C_{12} M_{21}^{II}}{p_2^{II}} \left(\frac{p_2^{II}}{p_1^I} h \right)^{\delta-1} \right) + \right. \right.$$

$$\left. \left. + L_{12}^I p_2^I \left(\frac{C_{21} M_{11}^{II}}{p_1^{II}} \left(\frac{p_1^{II}}{p_2^I} h \right)^{\delta-1} + \frac{C_{22} M_{21}^{II}}{p_2^{II}} \left(\frac{p_2^{II}}{p_2^I} h \right)^{\delta-1} \right) \right] \right\}, \qquad (134)$$

where $g(1)$ denotes a value of the function g, see Eq. (128), at $s = 1$; other quantities were already defined above.

Having found the dislocation density, the T-stress can be calculated using Eq. (121). Both, the calculation of the GSIF and the calculation of the T-stress were carried out only for the configuration A, specified in the Fig. 13. Table 2 contains the result of calculations of the GSIF and the T-stress, and illustrates the convergence of the numerical scheme with increasing number of terms N_f in the truncated series (129) while keeping the number of collocation point N_B equal to 10. Apparently, the results are in a good accordance with those obtained using FEM.

N_f	GSIF – H [MPa.m$^{1-\delta}$]	T – stress [MPa]
10	5.45214	-48.72973
20	6.31186	-48.12727
30	6.42548	-48.05871
40	6.44138	-48.05004
50	6.44394	-48.04889
60	6.44439	-48.04879
70	6.44447	-48.04886
80	6.44448	-48.04891
90	6.44448	-48.04885
100	6.44448	-48.04893

Table 2 Calculations of the GSIF and the T-stress using the dislocation technique, $N_B = 10$.

Example of the courses of stresses and displacements for the solution of the T-stress term are using the relations (63)-(66) and (74)-(75) depicted in the following Fig. 24. The corresponding courses of the auxiliary solution are shown in the Fig. 25. Both figures are for the configuration A (see Fig. 13) and the circular path with the radius R=1mm centred at the crack tip.

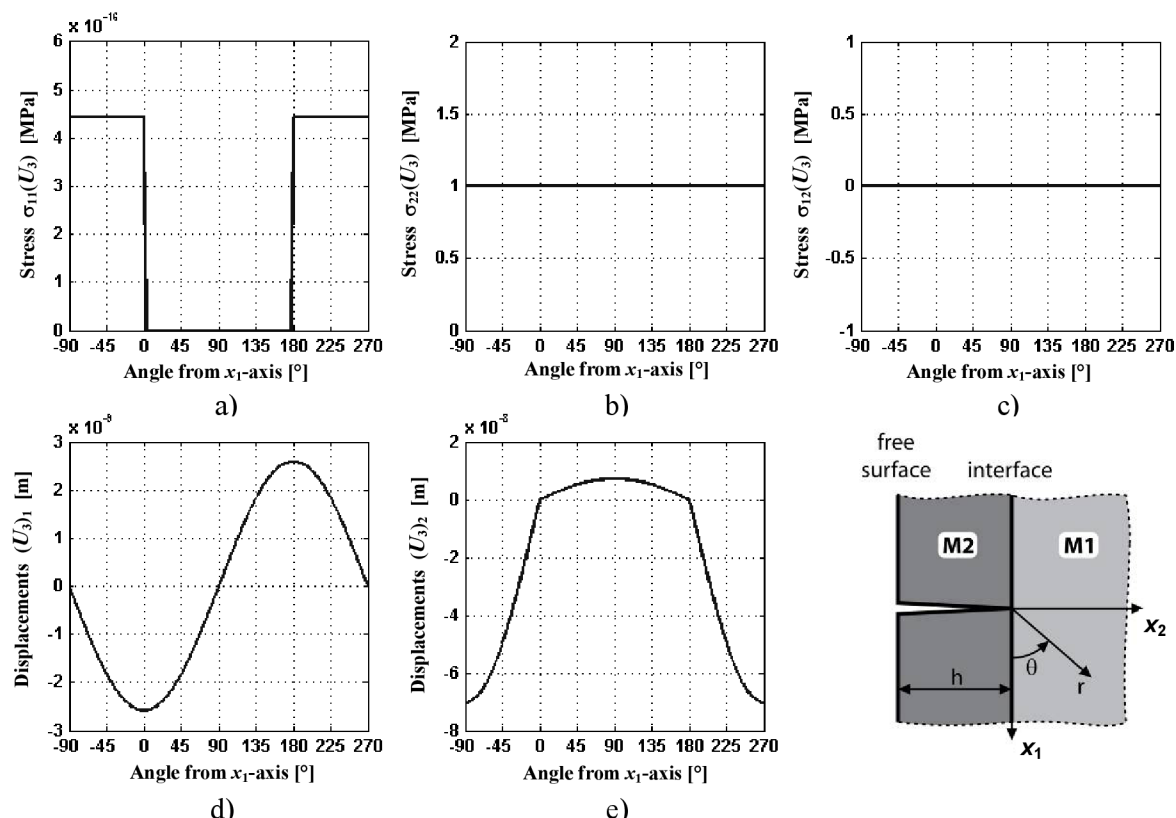**Fig. 24** The courses of the stress fields for the T-stress term: a) – c), and the displacement components, d)- e), along the circular path with the radius $R = 1$ mm for the configuration A.
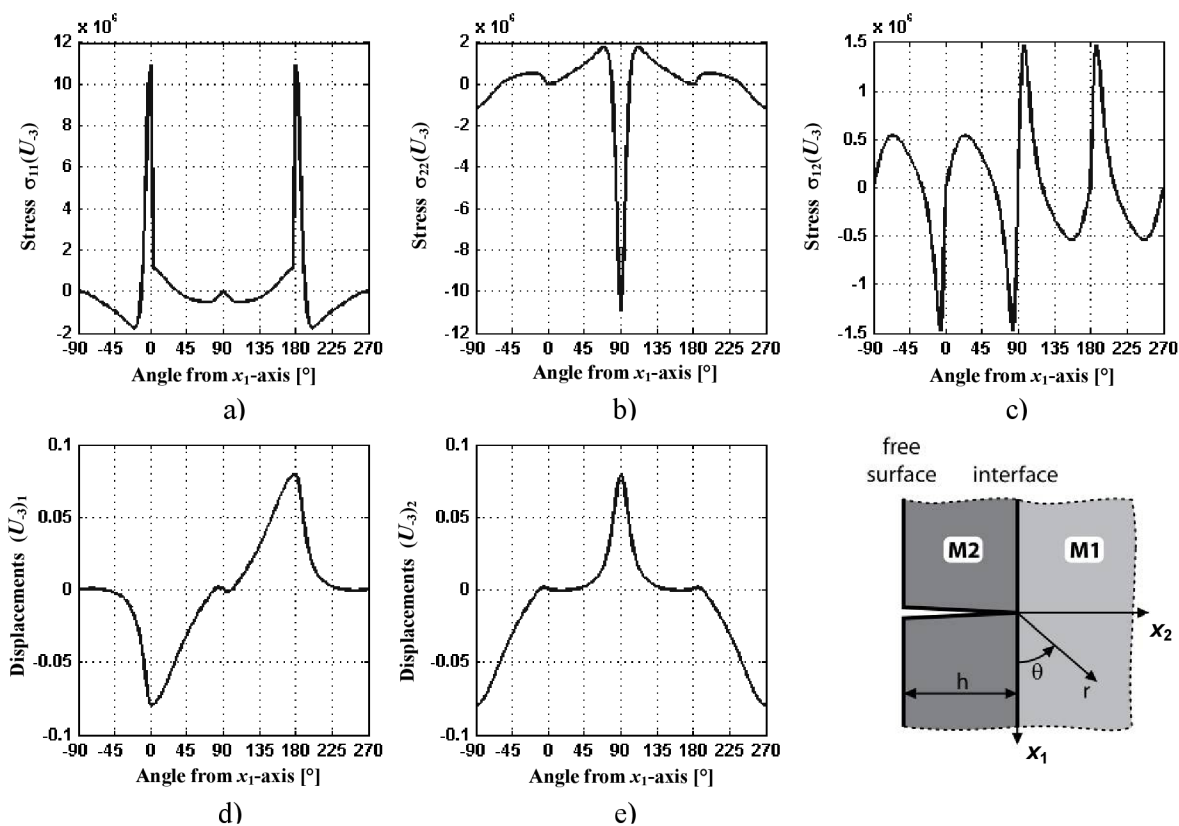

Fig. 25 The courses of the auxiliary stress fields for the T-stress term: a) – c), and the auxiliary displacement components, d)- e), along the circular path with the radius $R = 1$ mm for the configuration A.

6 Solution of the crack bridging problem

6.1 Model of the crack bridging

For a simple sliding with a constant τ_s, Aveston et al.[4]; Budiansky et al.[14]; Budiansky and Amazigo [12]; Marshall et al. [59] suggested a model of bridging fibres represented by a continuous distribution of bridging springs obeying the quadratic bridging law

$$v\left(x_2\right) = \left(\frac{\sigma_{br}\left(x_2\right)}{\beta}\right)^2, \tag{135}$$

where $v(x_2)$ is the displacement of the upper crack face (one half of the COD) and the constant β is defined as follows

$$\beta = \left[\frac{4c_f^2 E_f E^2 \tau_s}{R_f\left(1-c_f\right)^2 E_m^2}\right]^{1/2}, \tag{136}$$

where R_f is the fibre radius, E_f, E_m are material characteristics of the fibre and the matrix respectively, c_f fibre fracture volume and τ_s is a interface slipping shear resistance stress. Relation (135) follows from an estimate of the extra elastic elongation of a long bridging fibre that occurs in regions on the two sides of a matrix crack wherein frictionally constrained sliding occurs.

Under the assumption that the strength of the fibres, σ_{0f}, has a single, deterministic value, failure occurs when the bridging spring stress at the original crack tips reaches $\sigma = c_f \sigma_{0f}$. Because of fibres/matrix slip, the fibre stress decays linearly from the crack mid-plane. Since the stress on the fibres has a maximum value in the plane of the matrix crack, the assumption of a single strength value of fibres leads to the conclusion that fibres break in the plane of the crack. Consequently, the prediction of composite toughness and strength may be unduly conservative. The reason is that with dispersion in the fibre tensile strength, fibres may fracture within the matrix rather than at bridged faces of the matrix crack, thereby leading to frictionally constrained fibre pullout before final failure occurs, and so leading to enhanced composite strength. Apparently, fractured fibres still contribute to the bridging stresses as they have to be pulled out from the matrix. The relative contribution of intact fibres, which act as elastic ligaments between the crack faces, and broken ones within the matrix, which are eventually pulled out, is analysed assuming that the fibre strength follows the Weibull statistics [94]. This gave an explicit expression for the average stress transferred by the fibres across crack given by

$$\hat{\sigma}_{br} = \underbrace{\sigma_{br} \exp\left[-\left(\frac{\sigma_{br}}{c_f \Sigma}\right)^{m_w+1}\right]}_{\text{fraction of intact fibres}} + \sigma_P \underbrace{\left\{1 - \exp\left[-\left(\frac{\sigma_{br}}{c_f \Sigma}\right)^{m_w+1}\right]\right\}}_{\text{fraction of broken fibres}}, \tag{137}$$

where σ_P is the average stress exerted by the broken fibres pulled out from the matrix, and $\exp\left[-\left(\sigma_{br}/c_f\Sigma\right)^{m_w+1}\right]$ stands for the fraction of intact fibres in the crack wake. The fibre strength distribution is introduced through the parameter $\Sigma = \left(m_w+1\right)^{1/(m_w+1)} \sigma_{0f}$, which includes the information on the fibre tensile properties given by the Weibull modulus m_w and the fibre characteristic strength σ_{0f}. Physically, there is typically one flaw of strength σ_{0f} in a length l_{cf} of fibre and $l_{cf} = R_f\sigma_{0f}/\tau_s$ is twice the fibre slip length at an applied stress of σ_{0f}.

Using a simple shear-lag approach, the stress transferred by the broken fibres as they are pulled out from the matrix can be expressed as

$$\sigma_P = \frac{2c_f\tau_s}{R_f}\left(\langle h\rangle - v\right),$$

(138)

where $\langle h\rangle$ is the average distance from the fibre failure position to the crack plane for the broken fibres which was computed in [94] as

$$\langle h\rangle = \frac{R}{2\tau_s}\frac{\Sigma}{m_w+1}\Gamma\left(\frac{m_w+2}{m_w+1}\right) = \frac{l_{cf}}{2}\frac{1}{\left(m_w+1\right)^{m_w/(m_w+1)}}\Gamma\left(\frac{m_w+2}{m_w+1}\right),$$

(139)

where Γ is the Gamma function. Fibre pullout, thus, scales directly with the characteristic length l_{cf}.

6.2 Bridged crack modelling using the weight function method

It should be noted that an important task in the analysis of a component with a bridged crack is the calculation of the bridging stress intensity factor for a specified bridging stress-crack opening displacement relationship. There are a great number of methods available for the determination of stress intensity factors such as e.g. the finite element method with contact elements, the boundary element method, the boundary collocation method, or the weight function method. High efficiency of the weight function method consists in that once the weight function(s) are known the bridging intensity factor can be easily calculated for any bridging stress distribution by evaluating the integral of the form of Eq.(27). Moreover, it allows setting up a bridging stress-crack opening displacement relationship by analysing the experimental crack opening displacement data and solving an integral equation. The weight function method has been extensively used to the modelling of bridged crack problems [21]. For a complicated domain, the weight function has to be obtained numerically, e.g. from FEM calculations [78]. As to a crack impinging on the bi-material interface, such calculations have not been reported yet. The weight function is obtained numerically by performing a number of calculations of the generalised stress intensity factor due to unit line load applied to the crack face at arbitrary points. To this end, an application of the reciprocal theorem seems to be very efficient.

6.2.1 Bridging stress - recurrent calculations

To calculate the bridging stress along the crack face, the crack face displacements in dependence on given load are needed. The recurrent calculations are used and consist of the following steps:

1) In the first step, the magnitude of loading stress σ_1 is estimated and the displacement of the upper crack face for unbridged crack is calculated:

$$v_{appl(1)}\left(x_2\right) = v_{appl0}\left(x_2\right)\sigma_1,$$

(140)

where v_{appl0} is the displacement of the upper crack face caused by the unit stress σ_0.
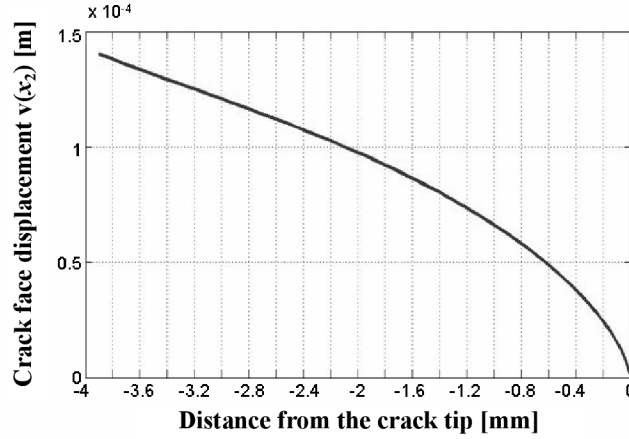
Fig. 26 Displacement of the upper crack face caused by the unit loading σ_0.

2) After the first step (n=1) of the recurrent calculation of the loading stress σ, an estimate of the total displacement of the upper crack face is recurrently refined in several sub-steps. In the first sub-step of the recurrent calculation the total displacement, $v_{n,1}$, n=1, is set equal to $v_{br(n,m_n)} < 0$, n=1 (i.e. the bridged crack face opening will be equal to the unbridged crack face opening in case of loading stress σ_l). Then the bridging stress is computed via one of the following relation (bridging law) – a) is a already mentioned simple quadratic bridging law and b) is an advanced bridging law taking into consideration the statistical distribution of the fibre strength along the fibre length – see [43] or [45]:

$$a) \quad \sigma_{br(n,1)}\left(x_2\right) = \beta\sqrt{v_{n,1}\left(x_2\right)}, \ n = 1 \tag{141}$$

$$b) \quad \hat{\sigma}_{br(n,1)} = \sigma_{br(n,1)} \exp\left[-\left(\frac{\sigma_{br(n,1)}}{c_f \Sigma}\right)^{m_w+1}\right] + \sigma_{P(n,1)}\left\{1 - \exp\left[-\left(\frac{\sigma_{br(n,1)}}{c_f \Sigma}\right)^{m_w+1}\right]\right\}, \tag{142}$$

$$\underbrace{\hspace{5.5cm}}_{\text{fraction of intact fibres}} \qquad \underbrace{\hspace{5.5cm}}_{\text{fraction of broken fibres}}$$

where $\sigma_{br(n,1)}\left(x_2\right) = \beta\sqrt{v_{n,1}\left(x_2\right)}$, $n = 1$, $\sigma_{P(n,1)}\left(x_2\right) = \dfrac{2c_f \tau_s}{R_f}\left(\langle h\rangle - v_{n,1}\left(x_2\right)\right)$, $n = 1$. This makes possible to estimate the corresponding crack face displacement $v_{br(n,1)}$ using the FEM solution for the crack face displacement due to isolated force F acting in position x_{2i} .from the relation

$$v_{br(n,1)}\left(x_2\right) = \sum_i v_{br0}\left(x_2, x_{2i}\right)\hat{\sigma}_{br(n,1)}\left(x_{2i}\right)S\left(x_{2i}\right), \tag{143}$$

where $v_{br0}(x_2, x_{2i})$ is the crack face displacement due to the isolated force F acting at the point x_{2i}, see Fig. 27, $S(x_{2i})$ is the area per node at the point x_{2i} and the summation is performed over all node rows behind the crack tip.

3) In next sub-steps the total crack face displacement is refined as follows:

$$v_{n,m_n+1}\left(x_2\right) = v_{n,m_n} \frac{v_{appl(n)}\left(x_2\right)}{v_{n,m_n}\left(x_2\right) - v_{br(n,m_n)}\left(x_2\right)}, \ n = 1, \tag{144}$$

where $v_{br(n,m_n)} < 0$ is the crack face displacement due to the bridging stress $\hat{\sigma}_{br(n,m_n)}\left(x_2\right) = \hat{\sigma}_{br(n,m_n)}\left[v_{n,m_n}\left(x_2\right)\right]$.

Note that for the exact value of $v_{br}(x_2)$ the ratio in Eq. (144) equals to one. The recurrent calculation stops when

$$\left(\frac{v_{n,m_n+1}\left(x_2\right)-v_{n,m_n}\left(x_2\right)}{v_{n,m_n+1}\left(x_2\right)}\right)^2 < TOL, \tag{145}$$

where the left side of the inequality is a square of the approximation in the actual and preceding step over the approximation in actual step and *TOL* is a prescribed tolerance.
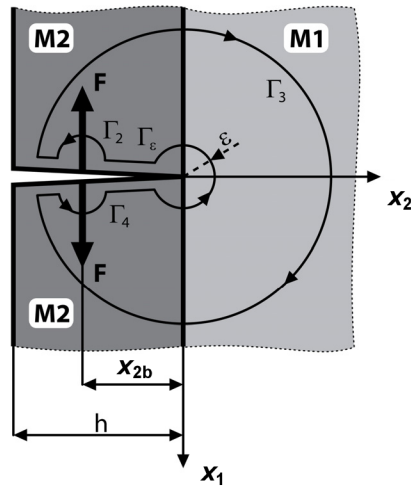
Fig. 27 A pair of line forces acting on the crack faces and the integration path.
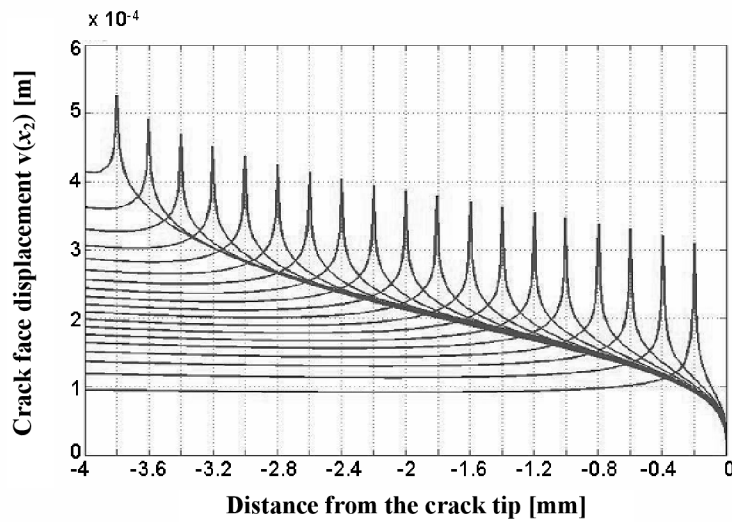
Fig. 28 Displacement of the upper crack face for a number of positions of the applied line load.

6.2.2 Weight function - application of the Ψ-integral

Now assume that a pair of line forces acts on the crack faces at a point x_{2b}, see Fig. 27. Other loading is absent. Eq. (20) modifies with help of Eq. (22) as

$$\int_{\Gamma_3}\left[\sigma_{ij}\left(\mathbf{U}\right)n_i\ r^{-\delta_1}u_{-1_j}-\sigma_{ij}\left(r^{-\delta_1}\mathbf{u}_{-1}\right)n_i U_j\right]\mathrm{d}s+2\mathbf{F}r^{-\delta_1}\mathbf{u}_{-1}=H\Psi\left(r^{\delta_1}\mathbf{u}_1,r^{-\delta_1}\mathbf{u}_{-1}\right). \quad (146)$$

Γ_3 is an arbitrary contour enclosing a domain containing both the crack tip and the pair of line forces. By definition, the weight function $W(x_{2b},h)$ follows as

$$W\equiv\frac{H}{|\mathbf{F}|}=\frac{1}{|\mathbf{F}|}\frac{\int_{\Gamma_3}\left[\sigma_{ij}\left(\mathbf{U}\right)n_i\ r^{-\delta_1}u_{-1_j}-\sigma_{ij}\left(r^{-\delta_1}\mathbf{u}_{-1}\right)n_i U_j\right]\mathrm{d}s+2\mathbf{F}r^{-\delta_1}\mathbf{u}_{-1}}{\Psi\left(r^{\delta_1}\mathbf{u}_1,r^{-\delta_1}\mathbf{u}_{-1}\right)}. \quad (147)$$

A finite element solution $\mathbf{U}^h$ was used as an approximation for $\mathbf{U}$ in Eq. (147). Having calculated a value of the weight function W for sufficiently large number of line force positions, the generalized bridging stress intensity factor, H_{br}, can be obtained for an arbitrary bridging stress distribution $\sigma_{br}(x_2)$ as

$$H_{br}=\int_{-h}^{0}W\left(x_2,h\right)\sigma_{br}\left(x_2\right)\mathrm{d}x_2. \quad (148)$$

With elastic constants of two layers M1 and M2 specified in the preceding section, the weight function were calculated for several ratio of the layer thicknesses h/B. The results are presented in Fig. 29 in dimensionless form such that the product $W.h^\delta$ is plotted against the dimensionless distance from the crack tip $-x_2/h$. The influence of the longitudinal modulus E_L is demonstrated in Fig. 30.
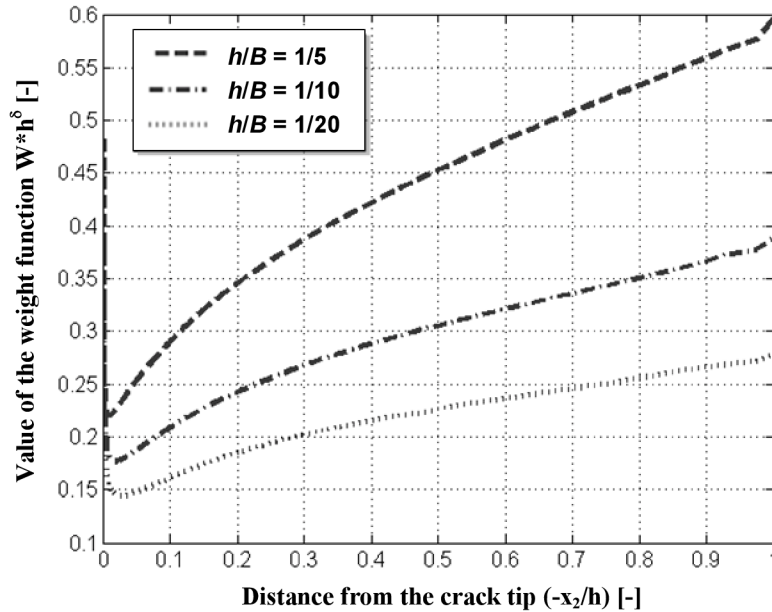
Fig. 29 Bi-material normalized weight function against the dimensionless distance from the crack tip for several values of the ratio h/B.
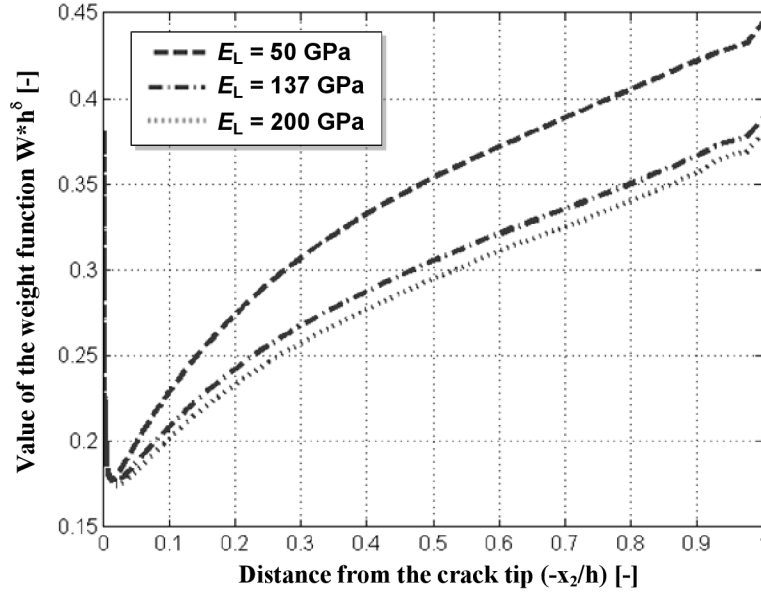
Fig. 30 Bi-material normalized weight function against the dimensionless distance from the crack tip for several values of the longitudinal modulus E_L.

6.3   Bridged crack modelling using the CDD technique

An integral equation is obtained by choosing the dislocation distribution to meet the traction conditions along of the line of the crack and within the crack bridging zone. Since the material interface and the crack plane correspond to the material symmetry planes, and the specimen is subjected to simple tensile loading conditions, the Burgers vector component b_{x_2} is equal to zero. The integral equation then reads

$$\sigma_{11}^{appl}\left(x_2\right)+\hat{\sigma}_{br}\left(v\left(x_2\right)\right)+\frac{1}{2\pi}\mathrm{Re}\left\{\sum_{\beta=1}^{2}L_{1\beta}^{II}\sum_{\alpha=1}^{2}M_{\beta\alpha}^{II}\left(B_{\alpha 1}^{II}\right)^{-1}\right\}\int_{-h}^{0}\frac{b_1\left(x_{2o}\right)}{x_{2o}-x_2}dx_{2o}+\int_{-h}^{0}b_1\left(x_{2o}\right)K_{x_1x_1}\left(x_2,x_{2o}\right)dx_{2o}=0. \quad (149)$$

$\sigma_{1i}^{appl}\left(x_2\right)$ denotes the negated stresses in $x_1=0$ produced by the given boundary loads, acting on a specimen with boundary $\partial\Omega$, but without cracks and dislocations, and $\hat{\sigma}_{br}\left(\delta\left(x_2\right)\right)$ is the bridging stress from Eqs. (141) or (142). The integral equation (149) must be complemented with the condition

$$v\left(x_2\right)=\frac{1}{2}\int_{x_2}^{0}b_1\left(x_{2o}\right)\mathrm{d}\,x_{2o}, \quad (150)$$

which relates the crack face displacement v to the dislocation density b_{x_l}. The regular kernel $K_{x_lx_l}(x_2, x_{2o})$ was obtained from the truncated semi-analytical solution of [37]. The regular kernel describes the interaction of a dislocation with the bi-material interface and with the free surface as well. $K_{x_lx_l}(x_2, x_{2o})$ possesses a complicated structure and depends on elastic constants of both materials and on the layer thickness. It can expressed as the truncated series

$$K_{x_1x_1}\left(x_2,x_{2o}\right)=\sum_{n=1}^{N_K}\frac{k_{1,n}'}{k_{2,n}'x_{2o}-k_{3,n}'x_2-k_{4,n}'}. \quad (151)$$

The $k_{i,n}'$ are the constants developed from the alternating technique discussed above. The substitutions

$$s = 2\frac{x_{2o}}{h} + 1, \quad t = 2\frac{x_2}{h} + 1 \tag{152}$$

allow to reduce the integral equation (149) to the form

$$\sigma_{11}^{appl}(x_2) + \hat{\sigma}_{br}(v(x_2)) + \frac{1}{2\pi}\mathrm{Re}\left\{\sum_{\beta=1}^{2}L_{1\beta}^{II}\sum_{\alpha=1}^{2}M_{\beta\alpha}^{II}(B_{\alpha 1}^{II})^{-1}\right\}\int_{-1}^{1}\frac{b_1(s)}{s-t}ds + \int_{-1}^{1}b_1(s)K_{x_1x_1}(t,s)ds = 0, \tag{153}$$

where

$$K_{x_1x_1}(t,s) = \sum_{n=1}^{N_K}\frac{k_{1,n}}{k_{2,n}s - k_{3,n}t - k_{4,n}}. \tag{154}$$

The procedure involves the reduction of the integral equation and constraints to a system of algebraic equations using the collocation technique.

The dislocation density is sought in the form $b_1(s) = (1-s)^{\delta-1}(1+s)^{1-\delta}g(s)$, where $g(s)$ is a bounded function. As mentioned elsewhere [26], this choice means that $b_1(-1)$ must vanish, i.e. that crack faces at the mouth are forced to be parallel and the solution is over-constrained. Nevertheless, this incorrect end-point behaviour at the crack mouth had a negligible effect on the calculated stress intensity factor.

Note that a more acceptable form of the density function can be found in the work [18].

$$b_1^*(s) = \frac{g(s)}{(1-s)^{1-\delta}} \tag{155}$$

The used quadrature method has to be adapted to the singularities of $b_1^*(s)$ using Jacobi polynomials $P_n^{(\delta-1,0)}(s)$ at all. The form of the density function $b_1^*(s)$ disables to receive the closed form solution of the regular kernel $K_{x_1x_1}(s, t)$, which has to be approximated [74]. To avoid the application of $P_n^{(\delta-1,0)}(s)$ polynomials, the following approach of the density function can be used [18]

$$b_1^{**}(s) = b_{-1}g_{-1}(s) + \left(\frac{1+s}{1-s}\right)^{1-\delta}g(s) \tag{156}$$

where $g_{-1}(s)$ is some known, bounded function on [−1, 1] such that $g_{-1}(s) = -1$ and b_{-1} is an unknown constant, which equals $b_1^{**}(-1)$. This equality serves as an additional consistency condition. This form of the density function corrects the crack opening at the crack mouth without the influence on the stress intensity factor. Because the objective of the paper is to find the stress intensity factor, the crack mouth opening correction will be omitted below.

The integral equation may be solved using the Gauss-Jacobi quadrature. The function $g(s)$ is sought in the form of linear combination of Jacobi polynomials $P_n^{(\delta-1,1-\delta)}(s)$

$$g(s) = \sum_{n=0}^{\infty}c_nP_n^{(\delta-1,1-\delta)}(s) \cong \sum_{n=0}^{N_B}c_nP_n^{(\delta-1,1-\delta)}(s) \tag{157}$$

This allows to express the integral containing the regular kernel $K_{x_1x_1}(t,s)$ in the closed form by integrating each component of the truncated series in Eq. (151). It is useful to apply the theory of the curve complex integrals developed by [67] because of the ambiguous behaviour of the $(1-s)^{\delta-1}(1+s)^{1-\delta}$ around the points $s = \pm 1$. Hence, after the integration, the regular part of the integral equation (153) can be written as

$$\int_{-1}^{1} b_1(s) K_{x_1 x_1}(t,s) ds = \sum_{n=1}^{N_K} \int_{-1}^{1} \frac{k_{1,n} b_1(s) ds}{k_{2,n} s - k_{3,n} t - k_{4,n}} = \sum_{n=1}^{N_K} \frac{k_{1,n}}{k_{2,n}} \int_{-1}^{1} \left(\frac{1+s}{1-s}\right)^{1-\delta} \frac{k_{1,n} g(s) ds}{s - (k_{3,n} t + k_{4,n})/k_{2,n}} = \tag{158}$$

$$= \sum_{n=1}^{N_K} \frac{k_{1,n}}{k_{2,n}} \frac{2\pi i e^{i(1-\delta)\pi}}{1 - e^{i(1-\delta)2\pi}} \left[\left| \frac{(k_{3,n}t + k_{4,n}) + k_{2,n}}{(k_{3,n}t + k_{4,n}) - k_{2,n}} \right|^{1-\delta} g((k_{3,n}t + k_{4,n})/k_{2,n}) - (\alpha_n s^n + \ldots + \alpha_0) \Big|_{s=(k_{3,n}t+k_{4,n})/k_{2,n}} \right],$$

where α_n are the coefficients of the pole at the infinity of the function $b_1(z) = (1-z)^{\delta-1}(1+z)^{1-\delta} g(z)$.

The boundary conditions along crack faces, $\sigma_{11} = \sigma_{12} = 0$, are controlled at the collocation points $t = t_i$, $i = 0,1\ldots N_B - 1$ given by

$$t_i = \cos\left(\frac{\pi}{2} \frac{2i+1}{N_B}\right). \tag{159}$$

Using Eqs. (154) and (157) in the integral equation (153) and employing the integral relations given in [19] one obtains the system of algebraic equations through which the unknown coefficients c_n can be evaluated:

$$\sigma_{11}^{appl}(t_i) + \frac{1}{2} \text{Re} \left\{ \sum_{\beta=1}^{2} L_{1\beta}^{II} \sum_{\alpha=1}^{2} M_{\beta\alpha}^{II} (B_{\alpha1}^{II})^{-1} \right\} \sum_{n=0}^{N_B} c_n \left[\cot(\pi\delta)(1-t_i)^{1-\delta}(1+t_i)^{\delta-1} P_n^{(\delta-1,1-\delta)}(t_i) - \right.$$

$$\left. \frac{\Gamma(\delta)\Gamma(n-(1-\delta)+1)}{\Gamma(n+1)} F\left(n+1,-n,1-(1-\delta);\frac{1-t_i}{2}\right) \right] + \tag{160}$$

$$+ \sum_{m=1}^{N_k} \frac{k_{1,m}}{k_{2,m}} \frac{2\pi i e^{i(1-\delta)\pi}}{1 - e^{i(1-\delta)2\pi}} \left[\left| \frac{(k_{3,m}t_i + k_{4,m}) + k_{2,m}}{(k_{3,m}t_i + k_{4,m}) - k_{2,m}} \right|^{1-\delta} \sum_{n=0}^{N_B} c_n P_n^{(\delta-1,1-\delta)}((k_{3,m}t_i + k_{4,m})/k_{2,m}) - (\alpha_m s^m + \ldots + \alpha_0) \Big|_{s=(k_{3,m}t_i+k_{4,m})/k_{2,m}} \right] = 0,$$

where $F(n_1,n_2;n_3;x_1)$ stands for the hypergeometric function, $\Gamma(n)$ is the Gamma function and $i = 0,1..N_B - 1$. The strength of the singularity in stress may be quantified in the usual way by defining the local generalized SIF H_{tip}. Using the function-theoretic methods [19], [26] one obtains

$$H_{tip} = \lim_{r \to 0} \sqrt{2\pi} r^{1-\delta} \sigma_{11}(r, \theta = \pi/2) =$$

$$= \sqrt{2\pi} h^{1-\delta} g(1) \text{Re} \left\{ \frac{i e^{(1-\delta)i\pi}}{1 - e^{2\pi i(1-\delta)}} \left[L_{11}^I \left(C_{11} \left(M_{11}^{II} (B_{11}^{II})^{-1} + M_{12}^{II} (B_{21}^{II})^{-1} \right) \left| \frac{p_1^{II}}{p_1^I} \right|^{-\delta} + \right. \right. \tag{161}$$

$$+ C_{12} \left(M_{21}^{II} (B_{11}^{II})^{-1} + M_{22}^{II} (B_{21}^{II})^{-1} \right) \left| \frac{p_2^{II}}{p_1^I} \right|^{-\delta} \right) + L_{12}^I \left(C_{21} \left(M_{11}^{II} (B_{11}^{II})^{-1} + M_{12}^{II} (B_{21}^{II})^{-1} \right) \left| \frac{p_1^{II}}{p_2^I} \right|^{-\delta} +$$

$$+ C_{22} \left(M_{21}^{II} (B_{11}^{II})^{-1} + M_{22}^{II} (B_{21}^{II})^{-1} \right) \left| \frac{p_2^{II}}{p_2^I} \right|^{-\delta} \right) \right] \right\},$$

where $g(1)$ denotes a value of the function $g(s)$, see Eq. (157), at $s = 1$; other quantities were already defined above.

6.4 Numerical results

At first the results of numerical analysis based upon the weight function method are presented. The advanced bridging model described in the section 6.1 was applied with the fibre volume fraction $c_f = 0.4$, the fibre radius $R_f = 7$ μm, the sliding resistance $\tau_s = 6$ MPa, the fibre Young modulus $E_f = 228\ 000$ MPa, and the matrix Young modulus $E_m = 76\ 000$ MPa. A parametric study was performed in order to examine an influence of the Weibull modulus m_w and the fibre characteristic strength σ_{0f}. As stated in the section 6.2.1, the total displacements of the crack surface $v = v_{appl} + v_{br}$ is to be derived. Fig. 31 reveals the influence of the Weibull modulus upon the crack opening displacement. As expected, the lower value of m_w leads to the lower crack opening due to higher bridging stress. Similarly, higher value of the fibre characteristic strength σ_{0f} leads to higher bridging stress, and as a consequence, the crack opening displacement is reduced, see Fig. 32. Similar results as for the statistical model can be found in the author's contribution [91] also for the simple Budiansky's model.

Fig. 31 Applied, closure and total crack opening displacement for several values of the Weibull modulus m_w, $\sigma_{0f} = 2300$ MPa. The applied tensile loading: a) $\sigma_0 = 90$ MPa, b) $\sigma_0 = 140$ MPa.

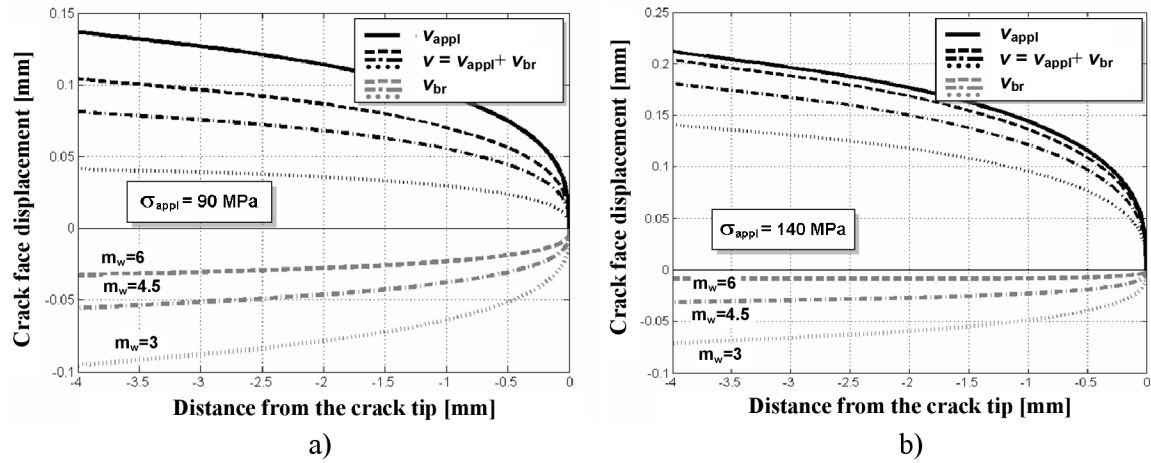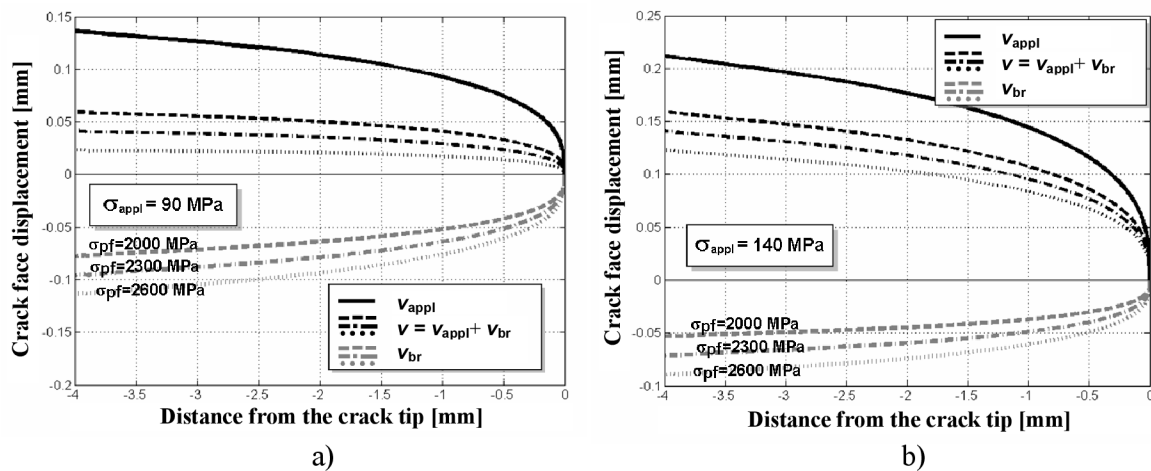**Fig. 32** Applied, closure and total crack opening displacement for several values of the Weibull modulus m_w, $\sigma_{0f} = 2300$ MPa. The applied tensile loading: a) $\sigma_0 = 90$ MPa, b) $\sigma_0 = 140$ MPa.

Having calculated the total displacements of the crack surface, the bridging stress distribution can be obtained and, consequently, the generalized bridging stress intensity

factor, H_{br} can be evaluated from Eq. (148). The results of these calculations are presented for the advanced statistical model in the Fig. 33, where the remote, bridging, and local generalized stress intensity factors are plotted as functions of the applied tensile loading of the bi-material specimen σ_0 for several values of the Weibull modulus and the fibre characteristic strength σ_{0f}.
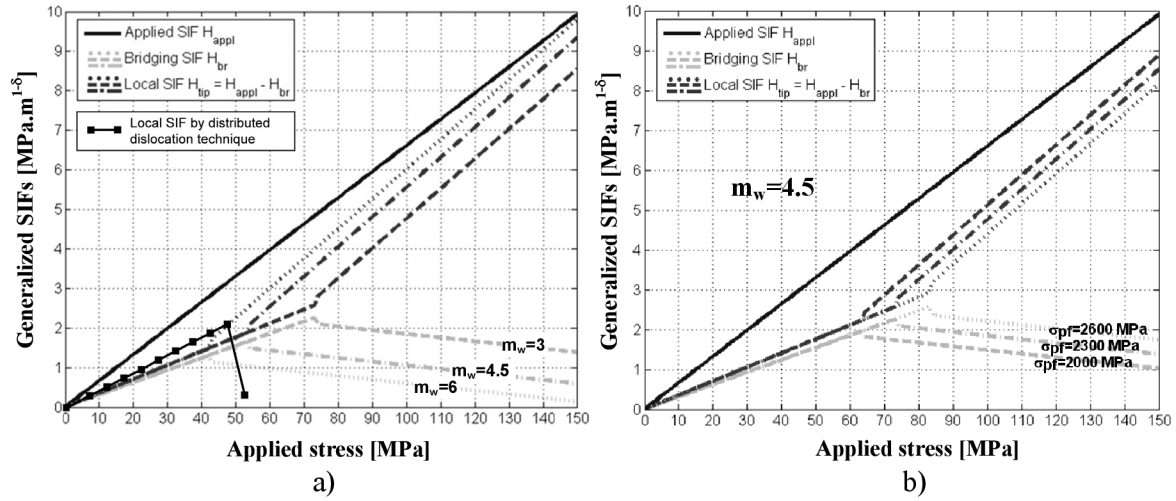
Fig. 33 Remote, bridging, and local GSIFs (for the advanced statistical model) plotted as functions of the applied tensile loading σ_0 for a) several values of the Weibull modulus, b) several values of the fibre characteristic strength σ_{0f}.

It is evident that the local generalized SIF decreases with the decrease of the Weibull modulus m_w and with the increase of the characteristic fibre strength σ_{0f}. Also observe that the bridging generalized SIF (grey lines) begins to decrease with loading when the broken fibres are pulled out from the matrix. As a consequence, the resulting local generalized SIF begins to increase more rapidly with loading. When doing the same analysis with the simpler Budiansky's model, all fibres are broken within very small change of the applied tensile stress σ_0 (when the bridging stress reaches the critical value of the fibre strenght). Consequently, the bridging GSIF H_{br} drops to zero. The local GSIF H_{tip} then reaches the value of H_{appl} and no more bridging effect is present.

It is a matter of interest to compare the calculations based upon the weight functions method with the results obtained using the distribution dislocation technique (DDT) according to Eq. (161). So far there are available only numerical data for the first stage of loading when the broken fibres are not massively pulled out from the matrix. There exist certain numerical problems for the subsequent stage of loading which were not resolved satisfactorily yet. Nevertheless, Fig. 33 shows that the results obtained via DDT in the first stage of loading are in a good accordance with the results obtained via weight functions method.

Remark 5: A method of solution should be sought for the situation when the preferred directions of the orthotropic material may not coincide with the reference axes in addition to having the crack and/or the material interface with an arbitrary orientation. Apparently, the concept of generalized anisotropic bi-material applies to such situations. In the case of the generalized anisotropic bi-material some aspects of the solution take place. Because of the participation of the all components of the displacement vector and stress tensor, the potentials describe the stress and displacement field must be extended to three ones, as well as the number of the eigenvalues characterizing each material.

7 Fracture criterion for the assessment of the general stress concentrator stability in orthotropic media

7.1 Fracture criterion

As it was presented in the work [48], both energy and stress criteria are necessary conditions for fracture but neither one nor the other are sufficient. Experiments by Parvizi et al. - [72] on transverse cracking in cross-ply laminates corroborate this assumption. Thanks to the singularity at the tip of the notch, the incremental form of the energy criterion gives a lower bound of admissible crack lengths. On the contrary, the stress criterion leads to an upper bound. The consistency between these two conditions provides a general form of a criterion for the crack nucleation. It enjoys the desirable property of coinciding with the usual Griffith criterion to study the crack growth and with the stress criterion for the uniform traction along a straight edge.

7.1.1 The energy criterion

We consider the initial state of a loaded structure to be elasto-static. The equilibrium state is characterized by a potential energy W_p and a zero kinetic energy $W_k = 0$. Next, we consider the same structure after the onset of a new crack or the growth of a pre-existing one. The start point of the energy criterion is an unquestionable balance between these two states:

$$\delta W_p + \delta W_k + G_c \delta a = 0. \tag{162}$$

Here, δW_p and δW_k are the changes respectively in potential and kinetic energy. The newly created crack surface is denoted δa (length per unit thickness) and G_c is the fracture energy per unit surface, the so-called toughness. Since the initial state is static δW_k ≥0 and a necessary condition for fracture derives from (162):

$$-\frac{\delta W_p}{\delta a} \geq G_c \quad \Rightarrow \quad 0 \geq \delta W_p + G_c \delta a. \tag{163}$$

This incremental form of the energy criterion is the foundation of Finite Fracture Mechanics (FFM). It requires the knowledge of the crack increment surface δa. If the crack grows continuously, the above condition must hold for any small surface change δa, then considering the limit $\delta a \to 0$ leads to the differential (Griffith) form of (163):

$$-\frac{\delta W_p}{\delta a} = G \geq G_c, \tag{164}$$

where G is the energy release rate. Nevertheless, there are some contra-indications to the use of the differential form (164) as explained in the section 4.3.

7.1.2 The stress criterion

The stress criterion is based on the data of a critical tension σ_c (or shear τ_c), the so-called strength, that a material can bear before it breaks. The fracture of a surface occurs if:

$$\sigma \geq \sigma_c \ (\text{or} \ \tau \geq \tau_c), \tag{165}$$

where σ and τ are the tension and shear components of the stress tensor acting on the surface. Such a criterion sounds like a necessary and sufficient condition for the failure. A counter example will evidence that in fact it is only a necessary one.

Applied to a crack onset at a notch, these two criteria lead to the following paradox. The Griffith criterion (164) is unable to predict such a mechanism. The energy release rate

G vanishes and thus can never reach the critical toughness G_c. On the other hand, the notch tip is singular, the stress field tends to infinity when approaching this point and then tension and shear stress components are always above the material strength. The stress criterion would thus conclude systematically to a crack onset whatever the applied load. The two criteria are contradictory. Moreover, neither one nor the other conclusion agrees with the experiments. It can be observed that such a notch is a privileged site for the crack nucleation and the fracture does occur at this point but not for any small applied load.

The main conclusion is that, when fracture occurs, the two criteria (energy and strength) are fulfilled simultaneously, even if one often hides the other. Both are necessary conditions and together they seem to form a sufficient one. Based on this ascertainment, a criterion for the crack onset at a notch is derived in the next section using the singular stress field around the notch tip. It ensures that the two criteria hold true. Giving both the toughness G_c and the strength σ_c brings us to define a characteristic length for the crack onset. The failure is assumed to be a sudden and quasi-spontaneous mechanism as proposed e.g. by [5], [72] and [102].
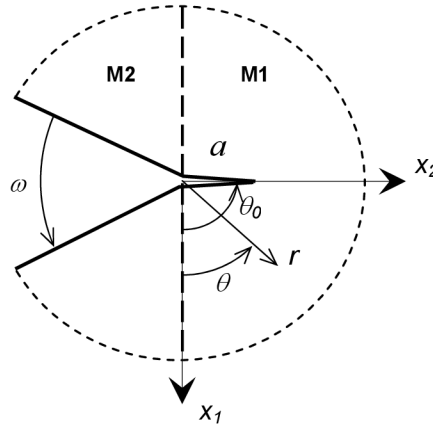
Fig. 34 The cracked notch in a heterogeneous material.

7.1.3 The crack initiation length

The potential energy change at a crack onset in the direction θ_0 is written [48]:

$$-\delta W_p = H^2 K(\omega, \theta_0) a^{2\delta} d \tag{166}$$

where a is the small newly created crack length and d the width of the specimen (considering plane elasticity). The coefficient $K(\omega, \theta_0)$ is a scaling term depending on the local geometry (ω) and on the direction of fracture (θ_0) - see [49]. The condition (163) becomes:

$$-\delta W_p \geq G^c a d \quad \Rightarrow \quad H^2 K(\omega, \theta_0) a^{2\delta-1} \geq G_c. \tag{167}$$

The stress intensity factor H is proportional to the applied load by κ :

$$H = \kappa \cdot \sigma_{appl} \tag{168}$$

and (167) is a lower bound for the increment lengths a :

$$a^{2\delta-1} \geq \frac{G_c}{K(\omega, \theta_0) \kappa^2 \sigma_{appl}^2} \quad (\text{where } 2\delta - 1 > 0). \tag{169}$$

Since the applied load at onset cannot be infinitely large, the increment length a cannot be infinitely small. At onset, there is a jump from 0 to a which is an illustration of the FFM. Of course, this lower bound must be compatible with the asymptotic framework, it has to be small with respect to a characteristic length of the structure. However, it is

essential to recall that the energy balance is only a necessary condition.

The failure is assumed to occur spontaneously, which seems reasonable since the critical traction acts uniformly all over the fracture surface. This condition will be extended to the present case to provide an upper bound for the crack extension length. The singular tension σ_θ (i.e. the component $\sigma_{\theta\theta}$ of the stress tensor) at a distance a from the tip in the direction θ_0 reads:

$$\sigma_\theta\left(a,\theta_0\right)=Ha^{\delta-1}s_\theta\left(\theta_0\right)+....$$ (170)

It is a decreasing function of a. If the condition (165) holds at any point between 0 and a, it becomes an upper bound for a:

$$\sigma_\theta\left(a,\theta_0\right)\geq\sigma_c\Rightarrow a^{1-\delta}\leq\frac{\kappa\sigma_{appl}s_\theta\left(\theta_0\right)}{\sigma_c}\quad\text{(where }1-\delta>0\text{)}$$ (171)

Once again, this bound must be small in order to be sure that higher order terms in (170) are negligible.

For a small applied load σ_{appl}, (169) leads to a high lower bound while (171) defines an incompatible low upper bound, thus for a monotonically increasing load the solution is achieved when equality holds in both (169) and (171). The increment length derives from these two equalities:

$$a_0=\frac{G_c s_\theta^2\left(\theta_0\right)}{K\left(\omega,\theta_0\right)\sigma_c^2}$$ (172)

The structure embedding the micro-crack with length a_0 is in equilibrium in the sense that the elastic solution is characterized by the absence of a kinetic energy. However, it is highly unstable from the point of view of the growing crack. The energy release rate at the tip of the newly created crack is an increasing function of its length and moreover is still above the critical toughness G_c in appropriate direction:

$$G\left(a_0\right)=2\delta G_c\quad\left(\delta>1/2\right),$$ (173)

where $G(a_0)$ is computed using (166) and considering a small increment δa to a_0:

$$G\left(a_0\right)=-\lim_{\delta\ell\to0}\frac{W_p\left(a_0+\delta a\right)-W_p\left(a_0\right)}{\delta a}$$ (174)

Here, $W_p(a_0)$ denotes the potential energy of a structure embedding a crack with length a_0. In a first step the crack length jumps from 0 to a_0 and then grows continuously.

There are two particular cases. If $\delta=1$ (the straight edge, $\omega=\pi$) the stress criterion does not provide any upper bound:

$$a\geq\frac{G_c s_\theta\left(\theta_0\right)^2}{K\left(\pi,\theta_0\right)\sigma_c^2}$$ (175)

If $\delta=1/2$ (the crack tip $\omega=0$), it is the energy criterion that does not impose any lower bound:

$$a\leq\frac{G_c s_\theta\left(\theta_0\right)^2}{K\left(0,\theta_0\right)\sigma_c^2}.$$ (176)

The crack increment length can be taken as small as needed and the differential approach of Griffith is permitted.

7.1.4 The crack onset criterion

It is now commonly admitted that the intensity factor H is the relevant parameter to define a crack onset criterion at a notch. It takes the Irwin-like form:

$$H \geq H_c, \tag{177}$$

where H_c is the critical value of the stress intensity factor. Herein, it will be derived in terms of material toughness G_c and strength σ_c (or τ_c). Replacing for (172) in (167) or (171) leads to a condition for a crack onset in the direction θ_0:

$$H \geq \left(\frac{G_c}{K(\omega, \theta_0)} \right)^{1-\delta} \left(\frac{\sigma_c}{s_\theta(\theta_0)} \right)^{2\delta-1}. \tag{178}$$

The direction of fracture θ_c can be determined by the minimum value of the right-hand side of (178). Note, that in a homogeneous material, if the fracture properties are isotropic, i.e. independent of the direction of fracture, G_c and σ_c are constant and θ_c is characterized by:

$$K(\omega, \theta_c)^{1-\delta} s_\theta(\theta_c)^{2\delta-1} \geq K(\omega, \theta_0)^{1-\delta} s_\theta(\theta_0)^{2\delta-1}, \quad \forall \theta_0, \, 0 < \theta_0 < 2\pi - \omega. \tag{179}$$

This condition coincides with the G-max branching criterion for a crack ($\delta = 1/2$) [50].

If the direction θ_c is known, function $s_\theta(\theta_c)$ can be normalized ($s_\theta(\theta_c) = 1$) and this enjoys the following very nice property that it coincides with the Griffith criterion for a crack ($\delta = 1/2$) and with the strength criterion for a straight edge ($\delta = 1$).

For a notch in a homogeneous isotropic material under symmetric loading the fracture direction is known $\theta_c = \pi - \omega/2$, thus we can define a critical value H_c of H as a function of the material properties σ_c and G_c and of the notch angle ω (through δ and K):

$$H_c \geq \left(\frac{G_c}{K(\omega)} \right)^{1-\delta} \sigma_c^{2\delta-1}. \tag{180}$$

where $K(\omega)$ stands for $K(\omega, \pi - \omega/2)$.

7.2 Perturbation analysis

In the case of a matrix crack impinging on the interface, a differential energy analysis is unsuitable due to the discontinuity in the elastic properties: finite crack extensions a_d, a_p are to be considered (instead of infinitesimal one) and the competition between deflection and penetration at the interface is evaluated using the condition that the crack will follow the path which maximizes the additional energy ΔW released by the fracture. If crack deflection occurs preferentially to penetration at the interface, the following condition must be satisfied:

$$\Delta W_d = \delta W_d - G_c^i a_d > \Delta W_p = \delta W_p - G_c^1 a_p, \tag{181}$$

where G_c^i is the interface toughness, G_c^1 is the toughness of the material M1 and δW is a change of the potential energy between the original and new crack position. It is also worth remarking that the differential form of the condition (181) is identical to the maximum energy release rate condition in the case of the homogenous material. Matched asymptotic procedure is used to derive the change of potential energy. Consider the singularity of the stress field at the crack tip impinging the material interface having the form $r^{\delta-1}$, with r being the radial coordinate emanating from the crack tip, and with $\delta \in (0, 1)$. Further

consider a perturbation of the domain Ω with crack impinging the interface between materials M2 and M1 as shown in Fig. 35; the perturbation is a deflected (double) crack extension of length a_d or penetrating crack extension of length a_p with the small perturbation parameter ε defined as
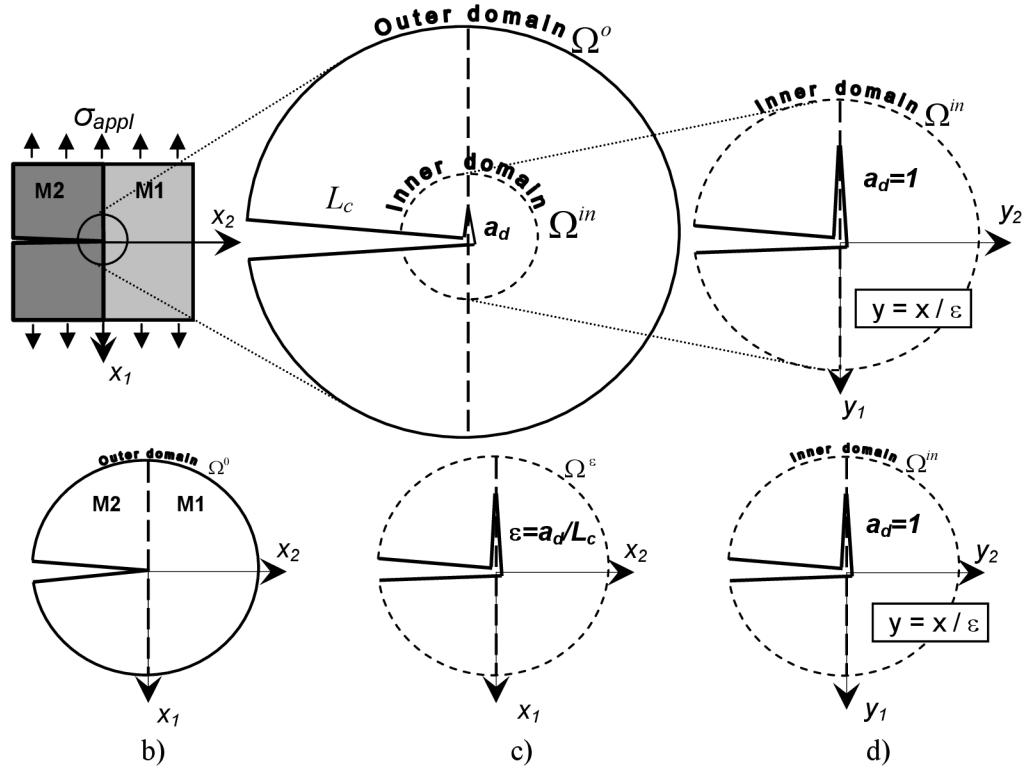
Fig. 35 Outer and Inner domain used in the matched asymptotic analysis (in case of the singly deflected crack) - zoomed-in view of crack neighbourhood perturbed by a small crack extension b) – d) coordinate systems of the outer and inner domain.

$$\varepsilon = \frac{a}{L_c} \ll 1, \quad a = a_p, a_d, \tag{182}$$

where L_c is the characteristic length of Ω. A second scale to the problem can be introduced, represented by the scaled-up coordinates

$$y_i = \frac{x_i}{\varepsilon}, \quad \text{or} \quad (y_1, y_2) = \left(\frac{x_1}{\varepsilon}, \frac{x_2}{\varepsilon}\right), \tag{183}$$

which provides a zoomed-in view into the region surrounding the crack.

7.2.1 Matched asymptotic procedure

Matched asymptotic procedure [55] is used to derive the change of potential energy. Consider a perturbation of the domain Ω with crack impinging the interface; the perturbation is a deflected (double) crack extension of length a_d or penetrating crack extension of length a_p with the small perturbation parameter ε - (182). A second scale to the problem can be introduced, represented by the scaled-up coordinates $y = x/\varepsilon$, or $(y_1, y_2) = (x_1/\varepsilon, x_2/\varepsilon)$ which provides a zoomed-in view into the region surrounding the crack. The displacement $\mathbf{U}^\varepsilon$ of the perturbed elasticity problem due to the crack extension can be expressed in terms of the regular coordinate x and the scaled-up

coordinate y as $\mathbf{U}^{\varepsilon}(x)=\mathbf{U}^{\varepsilon}(\varepsilon y)=\mathbf{V}^{\varepsilon}(y)$. Consider now the asymptotic expansion for $\mathbf{U}^{\varepsilon}$ (which is also known as the ''outer expansion'') and for $\mathbf{V}^{\varepsilon}$ (which is also known as the ''inner expansion'')

$$\mathbf{U}^{\varepsilon}(x)=k_0(\varepsilon)\mathcal{U}_0(x)+k_1(\varepsilon)\mathcal{U}_1(x)+...=\sum_{i=0}^{\infty}k_i(\varepsilon)\mathcal{U}_i(x), \quad \text{outer expansion}, \tag{184}$$

where $\lim_{\varepsilon\to 0}k_{i+1}(\varepsilon)/k_i(\varepsilon)=0, \quad \forall i=1,2,...$ and $\{\mathcal{U}_1,\mathcal{U}_2,...\}$ form a set of linearly independent basis functions, and the inner asymptotic expansion is possible to write in the following form – for more details see [101]:

$$\mathbf{V}^{\varepsilon}(y)=F_0(\varepsilon)\mathcal{V}_0(y)+F_1(\varepsilon)\mathcal{V}_1(y)+...=\sum_{i=0}^{\infty}F_i(\varepsilon)\mathcal{V}_i(y), \quad \text{inner expansion}, \tag{185}$$

where $\lim_{\varepsilon\to 0}F_{i+1}(\varepsilon)/F_i(\varepsilon)=0, \quad \forall i=1,2,...,\quad F_0(\varepsilon)=1, \quad \mathcal{V}_0(y)=\mathbf{U}^0(0)=0$ and $\{\mathcal{V}_0,\mathcal{V}_1,\mathcal{V}_2,...\}$ form a set of linearly independent basis functions. The basis functions $\{\mathcal{U}_i\}$ satisfy the elasticity problem on the same domain $\Omega\approx\Omega^{\varepsilon}$ but with zero body force and with homogeneous boundary conditions. From the matching conditions of the outer and inner asymptotic expansion, the asymptotic expansion coefficients $k_0(\varepsilon)$, $k_1(\varepsilon)$,.. and $F_0(\varepsilon)$, $F_1(\varepsilon)$,...can be found:

$$\mathbf{U}^{\varepsilon}(x=\varepsilon y)=H\varepsilon^{\delta_1}\rho^{\delta_1}\mathbf{u}_1(\theta)+T\varepsilon\rho\mathbf{u}_3(\theta)+k_1(\varepsilon)\left[K_{1d(p)}\varepsilon^{-\delta_1}\rho^{-\delta_1}\mathbf{u}_{-1}(\theta)+....\right]+$$
$$+k_2(\varepsilon)\varepsilon\rho\mathbf{u}_3(\theta)+...=$$
$$=\mathbf{V}^{\varepsilon}(y)=F_1(\varepsilon)\left[\rho^{\delta_1}\mathbf{u}_1(\theta)+K_{1d(p)}\rho^{-\delta_1}\mathbf{u}_{-1}(\theta)+K_{2d(p)}\rho^{-1}\mathbf{u}_{-3}(\theta)+...\right]+ \tag{186}$$
$$+F_2(\varepsilon)\left[\rho\,\mathbf{u}_3(\theta)+K'_{1d(p)}\rho^{-\delta_1}\mathbf{u}_{-1}(\theta)+K'_{2d(p)}\rho^{-1}\mathbf{u}_{-3}(\theta)+....\right]+$$
$$+F_3(\varepsilon)\left[\rho^{\delta_1}\mathbf{u}_1(\theta)+K_{1d(p)}\rho^{-\delta_1}\mathbf{u}_{-1}(\theta)+K_{2d(p)}\rho^{-1}\mathbf{u}_{-3}(\theta)+...\right]+...$$

To derive the relations for the unknown functions $k_1(\varepsilon)$, $k_2(\varepsilon)$, $F_1(\varepsilon)$, $F_2(\varepsilon)$, $F_3(\varepsilon)$ the corresponding terms (with the same power exponent δ) are to be compared.

$$H\varepsilon^{\delta_1}\rho^{\delta_1}\mathbf{u}_1(\theta)=F_1(\varepsilon)\rho^{\delta_1}\mathbf{u}_1(\theta)\Rightarrow F_1(\varepsilon)=H\varepsilon^{\delta_1} \tag{187}$$

$$T\varepsilon\rho\,\mathbf{u}_3(\theta)=F_3(\varepsilon)\rho\,\mathbf{u}_3(\theta)\Rightarrow F_3(\varepsilon)=T\varepsilon \tag{188}$$

$$k_1(\varepsilon)K_{1d(p)}\varepsilon^{-\delta_1}\rho^{-\delta_1}\mathbf{u}_{-1}(\theta)=F_1(\varepsilon)K_{1d(p)}\rho^{-\delta_1}\mathbf{u}_{-1}(\theta)\Rightarrow k_1(\varepsilon)=H\varepsilon^{2\delta_1} \tag{189}$$

Finally, the following asymptotic expansion $\mathbf{V}^{\varepsilon}(y)$ is obtained (by substitution of relations (187), (188) and (189) into (186)):

$$\mathbf{U}^{\varepsilon}(x=\varepsilon y)=\mathbf{V}^{\varepsilon}(y)=H\varepsilon^{\delta_1}\left[\rho^{\delta_1}\mathbf{u}_1(\theta)+K_{1d(p)}\rho^{-\delta_1}\mathbf{u}_{-1}(\theta)+K_{2d(p)}\rho^{-1}\mathbf{u}_{-3}(\theta)+...\right]+$$
$$+T\varepsilon\left[\rho\,\mathbf{u}_3(\theta)+K'_{1d(p)}\rho^{-\delta_1}\mathbf{u}_{-1}(\theta)+K'_{2d(p)}\rho^{-1}\mathbf{u}_{-3}(\theta)+....\right]+... \tag{190}$$

The terms in the expansions are ordered with respect to the increasing power of the parameter ε.

With an eye on applications we will distinguish between two cases: a) crack perpendicularly impinging an interface, b) inclined crack impinging a interface.

7.2.2 Crack perpendicularly impinging an interface

The asymptotic expansion of the displacements for the initial state $\mathbf{U}^0(x)$ (main crack terminating on the interface and no crack extension of length a is present) is possible to write in the following form, see the Section 4.1.3

$$\mathbf{U}^0(x) = \mathbf{U}^0(0) + H_1 r^{\delta_1} \mathbf{u}_1(\theta) + H_2 r^{\delta_2} \mathbf{u}_2(\theta) + Tr^{\delta_3} \mathbf{u}_3(\theta) + \ldots = \sum_{i=1}^{\infty} k_i r^{\delta_i} \mathbf{u}_i(\theta), \quad \delta_3 = 1, \quad (191)$$

where H_1 and H_2 are the generalized stress intensity factors, $\mathbf{u}_1(\theta)$ and $\mathbf{u}_2(\theta)$ are the angular distributions of the displacements corresponding to the singular terms in the stress asymptotic expansion and $\mathbf{u}_3(\theta)$ is the angular distribution of displacements for the T-stress – as discussed in the section 4.1.4. In the following we will consider $\mathbf{U}^0(0) = 0$. GSIFs H_1 and H_2 are calculated using relations (22) and (23) as already discussed in 4.1.3.

Remark 6: In the case of aligned orthotropic bi-materials and a crack perpendicularly impinging at the interface, the GSIFs H_1 and H_2 closely relates to the mixed mode loading and characterize symmetric and antisymmetric modes. Observe that the subscripts 1 and 2 mark the order of corresponding terms in the asymptotic expansion (185) and not the loading modes. Hence, a carefull analysis is required to specify to which loading mode a particular GSIF pertains.

The outer asymptotic expansion of $\mathbf{U}^\varepsilon$ (when the small crack extension has originated) is possible to write as

$$\mathbf{U}^\varepsilon(x) = \mathbf{U}^0(x) + k_1(\varepsilon) \left[K_{1d(p)} r^{-\delta_1} \mathbf{u}_{-1}(\theta) + \ldots \right] + k_3(\varepsilon) r \mathbf{u}_3(\theta) + \ldots \quad (192)$$

Linearly independent basis functions $\{\mathcal{V}_0, \mathcal{V}_1, \mathcal{V}_2, \ldots\}$ of the inner expansion (185) are as follows

$$\mathcal{V}_0(y) = \mathbf{U}^0(0) = 0,$$

$$\mathcal{V}_1(y) = \rho^{\delta_1} \mathbf{u}_1(\theta) + K_{1d(p)} \rho^{-\delta_1} \mathbf{u}_{-1}(\theta) + K_{2d(p)} \rho^{-1} \mathbf{u}_{-3}(\theta) + \ldots, \quad \rho = \frac{r}{\varepsilon}, \quad (193)$$

$$\mathcal{V}_2(y) = \rho \, \mathbf{u}_3(\theta) + K'_{1d(p)} \rho^{-\delta_1} \mathbf{u}_{-1}(\theta) + K'_{2d(p)} \rho^{-1} \mathbf{u}_{-3}(\theta) + \ldots, \quad \rho = \frac{r}{\varepsilon}$$

The first terms on the right hand side of (193) express the asymptotic behaviour of the functions $\mathcal{V}_i$ for $\rho \to \infty$. In equation (193) $\mathbf{u}_{-3}(\theta)$ denotes the dual (auxiliary) solution for the T-stress which has been already discussed in the chapter 4.1.4. The coefficients $K_{1d(p)}$ and $K_{2d(p)}$ are computed on the inner domain Ω^{in}, which is unbounded for $\varepsilon \to 0$ but in the model employed in the finite element calculation, Ω^{in} is approximated by a circular region with radius R much larger than the crack extension length $a_{d(p)}$. On the circle boundary, the condition of the type $\mathbf{U}\big|_{\partial\Omega^{in}} = \rho^{\delta_1} \mathbf{u}_1(\theta)$ is prescribed. $K_{1d(p)}$ and $K_{2d(p)}$ are calculated as follows:

$$K_{1d(p)} = \frac{\Psi\left(\mathcal{V}_1^h(\rho,\theta), \rho^{\delta_1} \mathbf{u}_1\right)}{\Psi\left(\rho^{-\delta_1} \mathbf{u}_{-1}, \rho^{\delta_1} \mathbf{u}_1\right)}, \quad K_{2d(p)} = \frac{\Psi\left(\mathcal{V}_1^h(\rho,\theta), \rho \mathbf{u}_3\right)}{\Psi\left(\rho^{-1} \mathbf{u}_{-3}, \rho \mathbf{u}_3\right)}, \quad \mathcal{V}_1^h\text{- FE approx. to } \mathcal{V}_1 . \quad (194)$$

The coefficients $K'_{1d(p)}$ and $K'_{2d(p)}$ in (193) are calculated in a similar way with boundary condition $\mathbf{U}\big|_{\partial\Omega^{in}} = \rho \mathbf{u}_3(\theta)$ prescribed on the circular region boundary.

$$K'_{1d(p)} = \frac{\Psi\left(\mathcal{V}_2^h(y), \rho^{\delta_1}\mathbf{u}_1\right)}{\Psi\left(\rho^{-\delta_1}\mathbf{u}_{-1}, \rho^{\delta_1}\mathbf{u}_1\right)}, \quad K'_{2d(p)} = \frac{\Psi\left(\mathcal{V}_2^h(y), \rho\mathbf{u}_3\right)}{\Psi\left(\rho^{-1}\mathbf{u}_{-3}, \rho\mathbf{u}_3\right)}, \mathcal{V}_2^h\text{-FE approx. to } \mathcal{V}_2 \qquad (195)$$

The incremental energy release rate (ERR) $G_{d(p)}$, related to the unperturbed state $\mathbf{U}^0$ (without the crack extension) and perturbed state $\mathbf{U}^\varepsilon$ (with the small finite crack extension), is defined as

$$G_{d(p)} = -\frac{\delta W}{a_{d(p)}} = -\frac{W^\varepsilon - W^0}{\varepsilon_{d(p)} L} =$$

$$= -\frac{1}{2\varepsilon_{d(p)} L} \int_\Gamma \left(\sigma_{kl}\left(\mathbf{U}^\varepsilon\right) n_k U_l^0 - \sigma_{kl}\left(\mathbf{U}^0\right) n_k U_l^\varepsilon\right) ds = -\frac{1}{2\varepsilon_{d(p)} L} \Psi\left(\mathbf{U}^\varepsilon, \mathbf{U}^0\right) = \qquad (196)$$

$$= -\frac{1}{2L} H^2 K_{1d(p)} \varepsilon^{2\delta_1 - 1} \Psi\left(\rho^{-\delta_1}\mathbf{u}_{-1}(\theta), \rho^{\delta_1}\mathbf{u}_1(\theta)\right) - \frac{1}{2L} HT K'_{1d(p)} \varepsilon^{\delta_1} \Psi\left(\rho^{-\delta_1}\mathbf{u}_{-1}(\theta), \rho^{\delta_1}\mathbf{u}_1(\theta)\right) -$$

$$- \frac{1}{2L} HT K_{2d(p)} \varepsilon^{\delta_1} \Psi\left(\rho^{-1}\mathbf{u}_{-3}(\theta), \rho\mathbf{u}_3(\theta)\right) - \frac{1}{2L} T^2 K'_{2d(p)} \varepsilon^{2-1} \Psi\left(\rho^{-1}\mathbf{u}_{-3}(\theta), \rho\mathbf{u}_3(\theta)\right)$$

where δW is the potential energy change, $\varepsilon_{d(p)} = a_{d(p)}/L_c$, H – Generalized Stress Intensity Factor and T is a T-stress. Observe, that line Γ is any contour surrounding the crack tip and the crack increment and starting and finishing on the stress-free faces of he primary crack. Among others, the crack extension faces along a_p or a_d respectively, form an admissible contour which allows to rewrite (196) as a work done along $a_{d(p)}$ and leads to the classical virtual crack closure method

$$G_{d(p)} = -\frac{1}{2a_{d(p)}} \int\limits_{a_{d(p)}} \left(\sigma_{kl}\left(\mathbf{U}^\varepsilon\right) n_k U_l^0 - \sigma_{kl}\left(\mathbf{U}^0\right) n_k U_l^\varepsilon\right) ds =$$

$$= \frac{1}{2a_{d(p)}} \int\limits_{a_{d(p)}} \sigma_{kl}\left(\mathbf{U}^0\right) n_k U_l^\varepsilon \, ds = \frac{1}{2a_{d(p)}} \int\limits_0^{a_{d(p)}} \sigma_{kl}\left(\mathbf{U}^0\right) n_k \Delta U_l^\varepsilon ds, \qquad (197)$$

where the integral along $a_{d(p)}$ means along two faces $a_{d(p)}^+$ and $a_{d(p)}^-$ and ΔU^ε denotes $\Delta U_l^\varepsilon = \left(U_l^\varepsilon\right)^+ - \left(U_l^\varepsilon\right)^-$ where the sign $+$ or $-$ refer to upper or lower crack face. The expression (197) is rather difficult to handle numerically since the singularities govern the behavior along $a_{d(p)}$.Nevertheless, it offers an idea to calculate the fracture mode mixity based upon the energy release rate (ERR). For $\delta_1 > 1/3$, the ratio of the debonding to the penetrating ERR follows from (196) as

$$\frac{G_d}{G_p} = \frac{K_{1d}\Psi_1 + \left(K'_{1d}\Psi_1 + K_{2d}\Psi_2\right)\eta_{d(p)}}{K_{1p}\Psi_1 + \left(K'_{1p}\Psi_1 + K_{2p}\Psi_2\right)\eta_{d(p)}} \left(\frac{a_d}{a_p}\right)^{2\delta_1 - 1}, \quad \text{where } \eta_{d(p)} = \frac{T}{H}\varepsilon_{d(p)}^{1-\delta_1},$$

$$\Psi_1 = \Psi\left(\rho^{-\delta_1}\mathbf{u}_{-1}(\theta), \rho^{\delta_1}\mathbf{u}_1(\theta)\right), \Psi_2 = \Psi\left(\rho^{-1}\mathbf{u}_{-3}(\theta), \rho\mathbf{u}_3(\theta)\right). \qquad (198)$$

Similar relation is obtained for $\delta_1 < 1/3$. The fracture mode mixity based on the stress intensity factor (SIF) concept is usually represented by the so-called local phase angle Ψ_K defined by $K = K_1 + iK_2 = |K|e^{i\Psi_K}$ where K is the complex stress intensity factor (SIF), associated to a reference length l according to the proposal by Rice [77]. The ERR based fracture mode mixity originally results from the application of the virtual crack closure method.

Consider a small but finite length a_d of a virtual crack extension along the interface. The energy release rate (ERR) associated to this crack extension is

$$G_d\left(a_d\right)=G_{dI}\left(a_d\right)+G_{dII}\left(a_d\right),\qquad(199)$$

where

$$G_{dI}\left(a_d\right)=\frac{1}{2a_d}\int_0^{a_d}\sigma_{22}\left(s,0\right)\Delta u_2\left(a_d-s\right)ds,\quad G_{dII}\left(a_d\right)=\frac{1}{2a_d}\int_0^{a_d}\sigma_{12}\left(s,0\right)\Delta u_1\left(a_d-s\right)ds.\qquad(200)$$

The Mode I component G_{dI} corresponds to the energy released by normal stresses acting through crack face opening displacements, and Mode II component G_{dII} corresponds to the energy released by shear stresses acting through crack face sliding displacements. The energetic mode mixity G_{dII}/G_{dII} for interface crack depends on a_d. The associated phase angle Ψ_G is defined as

$$\tan^2\Psi_G=\frac{G_{dII}\left(a_d\right)}{G_{dI}\left(a_d\right)},\quad 0\le\Psi_G\le\frac{\pi}{2}.\qquad(201)$$

Instead of Eqs. (200), the concept of Ψ-integral can be applied for to evaluate the phase angle Ψ_G. First observe that Eq. (200) can be written in the form

$$G_d=-\frac{1}{2a_d}\int_{a_d}\left(\sigma_{kl}\left(\mathbf{U}^\varepsilon\right)n_kU_l^0-\sigma_{kl}\left(\mathbf{U}^0\right)n_kU_l^\varepsilon\right)ds=$$

$$=\underbrace{-\frac{1}{2a_d}\int_{a_d}\left(\sigma_{22}\left(\mathbf{U}^\varepsilon\right)n_2U_2^0-\sigma_{22}\left(\mathbf{U}^0\right)n_2U_2^\varepsilon\right)ds}_{G_{dI}}\underbrace{-\frac{1}{2a_d}\int_{a_d}\left(\sigma_{21}\left(\mathbf{U}^\varepsilon\right)n_2U_1^0-\sigma_{21}\left(\mathbf{U}^0\right)n_2U_1^\varepsilon\right)ds}_{G_{dII}}.\qquad(202)$$

On the other side, assume any contour Γ surrounding the crack tip and write

$$G_d=-\frac{1}{2a_d}\int_\Gamma\left(\sigma_{kl}\left(\mathbf{U}^\varepsilon\right)n_kU_l^0-\sigma_{kl}\left(\mathbf{U}^0\right)n_kU_l^\varepsilon\right)ds=-\frac{1}{2a_d}\int_\Gamma\left(\sigma_{kl}\left(\mathbf{U}^\varepsilon\right)n_k\delta_{lj}U_j^0-\sigma_{kl}\left(\mathbf{U}^0\right)n_k\delta_{lj}U_j^\varepsilon\right)ds$$

$$=-\frac{1}{2a_d}\int_\Gamma\left(\sigma_{kl}\left(\mathbf{U}^\varepsilon\right)n_kn_ln_jU_j^0-\sigma_{kl}\left(\mathbf{U}^0\right)n_kn_ln_jU_j^\varepsilon\right)ds-\frac{1}{2a_d}\int_\Gamma\left(\sigma_{kl}\left(\mathbf{U}^\varepsilon\right)n_kt_lt_jU_j^0-\sigma_{kl}\left(\mathbf{U}^0\right)n_kt_lt_jU_j^\varepsilon\right)ds,\qquad(203)$$

where t_l is the unit tangential vector of Γ. The last two integrals in Eq. (203) are path-independent only if $n_ln_j=\delta_{lj}$, that is if Γ is a rectangle with its sides parallel to coordinate axes. In such a case, the last two integrals correspond to G_{dI} and G_{dII} respectively. Thus, the ERR based phase angle Ψ_G for deflected crack can be calculated by substituting for G_{dI} and G_{dII} from Eq. (203) to (201). Note that the ERR and the SIF based measures of mode mixity for an interface crack, phase angle Ψ_G and Ψ_K, are related see [58]:

$$\cos\left(2\Psi_G\right)=\sqrt{\frac{\sinh\left(2\pi\varepsilon_o\right)}{2\pi\varepsilon_o\left(1+4\varepsilon_o^2\right)}}\cos\left[2\Psi_K+2\varepsilon_o\ln\frac{a_d}{2L}+\arg\left[\frac{\Gamma\left(1/2+i\varepsilon_o\right)}{\Gamma\left(1+i\varepsilon_o\right)}\right]-\arctan\left(2\varepsilon_o\right)\right],\qquad(204)$$

where ε_o is an oscillation index – see [7], [24], [58] or [95].

7.2.3 Inclined crack impinging a interface

Asymptotic expansion for the primary inclined crack before the perturbation inception takes place reads

$$\mathbf{U}^0(x) = \mathbf{U}^0(0) + H_1 r^{\delta_1} \mathbf{u}_1(\theta) + H_2 r^{\delta_2} \mathbf{u}_2(\theta) + ..., \tag{205}$$

where only singular terms are considered. The GSIFs H_1 and H_2 can be again computed using relations (22) and (23).

The outer expansion for the perturbed domain Ω^ε is

$$\mathbf{U}^\varepsilon(x) = \mathbf{U}^0(x) + k_1(\varepsilon) K_{1d(p)} r^{-\delta_1} \mathbf{u}_{-1}(\theta) + k_2(\varepsilon) K_{2d(p)} r^{-\delta_2} \mathbf{u}_{-2}(\theta) + ... \tag{206}$$

The inner expansion for the perturbed domain Ω^ε reads

$$\mathbf{V}^\varepsilon(y) = F_1(\varepsilon) \left[\rho^{\delta_1} \mathbf{u}_1(\theta) + K_{1d(p)} \rho^{-\delta_1} \mathbf{u}_{-1}(\theta) + K_{2d(p)} \rho^{-\delta_2} \mathbf{u}_{-2}(\theta) + ... \right] + F_2(\varepsilon) \times$$
$$\times \left[\rho^{\delta_2} \mathbf{u}_2(\theta) + K'_{1d(p)} \rho^{-\delta_1} \mathbf{u}_{-1}(\theta) + K'_{2d(p)} \rho^{-\delta_2} \mathbf{u}_{-2}(\theta) + ... \right] + ... \tag{207}$$

The first terms in the brackets on the right-hand side of Eq. (207) describe the behaviour of functions $\mathcal{V}_i$ for $\rho \to \infty$. $\mathbf{u}_{-1}(\theta)$, $\mathbf{u}_{-2}(\theta)$ are dual (auxiliary) solutions to $\mathbf{u}_1(\theta)$, $\mathbf{u}_2(\theta)$, see above. The determination of the coefficients $K_{1d(p)}, K_{2d(p)}, K'_{1d(p)}, K'_{2d(p)}$, proceeds in a similar fashion as the coefficients K in the section 7.2.2, $K_{1d(p)}, K_{2d(p)}$ are calculated in the inner domain whose remote boundary $\partial \Omega^{in}$ is subjected to the boundary condition $\mathbf{U}|_{\partial \Omega^{in}} = \rho^{\delta_1} \mathbf{u}_1(\theta)$

$$K_{1d(p)} = \frac{\Psi\left(\mathcal{V}_1^h(y), \rho^{\delta_1} \mathbf{u}_1\right)}{\Psi\left(\rho^{-\delta_1} \mathbf{u}_{-1}, \rho^{\delta_1} \mathbf{u}_1\right)}, \quad K_{2d(p)} = \frac{\Psi\left(\mathcal{V}_1^h(y), \rho^{\delta_2} \mathbf{u}_2\right)}{\Psi\left(\rho^{-\delta_2} \mathbf{u}_{-2}, \rho^{\delta_2} \mathbf{u}_2\right)}, \quad \mathcal{V}_1^h \text{- FE approx. to } \mathcal{V}_1 \tag{208}$$

Similarly, the coefficients $K'_{1d(p)}, K'_{2d(p)}$ are calculated in the inner domain whose remote boundary $\partial \Omega^{in}$ is subjected to the boundary condition $\mathbf{U}|_{\partial \Omega^{in}} = \rho^{\delta_2} \mathbf{u}_2(\theta)$

$$K'_{1d(p)} = \frac{\Psi\left(\mathcal{V}_2^h(y), \rho^{\delta_1} \mathbf{u}_1\right)}{\Psi\left(\rho^{-\delta_1} \mathbf{u}_{-1}, \rho^{\delta_1} \mathbf{u}_1\right)}, \quad K'_{2d(p)} = \frac{\Psi\left(\mathcal{V}_2^h(y), \rho^{\delta_2} \mathbf{u}_2\right)}{\Psi\left(\rho^{-\delta_2} \mathbf{u}_{-2}, \rho^{\delta_2} \mathbf{u}_2\right)}, \quad \mathcal{V}_2^h \text{-FE approx. to } \mathcal{V}_2. \tag{209}$$

The incremental energy release rate (ERR) $G_{d(p)}$, related to the unperturbed state $\mathbf{U}^0$ (without the crack extension) and perturbed state $\mathbf{U}^\varepsilon$ (with the small finite crack extension), is defined as (see also Eq. (197))

$$G_{d(p)} = -\frac{W^\varepsilon - W^0}{a_{d(p)}} = -\frac{1}{2\varepsilon_{d(p)} L} \Psi\left(\mathbf{U}^\varepsilon, \mathbf{U}^0\right) = -\frac{1}{2L} H_1^2 K_{1d(p)} \varepsilon_{d(p)}^{2\delta_1 - 1} \Psi\left(\rho^{\delta_1} \mathbf{u}_1(\theta), \rho^{-\delta_1} \mathbf{u}_{-1}(\theta)\right) -$$
$$-\frac{1}{2L} H_1 H_2 \varepsilon_{d(p)}^{\delta_1 + d_2 - 1} \left[K'_{1d(p)} \Psi\left(\rho^{\delta_1} \mathbf{u}_1(\theta), \rho^{-\delta_1} \mathbf{u}_{-1}(\theta)\right) + K_{2d(p)} \Psi\left(\rho^{\delta_2} \mathbf{u}_2(\theta), \rho^{-\delta_2} \mathbf{u}_{-2}(\theta)\right) \right] - \tag{210}$$
$$-\frac{1}{2L} H_2^2 K'_{2d(p)} \varepsilon_{d(p)}^{2\delta_2 - 1} \Psi\left(\rho^{\delta_2} \mathbf{u}_2(\theta), \rho^{-\delta_2} \mathbf{u}_{-2}(\theta)\right) + ..,$$

The ratio of the debonding to the penetrating ERR follows from Eq.((210)) as

$$\frac{G_d}{G_p} = \frac{K_{1d}\Psi_1 + \left(K'_{1d}\Psi_1 + K_{2d}\Psi_2\right)\eta_d + K'_{2d}\Psi_2\eta_d^2}{K_{1p}\Psi_1 + \left(K'_{1p}\Psi_1 + K_{2p}\Psi_2\right)\eta_p + K'_{2p}\Psi_2\eta_p^2}\left(\frac{a_d}{a_p}\right)^{2\delta_1-1}, \quad \eta_d = \frac{H_2}{H_1}\left(\frac{a_d}{L}\right)^{\delta_2-\delta_1},$$

(211)

$$\eta_p = \frac{H_2}{H_1}\left(\frac{a_p}{L}\right)^{\delta_2-\delta_1}, \quad \Psi_1 \equiv \Psi\left(\rho^{\delta_1}\mathbf{u}_1(\theta), \rho^{-\delta_1}\mathbf{u}_{-1}(\theta)\right), \quad \Psi_2 \equiv \Psi\left(\rho^{\delta_2}\mathbf{u}_2(\theta), \rho^{-\delta_2}\mathbf{u}_{-2}(\theta)\right),$$

which corresponds to the relation obtained by the authors [109] in a different way, see their Eq. (18). An ERR based phase angle Ψ_G for deflected crack is defined as

$$\tan^2\Psi_G = \frac{G_{dII}(a_d)}{G_{dI}(a_d)}, \quad 0 \le \Psi_G \le \frac{\pi}{2}, \text{ where } G_{dII} = -\frac{1}{2a_d}\int_\Gamma\left(\sigma_{kl}\left(\mathbf{U}^\varepsilon\right)n_k t_l t_j U_j^0 - \sigma_{kl}\left(\mathbf{U}^0\right)n_k t_l t_j U_j^\varepsilon\right)ds,$$

(212)

$$G_{dI} = -\frac{1}{2a_d}\int_\Gamma\left(\sigma_{kl}\left(\mathbf{U}^\varepsilon\right)n_k n_l n_j U_j^0 - \sigma_{kl}\left(\mathbf{U}^0\right)n_k n_l n_j U_j^\varepsilon\right)ds, \quad t_l \text{ - unit tangential vector of } \Gamma.$$

7.2.4 Competition between the crack deflection and the crack penetration

The real competition between the crack deflection (along the interface) and the crack penetration can be assessed only with the knowledge of the toughnesses in the appropriate directions – for the deflection: the interface toughness G_c^i; for the penetration: the toughness of the material M1 - G_c^1. These values have to be specified on the base of the experiments (on the real specimens). This was not performed within this thesis. If these quantities are known, then the deflection occurs if the following condition is satisfied:

$$\frac{G_d}{G_p} > \frac{G_c^i}{G_c^1} \ .$$

(213)

And vice versa, if the inequality is of the opposite sign, the penetration is preferred before the deflection. Note, that the considered finite crack extensions of both, deflected and penetrating crack, must have the same lengths (a_d=a_p).

This energetic criterion (213) for the crack deflection gives only the information about the prospective propagation direction, however not any information whether the crack, terminating on the interface, will start the next propagation under the given loading or not. To this end also the stress criterion have to be used. The values of the tangential stresses at the crack extension tip have to be compared with the critical stresses σ_c of the material in appropriate direction. These critical values have to be also determined by the experiment.

8   Examples

The previous chapters described the fundamental theory necessary for the assessment of the general stress concentrators in anisotropic media. Description of the asymptotic stress field and subsequent definition of the fracture criterion has been studied. To make this work complete, several demonstration examples summarizing all outcomes will be presented. The problems of the crack terminating at right and arbitrary angle to the bi-material interface will be analyzed.

The fundamental question when assessing the general stress concentrators is how they will behave under the given loading conditions. This question includes a prediction of the further crack propagation direction (crack penetration or crack deflection along the interface – debonding of the interface) and also determination of the load under which the crack growth will occur.

For the finite element analysis of the stress and displacement field (on the bi-material model) the commercial system for the Finite Element Analysis ANSYS 10.0 has been used. The numerical calculations of the singularity exponent, GSIF, T-stress and problems of the fracture criteria were performed by force of the mathematical software MAPLE 10.0 and MATLAB 7.1.

8.1   Crack perpendicular to the bi-material interface in orthotropic media (with transversally isotropic surface layer)

The materials used within this example were purposely chosen to be transversally isotropic (special case of the orthotropic material - material properties in the plane perpendicular to the fibre direction L are isotropic - Fig. 36). This type of material is a typical representative when considering e.g. the laminate composites with layers reinforced by the long fibres and where the particular layers have different orientation. It can also be a case of the orthotropic material protected by some surface layer or coating. In the example, the major material directions in the specimen were chosen to be coincident with the coordinate system axes as shown in the Fig. 36. If these material directions are not coincident with the CS axes, the layer exhibits general anisotropic behaviour and in the given coordinate system the material compliance matrix (82) is more complicated and not symmetric. This case can also be solved using the above described theory with the only complication consisting in the higher number of needed elastic constants. The definition of these material properties for the calculations represents the main problem of the whole solution. The anisotropy itself doesn't represent any problem (thanks to the employment of the Lechnitskii-Stroh formalism).

8.1.1   Description of the stress field

Consider now a bi-material specimen as shown in Fig. 36 which is subjected to the tension load $\sigma_{appl} = 100$ MPa on its boundary. Material M1 represents the substrate and material M2 represents the transversally isotropic surface layer of the thickness h=4mm. Further consider the coupled DOFs of both materials along the loaded surfaces. A crack perpendicular to the interface between M1 and M2 is introduced in the middle of the surface layer. The orthotropic material M1 is described by 9 elastic constants, where 5 of them are independent and the transversally isotropic surface layer is described in the plane x_1x_2 by two independent elastic constants (specified in the Fig. 36).
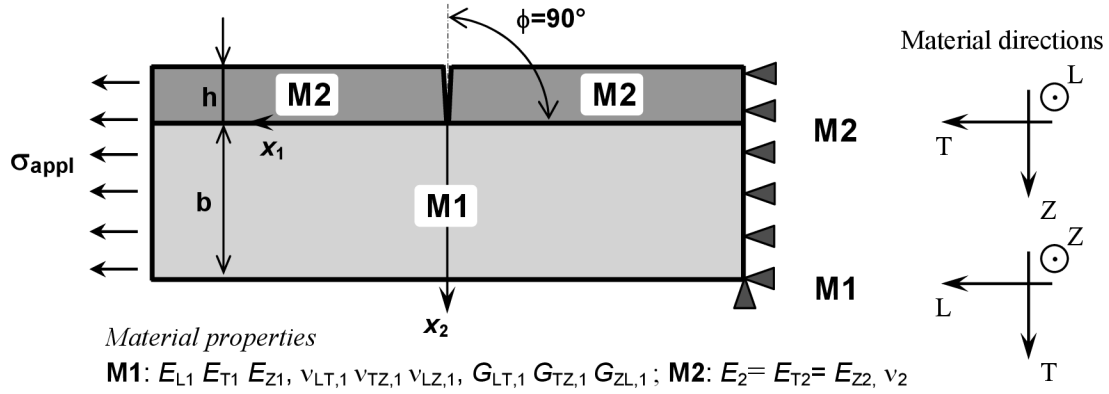
Fig. 36 Scheme of the solved bi-material configuration with a crack perpendicular to the bi-material interface.

For the parametric study there were chosen several material configurations by variation of Dundurs' parameter α - see Eq (87) and by setting Dundurs' parameter $\beta{=}0$. The isotropic material of the surface layer was set as a reference material with constant elastic properties $E{=}60000$ MPa, $\nu{=}0.238$ and the elastic properties of the orthotropic material were computed for each value of α using the relations (81)-(88) and setting the composite parameters $\lambda_1{=}0.1$, $\rho_1{=}2$, $\lambda_2{=}1$, $\rho_2{=}1$ - see (84). Note, that only the interval of the parameter $\alpha \in ({-}0{,}99, 0.4)$ has the physical meaning for the chosen material configuration and parameters λ, ρ (maximum range of α is $({-}1, 1)$). The resulting elastic properties of the orthotropic material M1 for the values of α outside the range $({-}0.99, 0.4)$ do not satisfy the following condition of a real material in the FE system ANSYS (the compliance matrix of the material properties has to be positively definite):

$$\left(1 - \nu_{LT,1}^2 \cdot \frac{E_{T,1}}{E_{L,1}} - \nu_{TZ,1}^2 \cdot \frac{E_{Z,1}}{E_{T,1}} - \nu_{LZ,1}^2 \cdot \frac{E_{Z,1}}{E_{L,1}} - 2 \cdot \nu_{LT,1} \cdot \nu_{TZ,1} \cdot \nu_{LZ,1} \cdot \frac{E_{Z,1}}{E_{L,1}}\right) > 0. \qquad (214)$$

If this condition is not fulfilled, the FE solution cannot be performed with this material. The FE solution is necessary for the GSIF determination and for the criteria solution.

The model for the FE analysis has been specially defined so that the mesh in the vicinity of the crack tip is uniform with linearly decreasing element size as approaching the singular point. In the region where the integration path crosses the interface a finer mesh was used (Fig. 37) in order to reduce the numerical errors in the integration process. However, when the model is required to be simpler (to contain a smaller number of elements), the mesh refinement is not required and the errors without this refinement are relatively small and in some cases they are insignificant. Nevertheless, the study of this influence is recommended to perform before any larger computations. In the next calculations the refinement will be considered to keep the eventual errors on the as low level as possible. Also a study of the influence of the whole mesh refinement on the results has been carried out. It was found that a much coarser mesh (in comparison to that one in Fig. 37) can also provide sufficiently good results, with no high deviations of GSIF values from the results obtained with a finer mesh. No special singular elements have been applied – only the standard quadratic plane 8-node elements are used in the FE model. Again, the simpler 4-node linear elements can be used as well leading to very similar results.
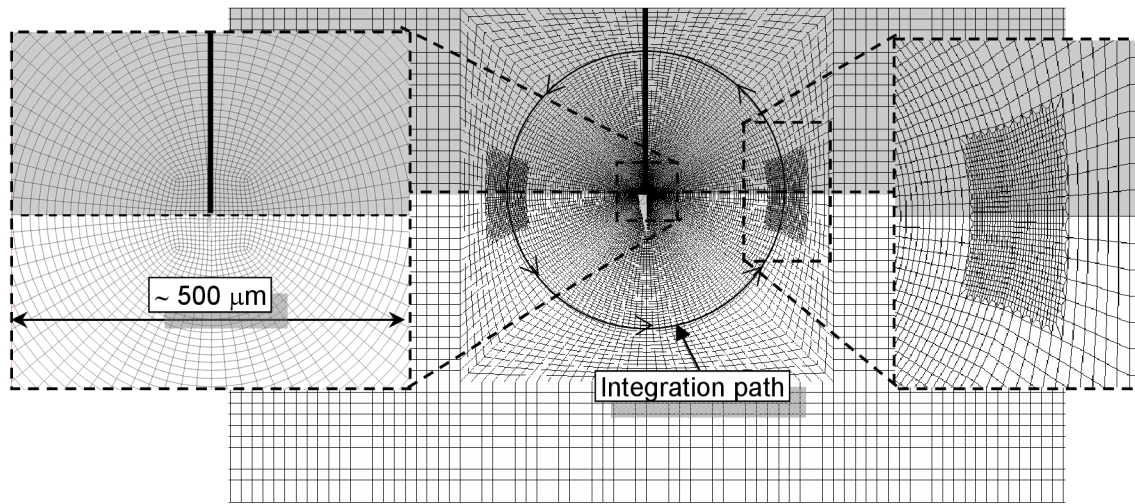
Fig. 37 Example of the FE mesh in the vicinity of the crack tip perpendicular to the bi-material interface with detail of the mesh refinement on the integration path at interface crossing.

The characteristic eigenvalues of the singularity δ_1, δ_2 (Table 3) has been calculated using the L.E.S. method analyzed in 0 and by employing mathematical software Maple 10, where the code for these calculations has been written. The corresponding generalized stress intensity factors H_1, H_2 (GSIF) and the T-stress T have been calculated using the Ψ-integral, based on the Betti´s reciprocal theorem – as described in 4.1.3 and 4.1.4. The calculations are carried out as a parametric study for several Dundurs' parameters α:

β=0, λ_1=0.1, ρ_1=2, λ_2=1, ρ_2=1, E_2=60000 MPa, ν_2=0.238					
α	Characteristic eigenvalue δ_1 [-]	Characteristic eigenvalue δ_2 [-]	GSIF – H_1 [$MPa.m^{1-\delta_1}$]	GSIF – H_2 [$MPa.m^{1-\delta_2}$]	T-stress – T [MPa]
-0.99	0.039521	0.070269	0.081	29.015	12528.0
-0.9	0.124150	0.220120	0.012	8.334	1193.2
-0.8	0.174523	0.307537	0.005	5.929	387.1
-0.7	0.212760	0.371383	0.003	4.993	159.9
-0.6	0.244859	0.421938	0.002	4.435	68.1
-0.5	0.273191	0.463121	0.002	3.997	24.8
-0.4	0.298994	0.496945	0.001	3.593	2.8
-0.3	0.323018	0.524661	0.001	3.193	-8.5
-0.2	0.345761	0.547175	0.001	2.796	-14.1
-0.1	0.367575	0.565216	0.001	2.410	-16.6
0	0.388725	0.579406	0.0004	2.049	-17.1
0.1	0.409413	0.590282	0.0003	1.718	-16.5
0.2	0.429803	0.598308	0.0003	1.424	-15.2
0.3	0.450028	0.603876	0.0002	1.164	-13.5
0.4	0.470199	0.607312	0.0002	0.936	-11.6

Table 3 Values of the singularity exponents δ, GSIFs and T-stresses (calculated using the L.E.S. method) for several values of Dundurs' parameter α for orthotropic substrate and transversally isotropic surface layer with crack perpendicular to the interface.

Note here, that δ_1 corresponds to the stronger singularity, δ_2 to the weaker singularity and the characteristic eigenvalue of the singularity $\delta_3=1$ corresponds to the regular term T-stress. To all the characteristic eigenvalues δ_1 and δ_2 pertain the appropriate GSIFs H_1 and H_2 respectively. The mathematical software Matlab 7.1 has been used for the calculations of GSIFs and T-stresses. Observe that for the perpendicular crack the first singular term is negligible in comparison with the second one ($H_1 \ll H_2$) and most likely the non-zero value of H_1 is due to numerical errors. This phenomenon is possible to observe only for the case of the crack perpendicular to the bi-material interface and simultaneously for the case, where the principal material directions of both materials coincide with the chosen CS $x_1 x_2$ (Fig. 36). Apparently in the case investigated, the GSIF H_1 relates to the antisymmetric mode while H_2 relates to the symmetric mode, see also the remark in the section 7.2.2. This implies that near the singular point the stress and displacement fields evoked by this type of general stress concentrator under symmetric applied loading can be reliably described by use of only one singular and one regular term (T-stress). In case of the inclined crack or the material configuration with inclined major material directions, other singular terms should be taken into consideration (as will be presented in the following section) and assessed in terms of their importance. In this section which deals with the perpendicular crack, the first singular term will be omitted from the calculations.

Fig. 38 -Fig. 41, show the decomposition of the full stress and displacement field (around the vicinity of the crack tip) into individual terms. The thin dark (blue) curves are the stresses and displacements obtained from the FE analysis. As such these curves correspond to the full Williams-like asymptotic expansion (they contain all terms from this expansion). On the other side, there are two lighter (orange) curves which have been obtained from the asymptotic singularity analysis using the L.E.S. method and the Ψ-integral (GSIF and T-stress calculations). The thin light (orange) curves correspond to the singular solution where only one singular term in the asymptotic expansion is considered (the more dominant one). It means the displacements and stresses are described as follows: $\mathbf{U}^0 = H_2 \cdot r^{\delta_2} . \mathbf{u}_2(\theta), \quad \sigma_{ij} = H_2 \cdot r^{\delta_2 - 1} . f_{ij,2}(\theta)$. When consider one more term in the asymptotic expansion (T-stress in this case), then one obtain the light thick (orange) curve. Then the displacements and stresses are described using the following expansions: $\mathbf{U}^0 = H_2 \cdot r^{\delta_2} . \mathbf{u}_2(\theta) + T \cdot r \cdot \delta_{i2} \cdot \delta_{j2} \cdot \mathbf{u}_3(\theta); \quad \sigma_{ij} = H_2 \cdot r^{\delta_2 - 1} . f_{ij,2}(\theta) + T \cdot \delta_{i2} \cdot \delta_{j2}$. All figures clearly show that the more terms are considered, the more exact is the description of the stress and displacement field (in comparison with the Finite Element solution). The number of terms in the asymptotic expansion, which are necessary for the sufficiently exact description of the stress and displacement field, depends also on the bi-material configuration. Comparing the Fig. 38 with Fig. 39 or Fig. 40 with Fig. 41 one can observe that the more the radius of the integration path is approaching the singular point the more the FE stress and displacement fields are approaching the singular solution. The FE solution can thus contain some influence of the free surface when the integration path is close to it.

Fig. 38 Comparison of the stresses and displacements for $\alpha=-0.1$, $\beta=0$, obtained from the FE analysis and from the asymptotic singularity analysis including (or not including) the T-stress term, on the circular integration path of radius $R=1$mm.
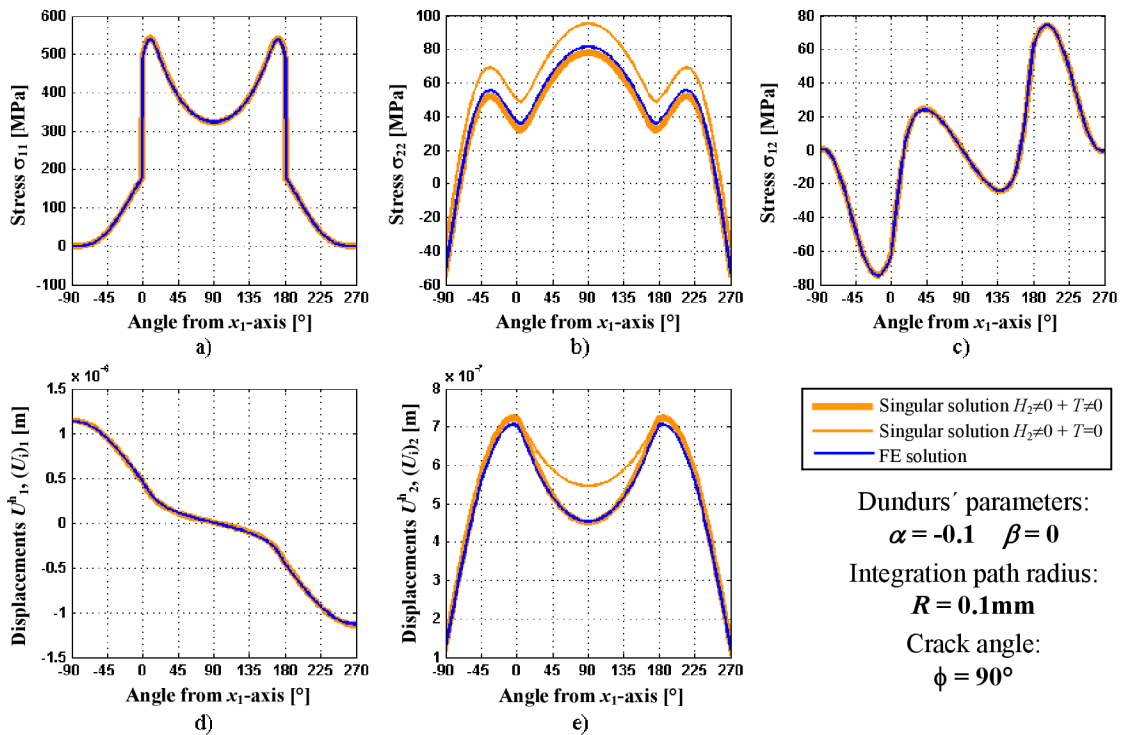
Fig. 39 Comparison of the stresses and displacements for $\alpha=-0.1$, $\beta=0$, obtained from the FE analysis and from the asymptotic singularity analysis including (or not including) the T-stress term, on the circular integration path of radius $R=0.1$mm.
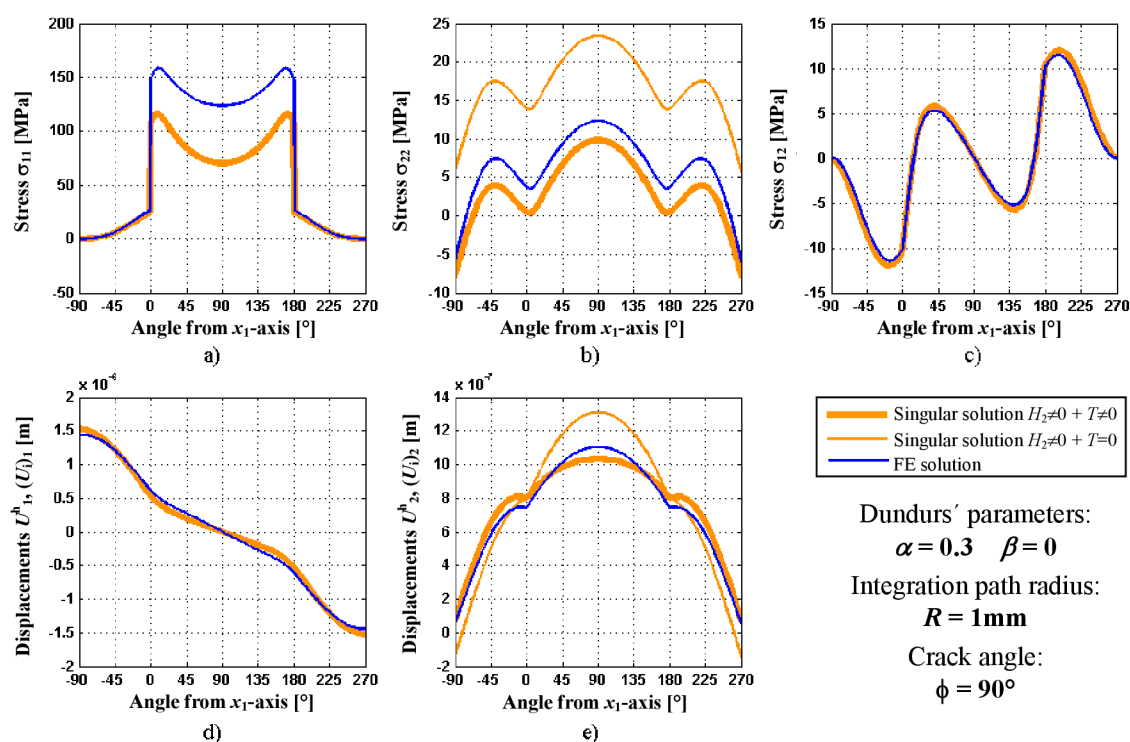
Fig. 40 Comparison of the stresses and displacements for α=0.3, β=0, obtained from the FE analysis and from the asymptotic singularity analysis including (or not including) the T-stress term, on the circular integration path of radius R=1mm.
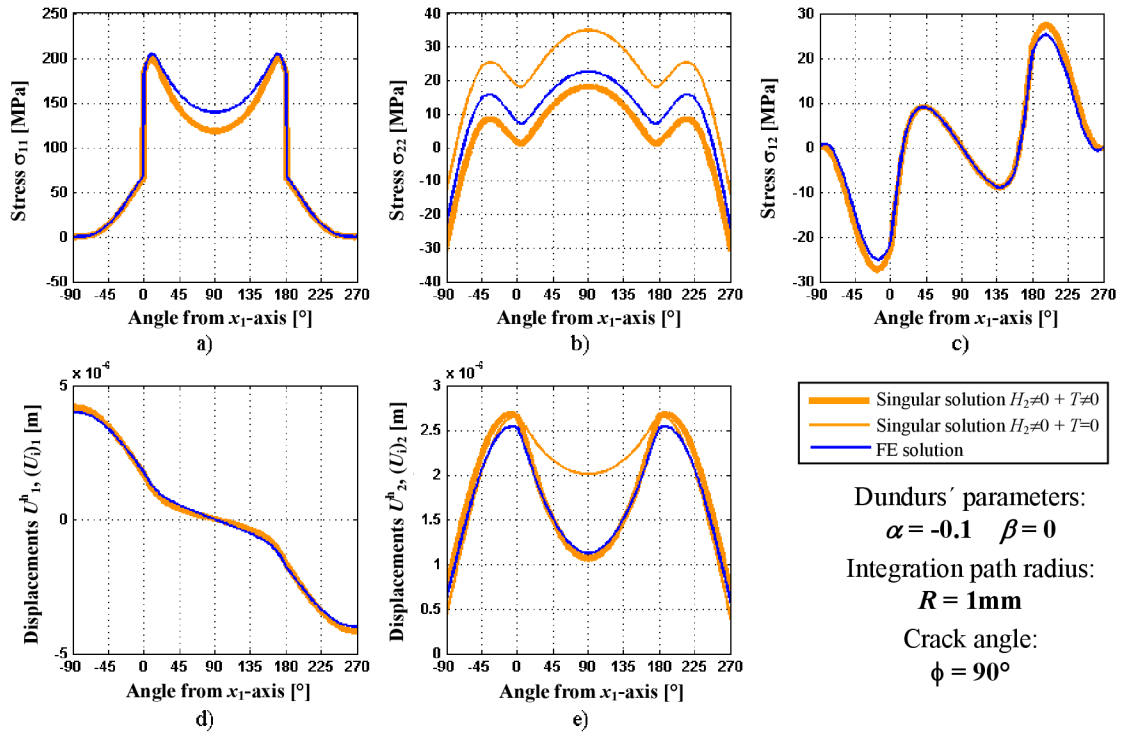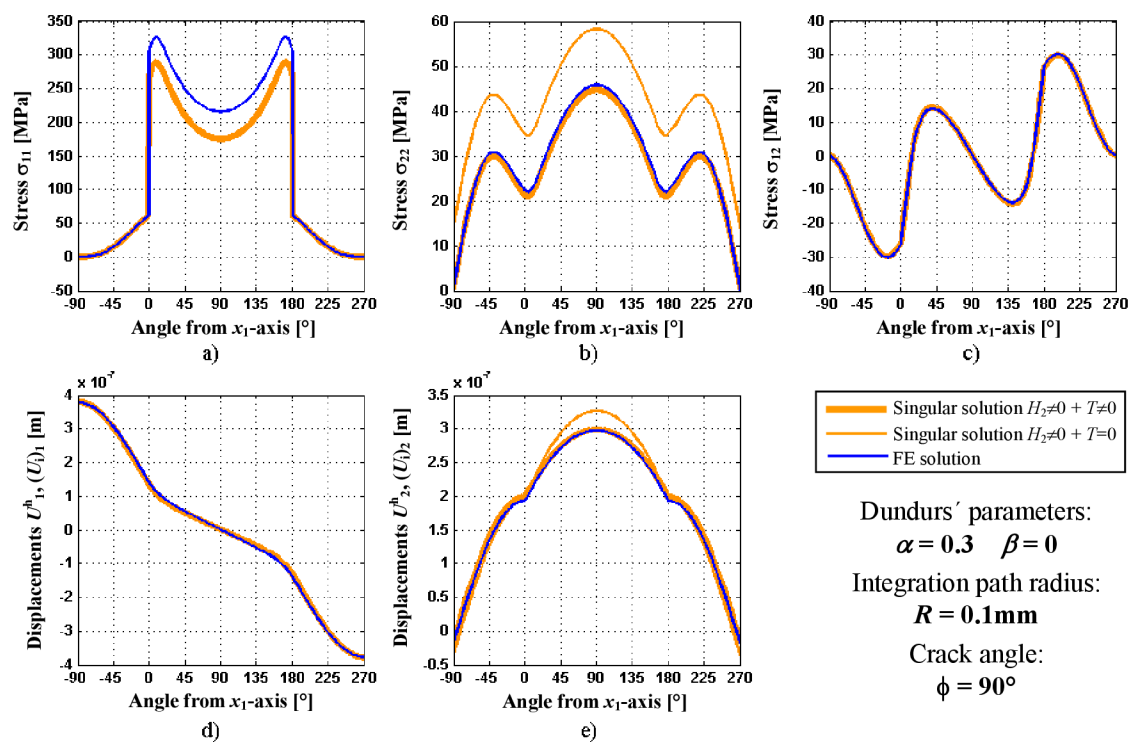

Fig. 41 Comparison of the stresses and displacements for α=0.3, β=0, obtained from the FE analysis and from the asymptotic singularity analysis including (or not including) the T-stress term, on the circular integration path of radius R =0.1mm.

8.1.2 Fracture criteria

The preceding results concern the description of the stress and displacement field near the crack tip at the bi-material interface. A tool for the decomposition of the "full" stress (displacement) fields (which can be obtained e.g. from the FE analysis) into asymptotic expansion was developed. This effort is now to be utilized in the fracture criterion, where the influence of particular asymptotic expansion terms on the resulting behaviour of the general stress concentrator will be assessed. To this end, the theory of the finite fracture mechanics and the matched asymptotic procedure (see 7.2.2) is to be employed. To predict the subsequent crack extension (under the given loading conditions), the change of the potential energy (and corresponding Energy Release Rate - ERR) caused by the increase of the main crack by some finite extension (in all possible propagation directions) have to be calculated. Using relations (194) and (195), the coefficients of the outer expansion (192) - $K_{1d(p)}$, $K_{2d(p)}$, $K'_{1d(p)}$ and $K'_{2d(p)}$, required also for the calculation of ERR $G_{d(p)}$ (196) are obtained. Analogical calculations as for GSIF or T-stress based on the Ψ-integral are used here. The required FE solution is performed using the FE model of the inner domain of circular shape as depicted in the Fig. 42. The FE code ANSYS 10.0 has been used again. Note that the mesh refinement at the area where the integration path crosses the interface is recommended (mesh in the Fig. 42 is not refined there):
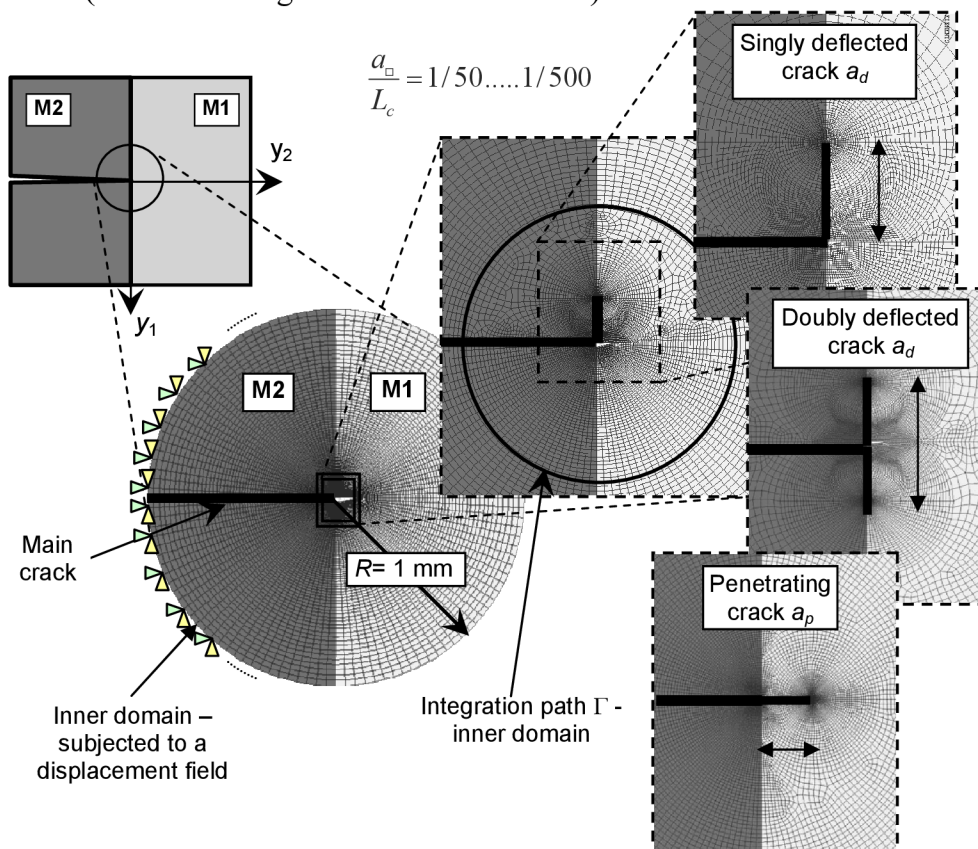
Fig. 42 Example of the FE mesh used for the case of a singly (doubly) deflected crack and penetrating crack.

The determination of the change of the ERR $G_{d(p)}$ - relation (196) (caused by the finite crack extension), requires a numerical solution of the stress and displacement field on the so-called inner domain by FEM. The ERRs are calculated from the change of the potential energy between the unperturbed state (main crack without extension) and perturbed state (main crack with small crack extension) – see (196).

The inner domain (Fig. 42) is subjected to the displacement field on the diameter $R=1$mm where for the calculation of parameters $K_{1d(p)}$ and $K_{2d(p)}$ the boundary condition (215) is used and for the parameters $K'_{1d(p)}$, $K'_{2d(p)}$ the boundary condition of type (216) is applied:

$$\mathbf{U}^0(x_1, x_2) = H_2 r^{\delta_2} \mathbf{u}_2(\theta) \quad \ldots\ldots \text{ where } H_2 = 1 \tag{215}$$

$$\mathbf{U}^0(x_1, x_2) = T r \, \mathbf{u}_3(\theta) \quad \ldots\ldots \text{ where } T = 1. \tag{216}$$

The characteristic eigenvalue δ_2 (corresponding to the more dominant singular term) and the functions $\mathbf{u}_2(\theta)$, $\mathbf{u}_3(\theta)$ are taken from the singularity analysis – see previous section 8.1.1. In the FE calculations, GSIF H_2 and the T-stress T are set equal to unit. The actual values of GSIFs and T-stresses (from Table 3) will be substituted later. Note, that the total length of doubly deflected crack extension a_d equals to the length of the singly deflected crack extension and to the penetrating crack extension a_p ($a_d = a_p$). The crack extension length is for the most part represented by the dimensionless parameter $\varepsilon = a_{d(p)}/L_c$ in pertinent relations.

The appropriate ERR G_{sd}, G_d, G_p are calculated for all possible directions using formula (196) where GSIF $H = H_2$ and the T-stress T are taken from the Table 3. All coefficients K, ERRs G, and their ratios for several parameters α are given in the Table 4 (for $\varepsilon = 1/50$) and Table 5 (for $\varepsilon = 1/500$).

$\beta=0$, $\lambda_1=0.1$, $\rho_1=2$, $\lambda_2=1$, $\rho_2=1$, $E_2=60000$ MPa, $\nu_2=0.238$, $\varepsilon = 1/50$								
					ERR for $T=0$		ERR for $T\neq 0$	
α	K_{1sd} [-] K_{1d} [-] K_{1p} [-]	K'_{1sd} [-] K'_{1d} [-] K'_{1p} [-]	K_{2sd} [-] K_{2d} [-] K_{2p} [-]	K'_{2sd} [-] K'_{2d} [-] K'_{2p} [-]	G_{sd} G_d G_p	G_{sd}/G_p G_d/G_p	G_{sd} G_d G_p	G_{sd}/G_p G_d/G_p
-0.9	-0.078111 -0.077071 -0.183052	-1.03 e-07 -4.40 e-07 -2.66 e-05	-5.14 e-04 -7.92 e-04 -3.69 e-02	-2.18 e-06 -1.96 e-06 -1.04 e-05	1.81 e-03 1.79 e-03 4.25 e-03	0.425 0.419	4.78 e-03 4.60 e-03 2.93 e-02	0.163 0.157
-0.7	-0.015780 -0.015266 -0.083535	-3.39 e-07 -5.98 e-07 -1.33 e-05	-5.39 e-04 -6.95 e-04 -1.22 e-02	-6.94 e-07 -5.42 e-07 -2.54 e-06	7.22 e-05 6.99 e-05 3.82 e-04	0.187 0.181	9.82 e-05 9.73 e-05 7.38 e-04	0.133 0.132
-0.5	-0.005948 -0.005926 -0.051630	-4.44 e-07 -5.64 e-07 -6.92 e-06	-5.02 e-04 -5.53 e-04 -5.44 e-03	-3.67 e-07 -2.60 e-07 -8.48 e-07	1.18 e-05 1.18 e-05 1.03 e-04	0.114 0.114	1.29 e-05 1.31 e-05 1.17 e-04	0.110 0.111
-0.3	-0.003356 -0.003503 -0.036793	-4.77 e-07 -5.00 e-07 -3.26 e-06	-4.54 e-04 -4.49 e-04 -2.38 e-03	-2.22 e-07 -1.47 e-07 -2.29 e-07	3.47 e-06 3.62 e-06 3.81 e-05	0.090 0.094	3.18 e-06 3.30 e-06 3.58 e-05	0.089 0.092
-0.1	-0.002565 -0.002716 -0.028200	-4.60 e-07 -4.25 e-07 -8.86 e-07	-4.19 e-04 -3.85 e-04 -6.93 e-04	-1.41 e-07 -8.78 e-08 -2.04 e-08	1.41 e-06 1.49 e-06 1.55 e-05	0.090 0.096	1.06 e-06 1.14 e-06 1.46 e-05	0.072 0.078
0.1	-0.002353 -0.002440 -0.022230	-4.04 e-07 -3.40 e-07 6.98 e-07	-4.22 e-04 -3.73 e-04 3.60 e-04	-8.97 e-08 -5.33 e-08 -1.71 e-08	6.56 e-07 6.80 e-07 6.19 e-06	0.105 0.109	4.15 e-07 4.61 e-07 6.76 e-06	0.061 0.068
0.3	-0.002360 -0.002357 -0.017410	-3.17 e-07 -2.49 e-07 1.60 e-06	-5.00 e-04 -4.43 e-04 1.11 e-03	-5.57 e-08 -3.17 e-08 -1.34 e-07	3.04 e-07 3.04 e-07 2.24 e-06	0.135 0.135	1.72 e-07 1.92 e-07 3.20 e-06	0.054 0.060

Table 4 Coefficients of the inner expansion, ERR of the deflected and penetrating crack (for a finite crack extension of the characteristic size $\varepsilon = 1/50$) and ratios of the ERR for singly (doubly) deflected and penetrating crack (*sd* – single deflection, *d* – double deflection, *p* – penetration).

α	K_{1sd} [-] K_{1d} [-] K_{1p} [-]	K'_{1sd} [-] K'_{1d} [-] K'_{1p} [-]	K_{2sd} [-] K_{2d} [-] K_{2p} [-]	K'_{2sd} [-] K'_{2d} [-] K'_{2p} [-]	ERR for $T=0$ G_{sd} G_d G_p	G_{sd}/G_p G_d/G_p	ERR for $T{\neq}0$ G_{sd} G_d G_p	G_{sd}/G_p G_d/G_p
-0.9	-3.02 e-02 -2.98 e-02 -7.77 e-02	-1.70 e-08 -3.70 e-08 -1.89 e-06	-1.76 e-04 -1.87 e-04 -2.74 e-03	-8.90 e-09 -5.81 e-09 -9.99 e-08	2.54 e-03 2.51 e-03 6.55 e-03	0.386 0.381	2.55 e-03 2.52 e-03 7.04 e-03	0.362 0.357
-0.7	-2.97 e-03 -2.87 e-03 -1.66 e-02	-2.90 e-08 -3.85 e-08 -6.32 e-07	-1.68 e-04 -1.72 e-04 -7.06 e-04	-9.85 e-09 -7.96 e-09 -2.98 e-08	2.46 e-05 2.37 e-05 1.37 e-04	0.175 0.168	2.47 e-05 2.40 e-05 1.43 e-04	0.173 0.168
-0.5	-7.54 e-04 -7.45 e-04 -6.51 e-03	-2.72 e-08 -3.01 e-08 -2.63 e-07	-1.33 e-04 -1.33 e-04 -3.11 e-04	-3.49 e-09 -2.26 e-09 -8.52 e-09	1.78 e-06 1.75 e-06 1.53 e-05	0.109 0.108	1.79 e-06 1.77 e-06 1.55 e-05	0.115 0.114
-0.3	-3.28 e-04 -3.36 e-04 -3.43 e-03	-2.52 e-08 -2.50 e-08 -1.11 e-07	-1.11 e-04 -1.10 e-04 -1.70 e-04	-2.45 e-09 -1.62 e-09 -2.51 e-09	3.03 e-07 3.10 e-07 3.17 e-06	0.089 0.091	3.01 e-07 3.08 e-07 3.14 e-06	0.096 0.098
-0.1	-2.06 e-04 -2.13 e-04 -2.15 e-03	-2.15 e-08 -2.00 e-08 -3.31 e-08	-1.10 e-04 -1.08 e-04 -1.17 e-04	-1.44 e-09 -8.63 e-10 -2.13 e-10	8.38 e-08 8.66 e-08 8.76 e-07	0.090 0.093	8.11 e-08 8.43 e-08 8.70 e-07	0.093 0.097
0.1	-1.63 e-04 -1.65 e-04 -1.50 e-03	-1.72 e-08 -1.52 e-08 1.18 e-08	-1.44 e-04 -1.42 e-04 -1.23 e-04	-9.02 e-10 -5.19 e-10 -1.62 e-10	3.00 e-08 3.04 e-08 2.75 e-07	0.106 0.108	2.83 e-08 2.91 e-08 2.79 e-07	0.101 0.104
0.3	-1.48 e-04 -1.45 e-04 -1.09 e-03	-1.22 e-08 -1.03 e-08 3.61 e-08	-2.43 e-04 -2.42 e-04 -2.03 e-04	-5.65 e-10 -3.15 e-10 -1.35 e-09	1.18 e-08 1.16 e-08 8.71 e-08	0.136 0.134	1.09 e-08 1.09 e-08 9.28 e-08	0.118 0.118

Table header parameters: $\beta=0$, $\lambda_1=0.1$, $\rho_1=2$, $\lambda_2=1$, $\rho_2=1$, $E_2=60000$ MPa, $\nu_2=0.238$, $\varepsilon = 1/500$

Table 5 Coefficients of the inner expansion, ERR of the deflected and penetrating crack (for a finite crack extension of the characteristic size $\varepsilon = 1/500$) and ratios of the ERR for singly (doubly) deflected and penetrating crack (sd – single deflection, d – double deflection, p – penetration).

Note that the results in the previous two tables present only a representative selection of all computed results. A complete set of results is displayed in the Fig. 43. The graphs show the dependency of the ratios G_{sd}/G_p (G_d/G_p) on Dundurs' parameter α for several crack extension lengths assuming either the T-stress term in the Williams-like asymptotic expansion is considered or not. Apparently, when the T-stress term is not considered, the ratios G_{sd}/G_p (G_d/G_p) are in fact independent of the crack extension size. This also follows from the relation (198), which simplifies to the plain ratio of K_{1sd} and K_{1p} (or K_{1d} and K_{1p}) if the T-stress is set to zero. Propably the small differences between curves, especially for the lower values of α are caused by both the accuracy of the numerical integration and the used element size in the FE model. When the T-stress is considered, the complete relation (198) has to be used. The dependency on the crack extension length is obvious. This property also follows from Eq. (198). The competition between the single or double deflection is characterized by the ratios G_{sd}/G_p and G_d/G_p. If $G_{sd}/G_p > G_d/G_p$ the single deflection is preferred before double deflection and vice versa. The competition between single (double) deflection and penetration is given by the relation (213). As stated already in 7.2.4, the final assessment of the propagation direction requires the knowledge of the material and interface toughness which have to be determined experimentally.

Note that for the assessment of the propagation direction, the mode mixity should be also taken into the account. It can strongly influence the criterion (213) and the decision about the further propagation direction. The mode mixity characterized by the phase angle

Ψ_G (204) influences the resulting interfacial toughness. The bigger the phase angle Ψ_G is, the higher interfacial toughness is reached. The dependence of the interfacial toughness on the mode mixity has been studied in several papers - e.g. [7]-[9] . It was suggested that the resulting interfacial toughness can be described for example by the relation $G_c^i = G_1 \cdot \left(1 + \tan^2 \Psi_G\right)$, where G_1 is the interfacial toughness for the zero phase angle Ψ_G.

It follows from this expression, that for the values of the phase angle Ψ_G higher than 40° or 50°, the resulting interfacial toughness starts to grow dramatically. The calculations of the phase angle Ψ_G were not performed within this thesis and it should be a point of interest of the subsequent work to involve another refining parameter in the criterion.
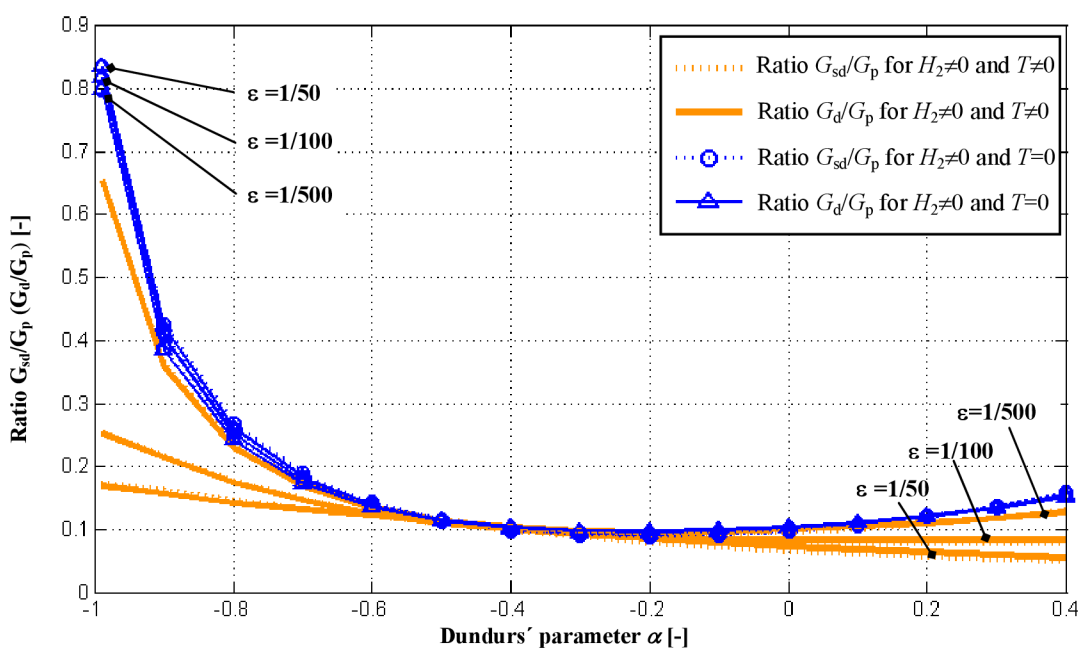
Fig. 43 The ratio of G_{sd}/G_p (G_d/G_p) as a function of Dundurs' parameter α for several values of the characteristic crack extension size ε.

When the T-stress term is considered, one can observe, that with decreasing ε the ratios G_{sd}/G_p (G_d/G_p) approach the limiting case when the T-stress is not considered. In other words, when the crack extension is too small, influence of the T-stress is not measurable. The length of the crack extension should be chosen in accordance with relation (172).

Observe also (in Fig. 43 or Table 4 and Table 5) that for the perpendicular crack the difference between the single and double deflection ERR ratios is very slight. This leads to a conclusion that it is not possible to decide for a certainty whether the single or double deflection will occur. The resulting behaviour will depend also on some other factors like the loading, geometry or bonding imperfections which will start up one of these deflection types.

8.2 Crack terminating at an arbitrary angle on the bi-material interface in orthotropic media (with transversally isotropic surface layer)

8.2.1 Description of the stress field

Solution to a similar problem as for the perpendicular crack is demonstrated for the case of the main crack inclined with respect to the interface. All the theory and calculations are in complete analogy to 8.1.1 with the only difference in the boundary conditions (97), where the condition of zero resulting force $T_i=0$ (98) is set for the angles corresponding to the inclined crack faces - $\theta = -\phi \cdot (\pi/180)$ and $\theta = (360-\phi) \cdot (\pi/180)$.
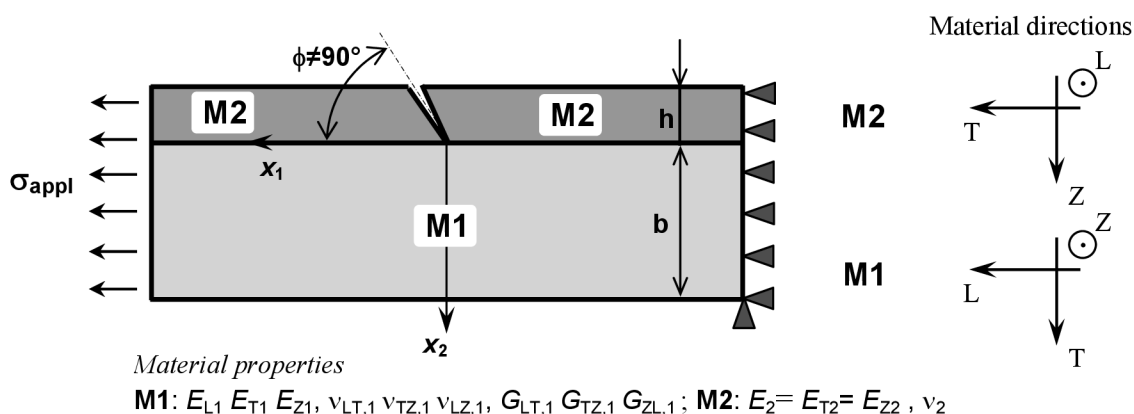
Fig. 44 Scheme of the solved bi-material configuration with crack situated at arbitrary angle to the bi-material interface.

In the same way as in the previous section 8.1.1 the characteristic eigenvalues of the singularity δ_1 and δ_2 have been calculated using the L.E.S. method (Table 6-Table 9). In contrast to the case of the perpendicular crack the characteristic eigenvalue $\delta_3=1$ does not generally exist, hence the T-stress was not calculated. The whole stress and displacement field is thus described only by the singular terms in the asymptotic expansion. The first singular term which was not involved for the perpendicular crack because GSIF H_1 was obviously zero is now getting to be significant. The more the crack is inclined from $\phi=90°$ the more significant the first singular term is. Therefore, the two generalized stress intensity factors H_1 and H_2 will be needed for description of the stress and displacement field. They are again computed using the Ψ-integral for several values of Dundurs' parameter α and for several inclination angles ϕ (see Table 6-Table 9). All the results from the mentioned Table 6-Table 9 are displayed in Fig. 45.

$\phi = 80°$	β=0, λ_1=0.1, ρ_1=2, λ_2=1, ρ_2=1, E_2=60000 MPa, v_2=0.238			
α	Characteristic eigenvalue δ_1 [-]	Characteristic eigenvalue δ_2 [-]	GSIF $-H_1$ [MPa.m$^{1-\delta_1}$]	GSIF $-H_2$ [MPa.m$^{1-\delta_2}$]
-0.99	0.039831	0.071713	6.01	39.57
-0.9	0.125243	0.223763	1.04	11.52
-0.8	0.176213	0.311326	0.53	8.08
-0.7	0.214963	0.374518	0.34	6.62
-0.6	0.247513	0.424068	0.24	5.68
-0.5	0.276235	0.464170	0.18	4.91
-0.4	0.302365	0.497030	0.13	4.23
-0.3	0.326649	0.524034	0.10	3.60
-0.2	0.349576	0.546164	0.07	3.02
-0.1	0.371489	0.564182	0.05	2.51
0	0.392632	0.578710	0.03	2.07
0.1	0.413186	0.590273	0.01	1.70
0.2	0.433277	0.599323	0.01	1.41
0.3	0.452982	0.606264	0.02	1.18
0.4	0.472322	0.611467	0.03	0.99

Table 6 Values of the singularity exponents, and GSIFs (calculated using the L.E.S. method) for several values of Dundurs' parameter α for orthotropic substrate and transversally isotropic surface layer with crack inclined to the interface at angle ϕ=80°.

$\phi = 70°$	β=0, λ_1=0.1, ρ_1=2, λ_2=1, ρ_2=1, E_2=60000 MPa, v_2=0.238			
α	Characteristic eigenvalue δ_1 [-]	Characteristic eigenvalue δ_2 [-]	GSIF $-H_1$ [MPa.m$^{1-\delta_1}$]	GSIF $-H_2$ [MPa.m$^{1-\delta_2}$]
-0.99	0.040770	0.076363	9.10	51.97
-0.9	0.128533	0.235353	1.83	15.86
-0.8	0.181276	0.323176	1.01	11.12
-0.7	0.221556	0.384145	0.68	8.87
-0.6	0.255457	0.430503	0.51	7.29
-0.5	0.285356	0.467298	0.39	6.00
-0.4	0.312473	0.497282	0.30	4.91
-0.3	0.337528	0.522179	0.23	3.98
-0.2	0.360979	0.543164	0.17	3.19
-0.1	0.383121	0.561086	0.11	2.55
0	0.404141	0.576596	0.06	2.04
0.1	0.424141	0.590222	0.02	1.66
0.2	0.443143	0.602423	0.02	1.39
0.3	0.461097	0.613626	0.05	1.21
0.4	0.477877	0.624256	0.08	1.08

Table 7 Values of the singularity exponents, and GSIFs (calculated using the L.E.S. method) for several values of Dundurs' parameter α for orthotropic substrate and transversally isotropic surface layer with crack inclined to the interface at angle ϕ=70°.

$\phi = 60°$	$\beta=0,\ \lambda_1=0.1,\ \rho_1=2,\ \lambda_2=1,\ \rho_2=1,\ E_2=60000$ MPa, $\nu_2=0.238$			
α	Characteristic eigenvalue δ_1 [-]	Characteristic eigenvalue δ_2 [-]	GSIF – H_1 [MPa.m$^{1-\delta_1}$]	GSIF – H_2 [MPa.m$^{1-\delta_2}$]
-0.99	0.042391	0.085323	13.66	67.91
-0.9	0.134086	0.256964	2.94	22.87
-0.8	0.189713	0.344368	1.71	16.06
-0.7	0.232480	0.400691	1.22	12.26
-0.6	0.268598	0.441210	0.94	9.50
-0.5	0.300441	0.472388	0.75	7.37
-0.4	0.329184	0.497687	0.59	5.70
-0.3	0.355472	0.519195	0.46	4.38
-0.2	0.379663	0.538290	0.34	3.35
-0.1	0.401937	0.555957	0.22	2.55
0	0.422352	0.572955	0.11	1.96
0.1	0.440892	0.589895	0.02	1.56
0.2	0.457504	0.607275	0.05	1.35
0.3	0.472145	0.625485	0.10	1.26
0.4	0.484812	0.644794	0.12	1.23

Table 8 Values of the singularity exponents, and GSIFs (calculated using the L.E.S. method) for several values of Dundurs' parameter α for orthotropic substrate and transversally isotropic surface layer with crack inclined to the interface at angle $\phi=60°$.

$\phi = 50°$	$\beta=0,\ \lambda_1=0.1,\ \rho_1=2,\ \lambda_2=1,\ \rho_2=1,\ E_2=60000$ MPa, $\nu_2=0.238$			
α	Characteristic eigenvalue δ_1 [-]	Characteristic eigenvalue δ_2 [-]	GSIF – H_1 [MPa.m$^{1-\delta_1}$]	GSIF – H_2 [MPa.m$^{1-\delta_2}$]
-0.99	0.044827	0.101046	16.80	89.23
-0.9	0.142156	0.292137	4.03	33.62
-0.8	0.201654	0.376067	2.50	22.91
-0.7	0.247675	0.423843	1.89	16.26
-0.6	0.286679	0.455550	1.53	11.72
-0.5	0.321059	0.479054	1.28	8.57
-0.4	0.351906	0.498214	1.05	6.33
-0.3	0.379693	0.515275	0.83	4.68
-0.2	0.404532	0.531772	0.60	3.43
-0.1	0.426330	0.548883	0.37	2.48
0	0.444952	0.567512	0.15	1.81
0.1	0.460412	0.588239	0.02	1.41
0.2	0.472954	0.611311	0.13	1.26
0.3	0.483002	0.636755	0.17	1.26
0.4	0.491024	0.664558	0.18	1.30

Table 9 Values of the singularity exponents, and GSIFs (calculated using the L.E.S. method) for several values of Dundurs' parameter α for orthotropic substrate and transversally isotropic surface layer with crack inclined to the interface at angle $\phi=50°$.
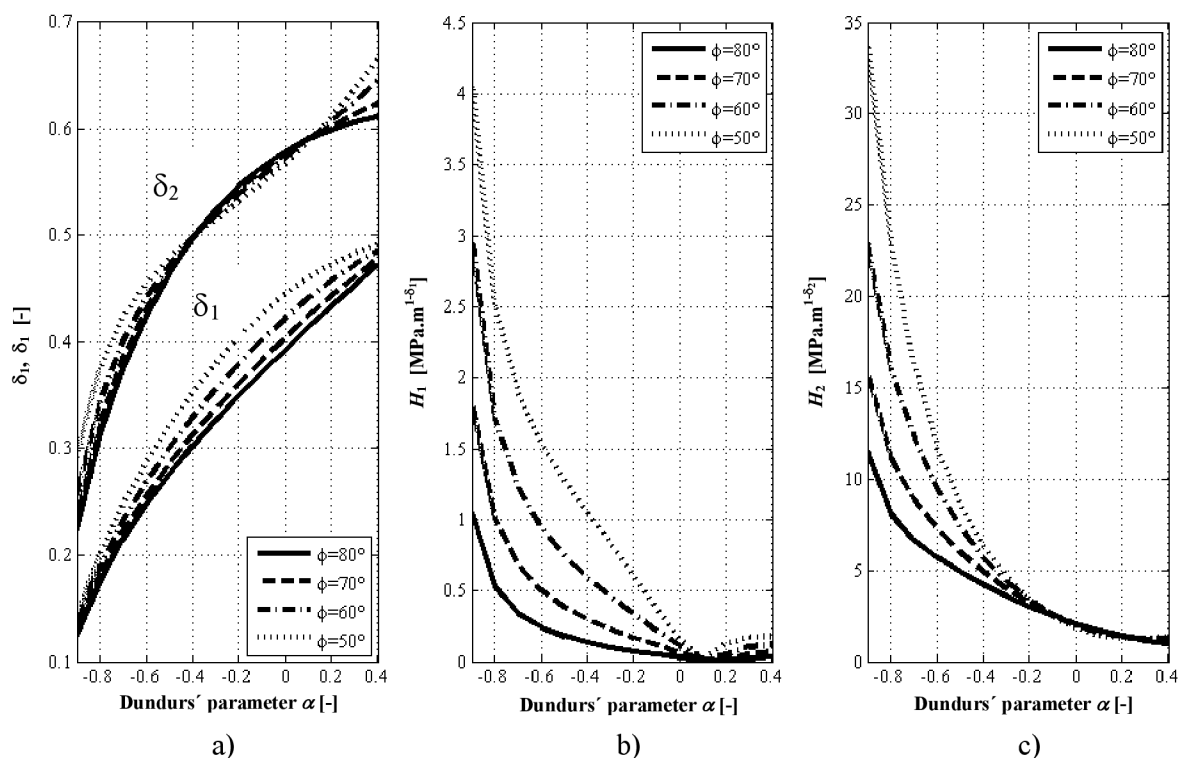
Fig. 45 Variation of the eigenvalues δ_1, δ_2 and of the Generalized Stress Intensity Factors H_1, H_2 with Dundurs' parameter α for several angles ϕ of the crack inclination with respect to the bi-material interface (Dundurs' parameter β=0).

Again, in analogy to the previous section, the decomposition of the "full" stress and displacement fields into asymptotic expansion (in the vicinity of the crack tip) was carried out. The first two terms are displayed in the Fig. 46 - Fig. 49. The thin dark (blue) curves refer to the stresses and displacements obtained from the FE analysis. The two lighter (orange) curves stand for the singular solution obtained using the L.E.S. method and the Ψ-integral. The thin light (orange) curves correspond to the singular solution where only the second singular term in the asymptotic expansion is considered. It means the displacements and stresses are described, for this case, as follows: $\mathbf{U}^0 = H_2 \cdot r^{\delta_2} . \mathbf{u}_2 \left(\theta \right)$; $\sigma_{ij} = H_2 \cdot r^{\delta_2 - 1} . f_{ij} \left(\theta \right)$. When both singular terms in the asymptotic expansion are considered, one then obtains the light thick (orange) curve. Then the displacements and stresses are described using the following expansions: $\mathbf{U}^0 = H_1 \cdot r^{\delta_1} . \mathbf{u}_1 \left(\theta \right) + H_2 \cdot r^{\delta_2} . \mathbf{u}_2 \left(\theta \right)$; $\sigma_{ij} = H_1 \cdot r^{\delta_1 - 1} . f_{ij,1} \left(\theta \right) + H_2 \cdot r^{\delta_2 - 1} . f_{ij,2} \left(\theta \right)$. All figures clearly show that by considering both singular terms, the description of the stress and displacement field is more precise and approaches the full FE solution.

Fig. 46 Comparison of the stresses and displacements around the inclined crack for φ=80°, α=0.1, β=0, obtained from the FE analysis and from the singular solution with consideration of a single or both singular terms, on the circular integration path of radius R=0.1mm.
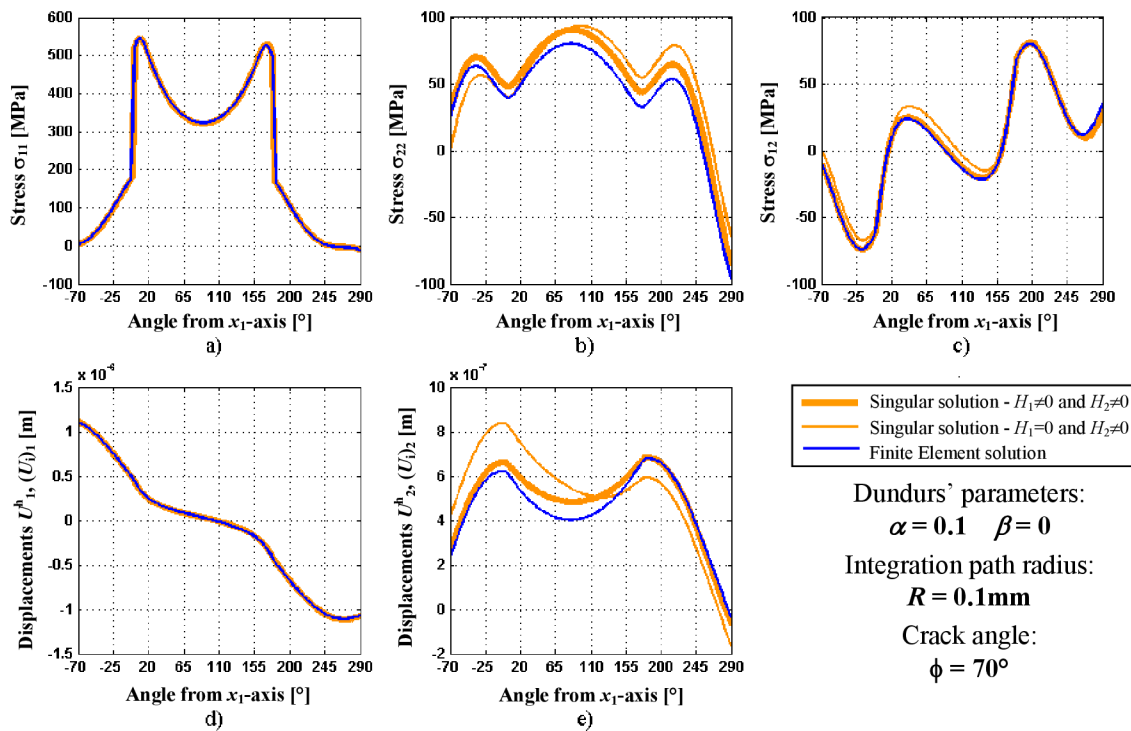
Fig. 47 Comparison of the stresses and displacements around the inclined crack for φ=70°, α=0.1, β=0, obtained from the FE analysis and from the singular solution with consideration of a single or both singular terms, on the circular integration path of radius R=0.1mm.
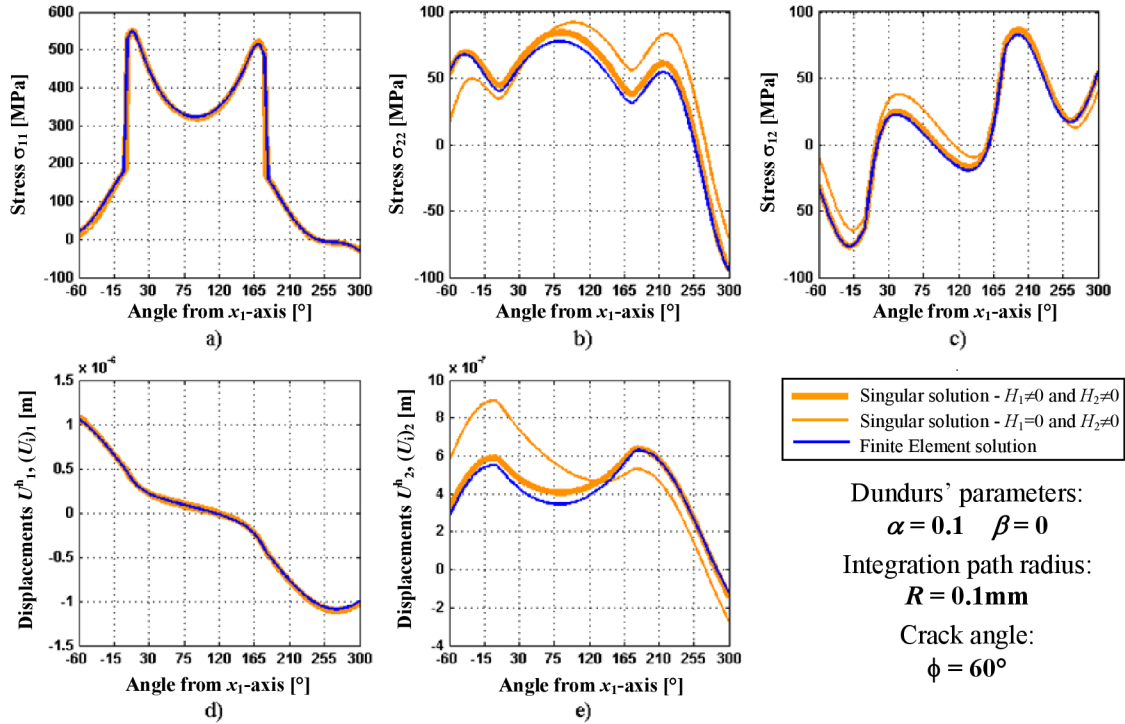
Fig. 48 Comparison of the stresses and displacements around the inclined crack for φ=60°, α=0.1, β=0, obtained from the FE analysis and from the singular solution with consideration of a single or both singular terms, on the circular integration path of radius R=0.1mm.

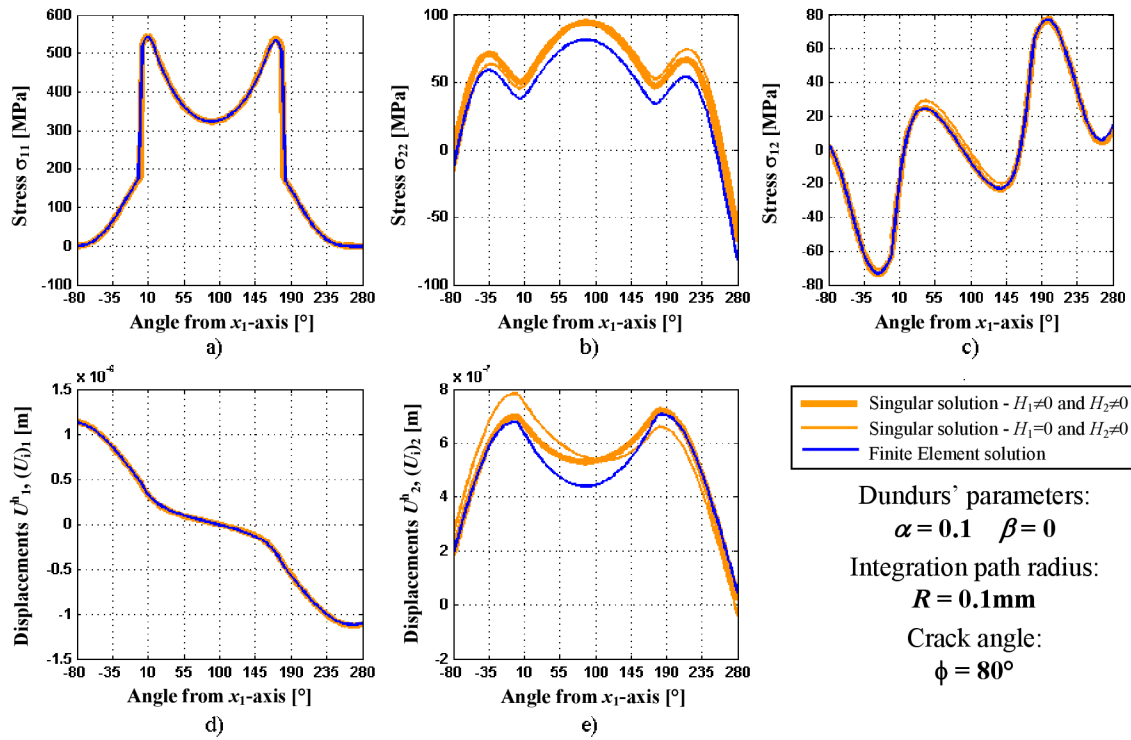**Fig. 49** Comparison of the stresses and displacements around the inclined crack for φ=50°, α=0.1, β=0, obtained from the FE analysis and from the singular solution with consideration of a single or both singular terms, on the circular integration path of radius R=0.1mm.
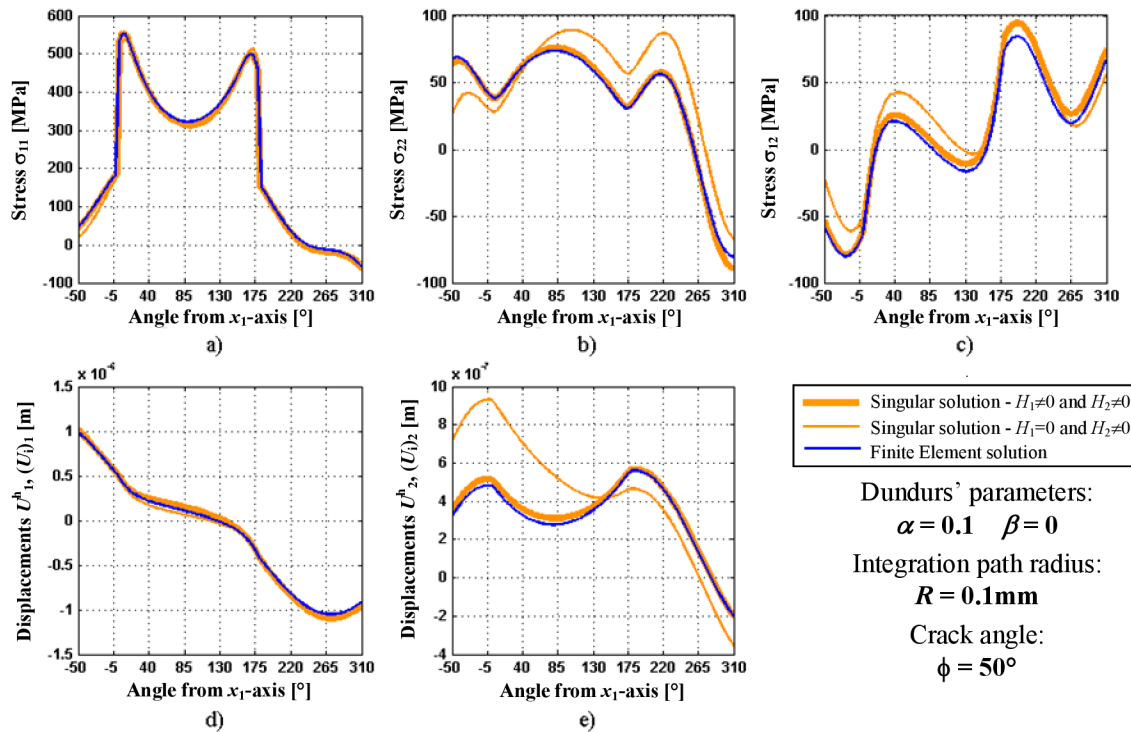
8.2.2 Fracture criteria

In the analogy to chapter 8.1.2 the values of ERRs for deflected and penetrating crack and their ratios were calculated. In the present case, the inner domain of circular shape with the diameter R=1mm measured in scaled up coordinates y (Fig. 42) is subjected to the displacement field along its boundary. For the calculation of parameters $K_{1d(p)}$, $K_{2d(p)}$ the boundary condition (217) is used and for the parameters $K'_{1d(p)}$, $K'_{2d(p)}$ the boundary condition of type (218) is applied:

$$\mathbf{U}^0(x_1,x_2)=H_1 r^{\delta_1}\mathbf{u_1}(\theta) \quad\ldots\ldots\text{where } H_1 = 1, \tag{217}$$

$$\mathbf{U}^0(x_1,x_2)=H_2 r^{\delta_2}\mathbf{u_2}(\theta) \quad\ldots\ldots\text{where } H_2 = 1. \tag{218}$$

The characteristic eigenvalues δ_1, δ_2 and the functions $\mathbf{u_1}(\theta)$, $\mathbf{u_2}(\theta)$ are taken from the singularity analysis – see section 8.1.1. All the other procedure and calculations are identical with that for the perpendicular crack.

The obtained variations of the ERRs on Dundurs' parameter α and on the crack inclination angle are displayed in the Fig. 50 a)-c). By comparing (217) and (218) with (215) and (216), one can see the difference in the considered terms of the Williams-like asymptotic expansion. For the perpendicular crack, the second singular term and the T-stress were considered, for the inclined crack the first two singular terms (and no T-stress) were considered. As was already mentioned, this is because, the significancy of the first singular term with the change of the crack inclination angle (from 90°) increases (for perpendicular crack it vanishes). This phenomenon is also possible to observe in the Table 6 - Table 9, where the crack inclination angle ϕ changes from 80° to 50°.

The appropriate ERR G_{sd}, G_d, G_p are again calculated for all possible directions using formula (210) where H_1 and H_2 are GSIFs from Table 6 - Table 9. Coefficients K, ERRs $G_{d,p}$, and their ratios for several parameters α are given (for $\varepsilon = 1/100$ and $\phi = 70°$) in the Table 10. All calculated results of ratios G_{sd}/G_p and G_d/G_p are shown, for several crack inclination angles, in Fig. 50. Results from Fig. 50 a)-d) are also summarized in the Fig. 51 for one chosen characteristic crack extension length ε=1/100. In Fig. 51 a) only one (first) singular term for ERR calculation is considered, while in Fig. 51 b) both singular terms are considered. By comparison of Fig. 51 a) and b) one can conclude that the influence of the second singular term on the ratios G_d/G_p is very significant and it can strongly affect the resulting verdict about the further propagation direction. The second singular term seems to be here more dominant for the fracture criterion than the first singular term. The other general conclusion which can be drawn for the inclined cracks is that the single deflection is preferred before the double deflection (especially for higher inclination angles). Also, with growing crack inclination (from the perpendicular direction) the probability of the crack deflection along the interface (with respect to the penetration) is increasing.

Furthermore remark, that the penetrating crack was assumed to grow perpendicularly towards the interface for the calculations of ERR G_p. Generally, when considering the main crack inclined, the further propagation direction can also be different from the perpendicular one. Commonly, one should compute the ERR for the crack extensions in several possible penetrating directions and then select that where the ERR is maximal. For our material configuration the maximal ERR for the penetration was always (when consider both singular terms in the criterion) in the direction perpendicular to the interface (modulus E_T is ten times lower than E_L – given by parameter λ_1=0.1) – see Fig. 52.
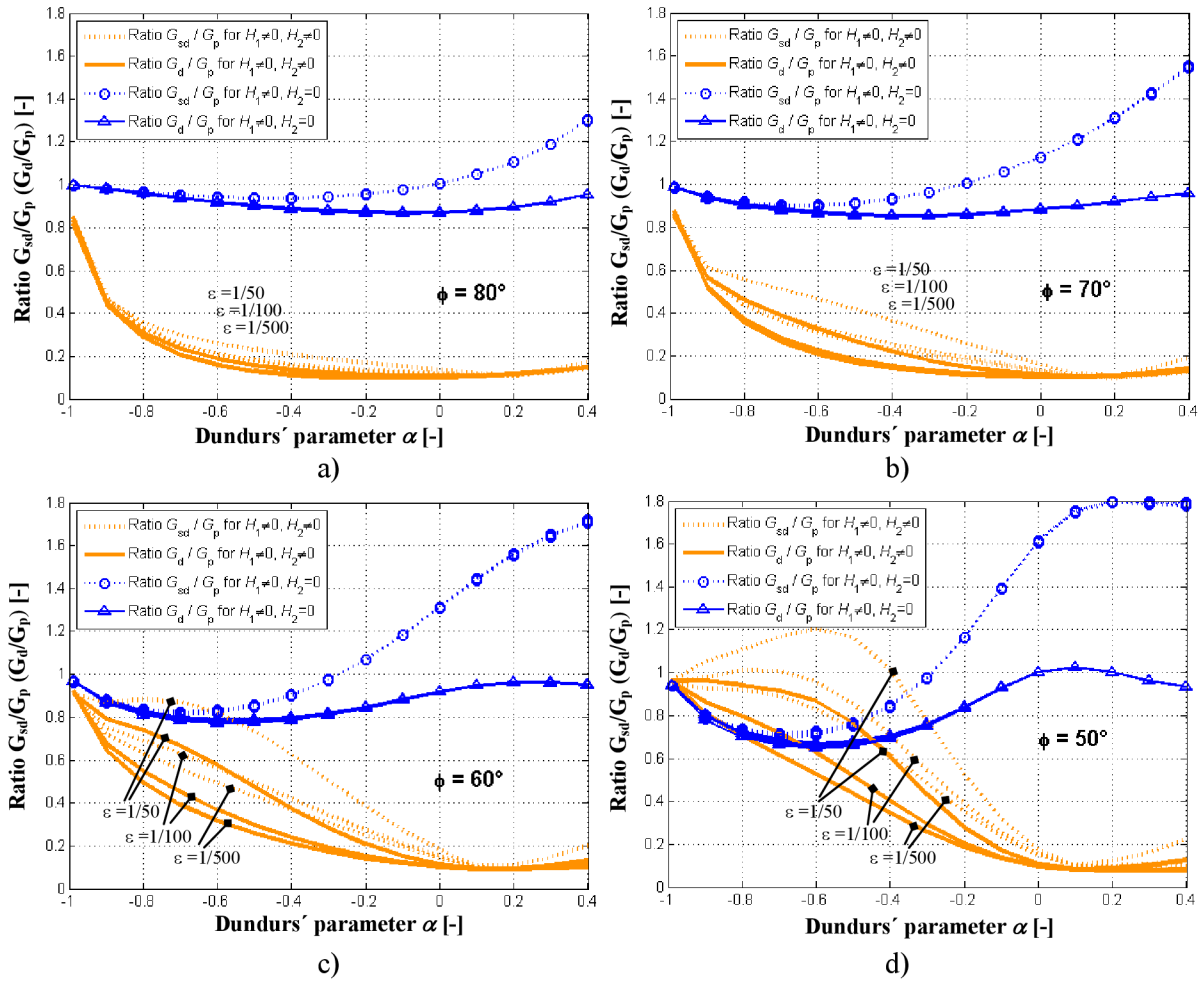
Fig. 50 Ratios G_{sd}/G_p and G_d/G_p as a function of Dundurs' parameters α for several valus of the characteristic crack extension length ε=1/50; ε=1/100; ε=1/500 and for several values of the crack inclination angle ϕ. a) ϕ=80°; b) ϕ=70°; c) ϕ=60°; d) ϕ=50°.

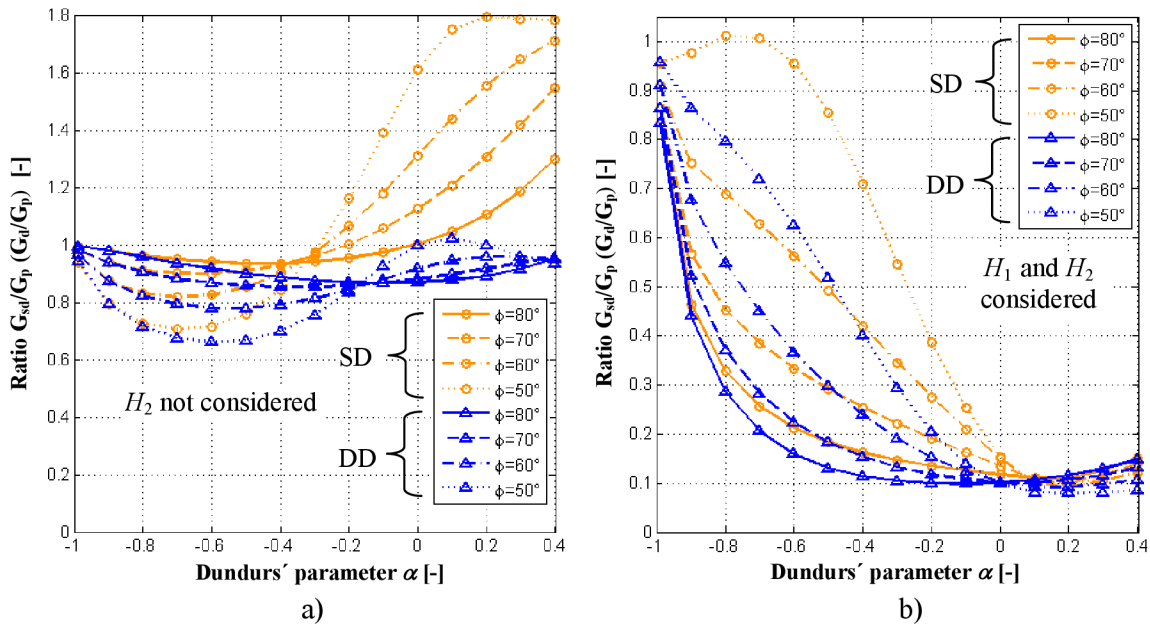**Fig. 51** Ratios G_{sd}/G_p and G_d/G_p as a function of Dundurs' parameters α for several values of the crack inclination angle ϕ (the characteristic crack extension length ε=1/100) a) the case when the second singular term is not considered (H_2=0); b) both H_1 and H_2 singular terms are considered.
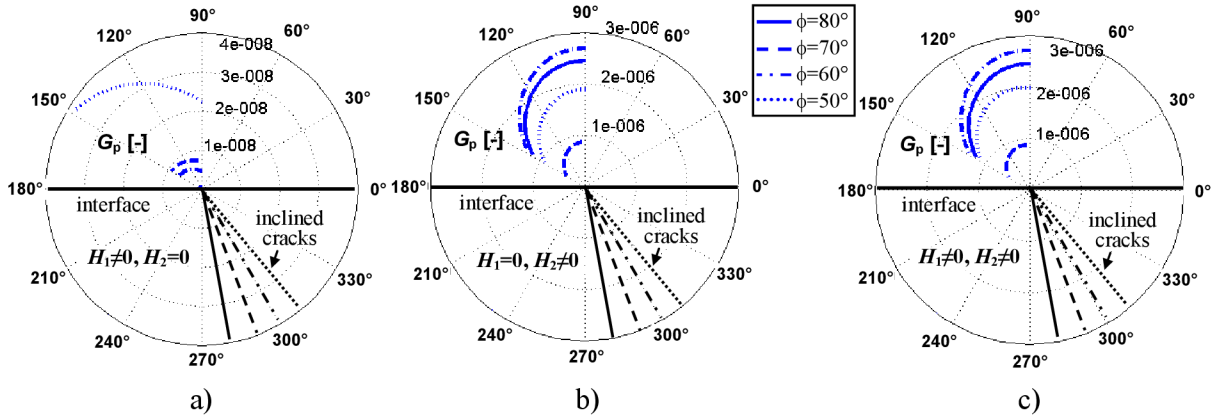
Fig. 52 Variation of the ERRs G_p with the angle of crack extension for α=0.1 and ε=1/100; a) the case when the second singular term is not considered (H_2=0); b) the case when the first singular term is not considered (H_1=0); c) both H_1 and H_2 singular terms are considered.

$\phi = 70°$	β=0, λ_1=0.1, ρ_1=2, λ_2=1, ρ_2=1, E_2=60000 MPa, ν_2=0.238, ε = 1/100							
					ERR for H_2=0		ERR for $H_2 \neq 0$	
α	K_{1sd} [-] K_{1d} [-] K_{1p} [-]	K'_{1sd} [-] K'_{1d} [-] K'_{1p} [-]	K_{2sd} [-] K_{2d} [-] K_{2p} [-]	K'_{2sd} [-] K'_{2d} [-] K'_{2p} [-]	G_{sd} G_d G_p	G_{sd}/G_p G_d/G_p	G_{sd} G_d G_p	G_{sd}/G_p G_d/G_p
-0.9	-0.165673 -0.165514 -0.176296	-0.013881 -0.010550 0.018405	-0.009590 -0.007281 0.012735	-0.049351 -0.045615 -0.109177	3.25 e-04 3.24 e-04 3.46 e-04	0.939 0.938	2.41 e-03 2.22 e-03 4.25 e-03	0.567 0.522
-0.7	-0.063845 -0.062524 -0.070758	-0.008290 -0.003871 0.009175	-0.006754 -0.003126 0.007508	-0.009442 -0.007168 -0.037660	1.38 e-05 1.36 e-05 1.53 e-05	0.902 0.883	9.51 e-05 7.00 e-05 2.47 e-04	0.385 0.283
-0.5	-0.032747 -0.030831 -0.035909	-0.005052 -0.001548 0.004429	-0.005243 -0.001613 0.004513	-0.003843 -0.002676 -0.021324	1.77 e-06 1.67 e-06 1.94 e-06	0.912 0.858	1.53 e-05 9.61 e-06 5.26 e-05	0.291 0.183
-0.3	-0.019336 -0.017173 -0.020091	-0.003273 -0.000678 0.002074	-0.004519 -0.001029 0.002625	-0.002158 -0.001554 -0.015120	2.92 e-07 2.59 e-07 3.04 e-07	0.962 0.855	3.76 e-06 2.24 e-06 1.70 e-05	0.222 0.132
-0.1	-0.012579 -0.010332 -0.011885	-0.002288 -0.000322 0.000805	-0.004110 -0.000799 0.001072	-0.001455 -0.001191 -0.012313	3.91 e-08 3.22 e-08 3.70 e-08	1.059 0.870	1.05 e-06 6.94 e-07 6.44 e-06	0.163 0.108
0.1	-0.008866 -0.006594 -0.007327	-0.001786 -0.000166 0.000005	-0.003552 -0.000681 -0.000374	-0.001053 -0.001072 -0.010666	6.58 e-10 4.89 e-10 5.44 e-10	1.211 0.901	2.68 e-07 2.54 e-07 2.51 e-06	0.107 0.101
0.3	-0.006726 -0.004440 -0.004729	-0.001581 -0.000090 -0.000706	-0.002445 -0.000516 -0.001284	-0.000680 -0.000968 -0.008519	4.34 e-09 2.86 e-09 3.05 e-09	1.424 0.940	1.04 e-07 1.05 e-07 9.00 e-07	0.116 0.117

Table 10 Coefficients of the inner expansion, ERR of the deflected and penetrating crack (for a finite crack extension of the characteristic size ε = 1/100 and crack inclination angle ϕ=70°) and ratios of the ERR for singly (doubly) deflected and penetrating crack (*sd* – single deflection, *d* – double deflection, *p* – penetration).

9 Discussion

It was shown that for the case of the perpendicular and inclined crack in anisotropic media there exist two real characteristic eigenvalues of the singularity δ_1 and δ_2 in the interval $(0,1)$ and hence also two generalized stress intensity factors (GSIFs) H_1 and H_2. Nevertheless, for the case of the perpendicular crack and symmetric loading it was shown that the value of one of the GSIFs (in our case H_1) is very small, practically approaching zero, and most likely the non-zero value of H_1 is due to numerical errors. Thus, the whole first singular term corresponding to δ_1 can be omitted for these configurations. Apparently, in such a case H_1 and H_2 relate to antisymmetric and symmetric loading respectively. At literature a reference was made that for the case of the perpendicular crack, the only one real characteristic eigenvalue of the singularity exists in the interval $(0, 1)$ – especially for isotropic bi-materials. However, it has been shown in this thesis and also in some other works – e.g. [56], that this statement does not hold for every bi-material configuration (especially when one considers anisotropic – orthotropic - bi-materials). In this case, there exist certain bi-material configurations for which two different real characteristic eigenvalues of the singularity exist in the interval $(0, 1)$. They exist only under the condition that the imaginary part of the eigenvalues δ_i is zero. Authors in [56] observed, that the non-zero complex roots occur for Dundurs' parameters $\beta \neq 0$. If $\beta = 0$ then the both roots seems to be always real with zero imaginary part for all crack inclination angles ϕ. However authors do not guarantee that this is the only sufficient condition and further investigations are required.

When describing the stress field in the vicinity of the crack perpendicular to the interface, the regular term in the Williams-like asymptotic expansion – called T-stress is recommended to be taken into the account. This term corresponds to the characteristic eigenvalue $\delta_3=1$. The T-stress consideration precises the description of the stress and displacement field and also precises the final fracture criterion for the case of the perpendicular crack. When one consider the inclined crack, then the same conclusion holds for another singular term (in our case that one corresponding to δ_1) which starts to be significant for the angles $\phi > 10°$. In these cases both singular terms should be used for the stress and displacement field description and fracture criterion definition.

The GSIF and T-stress calculations were performed using the postprocessing integration process in the mathematical software Matlab 7.1. However, it can be also involved directly into the Finite Element software using the programming language, which is in most of these codes implemented. The only limitation is that the appropriate programming language has to be capable to handle complex numbers. The alone FE calculation carried out on the 2D bi-material cracked model has no special needs or limitations. Only a refined mesh in the vicinity of the crack tip is required as in every crack problems.

Some other author's recommendations for the GSIF and the T-stress calculation:

☞ When integrating across the interface a finer FE mesh in comparison with the integration in homogeneous media it is advised to use – due to the presence of media discontinuity which can in some cases influence the further integration process.

☞ For the numerical integration of Ψ-integral, a simple trapezoidal or rectangular integration method is recommended to use instead of some advanced, e.g. Simpson's method, which in some cases result in an incorrect integration across the

interface (due to the discontinuity of the integrated function). When the mesh is not very coarse, also the simple integration formula leads to the sufficiently accurate results. Moreover, there is no necessity of keeping a special attention to the interface crossings. In addition, always is apparently convenient to integrate the Ψ-integral piecewise in each material (domain) and sum up the particular results. Integration in one step (from crack face to crack face) can lead to numerical errors.

☞ The T-stress can be also estimated directly from the FE analysis, when plotting the stress along the crack face and considering the stress magnitude when approaching the crack tip. These results should approximately correspond to the Ψ-integral calculations. However it is not recommended to use this method as the only one for the T-stress determination, since its results are dependent on the used material configuration and sometimes they can differ more then negligibly from the Ψ-integral calculations which should be closest to the exact value.

The same conclusions and recommendations concerning the FE mesh and integration process hold also for the calculations of the factors $K_{1d(p)}$, $K_{2d(p)}$, $K'_{1d(p)}$ and $K'_{2d(p)}$, which are used for the calculation of the ERRs and the definition of the fracture criteria.

The presented method for the definition of the fracture criteria, based on the Finite Fracture Mechanics and the matched asymptotic expansions represents an alternative way how to overcome the problems of the classical differential approach. When calculating the Energy Release Rate (ERR) for cracks terminating at the interface of two dissimilar materials, the differential approach leads to a zero or infinite ERR (depending on the type of the singularity) and therefore it is unusable for these applications. This problem is caused by the considered infinitesimal crack extension and the media discontinuity. The concept of the Finite Fracture Mechanics (FFM) offers the solution to this problem using the finite crack extension length. The disadvantage of this method is the necessity of the FE solution, which is used for the determination of the needed parameters. However, the FE solution is not complicated at all so in fact it doesn´t represent any problem. The length of the finite crack extension is to be determined by combining the energy and stress condition of the crack onset – as stated in the section 7.1.3. When the crack starts to grow, it happens usually by the small finite jumps of the main crack instead of the continuous propagation.

The advantage of the used combination of the FFM and the matched asympotitc expansion technique is that this method allows predition of prospective crack propagation direction. It can be done by calculating the additional released energy ΔW for a number of possible propagation directions and by selecting that which maximize the additional released energy ΔW. This approach therefore provides an alternative to the criteria based on the generalized factor of the strain energy density and related Sih´s approach discussed e.g. in the thesis [68], which become again too much complicated when considering generally anisotropic materials. The presented FFM based technique is universal for any type of general stress concentrator in whatever media. A solution to all these cases has the same complexity and also the same treatment. Moreover, several parameters (singular terms or regular term) can be simultanously considered by this approach to improve the crack stability prediction. It has been shown in the examples, that for some bi-material configurations also the second (weaker) term can quite significantly influence the propagation direction. Thus, it is not recommended to neglect them without any previous analysis. The theory of FFM was also applied on the problem of the multiple cracks in the thin surface layer under the temperature loading - presented in author's work [92].

10 Conclusion

10.1 Summary of the solved problems

It is possible to conclude, that the main aims of this thesis were realized. Briefly speaking, a complex computational tool for the assessment of the general stress concentrators in anisotropic media (especially cracks terminating at the interface of two dissimilar materials) was created. Technique based on the complex potential theory has been employed in combination with Finite Element Method.

The main particular outputs of this work are possible to summarize as follows:

☞ Using the complex potential theory and the Lechnitskii-Stroh formalism, a technique (the so-called L.E.S. method) for the calculation of the stress singularity exponents and description of the singular (regular) stress field in the vicinity of general stress concentrator in anisotropic media have been carried out. The characteristic eigenvalues of the singularity and corresponding eigenvectors have been calculated using this technique. The computational code is programmed in the mathematical software MAPLE 10.0. The method enables to characterize the singularities for cracks terminating at the interface at right (or arbitrary) angle and after light modifications it can also be used for the notch with its tip on the interface.

☞ Next to this approach, the Continuously Distributed Dislocation technique has been employed to attain the same objective (singularity analysis, description of the stress and displacement field and the GSIFs calculations). The results of both methods are compared and show a good agreement. A disadvantage of the CDD technique consists in that it is limited to the crack-like concentrators. The problems of the general notches are preferable to solve by use of the L.E.S. method or some other technique. Other methods for the singularity analysis of the general multimaterial notches have been also studied, however not widely used within this work.

☞ Using the Betti´s reciprocal theorem and the two state Ψ-integral, a powerful tool for the calculation of the Generalized Stress Intensity Factors - GSIF (amplitude of the singular term in the Williams-like stress asymptotic expansion) and T-stresses (non-singular term) has been developed. The Ψ-integral is used in combination with FEM and enables the calculation of GSIFs (or T-stresses) from the stress and displacement far fields of the singular point. Due to this fact, this technique doesn't need any special (or very fine) mesh to avoid errors caused by the presence of the singularity. Another significant property of the Ψ-integral, in comparison with M-integral or J-integral, is its integration path independency for any case of the general stress concentrator. The finite element calculations were carried out within the code ANSYS 10.0 and the post-processing, including the integration process for GSIF (T-stress) calculation, has been programmed in the mathematical software MATLAB 7.1.

☞ In the FE calculations the standard linear or quadratic plane elements can be used, without any special need of the mesh fineness. In the regions where the integration path crosses the interface a finer mesh is recommended, however not required.

☞ Since the aim of this work is to work up tools for the assessment of anisotropic (orthotropic) materials with interface, a possibility of application to laminates reinforced by the long fibres is also studied. If several layers of laminate fracture

and the crack is bridged by the fibres, the resulting stress field can be strongly influenced by these fibres - in positive sense (due to the crack closure effect). This effect can be captured using the generalized bridging stress intensity factor which reduces the GSIF calculated for the unbridged crack. The two different bridging models have been used and compared - simple Budiansky´s model and the advanced statistical model. A comparison with experimental data obtained on the same specimens has not been made yet, however when the results are qualitatively compared to the similar experiments made on a different type of specimen, the characteristic behaviour is the same. I.e. the statistical model leads to a higher predicted load under which all the fibres loose the ability to transfer any loads (all of the bridging fibres become broken). It can be explained as follows: according to the simple Budiansky's model, the fibre fracture always occurs in the plane of the crack. However in case of the statistical bridging model, the fibres can be broken (due to a statistical distribution of the fibre strength) also anywhere inside the matrix. They can still contribute to the bridging effect by the frictional constraint until they are completely pulled out from the matrix. In comparison with some of the earlier experiments, this model describes the reality more realistically.

☞ To utilize all the preceding effort devoted to the description of the stress and displacement fields near the crack tip at the interface in terms of Williams-like asymptotic expansion, a suggestion of the suitable fracture criterion has been made. It is applicable to the problems of cracks in anisotropic bi-materials terminating at the interface (at right or arbitrary angle). The theory of the finite fracture mechanics in combination with the matched asymptotic expansions technique has been employed here. This approach can overcome the classical differential analysis problem of zero or infinite energy release rate for the general stress concentrators. A relation for the energy release rate of the crack terminating at the interface of two different (anisotropic) materials has been derived. This relation can involve two parameters. Either the leading singular term of the Williams-like asymptotic expansion together with the T-stress (for perpendicular cracks) or the two singular terms (for inclined cracks). Thus, it is possible to assess an influence of the second term, on the crack stability. All the computations have again been made using an advantage of the FE analysis and of the already mentioned Ψ-integral.

☞ A direction of the prospective crack extension (crack penetration across the interface or the crack deflection) has been studied (for the crack terminating at the interface of the orthotropic substrate and the isotropic surface layer). The resulting propagation direction depends mostly on the bi-material configuration, on the character of the anisotropy and last but not least on the toughnesses of the substrate and the interface. If the crack penetrates to the next material, then it follows that penetration direction which maximizes the ERR for the chosen small crack extension. However, in case of the anisotropy of the substrate, also the toughness of this material can exhibit anisotropic behaviour. In that case the crack will follow that path which maximizes the additional released energy $\Delta W_p = \delta W_p - G_c^1 a_p$. When deciding between the penetration and the crack deflection, the ratios of ΔW of deflected and penetrated crack have to be calculated and compared with the corresponding ratios of toughnesses in deflected and penetrating direction. If the calculated ratio is higher than the ratio of material properties, the crack should deflect along the interface and vice versa.

☞ It was shown, for the case of the crack perpendicular to the interface, that in some cases, also a consideration of the T-stress can influences the resulting direction of the propagation (this problem is widely described in the discussion). Due to this reason, it is recommended to take also T-stress into the account. Influence of the T-stress strongly depends on the bi-material configuration and the material characteristics of both materials, so the importance of this term should be always assessed. On the contrary, for the case of the inclined cracks it is always recommended to consider both singular terms from the Williams's like asymptotic expansion for the definition of the fracture criteria (especially for cracks inclined more than 10° from the perpendicular state). The T-stress term was not proved to exist for the inclined cracks, at least for investigated configurations. The existence of the T-stress is closely related to the existence of the root $\delta=1$ of the eigenvalue-equation pertaining to a particular singularity problem. This is a necessary condition but it is still not clear whether this condition is also sufficient one.

☞ All the described theory and examples can be applied after the experimental verification and eventual model adjustment, for the assessment of general stress concentrators, and also for the designing of special "smart" materials, which will exhibit the predefined behaviour under the specific loading conditions. This is also the final aim of the whole effort put into this research. The possibilities of the further work are of course not closed yet and the suggestions, where to start the continuation work are stated in the following section.

10.2 Ideas for further research

The following points can serve as the author's suggestions for the subsequent work:

☞ One of the most important steps which is necessary to perform in the framework of the next work is the experimental validation of the presented results. Experiments were not performed within the framework of this thesis, because of its complexity, time consumption and above all the high expensiveness. It has to be worked out within the particular work or grant project to obtain any meaningful results. The main problem consists in the availability of suitable test specimens, what have been already shown as a relatively difficult issue. The aim of the experimental work should be in the first step focused on the measuring of the bi-material characteristics such as the interfacial toughness or the strength of the substrate. In the second step, a verification of the predicted crack propagation direction and load under which the crack starts to propagate should be performed.

☞ As a future work, a technique for the calculation of the mode mixity should be carried out, since as it was shown, consideration of this quantity can strongly influence the assessment of the crack propagation direction. Theory and related references for these calculations are stated in the thesis, see Eqs. (201)-(203).

☞ All the presented problems were performed within the 2D linear elasticity. It could be interesting to extend these pieces of knowledge into the 3D problem and to find the main differences between 2D and 3D interpretation. This can turn out to be helpful for the future implementation of the described theory into some FE code.

☞ By linking to the previous point, very useful for the practical usage of the whole problems could be the implementation of the described theory into some open FE code. Most of the commercial FE softwares have their own programming language, so most (or even all) of the calculations can be performed directly within a particular FE package. Some extending functions can be developed, e.g. for the calculation of the Generalized Stress Intensity Factors, T-stress and also for the final assessment of the crack stability under the given loading conditions.

☞ Some kinds of the advanced crack modelling techniques as Cohesive Zone Models (CZM) or Extended FEM (X-FEM) can be applied to the solution and verification of bi-material problems solved within this thesis.

Author's publications

[I] ŠEVEČEK, O. & KOTOUL, M., Řešení obecných koncentrátorů napětí v anisotropních prostředích, *In proc. of Multilevel design of advanced materials 2005*, ISBN 80-239-6145-4, FME BUT Brno, 2005, pp.215-222.

[II] ŠEVEČEK, O., PROFANT, T. & KOTOUL, M., Výpočet zobecněného součinitele intensity napětí pro trhlinu kolmou na rozhraní dvou anisotropních materiálů, *In proc. of Applied Mechanics 2006*, ISBN 80-7043-441-4, Srní, 2006, pp.93-94.

[III] ŠEVEČEK, O., KOTOUL, M., PROFANT, T., Fracture mechanics problems in anisotropic bimat. media, *In proc. of Únava a Lomová mechanika*, Žinkovy, 2006.

[IV] ŠEVEČEK, O., KOTOUL, M. & PROFANT, T., A construction of the fundamental solution for the dislocation in the anisotropic bi-material body by force of the FEM, *In proc. of Eng.Mechanics 2006*, ISBN 80-86246-27-2, Svratka, 2006, pp. 350-351.

[V] PROFANT, T., KOTOUL, M. & ŠEVEČEK, O., Stress field analysis near the semi-infinite crack tip terminating perpendicular to the interface between two orthotropic materials, *In proc. of Engineering Mechanics 2006*, Svratka, 2006, pp. 304-305.

[VI] PROFANT, T., ŠEVEČEK, O. & KOTOUL, M., Singularita napětí polonekonečné trhliny kolmé k rozhraní dvou ortotropních materiálů, *In proc. of Dynamika tuhých a deformovatelných těles*, ISBN 80-7044-782-6, Ústí n.Labem, 2006, pp. 175-182.

[VII] KOTOUL, M., ŠEVEČEK, O. & PROFANT, T., Calculation of K-Factor and T-Stress for Crack in Anisotropic bimaterials, *In proc. of 16th Europ. Conf. of Fracture Failure Analysis of Nano and Eng. Mat. & Structures*, ISBN 1-4020-4971-4, Alexandroupolis, Greece, 2006.

[VIII] PROFANT, T., KOTOUL, M. & ŠEVEČEK, O., Analysis of edge bridged crack in anisotropic bimaterial half-space, *Key Engineering Materials*, ISSN 1013-9826, Vol. 324-325, 2006, pp. 1143-1148.

[IX] ŠEVEČEK, O., PROFANT, T. & KOTOUL, M., Problematika přechodu trhlin přes rozhraní dvou ortotropních materiálů, *In Proc. of Computational Mechanics 2006*, ISBN 80-7043-477-5, Nečtiny, 2006, pp. 601-608.

[X] PROFANT, T., ŠEVEČEK, O. & KOTOUL, M., Analýza singularity napětí u trhlin na rozhraní dvou ortotropních materiálů, *In Proc. of Computational Mechanics 2006*, ISBN 80-7043-477-5, Nečtiny, 2006, pp. 483-490.

[XI] ŠEVEČEK, O. & PROFANT, T., Problematika obecných koncentrátorů na rozhraní dvou anisotropních materiálů, *In proc. of Multilevel Design of Advanced Materials 2006*, ISBN 80-239-8271-0, IPM ASCR Brno, 2006, pp. 155-162.

[XII] ŠEVEČEK, O., VYSLOUŽIL, T., PROFANT, T. & KOTOUL, M., A solution of the bridging problem of a crack in the thin orthotropic layer with tip on the interface of an orthotropic substrate, *In proc. of Applied Mechanics 2007*, ISBN 978-80-248-1389-9 Malenovice, 2007, pp.207-208.

[XIII] ŠEVEČEK, O., PROFANT, T. & KOTOUL, M., Crack propagation criteria for the crack terminating on the interface of a thin orthotropic layer and an orthotropic substrate, *In proc. of Engineering Mechanics 2007*, ISBN 978-80-87012-06-2, Svratka, 2007, pp. 350-351.

[XIV] KOTOUL, M., PROFANT, T., ŠEVEČEK, O. & KREJČÍŘ, M., Modelling of cracks crossing an interface between dissimilar elastic anisotropic materials, *Mat. Science Forum*, Trans Tech Publications, 2007, ISSN 0255-5476, Vol.567, No.1, pp.17-22.

[XV] PROFANT, T., ŠEVEČEK, O. & KOTOUL, M., The analysis of the stress and displacement field near the surface crack tip terminating perpendicular to the interface between two orthotropic materials, *Materials Science Forum*, Trans Tech Publications, 2007, ISSN 0255-5476, Vol.567, No.1, pp.137-140.

[XVI] KOTOUL, M., PROFANT, T., ŠEVEČEK, O. & KREJČÍŘ, M., Solution methods for general stress concentrators in anisotropic heterogeneous media, *Key Engineering Materials.*, ISBN 0-87849-448-0, Vol. 348-349, 2007, pp. 677-680.

[XVII] PROFANT, T., ŠEVEČEK, O. & KOTOUL, M., Calculation of K-factor and T-stress for cracks in anisotropic bimaterials, *Engineering Fracture Mechanics*, Vol. 75, 2008, pp. 3707-3726.

[XVIII] KOTOUL, M., PROFANT, T. & ŠEVEČEK, O., Dislocation tri-material solution in the analysis of bridged crack in anisotropic bimaterial half-space, *International Journal of Fracture*, Vol. 147, 2007, pp. 199-217.

[XIX] ŠEVEČEK, O. & PROFANT, T., Problems of the crack propagation across the interface of two orthotropic materials, *In proc. of Multilevel Design of Advanced Materials 2007*, ISBN 978-80-254-0793-6, IPM ASCR, Ostrava, 2007, pp. 53-60.

[XX] KOTOUL, M., PROFANT, T. & ŠEVEČEK, O., Analysis of multiple cracks in thin coating on orthotropic substrate, *In proc of: European Conference on Fracture 17*, Brno, 2008, pp. 2159-2166.

[XXI] PROFANT, T., KOTOUL, M. & ŠEVEČEK, O., Stronger and weaker singularity of an inclined crack terminating at the orthotropic bimaterial interface, *In proc of: European Conference on Fracture 17*, Brno, 2008, pp. 1150-1157.

[XXII] ŠEVEČEK, O., KOTOUL, M. & PROFANT, T., Crack propagation problems in orthotropic bimaterials, *In proc. of Multilevel Design of Advanced Materials 2008*, ISBN 978-80-254-3492-5, IPM ASCR, Velké Bílovice, 2008, pp. 7-14.

[XXIII] KOTOUL, M., ŠEVEČEK, O. & PROFANT, T., Analysis of multiple cracks in thin coating on orthotropic substrate under mechanical and residual stresses, *Under review in: Engineering Fracture Mechanics*, 2009.

References

[1]   AKISANYA, A. R. & FLECK, N.A., Interfacial cracking from the free-edge of a long bi-material strip, *Int.J.Solids Structures*, Vol. 34, 1997, pp. 1645-1665.

[2]   ANDERSON, T. L., Fracture Mechanics: fundamentals and applications, *CRC Press LLC*, 1995, Florida.

[3]   ANSYS Release 10.0, User´s Manual, *Swanson Analysis Sys. Inc.*, Pensylvania, 2005.

[4]   AVESTON, J., COOPER, G.A. & KELLY, A., The properties of fibre composites , *In proc. of National Physical Laboratory*, Guilford, IPC Science and Technology Press, Teddington, U.K., 1971, pp.15-26.

[5]   AVESTON, J. & KELLY, A., Theory of multiple fracture of fibrous composites, *J. Mater. Science*, Vol.8, 1973, pp. 352-362.

[6]   BABUSKA, I. & MILLER, A., The post-processing approach in the FEM, Part 2: The calculation of SIFs, *Int. Num. Meth. Engng*, Vol. 20, 1984, pp. 1111-1129.

[7]   BANKS-SILLS, L. & BONIFACE, V., Fracture mechanics of an interface crack between a special pair of transversely isotropic materials, *In: Chuang, T.J., Rudnicki, J.W. (Eds.), Multiscale Deformation and Fracture in Materials and Structures*, Kluwer Academic Publisher, Vol.60, 2000, pp. 183-204.

[8]   BANKS-SILLS, L. & ASHKENAZI, D., A note on fracture criteria for interface fracture, *Int.J. of Fracture*, Vol.103, 2000, pp. 177-188.

[9]   BANKS-SILLS, L., BONIFACE, V. & ELIASI, R., Developement of a methodology for determination of interface fracture toughness of laminate composites, *Int.J.of Solids and Structures*, Vol.42, 2005, pp. 663-680.

[10]   BARROSO, A., MANTIČ, V. & PARIS, F., Singularity analysis of anisotropic multimaterial corners, *International Journal of Fracture*, Vol. 119, 2003, pp. 1-23.

[11]   BROBERG, K. B., A note on T-stress determination using dislocation arrays, *Int. Journal of Fracture*, Vol.131, 2005, pp. 1-14.

[12]   BUDIANSKY, B. & AMAZIGO, J. C., Toughening by aligned, frictionally constrained fibres, *J.Mech. Phys. Solids*, Vol. 37, 1989, pp.93-109.

[13]   BUDIANSKY, B. & HUTCHINSON, J. W., Matrix fracture in fiber-reinforced ceramics, *J.Mech. Phys. Solids*, Vol. 34, 1986, pp.167-189.

[14]   BUDIANSKY, B., HUTCHINSON, J. W. & EVANS A.G., Matrix fracture in fiber-reinforced ceramics, *J. Mech. Phys. Solids*, Vol. 34, 1986, pp. 167-189.

[15]   COOK, T. S. & ERDOGAN, F., Stresses in bonded materials with a crack perpendicular to the interface, *Int. J. of Eng. Science*, Vol. 10, 1972, pp. 677-697.

[16]   DEMPSEY, J. P. & SINCLAIR, G. B., On the singular behavior at the vertex of a bi-material wedge, *J. Elasticity*, Vol.11, 1981, pp. 317-327.

[17]   DESMORAT, R. & LECKIE, F. A., Singularities in bi-materials: parametric study of an isotropic/anisotropic joint. *Eur. J. Mech. A/Solids*, Vol. 17, 1998, pp. 33-52.

[18]   DEWYNNE, J. N., HILS, D. A. & NOWELL, D., Calculation of the opening displacement of surface-breaking plane cracks, *Computational methods Appl. Mech. Eng.*, Vol.41, 1993, pp. 2425-2432.

[19] ERDOGAN, F., GUPTA, G. D. & RATWANI, M., Interaction between a circular inclusion and arbitrary oriented crack, *J. Appl. Mech.*, Vol.12, 1974, pp.1007-1013.

[20] ESHELBY, J. D., READ, W. T. & SHOCKLEY, W., Anisotropic Elasticity with Application to Dislocation Theory, *Acta Metallurgica*, Vol. 1, 1953, pp. 251-259.

[21] FETT, T., MUNZ, D. T., GERAGHTY, R.D. & WHITE, K.W., Bridging stress determination by evaluation of the R-curve, *Journal of European ceramic society*, Vol. 20, 2000, pp. 2143-2148.

[22] GROSS, D. & SEELIG, T., Fracture Mechanics – With Introduction to Micromechanics, *Springer*, 2006, Berlin.

[23] GRÖGER, R., Characterization of fracture-mechanical behavior of bimaterial V-notches using BEM, *Ph.D. Thesis*, FME BUT a IPM AVCR Brno, 2003, Brno.

[24] GUAGLIANO, M. & ALIABADI, M. H., Fracture and Damage Mechanics – Vol.8, *WITpress Southampton*, ISBN: 1-85312-669-1, 2006, Boston.

[25] GUPTA, V., ARGON, A. S. & SUO, Z., Crack deflection at an interface between two orthotropic media, *J. Applied Mechanics*, Vol.59, 1992, pp. 79-87.

[26] HILLS, D. A. & KELLY, D. N., Solution of Crack Problems – The distributed dislocation technique, *Kluwer Academic publisher*, 1996, Dordrecht.

[27] HE, M. J., EVANS., A. G. & HUTCHINSON, J. W., Crack deflection between dissimilar elastic materials: role of residual stresses, *Int. J. Solids structures*, Vol.31, 1994, pp. 3443-3455.

[28] HE, M. J. & HUTCHINSON, J. W., Crack deflection at an interface between dissimilar elastic materials, *Int. J. Solids Structures*, Vol.25, 1989, pp.1053-1067.

[29] HUI, C. Y. & RUINA, Why K? High order singularities and small scale yielding, *Int. Journal of Fracture*, Vol.72, 1985, pp. 97-120.

[30] HUTCHINSON, J. W., Crack deflection at an interface between dissimilar elastic materials:Role of residual stresses, *Int. J. Solids Struc.*, Vol.31, 1994, pp.3443-3455.

[31] HUTCHINSON, J. W. & SUO, Z., Mixed mode cracking in layered materials, *In: Advances in Applied Mechanics*, Vol.29, 1991, Academic Press, NY, pp. 63-191.

[32] CHANG, J. H. & WU, D. J., Calculation of mixed-mode stress intensity factors for a crack normal to a bimaterial interface using contour integrals, *Engineering Fracture Mechanics*, Vol.70, 2003, pp.1675-1695.

[33] CHEN, D. H., A crack normal to and terminating at a bimaterial interface, *Engineering Fracture mechanics*, Vol.49, 1994, pp.517-532.

[34] CHEN, F. H. K. & SHIELD, R. T., Conservation laws in elasticity of the J-integral type, *Z. Angw. Math. Phys. (ZAMP)*, Vol.28, 1977, pp.1-22.

[35] CHEN, S. H., WANG, T. C. & SHARON, K., A crack perpendicular to the bimat. interface in finite solid, *Int. J. of Solids and Struct.*, Vol. 40, 2003, pp.2731-2755.

[36] CHEN, Y. Z.., Closed form solutions of T-stress in plane elasticity crack problems, *Int. J. of Solids and Structures*, Vol.37, 2000, pp.1629-1637.

[37] CHOI, S. T. & EARMME, Y. Y., Elastic study on singularities interacting with interfaces using alternating technique Part I.: Anisotropic trimaterial, *Int. J. Solid Structures*, Vol.39, 2002, pp.943-957.

[38] CHOW, W. T. & ATLURI, S. N., SIFs as the fract. parameters for delamination crack growth in composite laminates. *Composites B*, 1997, pp.375-384.

[39] IM, S. & KIM, K. S., An application of two-state M-integral for computing the intensity of the singular near-tip field for a generic wedge, *Journal of the Mechanics and Physics of Solids*, Vol.48, 2000, pp.129-151.

[40] KFOURI, A. P., Some evaluations of elastic T-term using Eshelby´s method, *Int. J. of Fracture*, Vol.30, 1986, pp.301-315.

[41] KIM, J. & PAULINO, G. H., T-stress, mixed modes SIFs and cracks initiation angles in FGM, *Comput. Methods Appl. Mech. Eng.*, Vol.192, 2003, pp.1463-1494.

[42] KOTOUL, M., ŠEVEČEK, O. & PROFANT, T., Calculation of K-Factor and T-Stress for Crack in Anisotropic bimaterials, *In proc. of 16th Europ. Conf. of Fracture Failure Analysis of Nano and E. Mat. & Structures*, Alexandroupolis, Greece, 2006.

[43] KOTOUL, M., VYSLOUŽIL, T. & DLOUHÝ, I., Modelling the R-curve behaviour in chevron-notched specimen using weight functions , *In Advances in Fracture and Damage Mechanics IV*, Eastleigh, U.K., 2005, pp.217-225.

[44] KOTOUL, M., PROFANT, T., ŠEVEČEK, O. & KREJČÍŘ, M., Solution methods for general stress concentrators in anisotropic heterogeneous media, *Key Eng. Mat.*, ISBN 0-87849-448-0, Vol. 348-349, 2007, pp. 677-680.

[45] KOTOUL, M., PROFANT, T. & ŠEVEČEK, O., Dislocation tri-material solution in the analysis of bridged crack in anisotropic bimaterial half-space, *International Journal of Fracture*, Vol. 147, 2007, pp. 199-217.

[46] KREJČÍŘ, M., Výpočet vlastních hodnot asymptotického rozvoje napětí v okolí multimateriálového vrubu, *Diploma work*, FME BUT Brno, 2002.

[47] LACROIX, C., LEGUILLON, D. & MARTIN, E., The Influence of an interphase on the deflection of a matrix crack in a ceramic-matrix composite, *Composite science and technology*, Vol. 62, 2002, pp. 519-523.

[48] LEGUILLON, D., Strength or toughness? A criterion for crack onset at a notch, *Europ. Journal of Mechanics A/Solids*, Vol. 21, 2002, pp. 61-72.

[49] LEGUILLON, D. & SANCHEZ-PALENCIA, E., Computation of Singular Solutions in Elliptic Problems and Elasticity, *Masson*, 1987, Paris.

[50] LEGUILLON, D. & SANCHEZ-PALENCIA, E., Fracture in heterogeneous materials, weak and strong singularities, *New Advances in Computational Structural Mechanics, Studeis in Applied Mechanics*, Vol.32, 1992, pp. 423-434, Amsterdam.

[51] LEGUILLON, D., LACROIX, C. & MARTIN, E., Interface debonding ahead of a primary crack, *J. Mech. Phys. Solids*, Vol. 48, 2000, pp. 2137-2161.

[52] LEKHNITSKII, S. G., Těoria uprugosti anisotrop. těla, *Gostěchizdat*, 1950, Moskva.

[53] LEKHNITSKII, S. G., Někotoryje osnovnyje zadači matěmatičeskoj těoriji uprugosti, *Gostěchizdat*, 1953, Moskva.

[54] LEKHNITSKII, S. G., Anizotropnyje plastinki, *Gostěchizdat*, 1957, Moskva.

[55] LEKHNITSKII, S. G., Theory of Elasticity of an Anisotropic Body, *Holden-Day*, 1963, San Francisco.

[56] LIN, Y. Y. & SUNG, J. C., Singularities of an inclined crack terminating at an anisotropic bimaterial interface, *Int. J. Sol. Structures*, Vol.34, 1997, pp. 3727-3754.

[57] MAMMOLI, A. A., GRAHAM, A. L., REIMANIS, I. E., & TULLOCK, D. L., The effect of flaws on the propagation of cracks at bi-material interfaces, *Acta Metall. mater.*, Vol.43, 1995, pp. 1149-1156.

[58] MANTIC, V. & PARIS, F., Relation between SIF and ERR based measures of fracture mode mixity in interface cracks, *Int.J.Fracture*, Vol.130, 2004, pp. 557-569.

[59] MARSHALL, D.B. & COX, B. N., A J-integral method for calculating steady-state matrix cracking stresses in composites, *Mechanics of materials*, Vol.7, 1988, pp.127-133.

[60] MARTIN, E., PETERS, P.W.M., LEGUILLON, D. & QUENISSET, J.M., Conditions for matrix crack deflection at an interface in ceramic matrix composites, *Material science and engineering*, Vol. A250, 1998, pp.291-302.

[61] MARTIN, E., LEGUILLON, D. & LACROIX, C., A revisited criterion for crack deflection at an interface in a brittle bimaterial, *Composites Science and Technology*, Vol. 61, 2001, pp.1671-1679.

[62] MARTINEZ, D. & GUPTA, V., Energy criterion for crack deflection at an interface between two orthotropic media, *J. Mech. Phys. Solids*, Vol. 42, 1994, pp.1247-1271.

[63] MATLAB Release 14 User´s Manual, *The MathWorks, Inc.*, 2005, Massachusetts.

[64] MELIN, S., The influence of T-stress on the directional stability of cracks, *Int. Journal of Fracture*, Vol.114, 2002, pp. 259-265.

[65] MODI, M.B. & SITARAMAN, S.K., Interfacial fracture toughness measurement for thin film interfaces, *Engineering fracture mechanics*, Vol. 71, 2004, pp.1219-1234.

[66] MUNZ, D. & FETT, T., Ceramics – Mechanical Properties, Failure Behaviour, Materials Selection, *Springer*, 1999, Berlin.

[67] MUSCHELIŠVILI, N. I., Někotoryje osnovnyje zadači matěmatičeskoj těoriji uprugosti, *Gostěchizdat*, 1953, Moskva.

[68] NÁHLÍK, L., Šíření únavových trhlin v okolí rozhraní dvou elastických materiálů, Ph.D. Thesis (in Czech), FME BUT a IPM ASCR Brno, 2002, Brno.

[69] NAIR, S.V., EATON, H.E. & SUN, E.Y., Measurement of interface strength and toughness in shear of environmental barrier coatings on ceramic substrate at ambient and elevated temp., *Science and coating technology*, Vol. 200, 2006, pp.5175-5180.

[70] O´DOWD, N. P. & SHIH, C. F., Test geometries for measuring interfacial fracture toughness, *Int. J. Solids Structures*, Vol. 78, 1992 pp. 571-589.

[71] PAPADAKIS, P. J. & BABUŠKA, I., A numerical procedure for the determination of certain quantities related to the stress intensity factors in two-dimensional elasticity, *Computer methods in applied mech. & eng.*, Vol. 122, 1995 pp. 69-92.

[72] PARVIZI, A., GARRET, K. W. & BAILEY, J. E., Constrained cracking in glass fibre-reinforced epoxy cross-ply laminates, *J. Mater. Science*, Vol.23, 1978, pp. 195-201.

[73] PROFANT, T., ŠEVEČEK, O. & KOTOUL, M., Singularita napětí polonekonečné trhliny kolmé k rozhraní dvou ortotropních materiálů, *In proc. of Dynamika tuhých a deformovatelných těles 2006*, Ústí n. Labem, 2006, pp. 175-182.

[74] PROFANT, T., ŠEVEČEK, O. & KOTOUL, M., Calculation of K-factor and T-stress for cracks in anisotropic bimaterials, *Eng. Fract. Mech.*, Vol. 75, 2008, pp. 3707-3726.

[75] PROFANT, T., ŠEVEČEK, O. & KOTOUL, M., The analysis of the stress and displacement field near the surface crack tip terminating perpendicular to the interface between two orthotropic materials, *Materials Science Forum*, Trans Tech Publications, 2007, ISSN 0255-5476, Vol.567, No.1, pp.137-140.

[76] QIAN, Z. Q., On the evalution of wedge corner stress intensity factors of bi-material joints with surface tractions, *Computers and Structures*, Vol. 79, 2001, pp. 53 – 64.

[77] RICE, J. R., Elastic fracture mechanics concepts for interfacial cracks, *Journal of applied mechanics*, Vol.55, 1988, pp. 98-103.

[78] SARRAFI-NOUR, G. R., COYLE., T. W. & FETT, T., A weight function for the crack surface tractions in chevron-notched specimens, *Engineering fracture mechanics*, Vol.59, 1998, pp. 439-445.

[79] SEITL, S., Dvouparametrová lomová mechanika: chování krátkých únavových trhlin, *Disertační práce*, FME BUT a IPM ASCR Brno, 2003, Brno.

[80] SHIH, C. F. & ASARO, R. J., Elastic-plastic analysis of cracks on bimaterial interfaces: Part I – Small Scale Y., *ASME J. Applied Mechanics*, Vol. 55, 1988, pp. 299-316.

[81] SILLS, L.B., HERSHKOVITZ I. & WAVRZYNEK, P.A., Methods for calculating stress intensity factors in anisotropic materials: Part I , *Engineering fracture mechanics*, Vol. 72, 2005, pp. 2328 – 2358.

[82] SLADEK, J, SLADEK, V. & FEDELINSKI, P., Computation of the second fracture parameter in elastodynamics by the boundary element method, *Advances in Engineering Software*, Vol. 30, 1999, pp. 725 – 734.

[83] SODEN, P. D., HINTON, M. J. & KADDOUR, A. S., Lamina properties, Lay-up configurations and loading conditions for a range of fibre-reinforced composite laminates, *Composites Science and Technology*, Vol. 58, 1998, pp. 1011-1022.

[84] STERN, M. & SONI, M. L., On the computation of stress intensities at fixed-free corners, *Int. J. Solid Structures*, Vol. 12, 1976, pp. 331-337.

[85] STROH, A. N., Dislocation and Cracks in Anisotropic Elasticity, *Phil. Mag.*, Vol. 7, 1958, pp. 625-646.

[86] SUO, Z., Singularities, interfaces and cracks in dissimilar anisotropic media, *Proc. of Royal Society of London*, Vol. A 427, 1990, pp. 331-358.

[87] SUO, Z., Singularities interacting with interface and cracks, *International Journal of Solids and Structures*, Vol. 25, 1989, pp. 1133-1142.

[88] SUTRADHAR, A. & PAULINO, G. H., Symmetric Galerkin boundary element computation of T-stress and stress intensity factors for mixed mode cracks by the interaction integral method, *Engng. Anal. with Boundary Elems.*, Vol. 28, 2004, pp. 1335-1350.

[89] ŠEVEČEK, O., KOTOUL, M. & PROFANT, T., A construction of the fundamental solution for the dislocation in the anisotropic bi-material body by force of the FEM, *In proc. of Eng. Mechanics 2006*, ISBN 80-86246-27-2, Svratka, 2006, pp. 350-351.

[90] ŠEVEČEK, O. & PROFANT, T., Problematika obecných koncentrátorů na rozhraní dvou anisotropních materiálů, *In proc. of Multilevel Design of Advanced Materials 2006*, ISBN 80-239-8271-0, IPM ASCR Brno, 2006, pp. 155-162.

[91] ŠEVEČEK, O., VYSLOUŽIL, T., PROFANT, T. & KOTOUL, M., A solution of the bridging problem of a crack in the thin orthotr.layer with tip on the interface of an orthotr. substrate, *In proc. of Applied Mechanics 2007*, Malenovice, 2007, pp.207-208.

[92] ŠEVEČEK, O. & PROFANT, T., Problems of the crack propagation across the interface of two orthotropic materials, *In proc. of Multilevel Design of Advanced Materials 2007*, ISBN 978-80-254-0793-6, IPM ASCR, Ostrava, 2007, pp. 53-60.

[93] TAN, M. A.& MEGUID, S. A., Analysis of bimaterial wedges using a new singular finite element, *International Journal of Fracture*, Vol.88, 1997, pp. 373-391.

[94] THOULESS, M.D. & EVANS, A.G., Effects of pull-out on the mechanical properties of ceramic matrix composites, *In Acta Metall*, 1988, pp.517-522.

[95] TING, T. C. T., Anisotropic Elasticity: Theory and Applications, *Oxford University Press*, 1996.

[96] TING, T. C. T., Stress singularities at the tip of interfaces in polycrystals, *Damage and failure of interfaces*, Edited by Rossmanith, Balkema, Rotterdam, 1997.

[97] TING, T. C. T. & HOANG, P. H., Singularities at the tip of a crack normal to the interface of an anisotropic layered composite, *International Journal of Solids and Structures*, Vol. 20, 1984, pp. 439-454.

[98] TULLOCK, D. L., REIMANIS, I. E., GRAHAM, A. L. & PETROVIC, J.J., Deflection and penetration of cracks at an interface between two dissimilar materials, *Acta Metall. mater.*, Vol.42, 1994, pp. 3245-3252.

[99] VLK, M., Mezní stavy a spolehlivost, *Skriptum VUT v Brně*, 1.vydání, 1991.

[100] VOLINSKY, A.A., MOODY, N.R. & GERBERICH, W.W., Interfacial toughness measurements for thin films on substrate, *Acta Material.*, Vol. 50, 2002, pp.441-466.

[101] VU-QUOC, L. & TRAN, V. X., Singularity analysis and fracture energy-release rate for composites: Piecewise homogenous-anisotropic materials, *Comput. Methods Appl. Mech. Engrg*, Vol.195, 2006, pp.5162-5197.

[102] WANG, A. S. D. & CROSSMAN, F. W., Initiation and growth of transverse cracks and edge delamination in composite laminates, Part I. An energy method, *J. Comp. Mater. Suppl.*, Vol.14, 1980, pp. 71-108.

[103] WANG, H. F., GERBERICH., W. W. & SKOWRONEK, C. J., Fracture mechanics of Ti/Al$_2$O$_3$ interfaces, *Acta Metall*, Vol.41, 1993, pp. 2425-2432.

[104] WANG, T. C. & STAHLE, P., Stress state in front of a crack perpendicular to bimaterial interface, *Engineering Fracture Mechanics*, Vol.59, 1998, pp. 471-485.

[105] WEI, L., & TING, T. C. T., Explicit expression of the Barnett-Lothe tensor for anisotropic materials, *Journal of elasticity*, Vol.36, 1994, pp. 67-83.

[106] YANG, S., & YUAN, F. G., Determination and representation of the stress coefficient terms by path independent integrals in anisotropic cracked solids, *Int. Journal of Fracture*, Vol.101, 2000, pp. 291-319.

[107] YAU, J. F., WANG., S. S. & CORTEN, H. T., A mixed mode crack analysis of isotropic solids using conservation laws of elasticity, *ASME J. Appl. Mech.*, Vol.47, 1980, pp. 335-341.

[108] YING, X. & KATZ, N. I., A uniform formulation for the calculation of stress singularities in the plane elasticity of a wedge composed of multiple isotropic materials, *Comput. Math. Applic.*, Vol.14, 1987, pp. 437-458.

[109] ZHANG, Z. & SUO, Z., Split singularities and the competition between crack penetration and debond at a bimaterial interface, *Int.J.of Solids and Structures*, Vol.44, 2007, pp. 4559-4573.

[110] ZOU, L., HUANG, Y. & CHEN, R., The measurement and characterization of the interfacial toughness of composites by a three-point bending test, *Journal of the European Ceramic Society*, Vol. 23, 2003, pp.1987-1996.

Internet resources

[111] *http://www.sciencedirect.com* – On-line database of the scientific articles.

[112] *http://springerlink.metapress.com* – On-line database of the scientific articles.

Nomenclature

Notation	Description
a	Finite crack extension
a_p, a_d	Finite crack extensions of penetrating and deflected crack
adj	Adjoint matrix
$\mathbf{A}$, A_{ij}	Matrix of material characteristic eigenvalues and components s_{ij}
b_i	Burger's vector
$b^*_s(s)$	Density function
B	Thickness of the substrate (material without crack)
c_f	Fibre volume fraction
c_{ijkl}	Tensor of elastic constants
d_k	Elementary Burger's vector
$diag[...]$	Diagonal matrix
$\mathbf{D}$	System of equations for the solution of the δ exponent
$\mathbf{E_i}$	Transfer matrices
E_L, E_T, E_Z, E_{ij}	Young's moduli in longitudinal, transversal and Z-direction
E_f, E_m, E	Young's moduli of fibre and matrix and overall modulus
$f_{ij}(\theta)$	Angular distribution of the stress field
$f_j(z_j)$	Muschelishvilli´s complex potential
$f_k(y_0)$	Local density function of the Burger's vector
F	Line force acting on the crack faces (in the crack bridging problem)
$F_i(\varepsilon)$	Coefficients of the inner asymptotic expansion
$F_i(\theta)$	Angular distribution of the resulting force T_i
$g_i(\theta)$	Angular distribution of the displacement field
G_{LT}, G_{TZ}, G_{ZL}, G_{ij}	Shear moduli
G	Energy release rate
G_d, G_p	Energy release rate of the deflected and penetrating crack
G_c	Fracture toughness
G_c^i, G_c^1	Fracture toughness of the interface and of the material 1
$\mathbf{G_{w,i}}$	Material wedge of the multimaterial interface
$\langle h \rangle$	Average distance from the fibre failure position to the crack plane
h	Thickness of the surface layer
H	Generalized Stress Intensity Factor (GSIF)
H_1, H_2	GSIFs related to the stronger and weaker singularity
H_{appl}, H_{br}, H_{tip}	Applied, bridging and the local Generalized Stress Intensity Factor
H_c	Critical value of the GSIF
i	Imaginary unit

Im(...)	Imaginary part of the expression
$\mathbf{I}$	Identity matrix
$k_i(\varepsilon)$	Coefficients of the outer asymptotic expansion
$K_{1d}, K'_{1d}, K_{2d}, K'_{2d}$	Coefficients of the perturbed solution for the deflected crack
$K_{1p}, K'_{1p}, K_{2p}, K'_{2p}$	Coefficients of the perturbed solution for the penetrating crack
$K_{\mathrm{I}}, K_{\mathrm{II}}$	Stress intensity factors for loading mode I and II
K_{IC}	Fracture toughness
$K_{ij}, \mathbf{K}$	System of equations for the solution of the δ exponent
$\mathbf{K}_{\mathrm{N}}$	Product of the sequence of transfer matrices
l	Distance of the main crack from the interface
l_c	Total crack length
l_{cf}	Typical length of fibre with presence of one flaw
L	Measurement of the crack tip process zone
L_c	Characteristic size of the main crack
$L_{i\alpha}$	Matrix containing material characteristic eigenvalues.
m_w	Weibull shape coefficient
m,n	Characteristics of the material anisotropy
n_i	Normal pointing toward the origin of the coordinate system
N	Number of material wedges
N_B	Number of collocation points
p_α	Characteristic eigenvalues of the material
r	Polar coordinate
r_ε	Radius of the integration path approaching the zero
R	Radius of the integration path
R_f	Fibre radius
Re(...)	Real part of the expression
s, t	Substituted coordinates
s_{ij}	Components of compliance matrix
T	T-stress
T_i	Resulting force along the half-line leading from the singular point
$u_{k,l}$	Components of the strain tensor
$\mathbf{u}_i$	Angular distribution of the displacement field
$\mathbf{u}_{-i}$	Angular distribution of the auxiliary displacement field
$\mathbf{U}, \mathbf{V}$	Displacement field
U_i, U_{-1i}	Displacement field (vector), auxiliary (dual) displacement field
$U_j^0, \mathbf{U}^0$	Solution of displacements for the unperturbed state
$U_i^h, \mathbf{U}^{\mathrm{h}}$	Displacement field obtained by the Finite Element Analysis

U_j^ε, $\mathbf{U}^\varepsilon$	Solution of displacements for the perturbed state
$\mathbf{v}$, v_k	Eigenvector, components of the eigenvector
$v(x_2)$	Total displacement of the upper crack face
$v_{appl}(x_2)$	Crack face displacements of the unbridged crack under applied
$v_{br}(x_2)$	Bridging crack closure displacements
$\mathcal{V}_i$	Basis functions of the inner expansion
W_p, W_d	Change of the potential energy for crack penetration and deflection
W^0, W^ε	Potential energies of unperturbed and perturbed state
$W(x_2,h)$	Bridging weight function
x_1, x_2	Cartesian coordinates
x_{1o}, x_{2o}	Location of an isolated dislocation in Cartesian coordinates
y_1, y_2	Scaled up coordinates (for zoomed-in view)
z_α	Argument of the complex potential function
α, β	Dundurs' parameters
β	Bridging characteristics
Γ, Γ_i	Integration path
$\Gamma(n)$	Gamma function
δ, δ_i	Characteristic eigenvalue of the singularity
δ^*, δ_{-i}	Characteristic eigenvalue of the auxiliary solution
δ_{ij}	Kronecker´s delta
δa	Crack increment
δW	Change of the potential energy
δW_d, δW_p	Change of potential energy in case of crack deflection, penetration
ΔW	Additional energy
ε	Characteristic size of the perturbation
ε_{ij}	Components of the strain tensor
ε_o	Oscillation index
θ	Polar coordinate
θ_0	Direction angle of the crack extension.
κ	Constant proportional to the loading
λ	Characteristics of the material orthotropy
μ_i	Characteristic eigenvalues of the material
ν_{TZ}, ν_{ZL}, ν_{TL}, ν_{ij}	Poisson's ratio between appropriate directions
ρ	Zoomed variable r with factor ε
ρ	Characteristics of the material anisotropy
σ_c	Critical stress – strength of material
σ_{ij}	Components of the stress tensor

$\sigma_{ij}{}^{*}$	Auxiliary (dual) stress field
$\sigma_{ij\,(tip)}$	Stress field in the vicinity of the general stress concentrator
σ_0	Nominal tension load of the specimen
σ_{0f}	Fibre strength
σ_{br}	Bridging stress
σ_P	Average stress exerted by the broken fibres
Σ	Fibre strength distribution
τ_s	Interface slipping shear resistance stress
$\varphi(z)$	Muschelishvilli´s complex potential
ϕ	Angle between crack and interface
ϕ_j^J	Vector of complex coefficients
$\Phi(z_\alpha)$	Complex potential function
$\psi(z)$	Muschelishvilli´s complex potential
$\Psi(\Box, \Box)$	Ψ-integral
Ψ_G	Energy based mode mixity angle
Ψ_K	Stress intensity factor based mode mixity angle
ω_i	Polar sector of the multimaterial wedge
Ω^{in}	Inner domain
Ω^{o}	Outer domain
$\partial\Omega$	Boundary of the finite body

Abbreviations:

BEM	Boundary Element Method
C.C.	Complex conjugate
CDD	Continuously Distributed Dislocations
CS	Coordinate System
DDT	Distributed Dislocation Technique
ERR	Energy Release Rate
FEA	Finite Element Analysis
FEM	Finite Element Method
FFM	Finite Fracture Mechanics
GSC	General Stress Concentrator
GSIF	Generalized Stress Intensity Factor
LEFM	Linear Elastic Fracture Mechanics
L.E.S.	Lechnitskii Eshelby Stroh (method)

If not listed quantities occur in the text, then they have only a local meaning described directly on the place of the appearance and no other references to this quantity should be made in the following text.

Author's Curriculum Vitae

Oldřich Ševeček

Date of birth: 30. 01. 1980
Address: Jesenická 67, Šumperk 787 01
E-mail: sevecek@seznam.cz
Nationality: Czech
Marital status: Single

Education:

2004 - 2009	*Ph.D. Study* – Brno University of Technology, Faculty of Mechanical Engineering, Technická 2, 616 69 Brno
	Specialization: Engineering mechanics
	Ph.D. Thesis: Solution of general stress concentrators in anisotropic media by combination of FEM and the complex potential theory
1998 - 2004	*M.Sc. study program* – FME BUT, Technická 2, 616 69 Brno
	Specialization: Applied mechanics
	Diploma work: Computational and experimental analysis of the first vibration shape at simultaneous and contra-rotating precession of model rotor kit RK4
1994 - 1998	Vyšší odborná škola a Střední průmyslová škola, Gen. Krátkého 1, 787 01 Šumperk. *Specialization:* Management of engineering

Work experience:

2008 – onwards	FEM Specialist – Crash simulations, ŠKODA AUTO, a.s., Václava Klementa 869, 293 60 Mladá Boleslav.
2007	Solution of the grant project FRVŠ 2421/2007/G1
2004 – 2007	Teacher of subject Technical Mechanics II on FME BUT, Brno
	Cooperation on solution of grant projects GAČR: 106/05/H008, 101/05/0320, 106/06/0724, 101/05/P290

Personal skills:

Languages:	English: communication level, technical English Russian, German: basics
Computer skills:	Windows, Linux, MS Office, FE-systems ANSYS, ABAQUS, PAMCRASH, mathematical software MATLAB, MAPLE, CAD software AutoCAD, Catia, Inventor, basics of Pro/Engineer.
Driving license:	Category B

Hobbies: Travelling, photography, sports, IT

Awards:

06 / 2004	Dean's award for the excellent study results and the participation in the science-research activities on FME BUT